UNIVERSITY OF GLASGOW

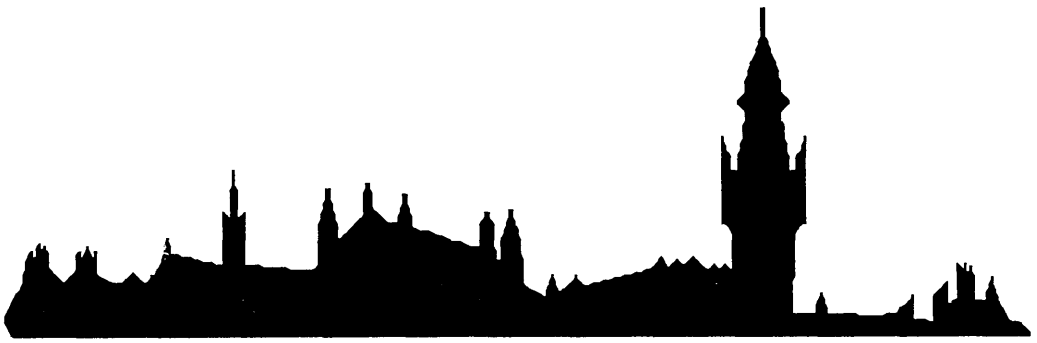

MAGNETIC RESONANCE STUDIES OF THE RED-PHOTOCHEMISTRY OF C-NITROSO DERIVATIVES, AND OF THE ACTION OF NO AND NO_2 ON BIOLOGICALLY IMPORTANT SUBSTANCES

by

Mohamed - Chérif BOUCENNA, B.Sc

being a thesis submitted for the degree of ***Doctor of Philosophy*** *in the Department of Chemistry*

SCOTLAND 1991

In the name of God, Most Gracious, Most Merciful.

Proclaim! In the name of thy Lord and Cherisher,
who created,
Created man, out of a mere clot of congealed blood,
Proclaim! And thy Lord is Most Bountiful,
He Who taught (the use of) the pen,
Taught man that which he knew not.

DEDICATED TO
MY WIFE DALILA-SONYA
AND
MY SON AMIR

ACKNOWLEDGEMENTS

It is with immense pleasure that I take this opportunity to thank my supervisor Dr Andrew L. Porte for showing patience and kindness towards me during the course of this thesis, and also for his constant encouragement, advice and invaluable guidance without which this work and the development of my own knowledge as a scientist would not have been possible.

My sincere thanks are also extented to Dr John S. Davidson for kindly providing me with a sample of solid 2-chloro-2-nitrosonorbornane, Dr David Rycroft and his technicians for their help in recording the high-resolution nuclear magnetic resonance spectra and finally the technical staff of this department for their assistance.

I am also indebted to my wife for her help, encouragement and moral support throughout the course of this work.

Last, but not least, my gratitude is also due to the Algerian government for financial support which is sincerely acknowledged, and for the assistance provided by the staff at the Algerian Embassy in London, and in particular to the Cultural Attaché, during my stay in Great Britain. I would also like to thank in particular Professor I.B. Thomson and Miss A.M. MacGregor, of the international office, for their help.

TABLE OF CONTENTS

CHAPTER ONE

CHAPTER TWO

REFERENCES

LIST OF FIGURES

SUMMARY

This thesis begins, chapter one, with a general introduction to the photochemistry of C-nitroso compounds, nitroxide radicals, and photochemical reactions of some optically active geminal chloronitroso derivatives of terpenes. The remaining chapters of the thesis then describe the author's work on two important aspects of C-nitroso systems.

1) Photochemical reactions in solid 2-chloro-2-nitrosonorbornane

Chapter two examines analyses of a sample of solid 2-chloro-2-nitrosonorbornane by means of infra red, mass spectroscopy and modern high resolution nuclear magnetic resonance spectroscopy. This work shows that the solid is racemic and dimeric, and contains mixtures of dd-,ll-, dl- and ld-isomers. It also enables the configuration at the >C(2)ClNO residue to be established. Detailed high resolution nuclear magnetic resonance spectroscopic studies show that in solutions, 2-chloro-2-nitrosonorbornane exists mainly in the monomeric form, in equilibrium with a small amount of the corresponding dimeric forms.

Irradiation of the solid with red visible light causes some white crystals and a brown viscous oil to be formed. The components of these two phases have been identified. In order to account for the observed photolysis products, a reaction mechanism is postulated. This invokes a Beckmann-like rearrangement reaction which may be of general synthetic use for converting geminal chloronitroso derivatives into lactams which may be of pharmacological interest.

In chapter three, information from the work described in chapter two is combined with work carried out by earlier investigators to show

how circular dichroism studies can be combined with high resolution nuclear magnetic resonance spectroscopy to enable the configurations at optically active >CClNO centres of other geminal chloronitroso terpene derivatives to be determined.

2) Action of NO and NO_2 on some biologically important substances

In chapter four, it is pointed out that the work described in chapters 1-3 of this thesis may have significance for the agricultural and medical toxicology, including carcinogenesis, of compounds containing nitrogen. This chapter describes the results obtained from detailed spectroscopic studies of reactions that take place when some steroids, fatty acids, pyrimidine bases and purine bases of biological interest are brought into contact with acidified solutions of sodium nitrite. These studies show that acidified sodium nitrite affects steroids and almost certainly carbohydrates. It isomerises unsaturated fatty acids, and therefore almost certainly affects the permeability of cell membranes. It affects pyrimidine bases and purine bases, and almost certainly nucleosides, nucleotides and nucleic acids. It also affects amino acids and proteins. Acidified sodium nitrite must interfere with the genetic code. NO and NO_2 must be implicated in some areas of carcinogenesis and in bacterial toxic shock.

CHAPTER ONE

INTRODUCTION

1.1 Photochemistry of C-nitroso compounds

Organic C-nitroso compounds can exist in monomeric or dimeric forms. The dimers can have either *cis*- or *trans*-geometry, or even both.

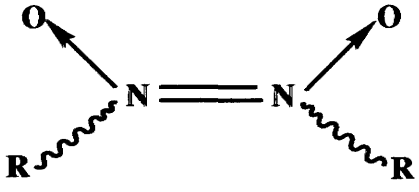

cis-dimer

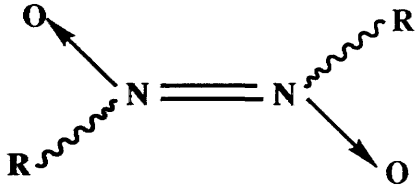

trans-dimer

In *solution,* the monomeric and the dimeric forms are in equilibrium.[1-5]

$$2\,R-NO \rightleftharpoons (R-NO)_2$$

blue colourless

The position of equilibrium depends on the nitrosite. Primary and secondary C-nitroso compounds tend to exist in dimeric forms, but the tertiary compounds are mostly monomers.[1] These differences can be accounted for by invoking both electronic and steric effects.[1,5-8]

Aliphatic C-nitroso monomers absorb red visible light at about 670 nm,[1,9,10] and it is this singlet ⟵ singlet, $^1\pi^* \longleftarrow {}^1n$ (nitrogen), transition that is responsible for the characteristic blue colour of the monomers, and for their interesting red-photochemical reactions. The dimers are not directly photolysed by red light but they may be converted to the monomeric forms by the action of heat[1,3,11,12] or by ultra-violet irradiation,[12,13] and then red-photolysed.

In simple aliphatic C-nitroso compounds, the C-N bond has a particularly low dissociation energy,[14,15] of about 34-41 kcal.mole^{-1}, and C-N bond cleavage can occur as a result of irradiation with red light. Current literature suggests that homolytic C-N bond cleavage, with the formation of alkyl radicals and nitric oxide, is common to the photolysis of C-nitroso compounds, and the basic photochemical processes have been summarised,[10] as in **Scheme 1.1**.

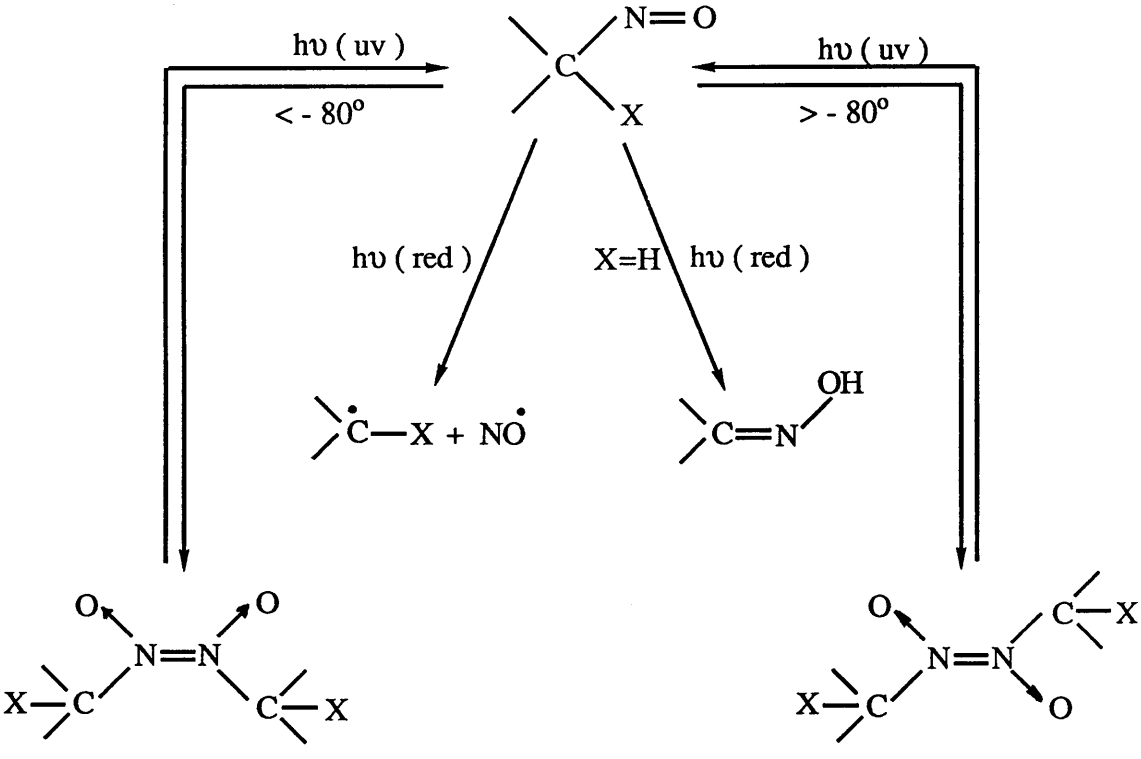

where X = H, alkyl, aryl, Cl, NO_2, $OCOCH_3$, CN.

Scheme 1.1

This scheme is a gross over-simplification. On red-photolysis, a mixture of paramagnetic nitroxide radicals and various diamagnetic products which include olefins, nitro- and nitrato- derivatives, gaseous nitrogen and oxides of nitrogen, are eventually formed.[16,17]

Photolyses of *solutions* of geminal substituted nitroso-alkanes,[14,18-21] and more recently of tertiary nitrosoalkanes,[22-24] have been studied by several groups of workers. Both *protic* and *aprotic* solvents have been used and it has been confirmed that the C-N bond breaks on red-irradiating these compounds. However, more recent work has shown that the irradiation processes do not proceed by the mechanisms invoked by earlier workers[25-27] in which C-X bond fission takes place and hydrogen atoms are abstracted from excited nitroso-alkanes.

The distribution of products is found to be markedly dependent on first, the structure of the nitrosoalkanes and second, on whether the solvent is *protic* or *aprotic*, and schemes are already available in the literature[18-20,23,24] to account for the photolysis products of *solutions* of simple geminal substituted alkanes.

In *aprotic* solvents, in the absence of air, the photolysis products are believed to be formed during the following photochemical processes.

$$R_1R_2CXNO \xrightarrow{h\upsilon} R_1R_2\dot{C}X + NO^{\bullet} \qquad (1)$$

$$R_1R_2CXNO + R_1R_2\dot{C}X \longrightarrow R_1R_2XC - \underset{\underset{O}{\|}}{N}{}^{\bullet} - CXR_2R_1 \qquad (2)$$

$$R_1R_2CXNO + 2\,NO \longrightarrow R_1R_2XC - \underset{\underset{N=O}{|}}{N} - O - NO \longrightarrow R_1R_2XC - N = N - ONO_2 \qquad (3)$$

$$R_1R_2XC - N = N - ONO_2 \xrightarrow{X = H} R_1R_2C = CR_2R_1 + N_2 + HNO_3 \qquad (4)$$

$$R_1R_2XC - N = N - ONO_2 \longrightarrow R_1R_2\dot{C}X + N_2 + \dot{NO_3} \qquad (5)$$

$$R_1R_2\dot{C}X + \dot{NO_3} \longrightarrow R_1R_2CX - ONO_2 \qquad (6)$$

$$\dot{NO_3} + NO^{\bullet} \longrightarrow 2\,\dot{NO_2} \qquad (7)$$

$$R_1R_2CXNO + \dot{NO_2} / \dot{NO_3} \longrightarrow R_1R_2XC - ONO + NO^{\bullet} / \dot{NO_2} \qquad (8)$$

$$R_1R_2\dot{C}X + \dot{NO_2} \longrightarrow R_1R_2XC - ONO \qquad (9)$$

Reaction (**5**) involving the breakdown of the intermediate diazonium nitrate formed in reaction (**3**) is the clue to understanding the formation of alkenes and other diamagnetic products.[18-20,22,28,29]

In red photolysis of *solutions* of C-nitroso compounds in *protic* solvents however, intermediates are readily dissipated by solvolysis which tends to dominate the whole reaction pattern, and additional diamagnetic products such as oximes, alkyl nitrites, *etc.* may then also be formed.[10,18-20]

Electron paramagnetic resonance studies[30,31] have shown that nitroxide radicals are very commonly formed in the photolysis of C-nitroso compounds. Two mechanisms have been postulated to account for the formation of these radicals. The first and the most important and acceptable mechanism, is the scavenger mechanism,[3,32,33] which is a natural consequence of the very efficient spin-trapping properties of C-nitroso compounds,[34,35] reactions (**1**) and (**2**). The alkyl radicals produced in reaction (**1**) are trapped by molecules of the parent nitroso compound, reaction (**2**). Very strong support for this mechanism comes from a number of studies, and in particular from an ingenious experiment, designed by de Boer,[36] involving the photolysis of 1-cyclopropyl-1-nitrosoethane, reaction (**10**). The nitroxide radical produced in this photolysis can only arise by trapping of the rearranged intermediate alkyl radical by unchanged 1-cyclopropyl-1-nitrosoethane.

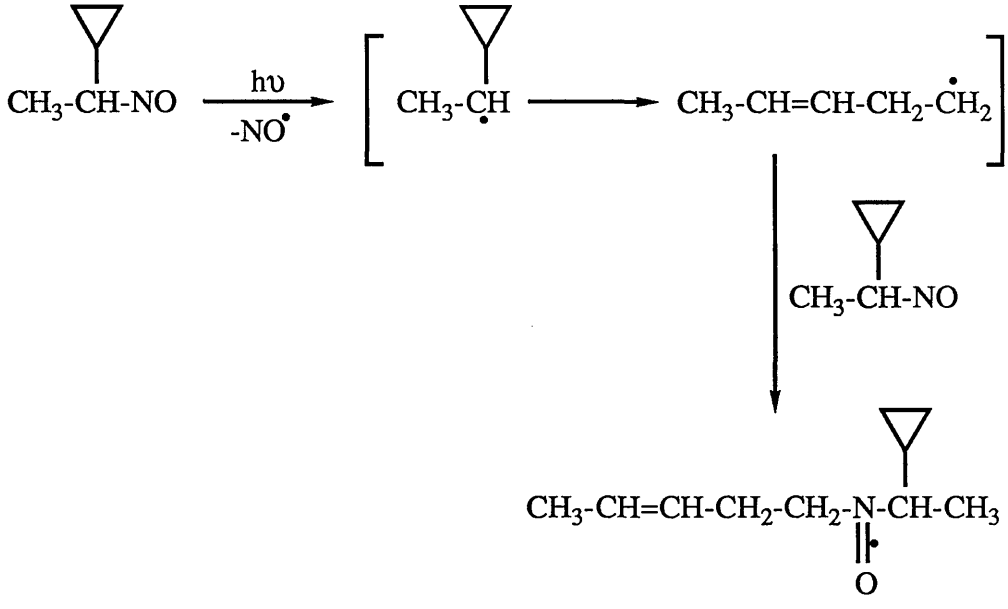

reaction **(10)**

There is some evidence that in some cases a second mechanism may also be involved.[36-38] In this, a long lived excited state of the nitroso compound collides with a second molecule to form a nitroxide, as shown in reaction **(11)**.

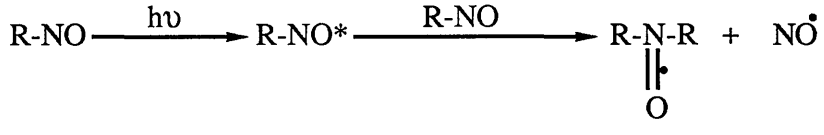

reaction **(11)**

1.2 Nitroxide radicals generated from C-nitroso compounds

The first authenticated organic free radical was triphenylmethyl, discovered by Gomberg in 1900,[39] and since then, many stable free radicals have been prepared. Most, but not all, radicals are highly reactive because of the presence of an unpaired electron, and have lifetimes of the order of micro-, or milli-seconds, unless they are

trapped within an inert matrix.

The first nitroxide radical to be isolated was porphyrexide **[1]**, a heterocyclic radical, that was identified as long ago as 1901.[40]

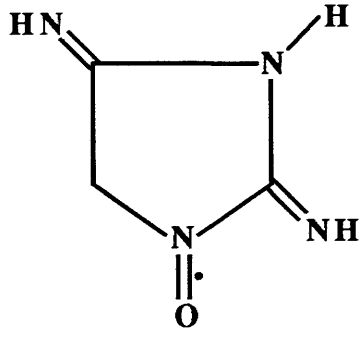

[1]

porphyrexide

Because of the presence of an unpaired electron, electron paramagnetic resonance spectroscopic techniques are ideally suited to studying the nitroxides. These techniques can also be used to investigate less stable nitroxide radicals that are formed as short lived intermediates in various reactions.

The simple molecular orbital picture, **Figure 1.1**, shows that in the nitroxide radicals, three π-electrons are distributed over the two molecular π-orbitals obtained from a linear combination of the atomic p_z orbitals of the nitrogen and oxygen atoms.[41]

The overlap of the $2p_z$ orbitals on nitrogen and oxygen results in a π-bonding orbital occupied by two electrons, and a π^*-antibonding orbital, occupied by only one electron, giving a net $N \overset{\bullet}{=} O$ bond order of 1.5, characterised by a bond energy of about 100 kcal.mole^{-1}. This

energy is half way between the values of 53 kcal.mole^{-1} found for a >N-O- single bond and 145 kcal.mole^{-1} found for a -N=O double bond.[42]

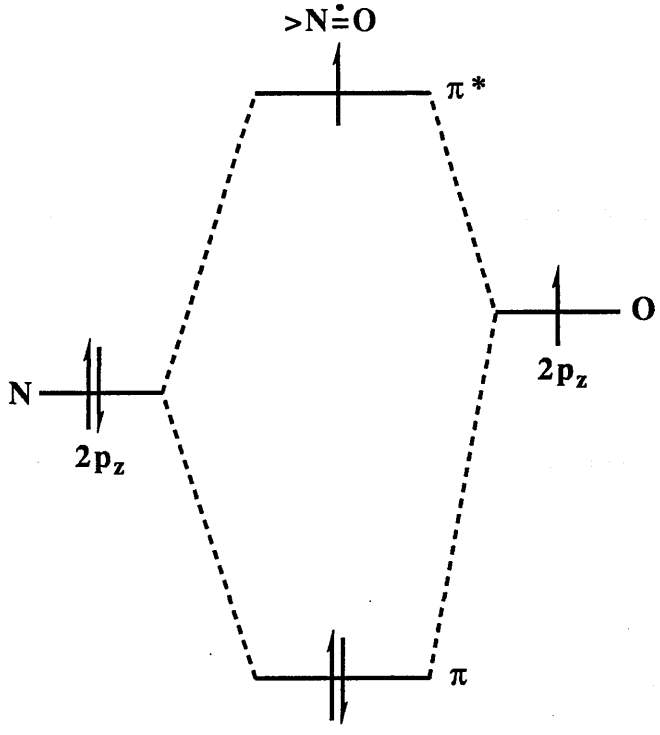

N: $1s^2[sp^2 \text{ hybrids}]^3 2p_z^2$ O: $1s^2 2s\ ^2 2p_x^1 2p_y^2 2p_z^1$

Figure 1.1

Detailed LCAO-SCF-MO calculations using the CNDO/2 approximation,[43] together with electron paramagnetic resonance measurements on various aliphatic nitroxides, have confirmed the above picture and both theoretical and experimental arguments show that the unpaired spin density on nitrogen and oxygen are of the order of 0.46 and 0.54 respectively.[44]

The organic nitroxide radicals show no tendency to dimerise at the nitrogen or oxygen atoms. However, the chemical stability of these radicals is markedly dependent on the environment of the nitroxide and on the nature of the groups attached to the nitrogen atom.[45]

Other magnetic resonance techniques, including nuclear magnetic resonance (NMR)[46] and electron nuclear double resonance (ENDOR)[47] spectroscopy have also occasionally been used to study nitroxides. They are particularly useful in measuring very small hyperfine coupling constants, and their absolute signs.

1.3 Photochemistry of the solid nitrosites of caryophyllene and humulene

Caryophyllene [2] is one of the major components of oil of cloves. Its structure was worked out by Barton[48] and Šorm,[49] and co-workers,

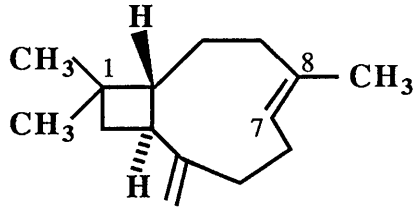

[2]

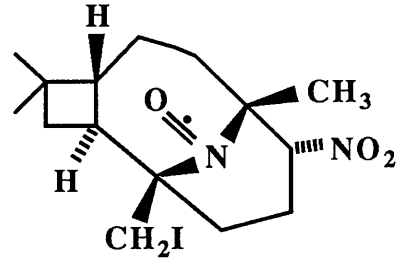

[3]

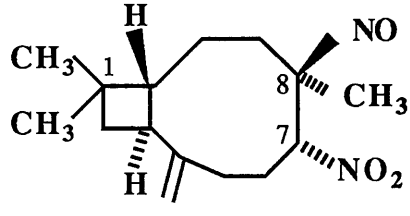

[4]

using standard organic degradative techniques, and by X-ray crystal structure analysis of the iodonitrosite, structure **[3]**,[50-52] a crystalline material formed when iodine is added to caryophyllene nitrosite. This X-ray analysis of the iodonitrosite unambiguously establishes the structure and stereochemistry of caryophyllene nitrosite **[4]**.

Caryophyllene nitrosite was first synthesised in 1898.[53] Although it used to be employed to characterise caryophyllene, its photochemistry was largely neglected until 1968. Mitchell *et al* examined the circular dichroism and rotatory dispersion spectra of *solutions* of caryophyllene nitrosite[54,55] and Hoffman's[56] early studies of the red photolysis of these *solutions* identified nitrogen and gaseous oxides of nitrogen[56] in the products. In 1968,[57,58] McConnell, Porte and co-workers used an electron paramagnetic resonance spectrometer to monitor the red- and ultra-violet irradiation of both *solution* and *solid* caryophyllene nitrosite and they showed that this substance is a versatile source of radicals. This work represents the first serious attempt to study the photolysis of *solid* C-nitroso compounds.

The sesquiterpene humulene **[5]** is one of the major components of oil of hops and, like caryophyllene, its structure was established by means of a combination of organic chemical degradation studies,[59-71] and X-ray analysis, this time of its silver nitrate adduct.[72-74]

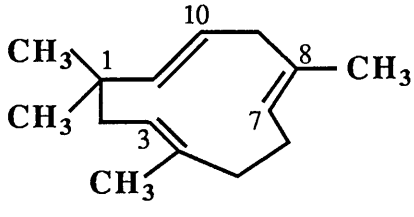

[5]

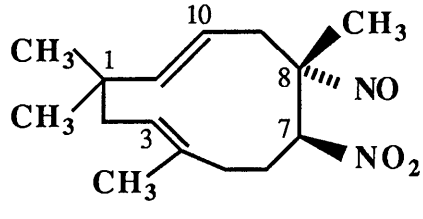

[6]

Humulene nitrosite **[6]** again was first prepared by Chapman who allowed humulene to react with N_2O_3[75,76] and it too was used by Mitchell and co-workers in their early work on the Cotton effect[54] and in their early studies of asymmetric photochemical reactions involving circularly polarised light.[55] Humulene nitrosite exists in two crystalline forms. Needles are obtained when it is rapidly recrystallised out of an ethanol solution. Platelets are also formed, in addition, when crystallisation is allowed to take place slowly from the same solvent.[30,77,78]

Very detailed spectroscopic studies and in particular, polycrystalline and single crystal electron paramagnetic resonance studies of caryophyllene nitrosite[17] and humulene nitrosite[77,78] have unravelled much of the photophysics and photochemistry of the complicated red-photolysis reactions of these solids. These investigations established the mechanisms of the photochemical reactions, and identified the following compounds in the products obtained: N_2, NO, NO_2, $NO_3^{\bullet}$, dinitro-derivatives **[7]**, a nitronitrato-derivative **[8]** in the case of caryophyllene nitrosite, olefinic isomers **[9]-[11]**, and in the case of the platelets of humulene nitrosite, caryophyllene derivatives.[16]

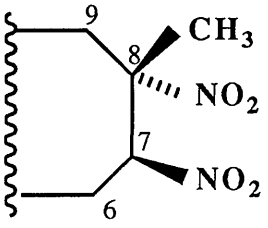

[7]

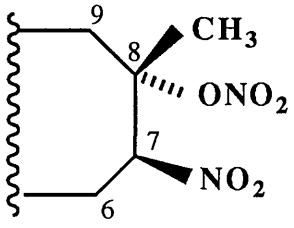

[8]

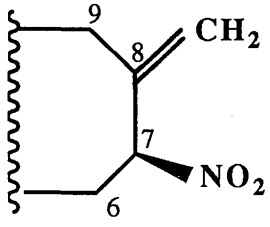

[9]

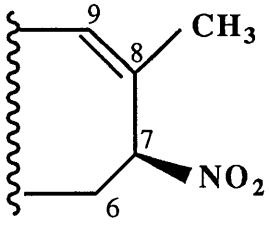

[10]

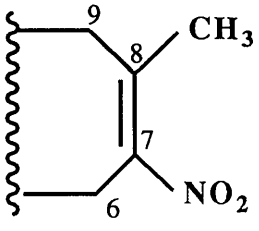

[11]

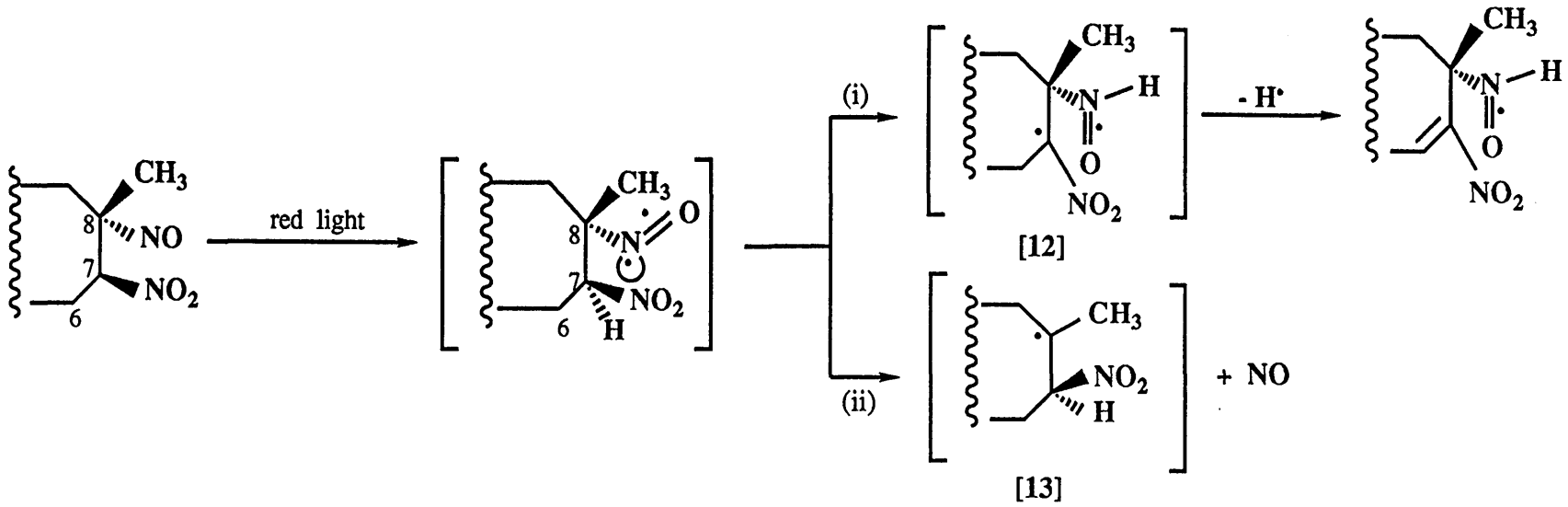
CH3
8
NO
7
NO2
6
red light
CH3
8
N
O
7
NO2
6
H
(i)
CH3
N
H
O
NO2
[12]
- H•
CH3
N
H
O
NO2
(ii)
CH3
NO2
H
[13]
+ NO

Scheme 1.2

The electron paramagnetic resonance studies[17,77,78] of the single crystals of the nitrosites of these sesquiterpenes show that the very early stages of the solid red photolyses involve two competing reactions, **Scheme 1.2**, in which the formation of the monoalkyl nitroxide radicals **[12]** are initially favoured relative to the alkyl radicals **[13]**. The radicals, **[12]**, decay very rapidly in *solution*, presumably to mixtures of the corresponding nitrones and hydroxylamines. The single-crystal electron paramagnetic resonance studies[17,77,78] provide a wealth of information about the photochemistry, photophysics, and the components of the tensors involved in the spin-Hamiltonians of these radicals, information that can only be obtained by studying the *solid state* reactions.

1.4 Photochemistry of geminal chloronitroso derivatives of the diterpenes

The interesting results that followed from the study of caryophyllene and humulene nitrosites,[16,17] when combined with the renewal of interest in the *solution* photochemical reactions of the geminal chloronitroso derivatives of the alkanes[18-20,22,79,80] implied that it would be worth while extending the examination of the photochemical reactions of C-nitroso solids to include the *solid* geminal chloronitroso derivatives of the *diterpenes*.

Even as far back as the 1930s, Mitchell and his co-workers[81,82] in Glasgow examined the Cotton effect and the red-photolysis reactions of *solutions* containing some geminal halonitroso alkane derivatives, and in the 1950s they extended this work to include diterpene derivatives.

Mitchell and Veitch[83] synthesized the derivatives **[14]-[19]** of 2-chloro-2-nitrosocamphane, which incorporate at the C(10)-position a series of chromophoric groups, R, of varying size and charge.

[14] R = CH_2Br

[15] R = COOH

[16] R = CH_2COOH

[17] R = CH_2COOCH_3

[18] R = $CH_2COOC_6H_5$

[19] R = CH_3

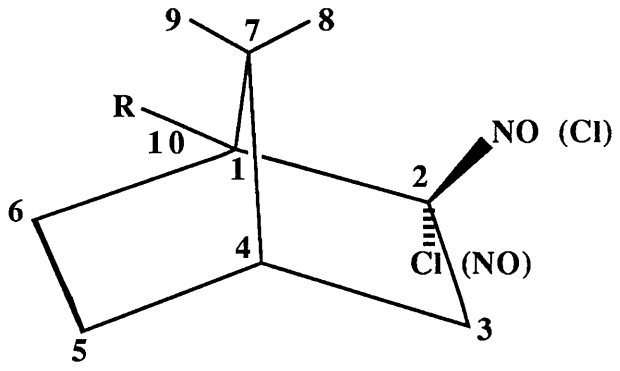

They found that the Cotton effect has the same sign in compounds **[14]** and **[15]**, but is opposite to that in the un-irradiated (-)-2-chloro-2-nitrosocamphane **[19]**. They also found that the rotatory dispersion curves of compounds **[15]** and **[19]** invert on irradiation with red-light, but the corresponding curve of compound **[14]** does not.

Hope and Mitchell[84] studied the 2-chloro-2-nitroso derivatives, **[20]**, **[21]** and **[22]**, of pinocamphane, carane and carvomenthone, respectively.

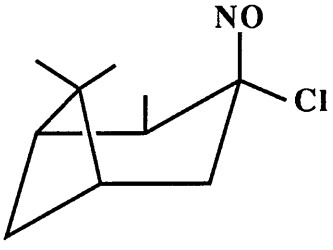

[20]

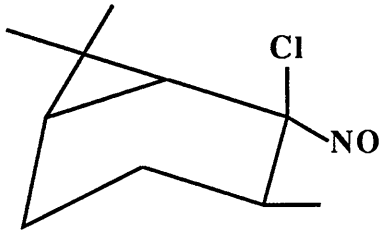

[21]

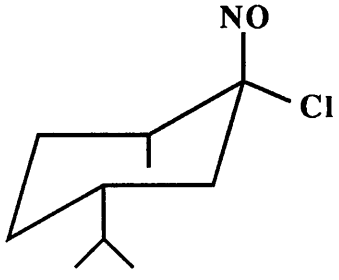

[22]

The rotatory dispersion curves of these compounds show small displacements in their absorption maxima after red-light irradiation, but the signs of the Cotton effects are not inverted, and on very doubtful grounds, Hope and Mitchell postulated that skeletal rearrangements occured in these cases, as shown below.

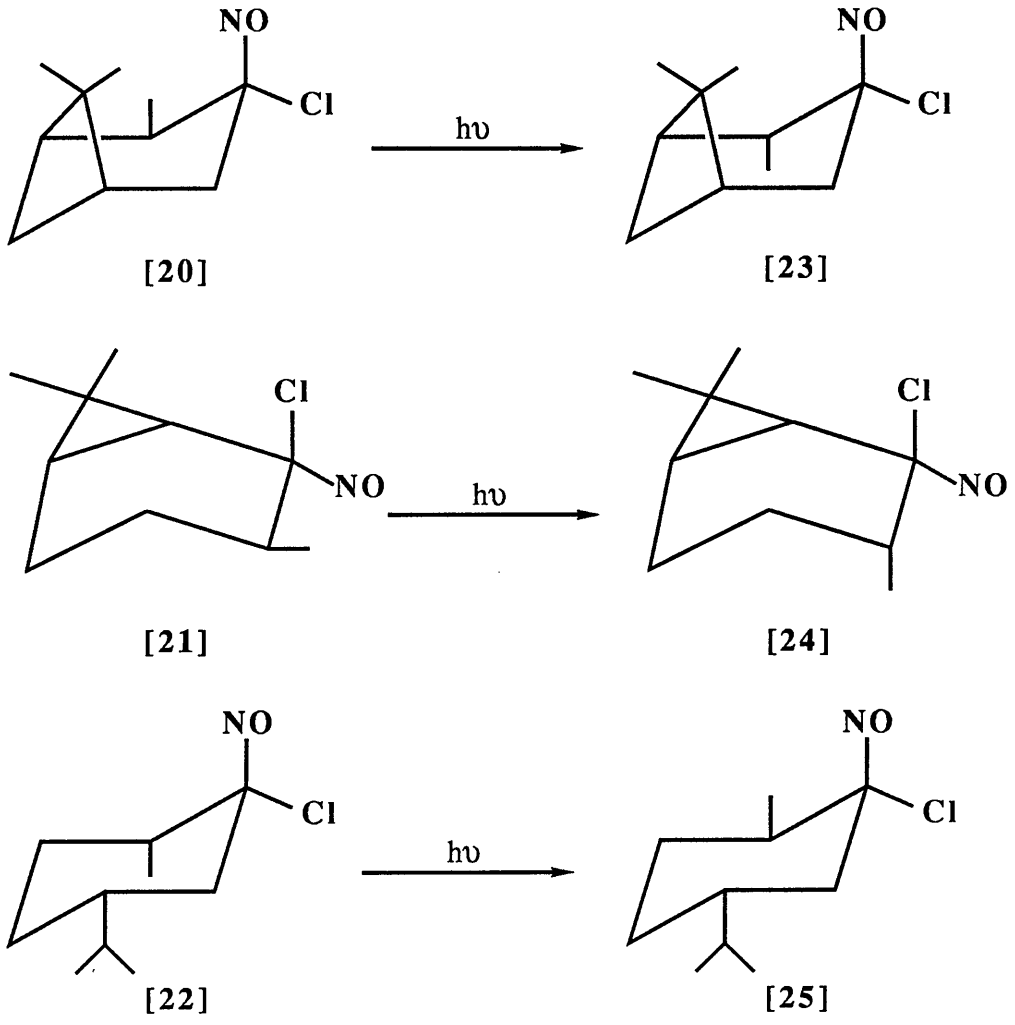

Powerful modern spectroscopic methods were not available to these workers, and therefore, they were not able to assign configurations at the >C(NO)(Cl) residues with certainty. Mitchell and his co-workers found[85,86] that the rotatory dispersion curve of an alcoholic solution of (-)-2-chloro-2-nitrosocamphane **[19]** is inverted when it is irradiated with

red-light, "without appreciable photolysis", and the absorption is displaced by 60 Å towards longer wavelengths, *if this irradiation lasts for only a short period of time*. They interpreted this in terms of a 2,2'-mutarotation in which the NO and Cl groups on C(2) are interchanged and the configuration at this carbon is thereby inverted, reaction **(12)**.

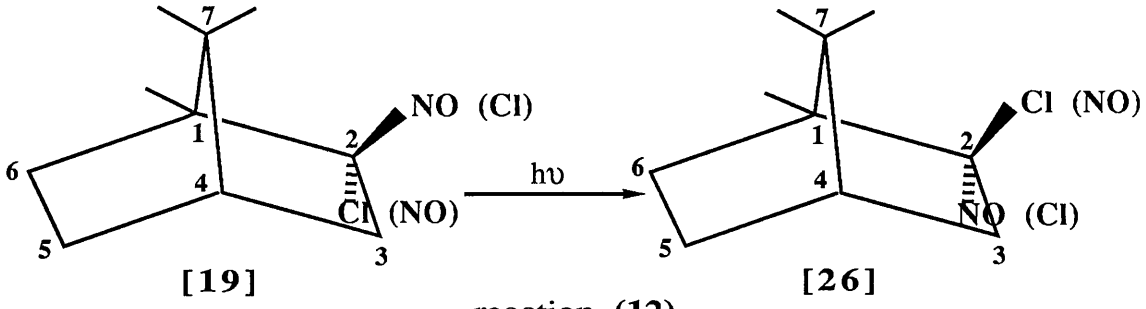

[19] **[26]**

reaction **(12)**

Hope and Mitchell[86] also noticed that the differences in the ultra-violet absorption spectra of the (-) and (+) pair of isomers of 2-chloro-2-nitrosocamphane, componds **[19]** and **[26]**, are similar to the differences in the corresponding spectra of bornyl and isobornyl chlorides, **[27]** and **[28]** respectively, whose structural configurations were already known to them. They therefore *assumed* the following correspondences.

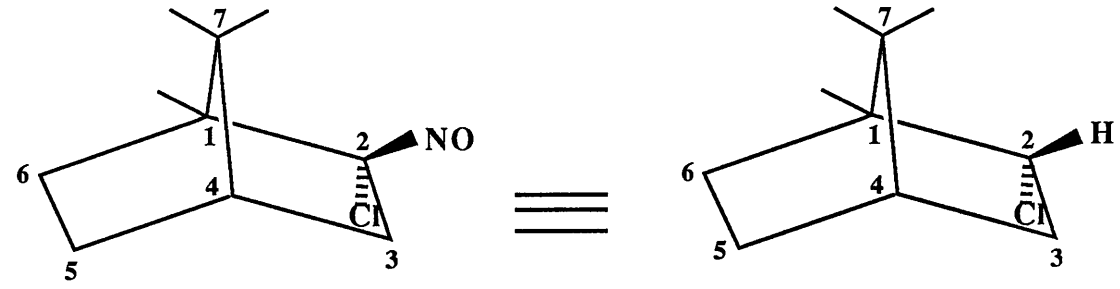

[19]
(-)-2-chloro-2-nitrosocamphane
un-irradiated

[27]
bornyl chloride

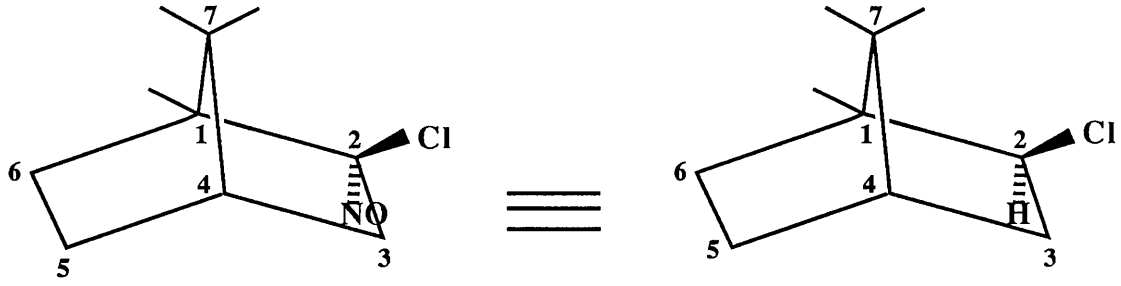

[26]
(+)-2-chloro-2-nitrosocamphane irradiated

[28]
isobornyl chloride

Much later studies on the photochemistry of **[19]**, carried out by Majeed and Porte,[87] showed that these configurations in fact are correct.

Davidson and Mitchell[88] *also* studied the Cotton effect in the geminal chloro-nitroso derivatives, (+)-10-bromo-2-chloro-2-nitroso-camphane **[14]**, (-)-2-chloro-2-nitrosocamphane **[19]**, and (-)-2-chloro-2-nitrosofenchane **[29]**. They also included 2-chloro-2-nitroso-norbornane, **[30]**, in their studies and found that its solutions are optically inactive.

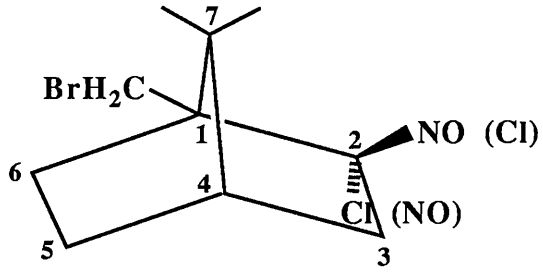

[14]

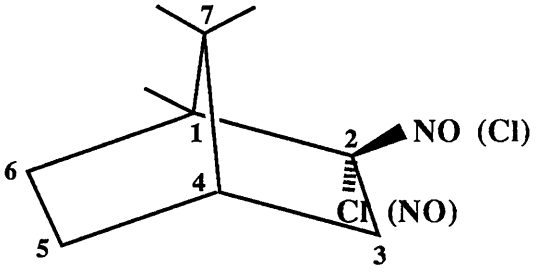

[19]

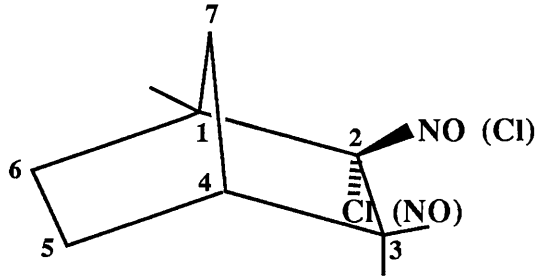

[29]

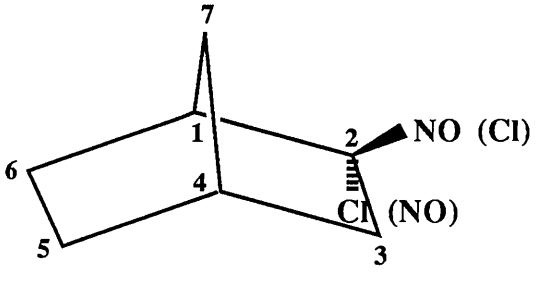

[30]

Their work confirmed Veitch's earlier circular dichroism and rotatory dispersion measurements[83] concerning compound **[14]** but, without giving any justification, they inverted the configuration at the >C(NO)(Cl) residue. Furthermore, they found that solutions of compounds **[19]** and **[29]** undergo photomutarotation on irradiation with red-light and they also showed that the sign of the Cotton effect in solutions of compound **[19]** is opposite to the signs found in compounds **[14]** and **[29]**. They further suggested that photomutarotation at the >C(NO)(Cl) residues can only take place if the NO group is in a sterically congested site of the molecule, *eg.* on the same side as the bridging $>C(CH_3)_2$ groups, in the camphane derivatives. However, further work by the same authors appears to disapprove this reasoning. Mitchell and Davidson finally suggested that the following intramolecular mechanism is involved in the photomutarotation of **[19]**, reaction **(13)**.

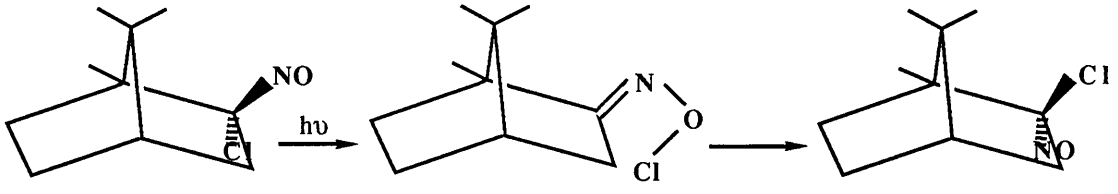

[19] **[31]** **[26]**

reaction **(13)**

When the molecule absorbs red-light, the NO group is activated, thereby increases in size, and is forced nearer to the chlorine atom. At the same time as the geometry is distorted, the C-N bond becomes double in character as the NO group is closely bound by the $>C(CH_3)_2$ bridge. The C-Cl bond breaks and the chlorine atom then bonds with the oxygen atom to form the postulated nitrosyl chloride intermediate **[31]**. This latter, since the excited NO chromophore is larger than the chlorine atom, isomerises to the axially NO-substituted isomer which is now more

stable. Finally, deactivation of the molecule takes place by degradation of its excess of energy to heat.

With the techniques then available to them, these early workers could not possibly have detected radicals formed in the photochemical reactions and, furthermore, they were unable to use their circular dichroism measurements to assign relative configurations at the >C(2)NOCl residues in their compounds. Veitch, for example, wrote the structure of (+)-10-bromo-2-chloro-2-nitrosocamphane as **[32]** whereas Davidson assigned structure **[33]** to it. Both, however, agreed on the configuration at C(2) for (-)-2-chloro-2-nitrosocamphane **[19]**. Nevertheless, none of these early workers was able to assign molecular configurations in their compounds, with any certainty, and as a result some of this earlier work is confusing and inconsistent.

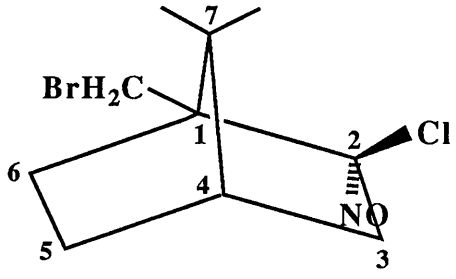

[32]

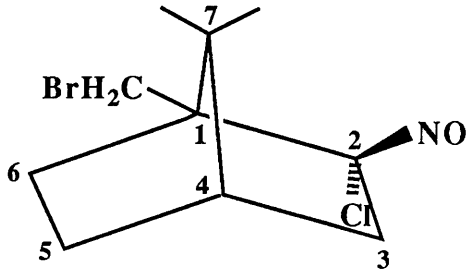

[33]

It was not until 1961 that the Glasgow X-ray crystallographers showed that[89] in the crystal structure of (+)-2-chloro-2-nitroso-10-bromocamphane, the un-irradiated isomer, the molecular structure and configuration are as in structure **[32]**, the structure chosen by chance by Veitch, and therefore the chlorine atom is on the same side as the bridging $>C(CH_3)_2$ group.

Majeed, Porte and co-workers carried out careful spectroscopic studies of the action of red light on solid (+)-10-bromo-2-chloro-2-nitrosonorbornane **[32]**[90] and on solid (-)-2-chloro-2-nitrosocamphane **[19]**.[87] These involved very detailed applications of nuclear magnetic resonance spectroscopy and electron paramagnetic resonance spectroscopy, and several important points emerged from their work. First, in the case of the geminal *chloronitroso* diterpene derivatives, ^{1}H n.m.r. signals arising from a neighbouring hydrogen nucleus cis- to the chlorine atom appear at lower applied fields, i.e. larger δ values, than signals from hydrogen atoms cis- to NO. On the other hand, in the case of the corresponding geminal *chloronitro* derivatives, it is the signals arising from the hydrogen atom cis- to NO_2 group which appear at lower applied field, i.e. larger δ value. Hence, careful analyses of the, complicated, ^{1}H n.m.r. spectra of these diterpenes derivatives enable the configurations at the chiral carbon centers to be determined and, furthermore, also signify when inversion of configuration takes place during the course of chemical reaction. These workers showed that the configurations at the >C(NO)(Cl) residues of solid (+)-10-bromo-2-chloro-2-nitrosocamphane and of solid (-)-2-chloro-2-nitrosocamphane are as in structures **[32]** and **[19]** respectively, and they also showed that the descriptions given by the earlier workers on the red-photolysis of these compounds are grossly oversimplified. They unravelled the mechanisms involved in the photomutarotation reaction of **[19]**, and they identified some very interesting rearrangement reactions that take place when the solids are red irradiated. They showed that in the case of (-)-2-chloro-2-

nitroso-camphane **[19]**, all the information obtained from the solution Cotton effect studies,[85,86,88] and from the analyses of the paramagnetic and diamagnetic products obtained from the irradiated solid, could be pieced together to construct mechanisms for the photochemical reactions that take place when **[19]** is irradiated with red light.[87] The sequence of reactions is summarized in the following pages, **Schemes 1.3-1.9**. Irradiation of the NO group in **[19]** causes an $^1\pi^* \longleftarrow {}^1n$ (nitrogen) transition to take place and the intermediate biradical **[34]** is formed, **Scheme 1.3**. This biradical either rearranges, as in Davidson's reaction **(13)**, to the chloro oxime **[31]**, or undergoes homolysis of its C(2)-N bond to give a radical intermediate **[35]** and nitric oxide. At this stage, formation of **[31]** strongly predominates, and it can then undergo reversible rearrangement back to the original (-)-2-chloro-2-nitrosocamphane **[19]** or its (+)-isomer **[26]**. Compound **[31]**, and possibly also the photochemically excited intermediate **[34]**, can also undergo Beckmann-like rearrangement to form an acyl-nitroxide **[36]**, as shown in **Scheme 1.4**, the reaction, in the case of **[31]**, being triggered by the inductive effect of the chlorine atom. It should be noted that the radical **[36]** has also been obtained by de Boer *et al.* by oxidation of the corresponding hydroxamic acid formed in similar Beckmann-like rearrangements when **[19]** reacts with aluminium chloride, or with $(CH_3)_2AlCl$ or $(CH_3)_3Al$.[91,92]

Other nitroxide radicals **[37]** and **[38]** are observed much later on in the irradiation, and it is believed that they are formed, as shown in **Scheme 1.7** by subsequent red irradiation of the mutarotated product **[26]** formed in reaction **(13)**. $^1\pi^* \longleftarrow {}^1n$ excitation of **[26]** causes

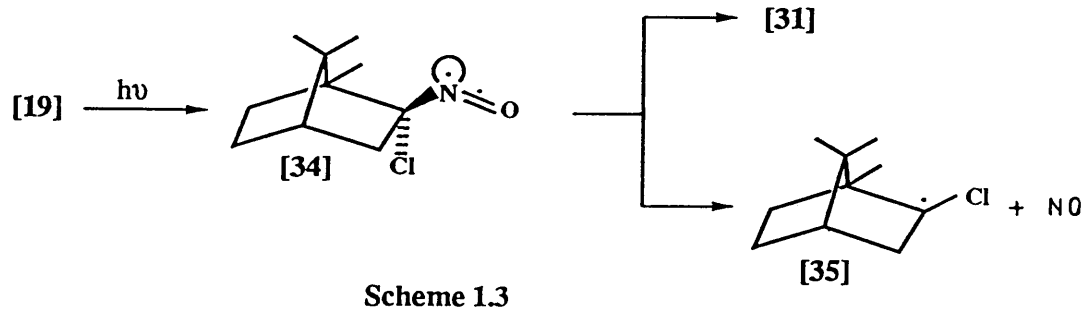

Scheme 1.3

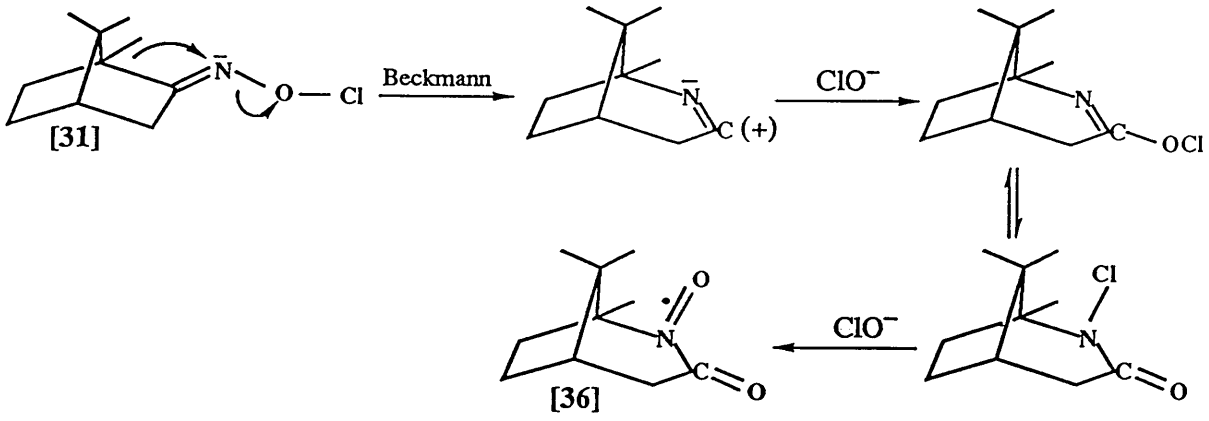

Scheme 1.4

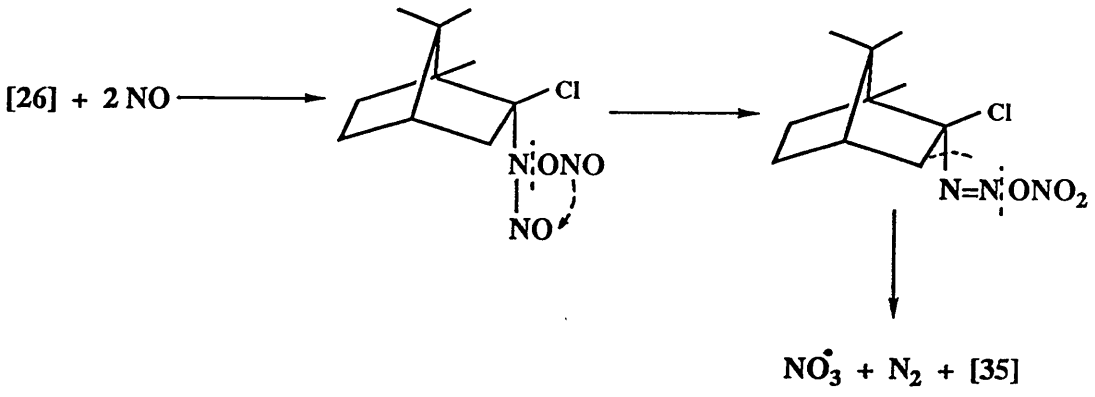

Scheme 1.5

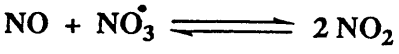

Scheme 1.6

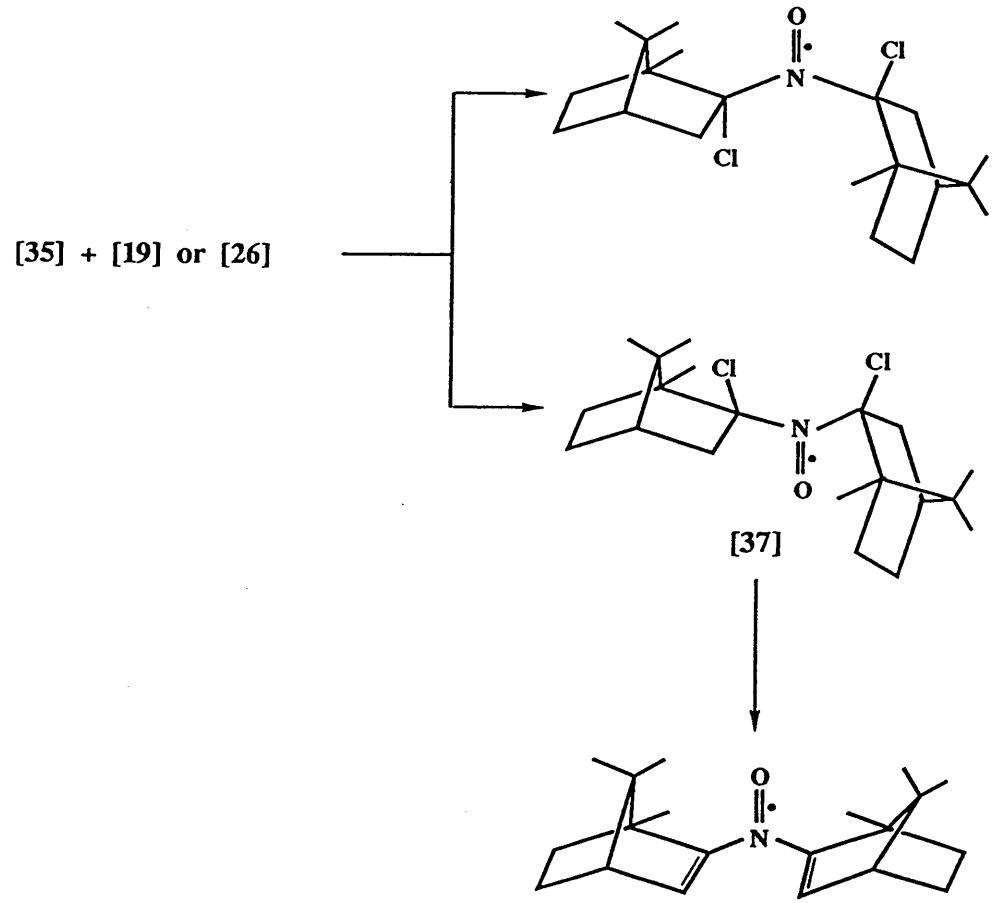

Scheme 1.7

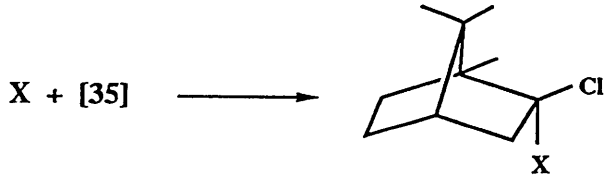

[26] X = NO
[39] X = NO_2
[40] X = ONO_2
[41] X = ONO

Scheme 1.8

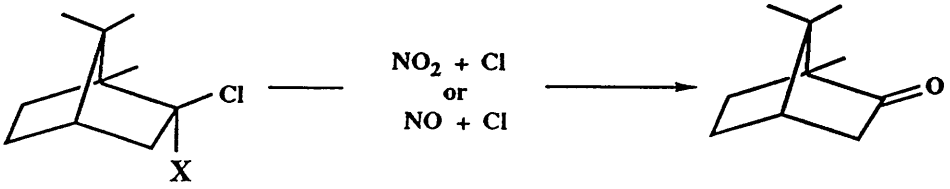

[40] X = ONO_2
[41] X = ONO

[42]

Scheme 1.9

homolysis of its C(2)-N bond, forming more of the radical **[35]** and nitric oxide, which then reacts with neighbouring molecules of the parent nitroso compounds, providing a third source of the radical **[35]** , an $NO_3^{\bullet}$ radical, and nitrogen as shown in **Scheme 1.5.**[16,17,19,22,79] The radical **[35]** is also scavenged by $NO_3^{\bullet}$ and $NO_2^{\bullet}$ radicals, in the sterically less-hindered *endo*-position to give the nitro-, nitrato- and nitrito- derivatives of camphane, **Scheme 1.8**, in which the configuration at C(2) is now inverted when compared with the original 2-chloro-2-nitrosocamphane, **[19]**.

The large amount of camphor **[42]**, **Scheme 1.9**, can be accounted for if the nitrato- and the nitrito-derivatives are unstable and decompose with loss of $ClNO_2$ and ClNO respectively. The camphor oxime detected in smaller amount may come directly from the geometrically similar chloro oxime **[31]**, or from the photoexcited intermediate **[34]**, when the photolysis has built up to produce a reasonable concentration of hydrogen atoms *via* the reactions shown in **Scheme 1.7**.

The early rotatory dispersion measurements[83,84,88] and the later magnetic resonance studies[87,90] all show quite clearly that the configurations at C(2) in compounds **[19]** and **[32]** significantly affect the first stages of these photochemical changes. Thus, in compound **[19]**, photomutarotation first takes place and is then followed by slower photochemical reactions, whereas in **[32]**, photolysis takes place *without photomutarotation* because the NO group is not confined by the $>C(CH_3)_2$ bridge.

Detailed examination of solid state red-photolysis reactions of geminal chloronitroso terpene derivatives appear to have been carried out only for (+)-10-bromo-2-chloro-2-nitrosocamphane **[32]**,[90] and for (-)-2-chloro-2-nitrosocamphane **[19]**,[87] although some preliminary studies have been carried out on *solutions* of 2-chloro-2-nitrosonorbornane **[30]**.[88] Synthetic **[30]** is racemic, so Davidson could not carry out Cotton effect and photomutarotation studies of *its solutions*. However, he found that this compound is essentially dimeric in ethanol and is essentially monomeric in benzene. He also noticed that when a potassium acetate-buffered ethanolic solution of **[30]** was irradiated with red light, hydrochloric acid, norcamphor and acetaldehyde oxime, $CH_3CH{=}NOH$, were produced, but at the time he carried out his work, it was not possible to study the red-photolysis of this substance in greater detail. The modern spectroscopic methods used by Majeed, Porte and their colleagues,[87,90] particularly the application of magnetic resonance techniques, should be able to unravel the structures, the configurations at the chiral >C(2)NOCl centres, and the details of the photochemical reactions of both the monomeric and the dimeric forms of this compound. For these reasons, and with these aims in mind, very detailed spectroscopic studies of 2-chloro-2-nitrosonorbornane **[30]** were carried out, with the results and the conclusions that are described in Chapter 2.

CHAPTER TWO

THE ACTION OF RED LIGHT ON 2-CHLORO-2-NITROSONORBORNANE

2.1 Experimental

Preparation of 2-chloro-2-nitrosonorbornane, its infra red, and its electron impact mass spectra

2-Chloro-2-nitrosonorbornane, i.e. 2-chloro-2-nitrosobicyclo-[2.2.1] heptane **[30]** is a white solid with a blue-green cast on its surface, and it melts at about 44° C to give a deep-blue liquid. It is very volatile and if it is left on a watch glass, it sublimes and disappears within a few hours. It dissolves in all common solvents to give a deep-blue solution which, as expected, is racemic. The vapour is lachrymatory.

The sample of 2-chloro-2-nitrosonorbornane used in this work was kindly donated by Dr J. S. Davidson who prepared it by allowing chlorine to react with the oxime **[44]** of synthetic norbornanone **[43]**. The synthesis involves the six stages shown below, in **Scheme 2.1**.[88]

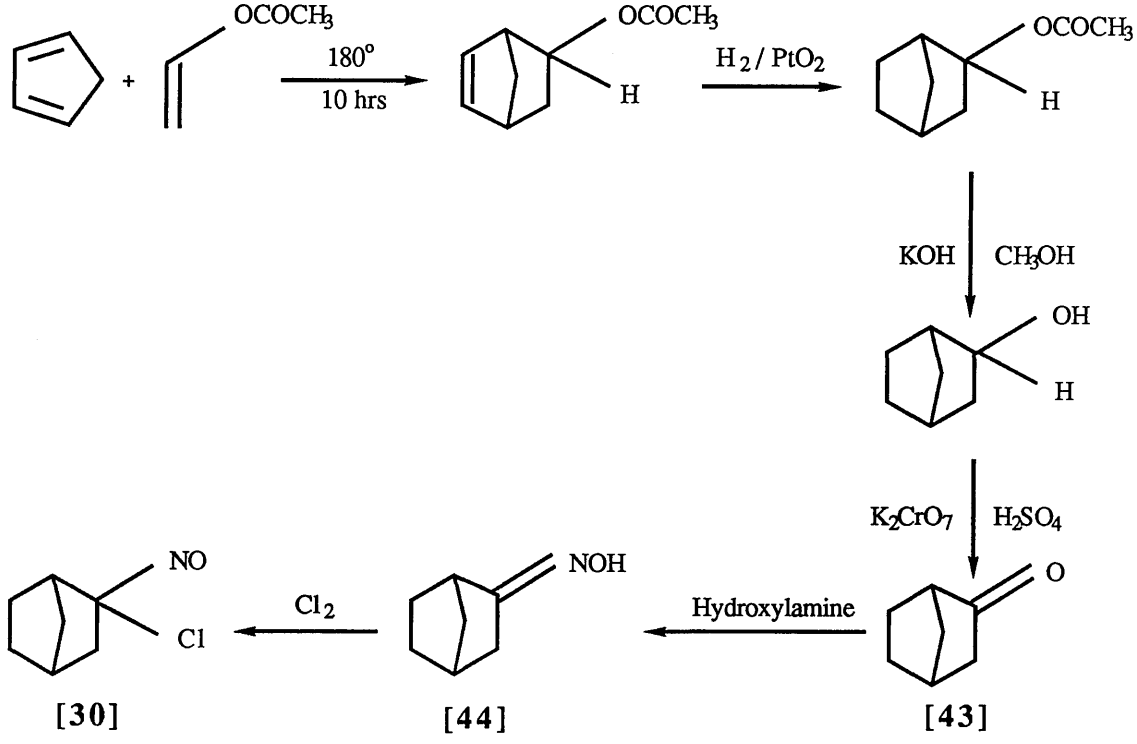

Scheme 2.1

The microanalysis data for this sample, listed in **Table 2.1**, are consistent with the structure $C_7H_{10}ClNO$ of 2-chloro-2-nitroso-norbornane.

The infra red spectrum of the solid is shown in **Figure 2.1**. The absorption peak in the region 1580-1570 cm^{-1}, characteristic[29,93] of the N=O stretching vibration of a C-nitroso monomer is absent, and furthermore, the vibrations expected from a cis-nitroso dimer in the regions 1420-1330 cm^{-1} and 1344-1323 cm^{-1} are also absent.[94,95] However, absorption at 1182 cm^{-1} that is present in the infra red spectrum,[94,95] implies that in the solid, 2-chloro-2-nitroso-norbornane is a trans-nitroso-dimer, as shown below. Detailed assignments of the vibrational frequencies in the infra red spectrum of 2-chloro-2-nitroso-norbornane are listed in **Table 2.2.**

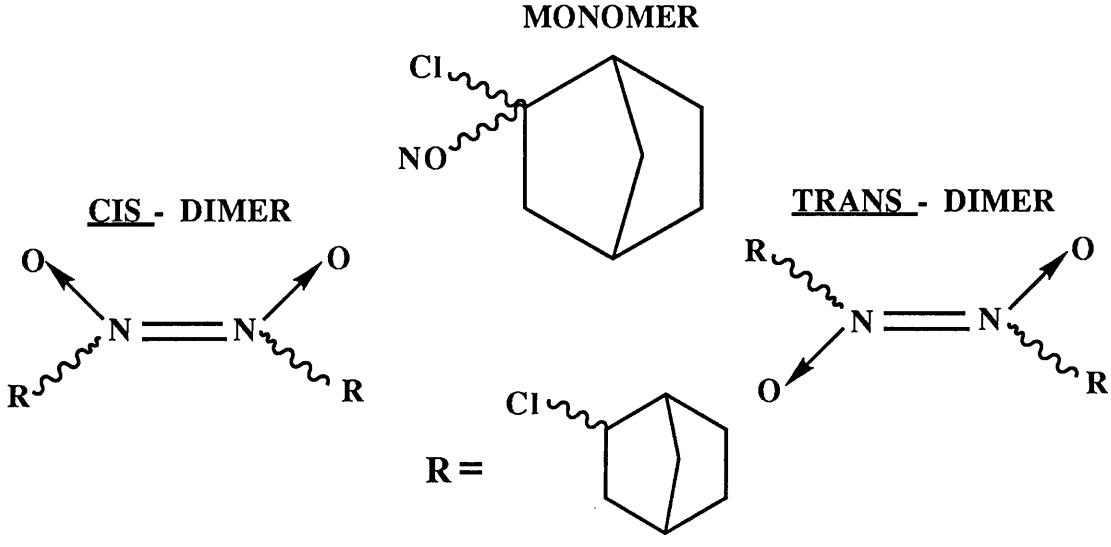

The heaviest fragments observed in the electron impact mass spectrum of the solid 2-chloro-2-nitrosonorbornane are at m/z=131 and 129. The parent peak for $C_7H_{10}ClNO$ is not observed since the NO group is cleaved in the mass spectrometer. A more complete description of the mass spectrum cracking pattern is given in detail, in Appendix 2, 2'.1'.

Table 2.1

Microanalysis data of 2-chloro-2-nitrosonorbornane

Element	% Composition [Found]	% Composition [Expected for $C_7H_{10}ClNO$]
C	52.59	52.64
H	6.34	6.32
Cl	22.28	22.25
N	8.73	8.77
O	10.06	10.00

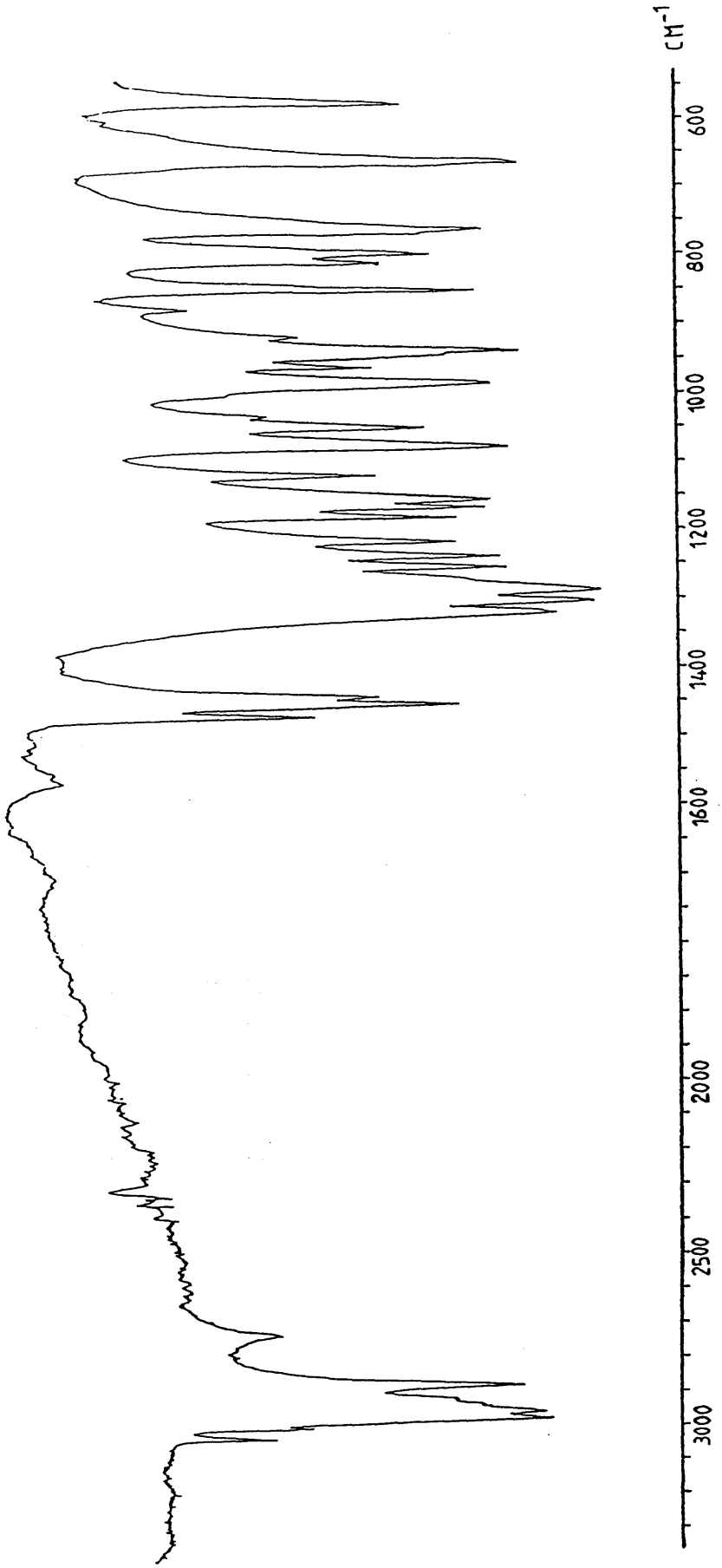

Figure 2.1 The infra red spectrum of solid 2-chloro-2-nitrosonorbornane, recorded in a KBr disc

Table 2.2

Infra red assignments for solid 2-chloro-2-nitrosonorbornane

Band/cm^{-1}	Assignment
3040 3001	C-H stretching vibrations of C(1)-H and C(4)-H
2979 2958 2938 2936	The antisymmetric stretching modes of $C(3)H_2$, $C(5)H_2$, $C(6)H_2$ and $C(7)H_2$
2925 2920 2880 2738	The symmetric stretching modes of $C(3)H_2$, $C(5)H_2$, $C(6)H_2$ and $C(7)H_2$
1472 1452 1442	The deformation vibrations of $C(3)H_2$, $C(5)H_2$, $C(6)H_2$ and $C(7)H_2$
1320 1302 1288	The wag vibrations of $C(3)H_2$, $C(5)H_2$, $C(6)H_2$ and $C(7)H_2$
1182	The N-O stretching vibration of a *trans*-dimer
800	The C-N-O residue skeletal bending mode of the dimer
763	The C-Cl stretching vibration

2.2 Nuclear magnetic resonance studies of 2-chloro-2-nitrosonorbornane

2.2.1 $CDCl_3$ solutions of 2-chloro-2-nitrosonorbornane

2-Chloro-2-nitrosonorbornane **[30]** dissolves in $CDCl_3$ to give a deep-blue solution whose $^{13}C-\{^1H\}$, and $^{13}C-\{^1H\}$ 90° and 135° Distortionless Enhancement by Polarization Transfer spectra (D.E.P.T.) are shown in **Figures 2.2A, 2.2B** and **2.2C** respectively. These spectra enable the resonances from C(1), C(2), C(3), C(4) and C(7) to be assigned, but they do not distinguish between signals from C(5) and C(6). The assignments from **Figure 2.2** are confirmed by the $^{13}C-^1H$ two dimensional HETeronuclear COrrelated spectrum (HETCOR) shown in **Figure 2.3**. **Figure 2.3** also enables the chemical shifts of 1-H, 3-H_{endo} and 4-H in the 200.132 MHz spectrum, shown in **Figure 2.4**, to be assigned. However, because of extensive overlapping in this spectrum, no other ^1H resonances could be unambiguously identified at this stage, and for this reason the $^1H-^1H$ two dimensional COrrelated SpectroscopY spectrum (COSY), shown in **Figure 2.5**, was recorded. By judiciously eliminating ambiguities and systematically using all the high-resolution spectra, shown in **Figures 2.2-2.5**, all ^{13}C chemical shifts, ^1H chemical shifts and $^1H-^1H$ coupling constants were eventually unambiguously assigned. These spin Hamiltonian parameters are listed in **Table 2.2**, and the calculated 200.132 MHz ^1H n.m.r. spectrum obtained by using them, is shown in **Figure 2.6**. The observed ^1H n.m.r. spectrum, **Figure 2.4** is compared with the calculated ^1H n.m.r. spectrum, **Figure 2.6**, in **Figure 2.7.**

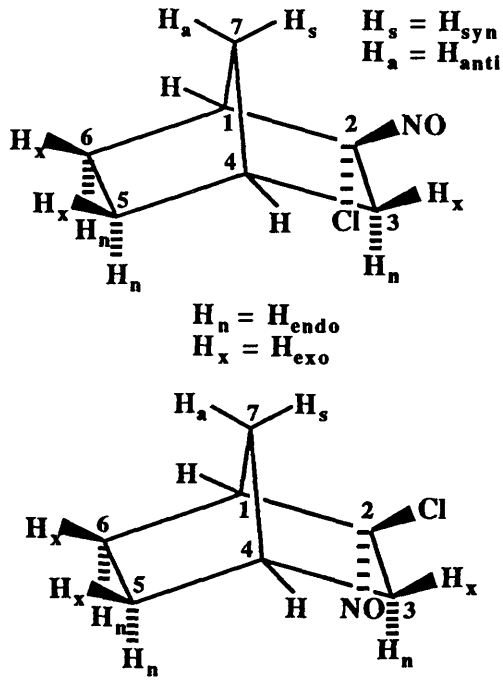

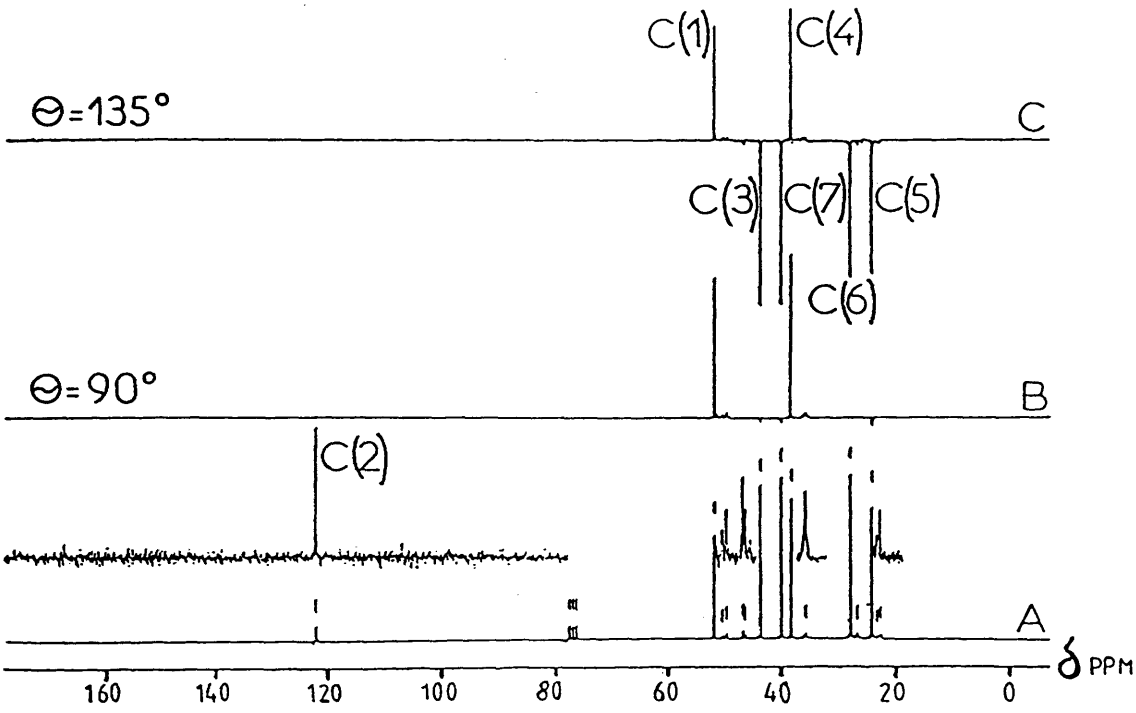

Figure 2.2 The $^{13}C-\{^{1}H\}$ n.m.r. spectrum, {**A**}, and corresponding $\Theta = 90^{o}$, {**B**}, and $\Theta = 135^{o}$, {**C**}, D.E.P.T. spectra of 2-chloro-2-nitrosonorbornane in $CDCl_3$ solution

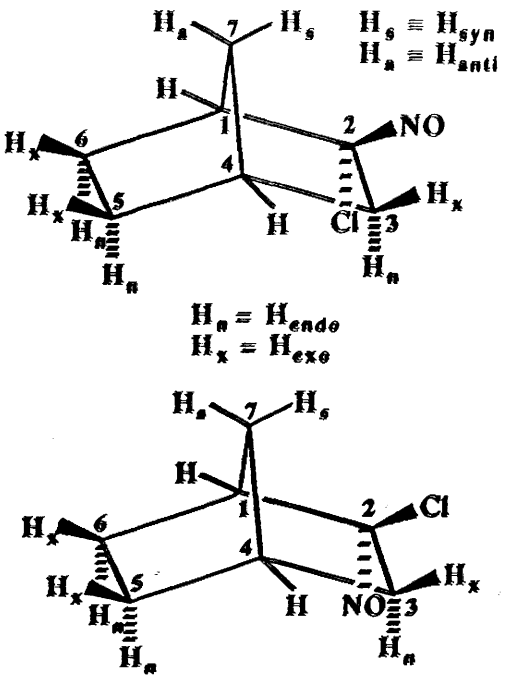

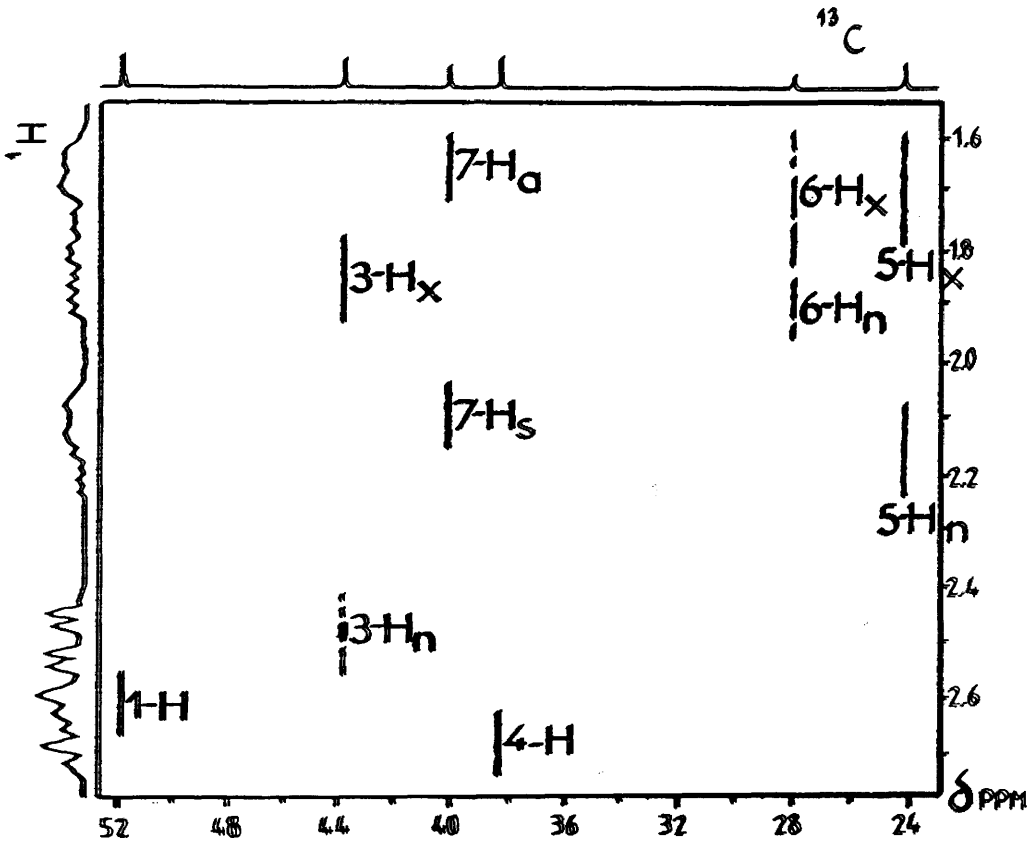

Figure 2.3 The ^{13}C- ^{1}H two dimensional correlation spectrum of 2-chloro-2-nitrosonorbornane in $CDCl_3$ sloution

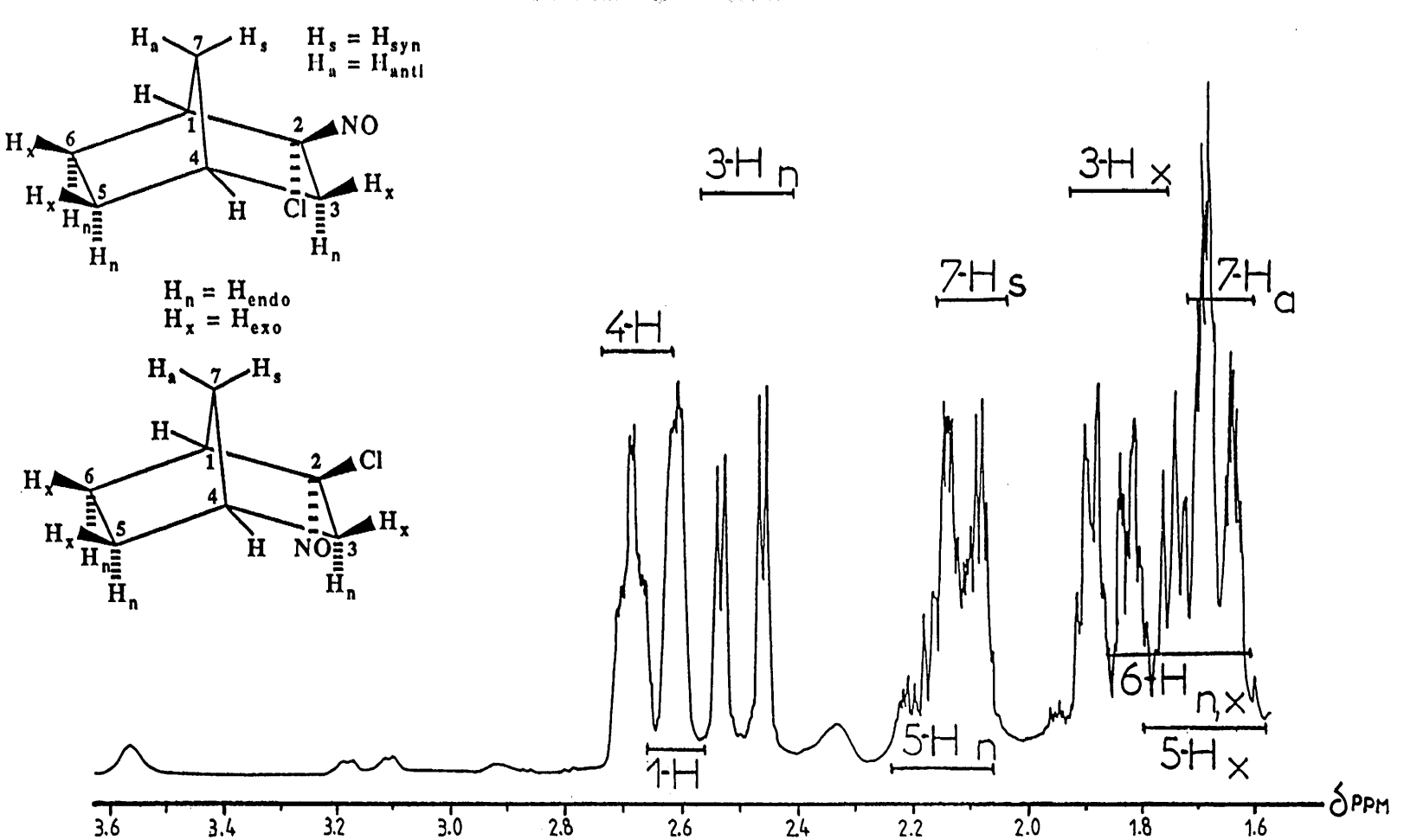

Figure 2.4 The 200.132 MHz ^1H n.m.r. spectrum of 2-chloro-2-nitrosonorbornane in $CDCl_3$ solution

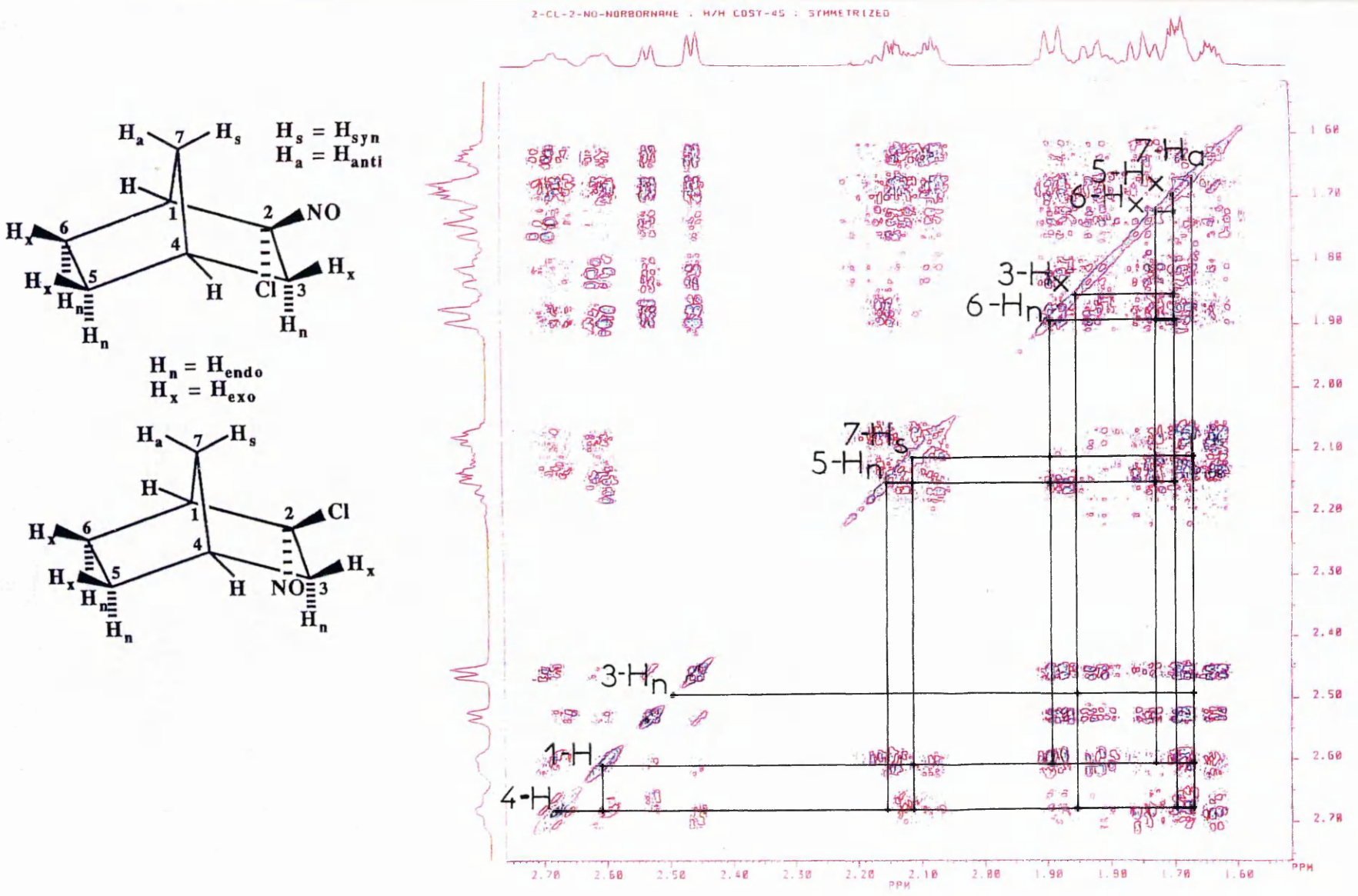

Figure 2.5 The ^1H-^1H two dimensional COSY spectrum of 2-chloro-2-nitroso-norbornane in $CDCl_3$ solution

Table 2.2

^{1}H and ^{13}C n.m.r. chemical shifts, δ_H and δ_C, and ^{1}H-^{1}H coupling constants ($J_{H,H}$) for 2-chloro-2-nitrosonorbornane in $CDCl_3$

δ_H(ppm)($CDCl_3$)

1-H	3-H_{endo}	3-H_{exo}	4-H	5-H_{endo}
2.602	2.490	1.849	2.678	2.150
5-H_{exo}	6-H_{endo}	6-H_{exo}	7-H_{syn}	7-H_{anti}
1.697	1.890	1.720	2.113	1.665

δ_C(ppm)($CDCl_3$)

C(1)	C(2)	C(3)	C(4)	C(5)	C(6)	C(7)
51.80	122.10	43.74	38.35	24.17	28.33	40.06

$J_{H,H}$/Hz

1-H,4-H	1-H,6-H_{exo}	1-H,6-H_{endo}	1-H,7-H_s
2.0	4.3	1.5	2.0
1-H,7-H_a	3-H_{exo},3-H_{endo}	3-H_{exo},4-H	3-H_{exo},5-H_{exo}
2.0	14.0	4.3	2.0
3-H_{endo},4-H	3-H_{endo},7-H_a	4-H,5-H_{exo}	4-H,5-H_{endo}
0.0	2.8	4.3	1.5
4-H,7-H_s	4-H,7-H_a	5-H_{exo},5-H_{endo}	5-H_{exo},6-H_{exo}
2.0	2.0	10.5	9.1
5-H_{exo},6-H_{endo}	5-H_{endo},6-H_{exo}	5-H_{endo},6-H_{endo}	5-H_{endo},7-H_s
4.0	4.0	9.1	2.6
6-H_{exo},6-H_{endo}	6-H_{endo},7-H_s	7-H_s,7-H_a	
10.5	2.6	10.0	

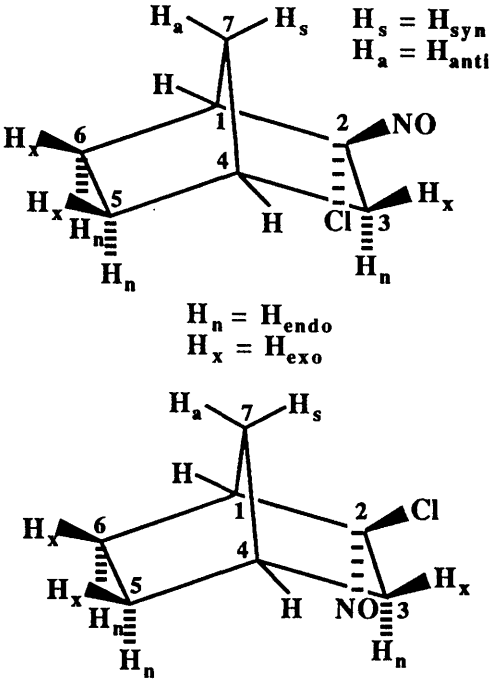

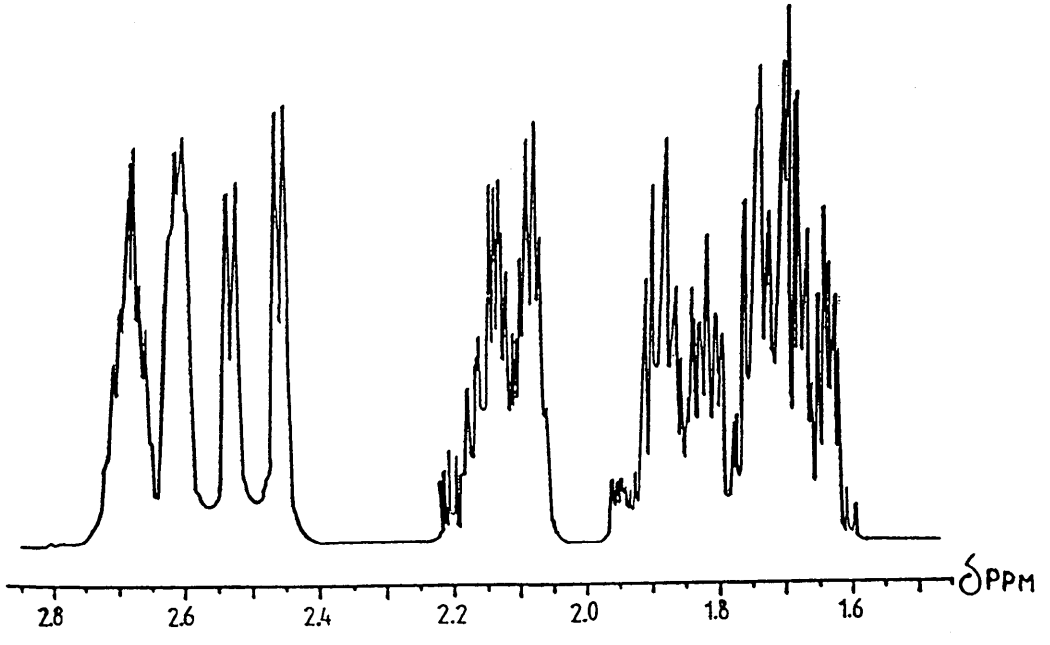

Figure 2.6 The calculated 200.132 MHz ^{1}H n.m.r. spectrum of 2-chloro-2-nitrososonorbornane

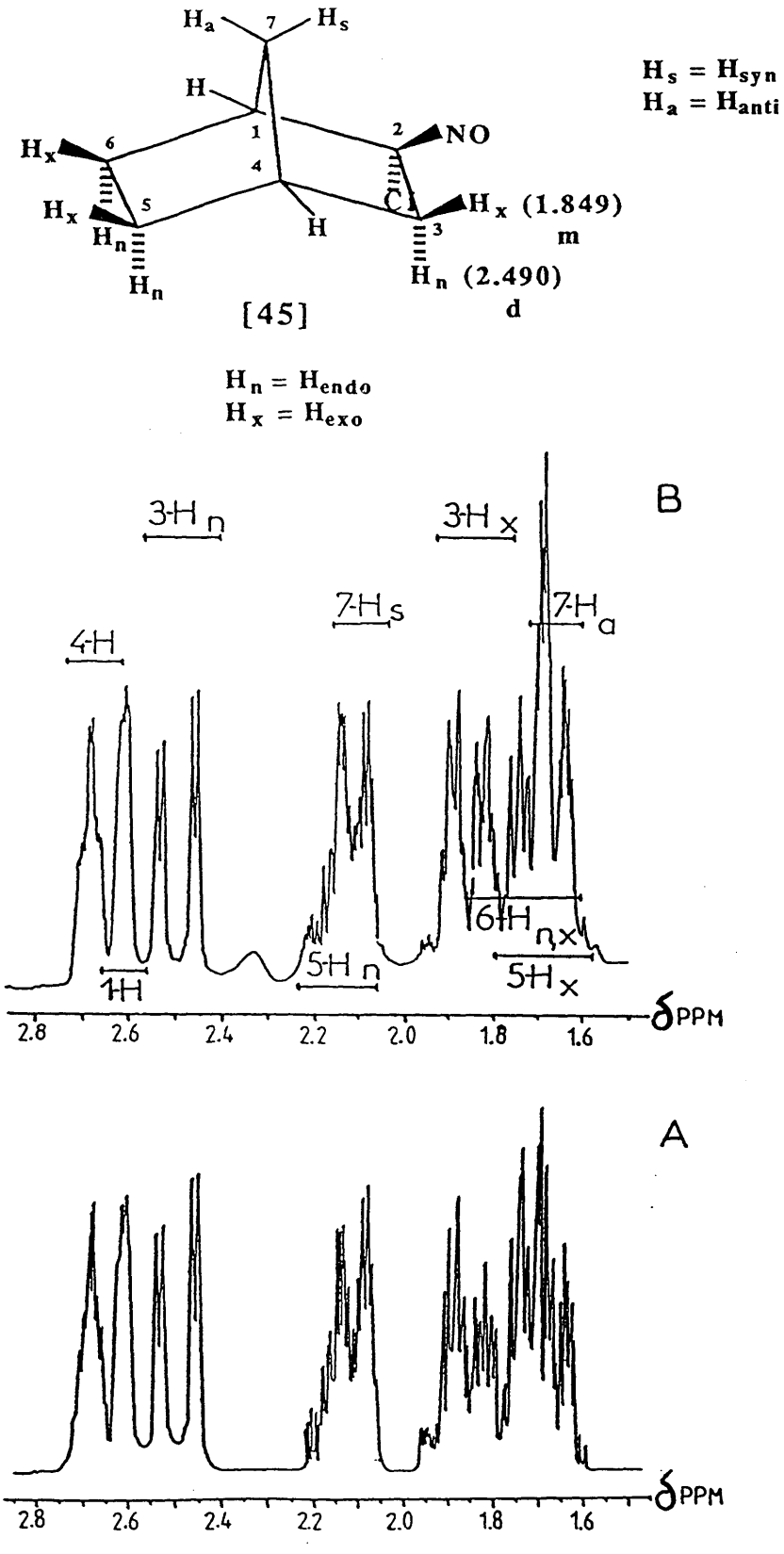

Figure 2.7 The calculated, {A}, and the observed, {B}, 200.132 MHz ^{1}H n.m.r. spectra of 2-chloro-2-nitrosonorbornane

Figures 2.4, 2.6 and **2.7**, the data listed in **Table 2.2** and the infra red spectrum of the solution, shown in **Figure 2.8**, establish that the major species present in $CDCl_3$ solution is the monomeric form of 2-chloro-2-nitrosonorbornane. Furthermore, ^1H n.m.r. signals of 3-H_{endo} lie at lower applied field than the signals from 3-H_{exo}. Hence, 3-H_{endo} is *cis* to the chlorine atom,[87,90] and the structure of the monomer is therefore established as that shown in **[45]**. The NO residue on C(2) is on the same side as the bridging >C(7)H_2 residue. The configuration at C(2) is the same as in 2-chloro-2-nitrosocamphane **[19]** and is opposite to the corresponding configuration in 2-chloro-2-nitroso-10-bromo-camphane **[32]**.[87,88,90]

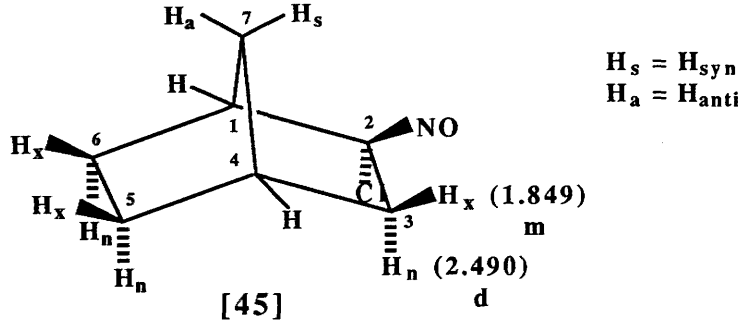

[45]

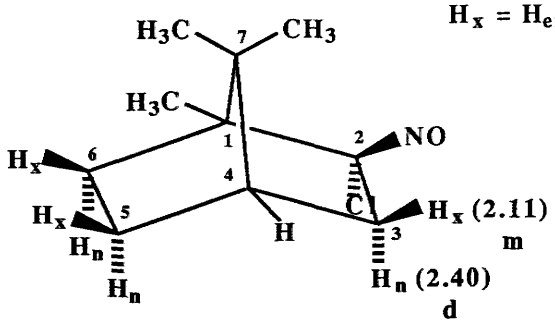

[19]

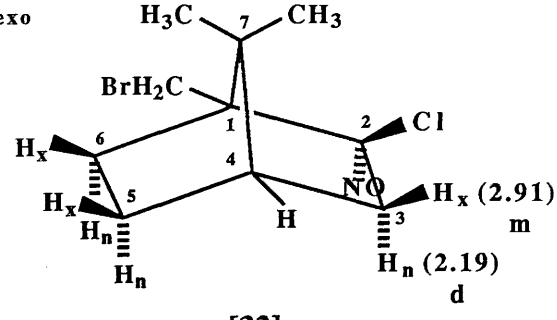

[32]

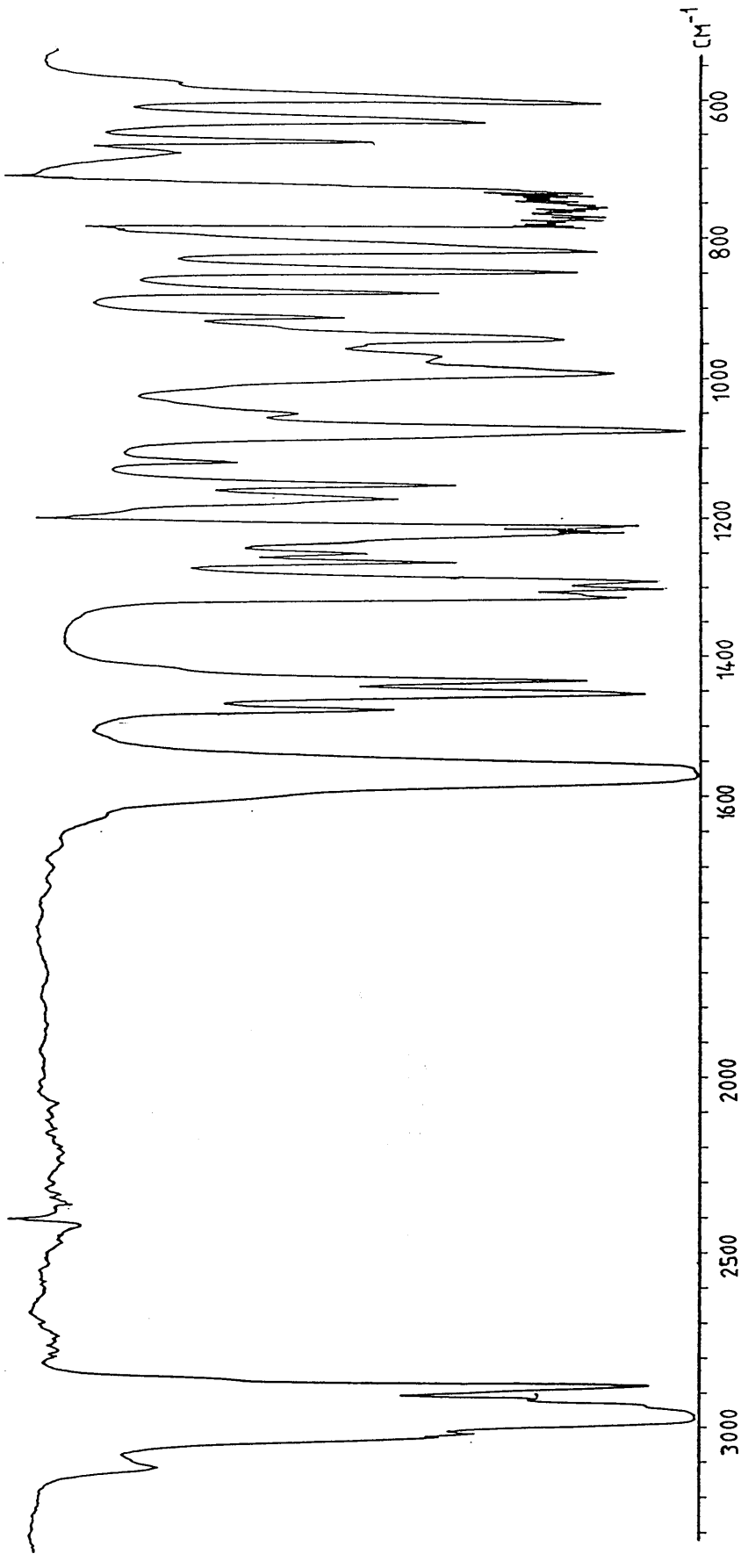

Figure 2.8 The infra red spectrum of a solution of 2-chloro-2-nitrosonorbornane in $CHCl_3$

^{1}H n.m.r. chemical shifts
^{13}C *n.m.r. chemical shifts*

$H_n = H_{endo}$
$H_x = H_{exo}$
$H_s = H_{syn}$
$H_a = H_{anti}$

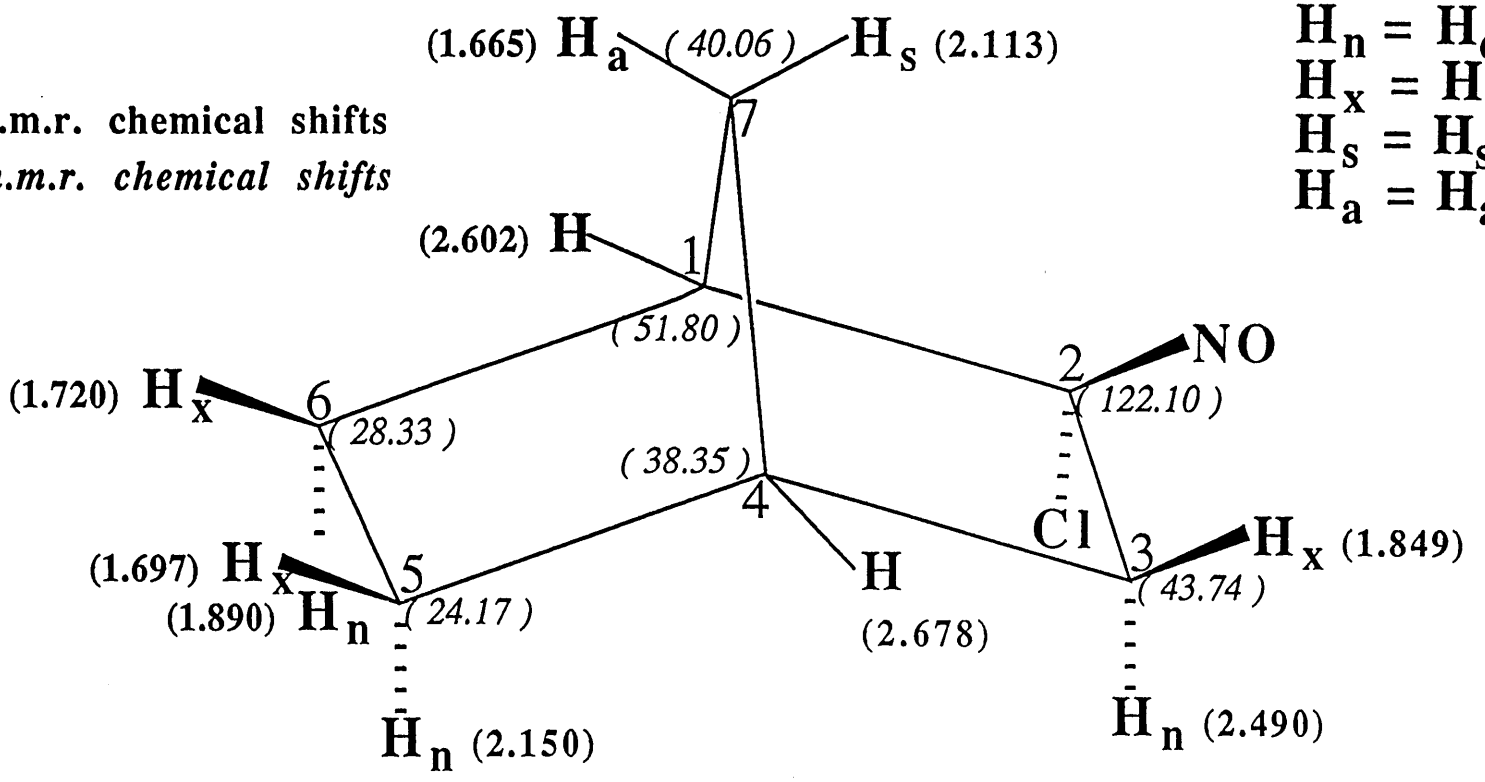

[45]

Figures 2.2A and **2.4** show that in $CDCl_3$ solutions of 2-chloro-2-nitrosonorbornane, the dominant species is the monomeric form. However, they also reveal the presence of small amounts of a second species which gives rise to additional broadened ^1H signals in **Figure 2.4** and extra very weak, ^{13}C signals in Figure **2.2A**. They are both shown in **Figure 2.9**. These signals are believed to arise from the diastereoisomers of the dimeric form **[46]**, and their ^{13}C chemical shifts are listed in **Table 2.3**.

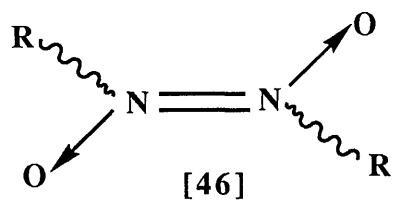

[46]

where **R** =

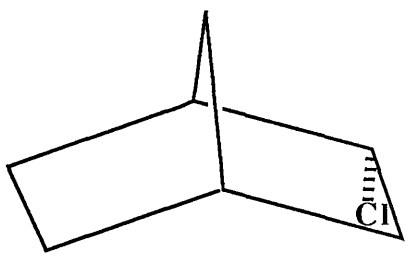

2.2.2 Solid 2-chloro-2-nitrosonorbornane

A 75.431 MHz ^{13}C Cross Polarization Magic Angle Spinning spectrum (^{13}C C.P.M.A.S.) of the solid is shown in **Figure 2.10A**. The chemical shifts of $^{13}C(1)$ and $^{13}C(3)$-$^{13}C(7)$ are very similar to the corresponding shifts in $CDCl_3$ solution, but the δ=122.10 ppm signal from the ^{13}C nucleus of the monomeric >C(2)NOCl residue in **[45]**, shown in **Figure 2.2A**, has moved upfield and has asymmetrically split into a doublet[94,95] at about δ=100 ppm in the solid, confirming that the solid is dimeric and exists in more than one form. The broadened multiplets arise from the coupling of the $^{13}C(2)$ nucleus to the ^{14}N and $^{35/37}Cl$ quadrupolar nuclei. Unlike magnetic dipole-dipole interactions, second order contributions arising from quadrupolar interactions do not completely average out on magic angle spinning in C.P.M.A.S. spectroscopy.

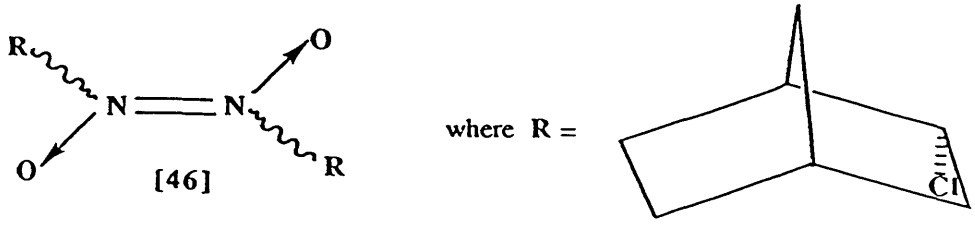

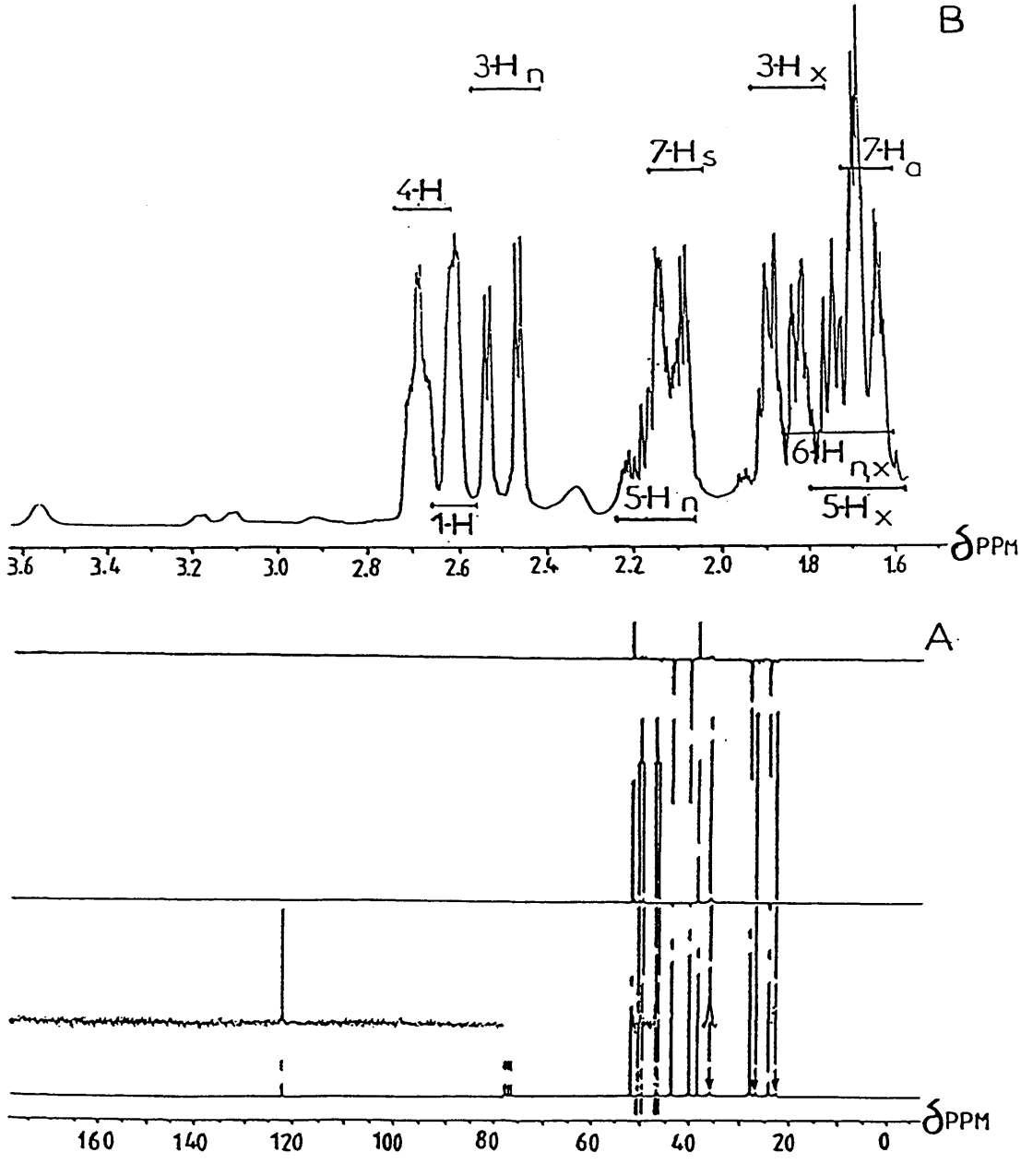

Figure 2.9 The ^{13}C-{^{1}H} n.m.r. spectrum, {A}, and the 200.132 MHz ^{1}H n.m.r. spectrum, {B}, of 2-chloro-2-nitrosonorbornane in $CDCl_3$ solution, at increased gain to show the weak signals from the dimeric form of the compound

Table 2.3

^{13}C n.m.r. chemical shifts of 2-chloro-2-nitrosonorbornane in $CDCl_3$ solution, showing the weak signals from the dimeric form of the compound

δ_C(ppm)($CDCl_3$)

C(1)		C(2)		C(3)	C(4)	C(5)	C(6)	C(7)
51.80	50.47	/	46.80	46.51	35.78	22.71	26.78	38.25

Table 2.4

^{13}C n.m.r. chemical shifts of solid 2-chloro-2-nitrosonorbornane

δ_C(ppm)

C(1)	C(2)		C(3)	C(4)	C(5)	C(6)	C(7)
50.429	104.364	98.019	47.479	36.767	24.235	26.925	39.22

^{13}C chemical shifts from the solid are listed in **Table 2.4** and when these data are combined with the observation that an absorption at 1182 cm^{-1} is present in the infra-red spectrum of the solid, and that absorptions at 1420 cm^{-1} and 1344-1323 cm^{-1} are absent, it now follows that the dimer in the solid has the *trans diazo - dioxide* form, shown in **[46]**.[29,96,97]

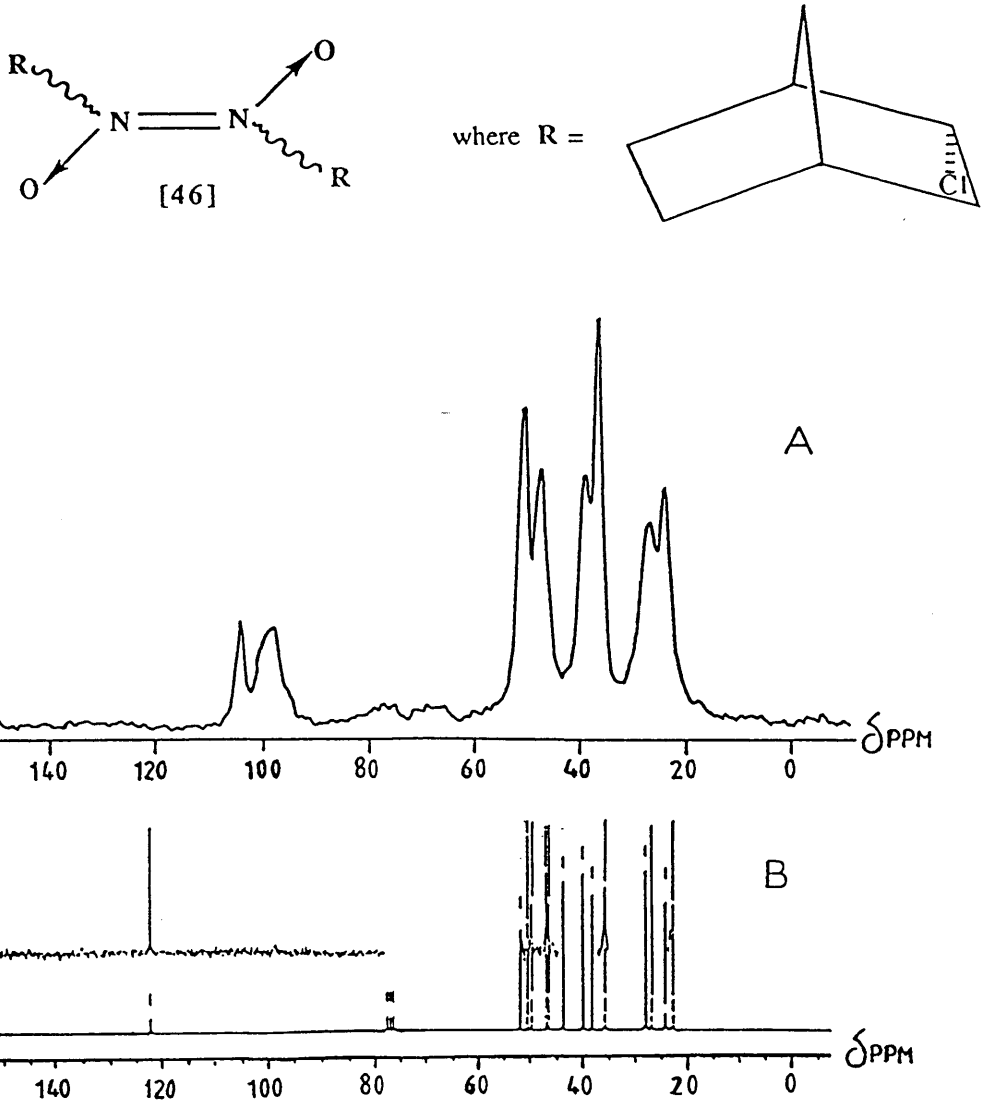

Figure 2.10 The ^{13}C C.P.M.A.S. spectrum, {A}, of solid 2-chloro-2-nitrosonorbornane, and the ^{13}C-{^{1}H} n.m.r. spectrum, {B}, of the dimer present in the $CDCl_3$ solution

The analysis of the ^{13}C C.P.M.A.S. spectrum, **Figure 2.10A**, establishes that in the *solid* structure, the dimer **[46]** shows only one set of $^{13}C(1)$,$^{13}C(3)$-$^{13}C(7)$ signals but pairs of weak ^{13}C signals are observed for both C(1) and C(3) in *solution*. It therefore follows that this structure possesses either a centre of symmetry or a 2-fold axis and it exists in diastereoisomeric forms dd, ll, dl and ld. In $CDCl_3$ solution, ^1H n.m.r. spectra from the monomers are sharp, whereas spectra from the dimer are broad. It therefore follows that in the equilibrium reaction, the monomer has a long life time and the dimer, **[46]**,

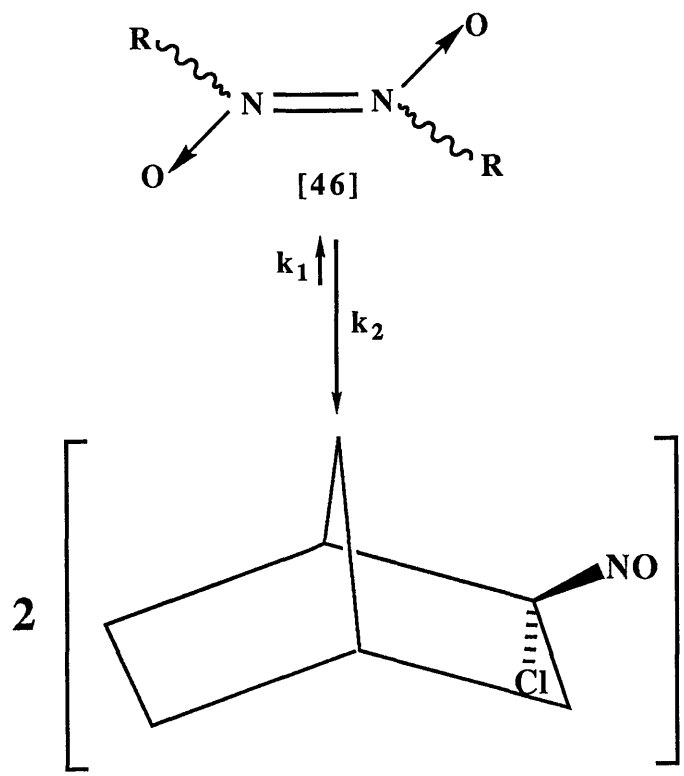

has a short life time on the n.m.r. time scale, i.e. $k_1 << k_2$. The intensities of the signals in **Figure 2.4** show that the equilibrium constant $K=k_1/k_2$ is of the order of 0.05±0.01.

A ^{13}C C.P.M.A.S. spectrum of solid 2-chloro-2-nitrosocamphane **[19]** is shown in **Figure 2.11A**, and its ^{13}C chemical shifts are listed in **Table 2.5**. This spectrum is quite different from the ^{13}C C.P.M.A.S. spectrum, shown in **Figure 2.10A**, of solid 2-chloro-2-nitroso-norbornane **[46]**. It is much more like the high resolution $^{13}C-\{^{1}H\}$ spectrum of its $CDCl_3$ solution,[87] **Figure 2.11B**, and it shows that the, almost spherically shaped, molecule of **[19]** is rapidly and randomly reorienting in the solid at room temperature.

Finally, a 30.405 MHz ^{15}N C.P.M.A.S. spectrum of the solid is shown in **Figure 2.12**. The nitrogen chemical shift of the nitroso group in the 2-chloro-2-nitrosonorbornane dimer is referenced to the nitrate signal in ammonium nitrate and is found at -67.232 ppm. The presence of a single ^{15}N peak confirms the earlier deductions that the dimer is either centrosymmetric or possesses a 2-fold axis of symmetry.

Table 2.5

^{13}C n.m.r. chemical shifts solid of 2-chloro-2-nitrosocamphane

δ_C(ppm)

C(1)	C(2)	C(3)	C(4)	C(5)
55.642	120.197	40.605	47.347	26.977
C(6)	C(7)	C(8)/C(9)	C(9)/C(8)	C(10)
29.728	51.932	21.235	20.066	13.148

^{13}C n.m.r. chemical shifts of 2-chloro-2-nitrosocamphane in $CDCl_3$ solution

δ_C(ppm)($CDCl_3$)

C(1)	C(2)	C(3)	C(4)	C(5)
55.47	145.04	40.31	46.75	26.45
C(6)	C(7)	C(8)/C(9)	C(9)/C(8)	C(10)
29.46	51.47	20.73	19.40	12.68

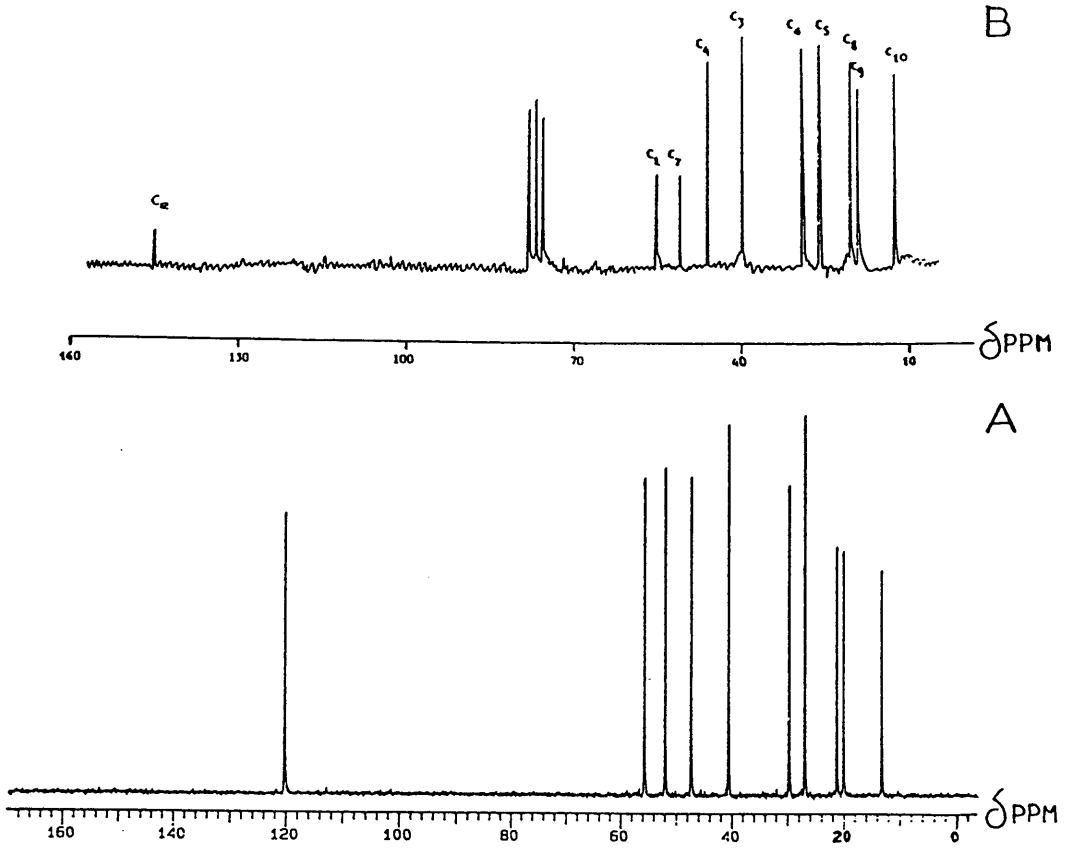

Figure 2.11 The ^{13}C C.P.M.A.S. spectrum, {**A**}, of solid 2-chloro-2-nitrosocamphane, and the ^{13}C-{^{1}H} n.m.r. spectrum, {**B**}, of its $CDCl_3$ solution

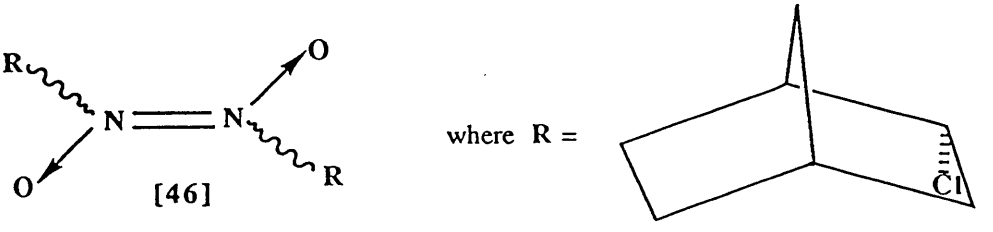

[46]

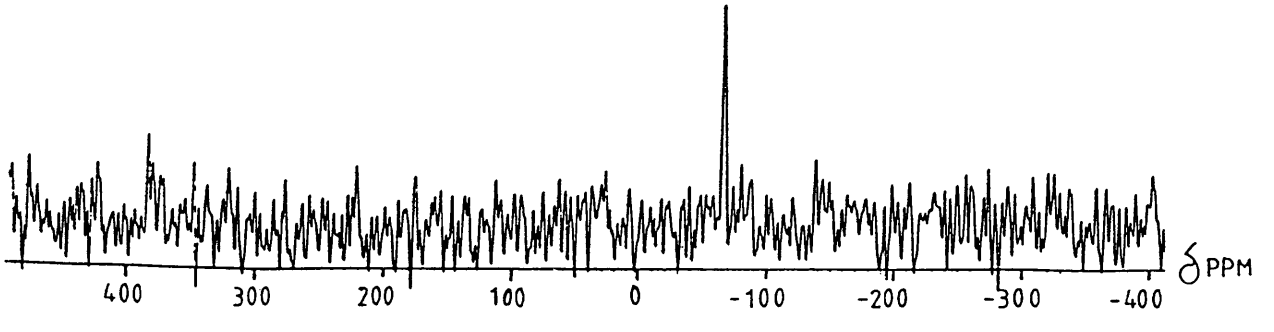

Figure 2.12 The ^{15}N C.P.M.A.S. spectrum of solid 2-chloro-2-nitrosonorbornane

2.3 Red photolysis reactions of 2-chloro-2 nitrosonorbornane

2.3.1 Experimental

A sample of solid 2-chloro-2-nitrosonorbornane **[46]** was placed in the equipment shown in **Figure 2.13**. This was evacuated, sealed and then exhaustively irradiated with red light at 290 K whilst the side A of the equipment was cooled in liquid nitrogen in order to trap any gaseous material that is produced during irradiation. Solid 2-chloro-2-nitroso-norbornane is white, i.e. it does not absorb any visible light. However, the blue-green cast on its surface implies the presence of monomeric vapour and it is this that is photolysed by red light. During photolysis, liquid products are formed. These dissolve the parent dimer and on red irradiation, the blue-green cast on the surface of the solid changes to a blue colour, after which the substance becomes a deep-blue liquid, which on exhaustive irradiation in vacuum then slowly changes to a brown viscous oil. During the irradiation, in the equipment shown in **Figure 2.13**, white crystals are formed on the inside wall, at the bend B of the reaction vessel. Since they grow at a site remote from the original starting material, it is believed that these are formed by photochemical reactions in the vapour. Despite a number of attempts using several procedures, it was not possible to separate the components of these crystals. Furthermore, it is believed that at least one of these components undergoes further reaction when the crystals are introduced into the mass spectrometer, possibly because of the high temperature (170°C), at the source of the instrument.

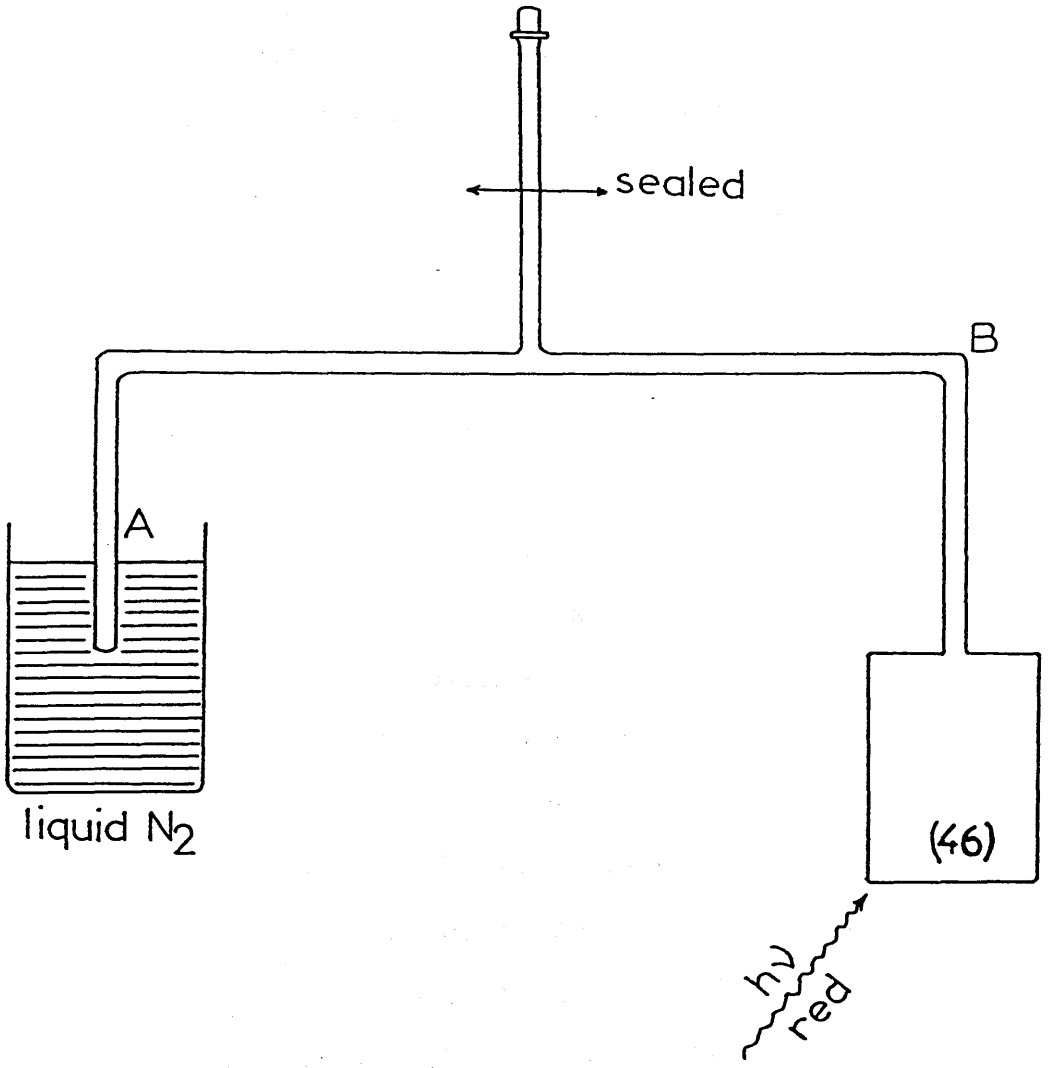

Figure 2.13

2.3.2 Spectroscopic studies of the white crystals

^{13}C-{^{1}H} D.E.P.T. spectra, for $\Theta=90^{o}$ and $\Theta=135^{o}$, obtained from a $CDCl_3$ solution of these white crystals, turn out to be particularly interesting. The relevant spectra are shown in **Figure 2.14**. Only >CH methine residues contribute to the $\Theta=90^{o}$ D.E.P.T. spectrum. The eight >CH peaks, in **Figure 2.14B**, immediately indicate that these white crystals consist of a mixture of four major components containing the [2.2.1]-bicycloheptane structure, and their relative intensities enable the pairs of >CH residues to be connected. **Figure 2.14B** also gives information about the relative amounts of each component present in the mixture. Similar analyses of the D.E.P.T. $\Theta=135^{o}$ spectrum, shown in **Figure 2.14C**, then enable connections within the methylene $>CH_2$ residues to be made, and eventually these procedures finally enable the four components present in the solution obtained from the white crystals to be identified. These turn out to be 2-norbornanone $C_7H_{10}O$, **[47]**, (10%), the norcamphor-oximes $C_7H_{11}NO$, **[48]** and **[49]**, (total=60%), in which -OH is *syn* to C(3) and -OH is *anti* to C(3) in relative proportions of 9:1 respectively, and a lactam $C_7H_{11}NO$, which could have either structure **[50]** or structure **[51]**, (30%). Only one of these lactams is present in the mixture in the white crystals. Detailed assignments of the n.m.r. data are shown in **Table 2.6**.[99]

A thorough analysis of the infra red spectum, **Figure 2.15**, of the white crystalline solid obtained from the apparatus, shown in **Figure 2.13**, supports the n.m.r. analyses already described, and confirms the presence of compounds **[47]**-**[49]**, and a lactam **[50]** or **[51]**. The infra red spectrum also shows that protonated forms of compounds **[48]**, **[49]**, and **[50]** or **[51]** are also present in the white crystals. These

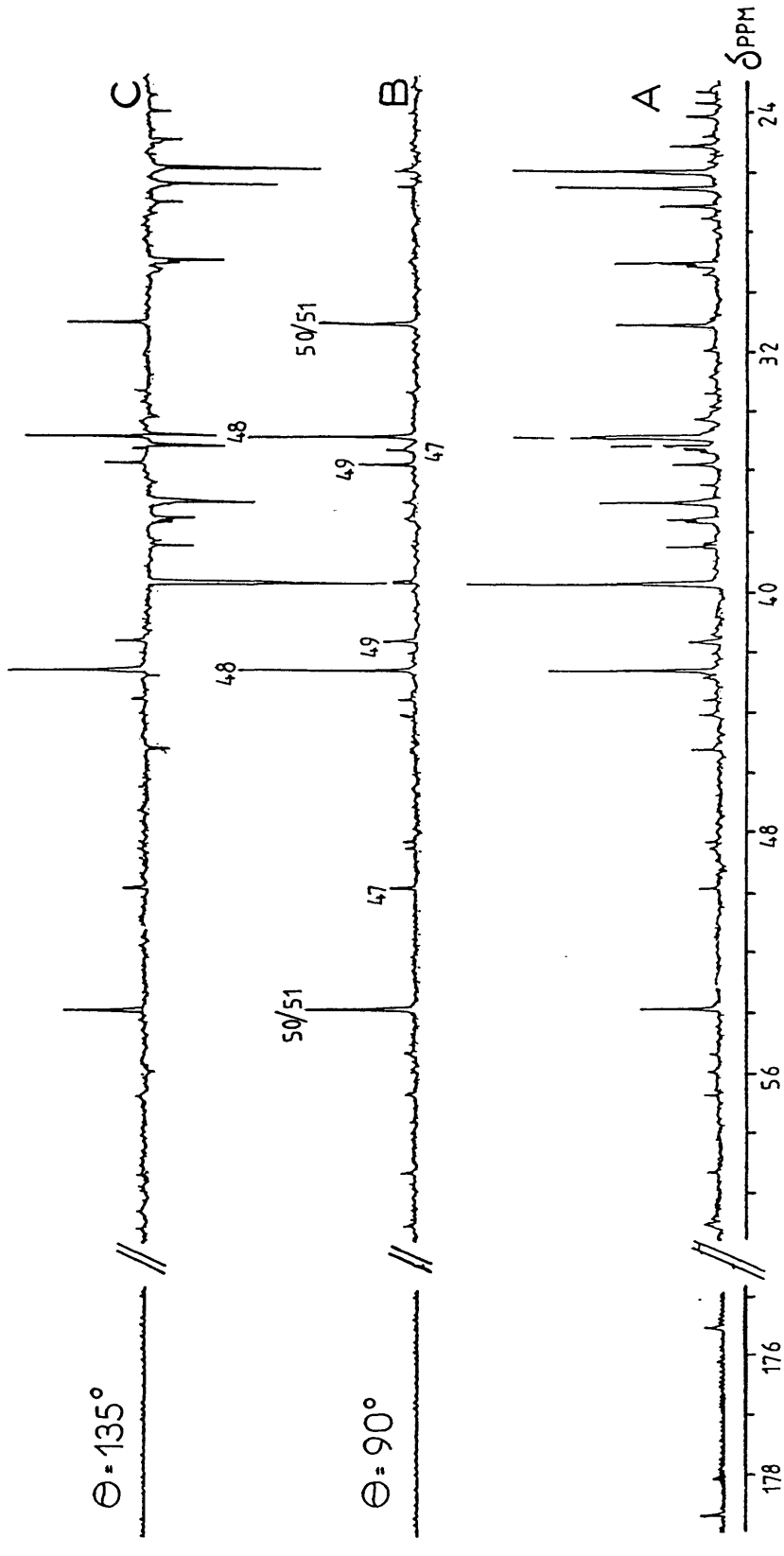

Figure 2.14 The ^{13}C-{^{1}H} n.m.r. spectrum, {A}, and corresponding Θ = 90°, {B}, and Θ = 135°, {C}, D.E.P.T. spectra of the white crystals in $CDCl_3$ solution

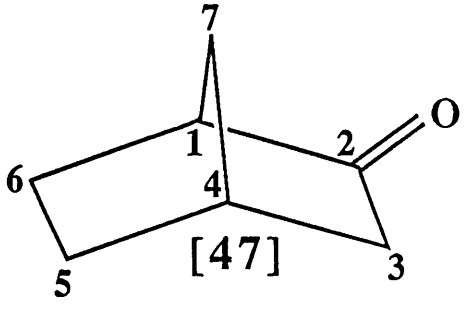

[47]

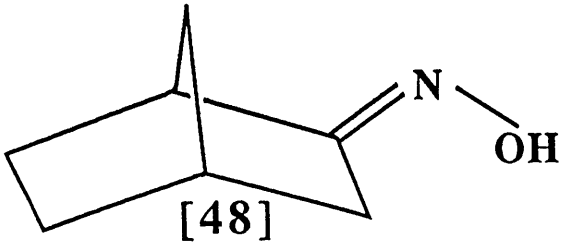

[48]

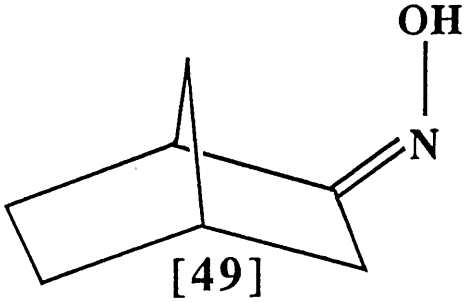

[49]

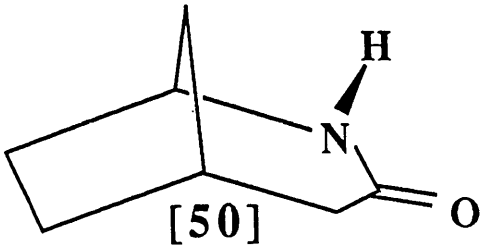

[50]

OR

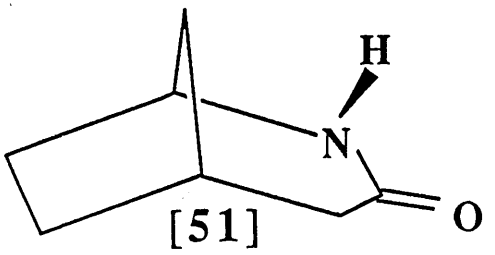

[51]

Substances present in the white crystals

Table 2.6

^{13}C n.m.r. chemical shifts of the components of the white crystals in $CDCl_3$

δ_c(ppm)($CDCl_3$)

2-Norbornanone **[47]**

C-1	C-2	C-3	C-4	C-5	C-6	C-7
49.83	/	45.23	35.28	27.14	24.15	37.59

Norcamphor-oxime **[48]**

C-1	C-2	C-3	C-4	C-5	C-6	C-7
42.63	178.60	34.84	34.89	26.00	26.55	39.73

Norcamphor-oxime **[49]**

C-1	C-2	C-3	C-4	C-5	C-6	C-7
41.65	178.00	37.66	35.77	25.12	26.55	38.49

Lactam **[50]/[51]**

C-1	C-2	C-3	C-4	C-5	C-6	C-7
53.87	175.27	37.04	31.12	29.04	35.19	39.73

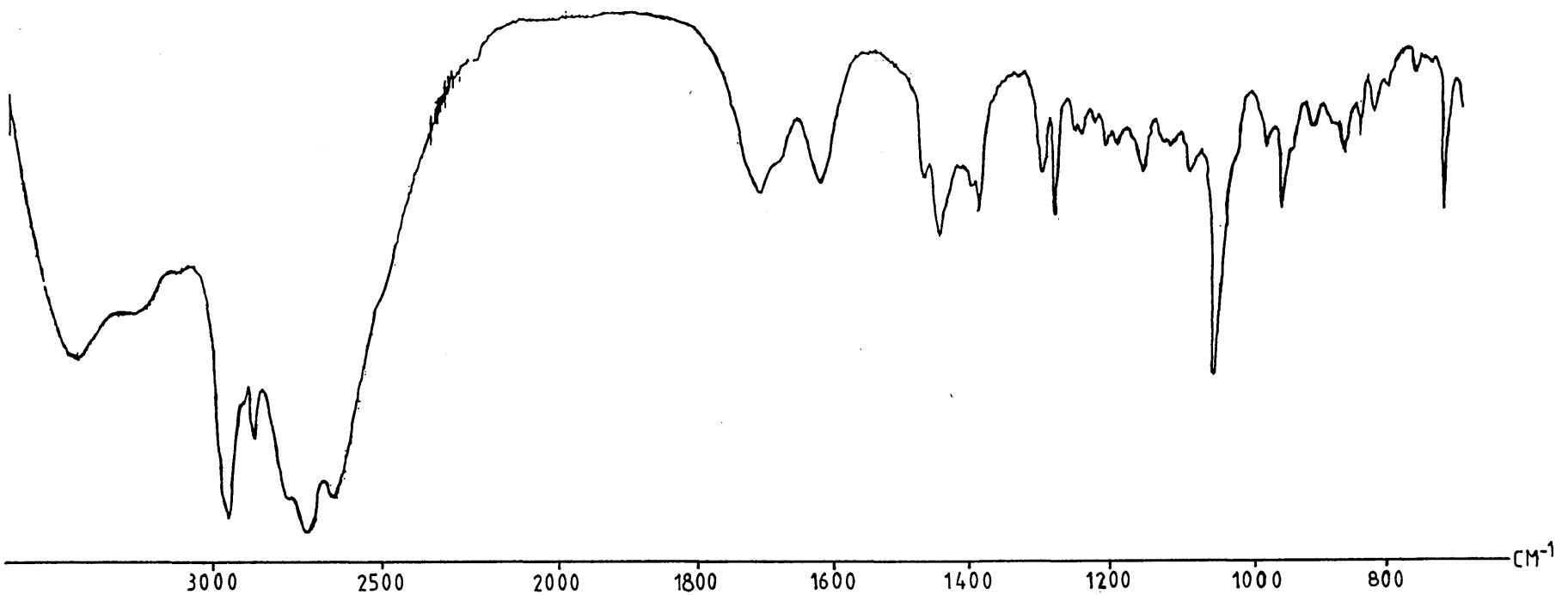

Figure 2.15 The infra red spectrum of the white crystals, recorded in a KBr disc

protonated forms are not detected in the n.m.r. or i.r. spectra of the $CDCl_3$ solution. Hence, the protonated forms must lose HCl when they are dissolved in $CDCl_3$. Detailed assignments of the i.r. data are given in **Table 2.7**. The electron impact mass spectrum of the white solid obtained, using a 70 eV electron beam, at 170°C only shows a parent peak from compound **[47]**. Parent peaks from compounds **[48]**, **[49]** and **[50]** or **[51]** are not detected, presumably because of the high temperature at the source of the mass spectrometer, but fragments from all of these compounds are readily detected. Details of the mass spectrum cracking pattern are given in Appendix 2, 2'.2'. Interestingly, the mass spectrum of the white crystals indicates that, in addition to fragmentation of the parent substances, at least one of compounds **[48]**, **[49]** and **[50]** or **[51]** undergoes still further rearrangements inside the mass spectrometer. Details of these reactions will be given later in the discussion.

Table 2.7

Infra red assignments for the components of the white crystals

Component	Assignment	Absorption
(3)	>C=O stretching	1715 cm^{-1}
(4) and (5)	bonded -OH >C=N stretching >N-O stretching	3400 cm^{-1} 1630 cm^{-1} 1055 cm^{-1} 960 cm^{-1}
(6) or (7)	>N-H stretching asymmetric and symmetric -NH_2^+ stretching >C=O stretching >N-H wagging	3200 cm^{-1} 3100 cm^{-1} 2780 cm^{-1} 2720 cm^{-1} 2650 cm^{-1} 1680 cm^{-1} 722 cm^{-1}

2.3.3 Spectroscopic studies of the brown viscous oil

Having fully identified the components of the white crystals, it was then easy to subtract their characteristic signals from the ^{13}C n.m.r. spectra of the brown viscous oil, shown in **Figure 2.16**, and then identify the extra components which are present in that mixture. The brown viscous oil was dissolved in $CDCl_3$, and then the ^{13}C-{^{1}H} and the ^{13}C-{^{1}H} D.E.P.T. spectra for Θ values of 90^{o} and 135^{o} were recorded, as shown in **Figures 2.16A**, **2.16B**, and **2.16C** respectively. Particular attention was then given to the intensity distribution in **Figure 16B**, in order to assess the number of pairs of >CH- residues, and to match these methine residues within the pairs. Seven pairs of methine peaks were identified, so there are at least seven compounds present in the brown viscous oil mixture. All of the characteristic ^{13}C n.m.r. signals arising from the four components present both in the white crystals and in the brown viscous oil, and their relative proportions in the brown viscous oil, were identified. These turn out to be 2-norbornanone $C_7H_{10}O$, **[47]**, (35%), the norcamphor-oximes $C_7H_{11}NO$, **[48]** and **[49]**, (total=15%), in relative proportion of -OH *syn* to C(3) and -OH *anti* to C(3) of 2:1, and a lactam $C_7H_{11}NO$, **[50]** or **[51]**, (20%). Their characteristic ^{13}C n.m.r. signals are shown in **Figure 2.17**. It should be noted that the relative amounts of compounds **[47]**-**[50]** or **[51]** present in the white crystals are not the same as the corresponding amounts in the brown oil. **Figure 2.18** shows the remaining major peaks in the corresponding n.m.r. spectra after removal of the spectra of compounds **[47]**-**[50]** or **[51]** from **Figure 2.16**.

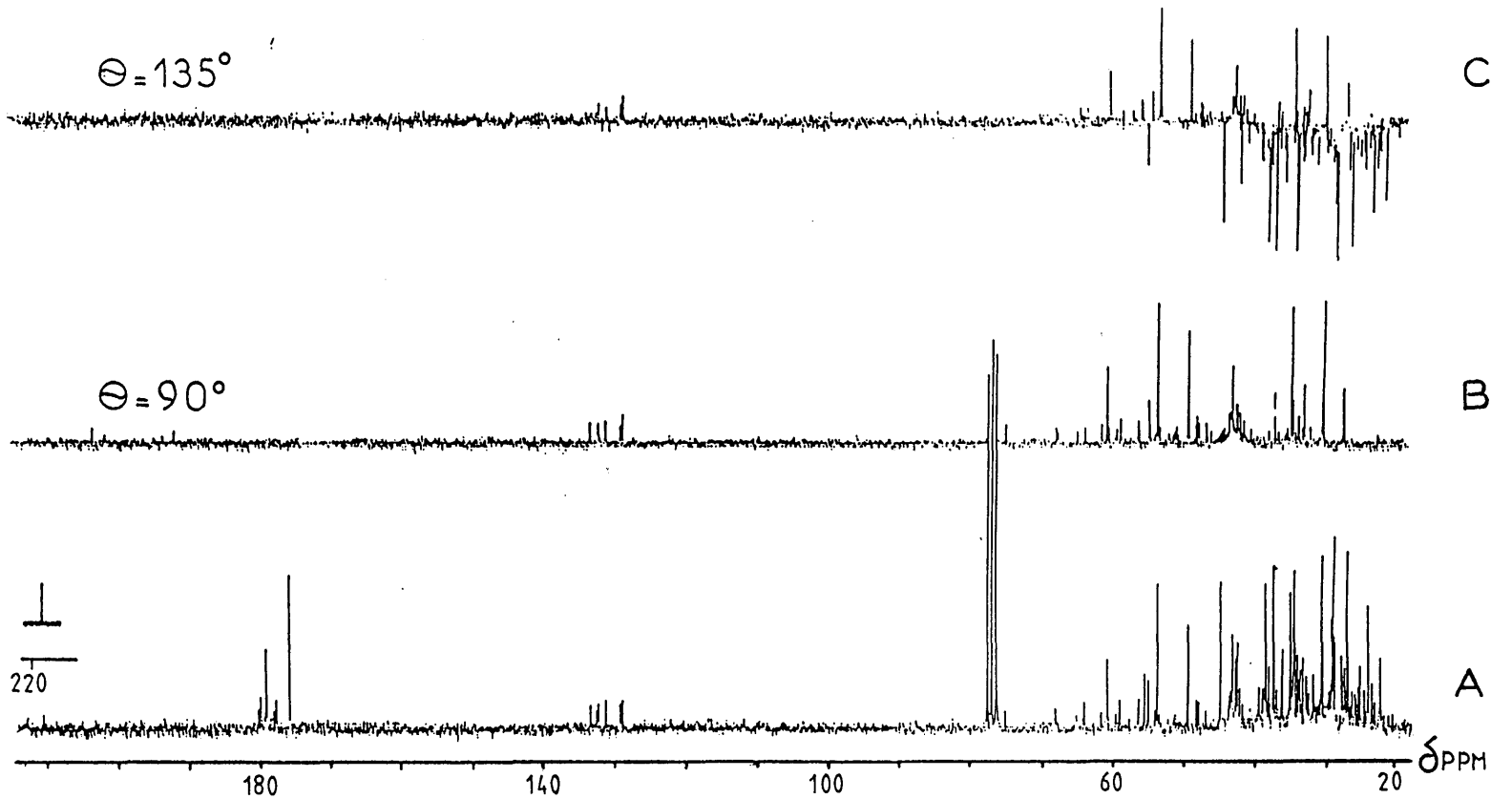

Figure 2.16 The ^{13}C-{^{1}H} n.m.r. spectrum, {A}, and corresponding $\Theta = 90^{o}$, {B}, and $\Theta = 135^{o}$, {C}, D.E.P.T. spectra of the brown viscous oil in $CDCl_3$ solution

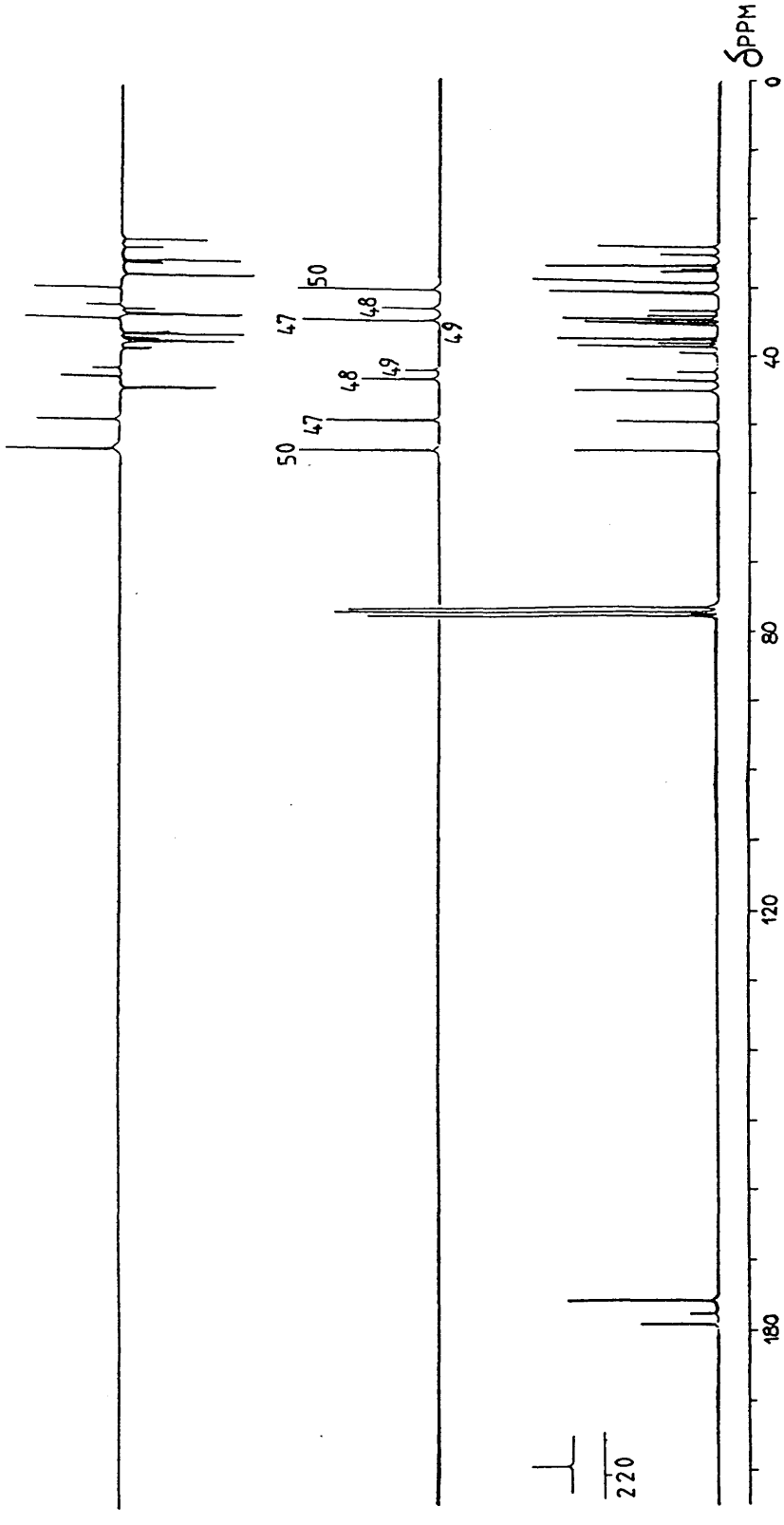

Figure 2.17

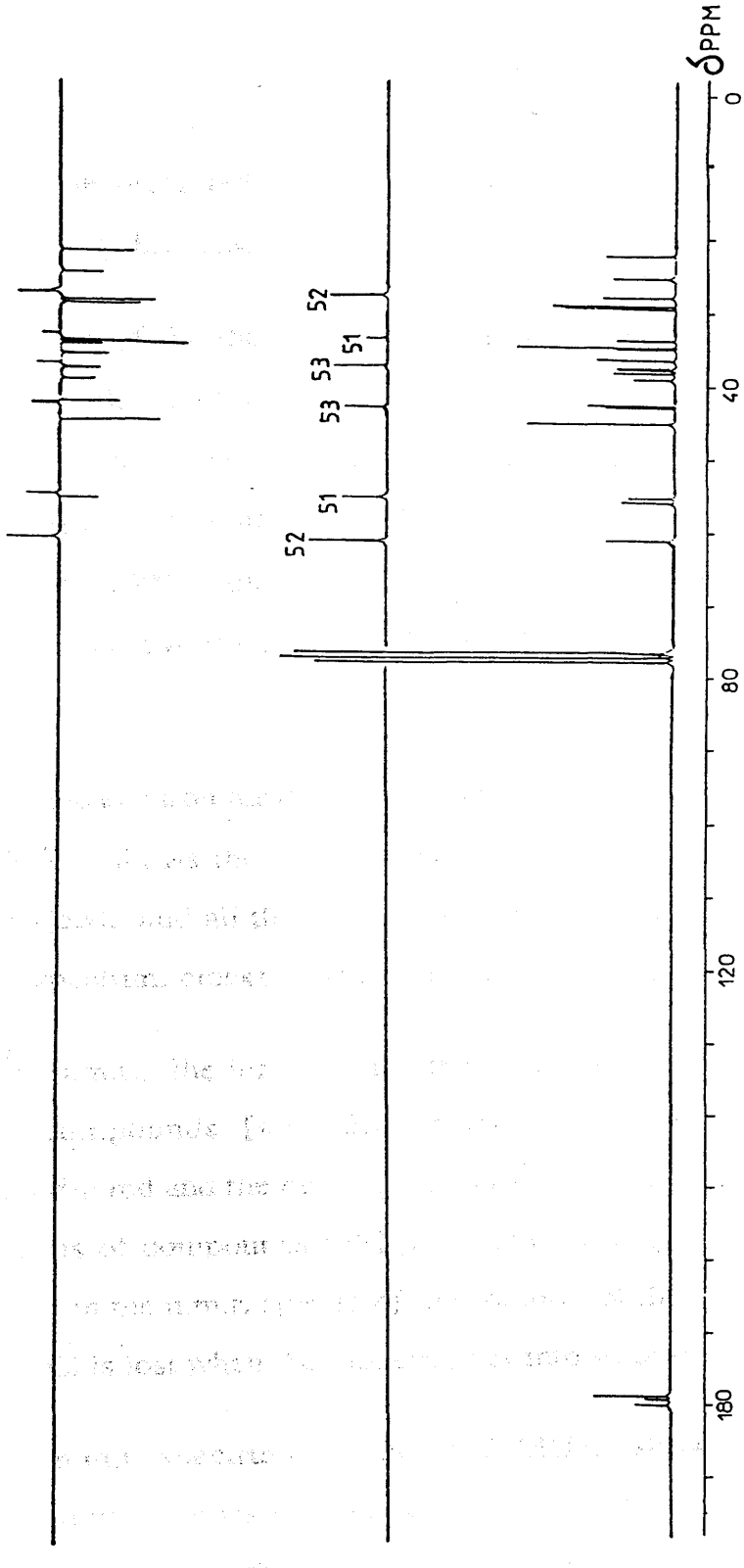

Figure 2.18

Figure 2.18 reveals the presence of three major components which are either structural isomers or stereoisomers of the lactam **[50]**. These three lactams **[51]-[53]** are present in relative proportions of 3 : 2: 1 respectively. Their characteristic ^{13}C n.m.r. signals are shown in **Figure 2.18**. The separated spectral assignments of compounds **[47]-[53]** are given in **Table 2.8.**

The analysis of the the infra red spectrum, **Figure 2.19**, of the brown viscous oil, clearly shows a >C=O stretching absorption frequency at 1715 cm^{-1}, characteristic of norbornanone **[47]**, a >C=N- stretching absorption at 1640 cm^{-1}, characteristic of the norbornanone oximes **[48]** and **[49]**, and with some overlap between these two regions, characteristic of the lactams, the >C=O stretching absorption at 1675 cm^{-1}.

Finally, the electron impact mass spectrum, using a 70 eV electron beam, at 170°C, shows the parent peaks of all the components of the mixture, **[47]-]53]**, and all the cracking patterns derived from them. A detailed mass spectrum cracking pattern is shown in Appendix 2, 2'.3'.

The ^{13}C n.m.r., the infra red and the mass spectra all confirm the presence of compounds **[47]-[53]** in the photolysis mixture. In addition, the infra red and the mass spectra also show the presence of the protonated forms of compounds **[48]-[53]**, and these protonated forms are not detected in the n.m.r. spectra of the solution of the brown viscous oil, because HCl is lost when the mixture goes into solution in $CDCl_3$.

The ^{1}H n.m.r. spectrum, at 200.132 MHz, shown in **Figure 2.20**, of the brown viscous oil shows a very extensive overlap of the characteristic regions of each component of the photolysis mixture, and

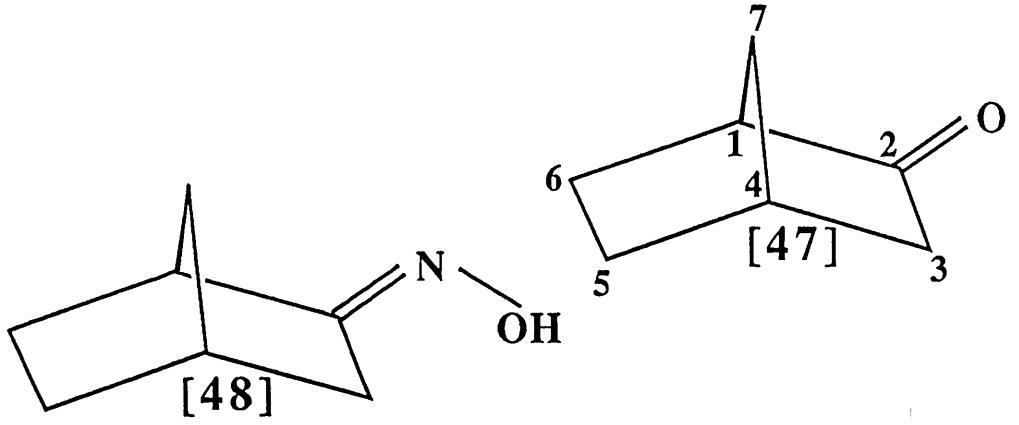

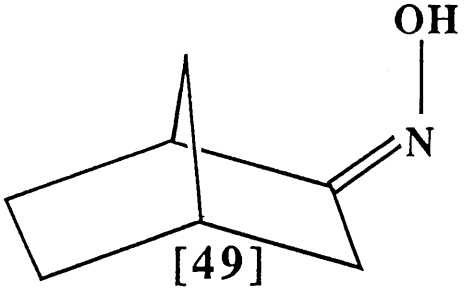

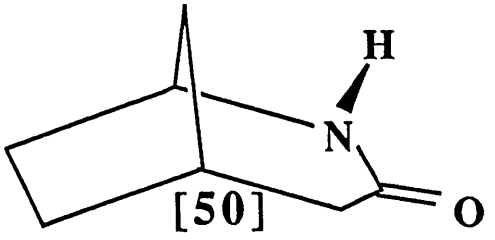

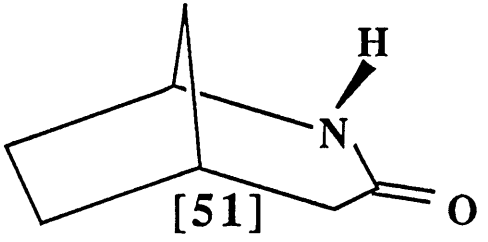

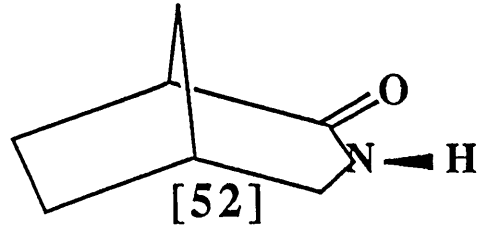

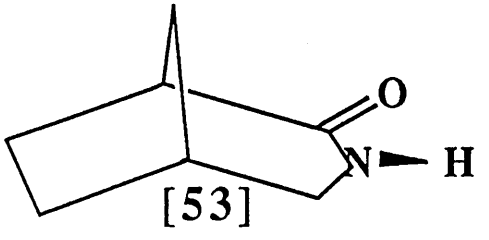

Substances present in the brown viscous oil

Table 2.8

^{13}C n.m.r. chemical shifts of the components of the brown viscous oil in $CDCl_3$

δ_c(ppm)($CDCl_3$)

2-Norbornanone **[47]**

C-1	C-2	C-3	C-4	C-5	C-6	C-7
49.51	218.64	44.90	34.94	26.77	23.83	37.28

Norcamphor-oxime **[48]**

C-1	C-2	C-3	C-4	C-5	C-6	C-7
43.32	178.98	33.92	33.12	26.77	27.15	39.43

Norcamphor-oxime **[49]**

C-1	C-2	C-3	C-4	C-5	C-6	C-7
42.20	177.66	37.28	34.94	25.22	27.05	38.01

Lactam **[50]**

C-1	C-2	C-3	C-4	C-5	C-6	C-7
53.80	175.73	38.45	30.49	28.76	34.34	37.33

Lactam **[51]**

C-1	C-2	C-3	C-4	C-5	C-6	C-7
55.00	178.98	38.86	33.52	29.03	36.10	37.45

Lactam **[52]**

C-1	C-2	C-3	C-4	C-5	C-6	C-7
60.85	179.86	44.90	27.52	22.11	28.84	34.44

Lactam **[53]**

C-1	C-2	C-3	C-4	C-5	C-6	C-7
42.68	179.17	55.57	37.33	25.01	34.63	42.48

Figure 2.19 The infra red spectrum of the brown viscous oil, recorded in a KBr disc

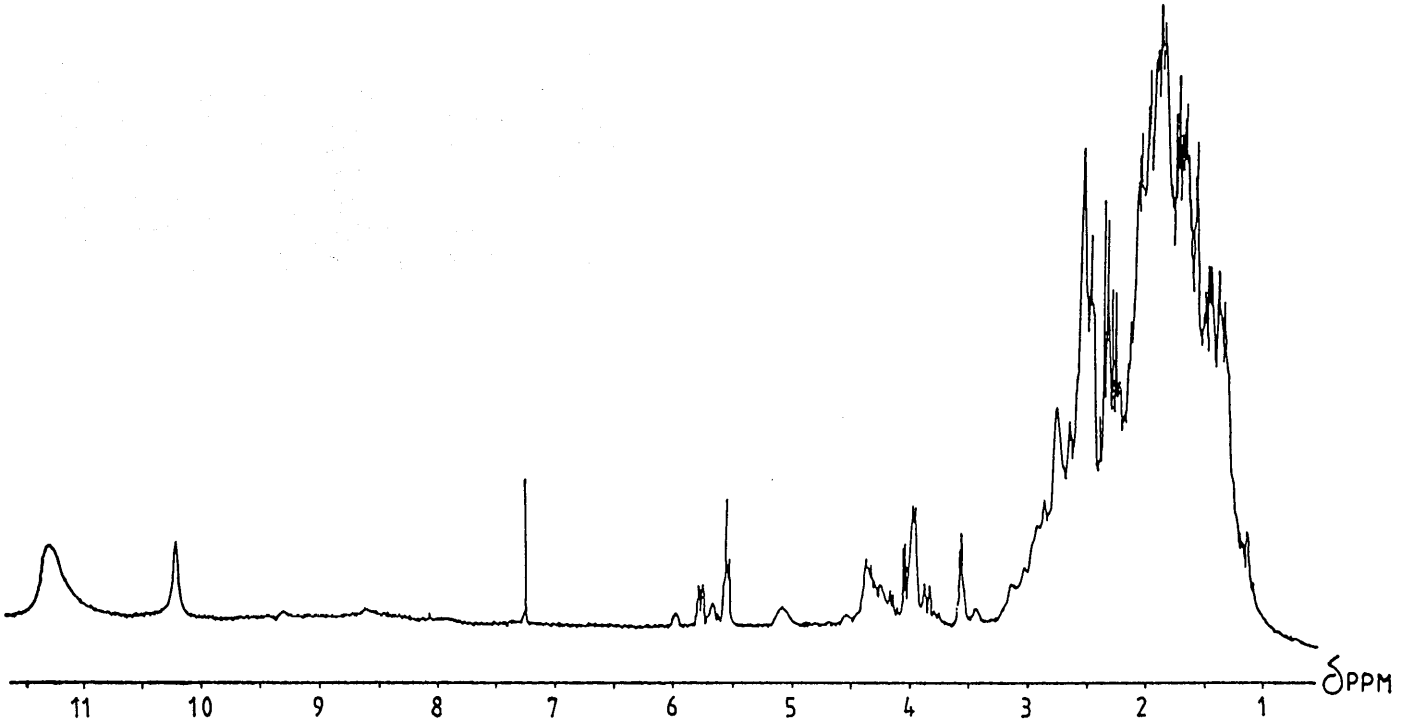

Figure 2.20 The 200.132 MHz ^{1}H n.m.r. spectrum of the brown viscous oil, in $CDCl_3$ solution

so, it was not possible to determine exactly the ^{1}H n.m.r. chemical shifts and the $J_{H,H}$ coupling constants of the compounds **[47]-]53]**. However, the ^{1}H n.m.r. spectrum confirms that all the components of the mixture possess the main skeletal frame shown below, where both X and Y vary from one component to another.

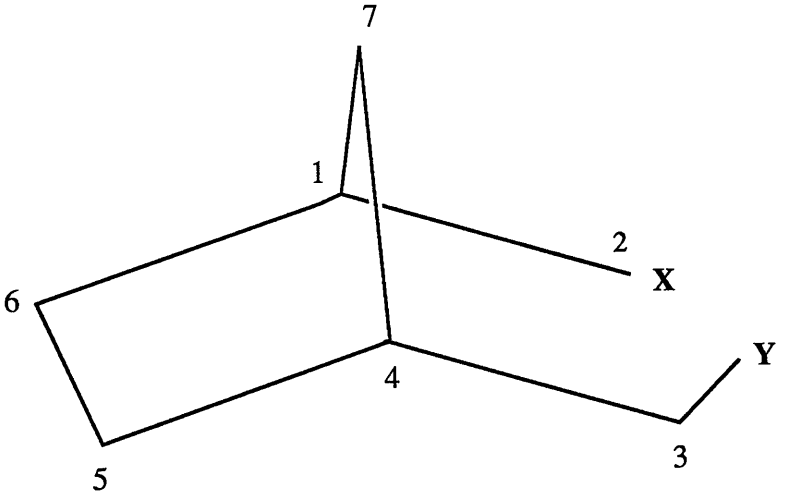

2.4 Summary and solid state photolysis reactions

At this point it is worth summarizing the important conclusions deduced so far. Analysis of the ^{13}C-{^{1}H} n.m.r. spectrum, the ^{13}C D.E.P.T., the two dimensional ^{13}C-^{1}H correlation, the ^{1}H, and the ^{1}H-^{1}H COSY n.m.r. spectra of 2-chloro-2-nitrosonorbonane **[45]**, in $CDCl_3$ solution, and of the C.P.M.A.S. spectra of the corresponding solid, show that the compound is mainly monomeric in the liquid phase, but has a *trans*-dimeric structure **[46]** in the solid form of this substance. These n.m.r. structural assignments are confirmed by analyses of infra red and mass spectra. The blue green cast on the surface of the solid implies that the vapour is monomeric.

At each stage of this work, attempts were made to detect paramagnetic species, in particular nitroxide radicals, completely without success.

Red irradiation of the solid, in equilibrium with its vapour, initially photolyses the vapour and produces liquid products. At that point, irradiation essentially involves the monomeric liquid phase, and the rate of photolysis then cooperatively speeds up. Photolysis of the liquid phase, appears to be similar to, but not the same as, the vapour phase photolysis. The vapour phase products include 2-norbornanone **[47]**, the two isomeric forms of norbornanone-oxime **[48]** and **[49]**, and a lactam **[50]** or **[51]**. Compounds **[47]**, **[48]** and **[49]** and the four isomeric lactams **[50]**-**[53]** are also present in the photolysis products of the liquid phase.

These results now enable mechanisms to be constructed for the photochemical reactions that take place when the solid is irradiated with

red light. The sequence of reactions is summarized in the **Scheme 2.2.** The initial red irradiation of the solid, in equilibrium with its vapour, causes photolysis of the vapour and produces liquid products. The irradiation then involves mainly the monomeric liquid phase.

When the NO group on **[45]** is irradiated with red light, it causes an $^1\pi^* \longleftarrow {}^1n$ (nitrogen) transition and the intermediate biradical **[54]** is formed. This rearranges to the isomeric chloro oximes **[55]** and **[56]**. At this stage, these chloro oximes either lead to the oximes **[48]** and **[49]** respectively as hydrogens are available via the side reaction shown in **Scheme 2.2**, or can undergo Beckmann-like rearrangement leading to **[57]** and **[58]** respectively, which in their turn further react with hydrogen to give **[50]/[51]** and **[52]/[53]** respectively.

The parent peaks of the oximes **[48]** and **[49]**, as well as the lactams **[50]-[53]** are not present in the mass spectrum of the white crystals because when these crystals are heated in the mass spectrometer, at 170°C, the components further rearrange to give **[59]** and **[60]**.

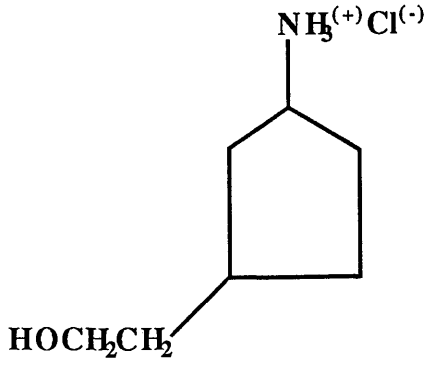

[59]

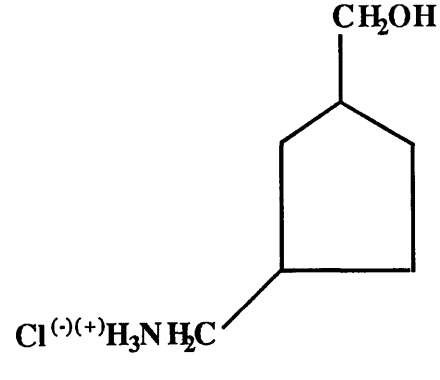

[60]

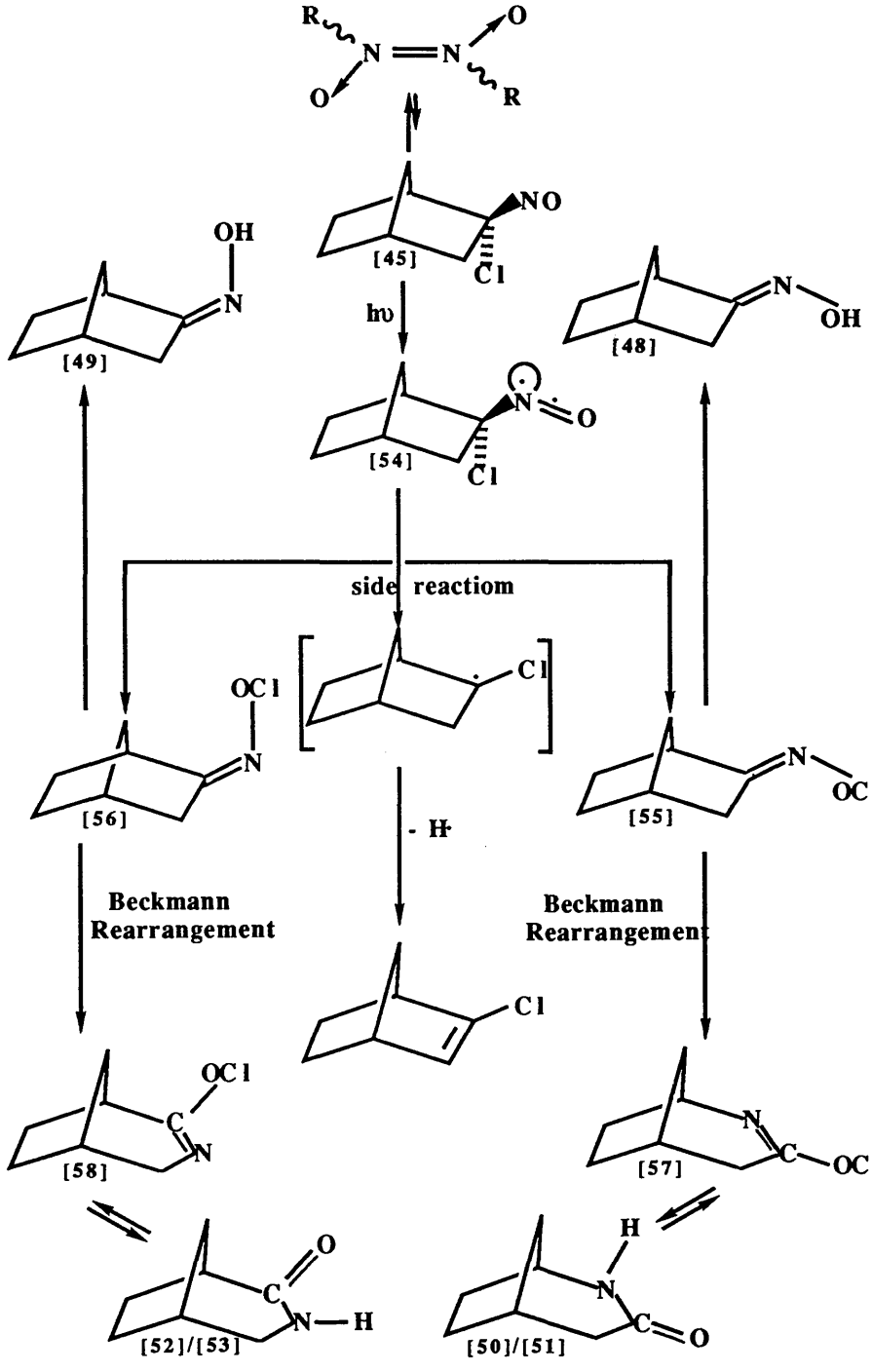
R
N
N
O
O
R
NO
Cl
[45]
hυ
OH
N
[49]
N
OH
[48]
N
O
Cl
[54]
side reactiom
OCl
N
[56]
Cl
- H
N
OCl
[55]
Beckmann
Rearrangement
Beckmann
Rearrangement
Cl
OCl
C
N
[58]
N
C
OCl
[57]
O
C
N—H
[52]/[53]
H
N
C
O
[50]/[51]

Scheme 2.2

As already noted, unlike the solid state photolyses studies discussed[16,17,77,78,87,90] in Chapter 1, at no time have nitroxide radicals been detected in these studies of the red photolysis of 2-chloro-2-nitrosonorbornane. The reason for this almost certainly is as shown in **Scheme 1.4**,[87] Chapter 1, in which the intermediate chloro oxime **[31]** undergoes Beckmann rearrangement followed by oxidation to the acyl nitroxide **[36]**. Two ClO^- ions (or two $ClO^\bullet$ radicals) are required in this scheme. Cage effects in the solid enable the product of the Beckmann rearrangement to react with its own ClO^- (or $ClO^\bullet$) residue, but, the reaction with a second ClO^- (or $ClO^\bullet$) residue can not take place in the much more loosely packed vapour or liquid. Hence, the reaction **Scheme 2.2** in the case of 2-chloro-2-nitrosonorbornane stops with the production of the intermediate lactams **[57]** and **[58]**.

APPENDIX TWO

2'.1' Electron impact mass spectrum of 2-chloro-2-nitrosonorbornane [45]

Mass	Relative Abundance (%)	Ion
131.0	7.95	$[C_7H_{10}{}^{37}Cl]^+$
129.0	23.86	$[C_7H_{10}{}^{35}Cl]^+$
94.1	10.23	$[C_7H_{10}]^+$
93.1	100.00	$[C_7H_9]^+$
91.0	29.55	$[C_7H_7]^+$
77.1	30.68	$[C_6H_5]^+$
67.1	36.36	$[C_5H_7]^+$
65.2	22.73	$[C_5H_5]^+$
41.0	13.64	$[C_3H_5]^+$

2'.2' Electron impact mass spectrum of the components of the white crystals

2-Norbornanone [47]

Mass	Relative Abundance (%)	Ion
110	12.1	$[C_7H_{10}O]^+$
94	15.0	$[C_7H_{10}]^+$
82	30.7	$[C_6H_{10}]^+$
81	11.5	$[C_6H_9]^+$
69	100.0	$[C_5H_9]^+$
68	27.3	$[C_5H_8]^+$
67	23.1	$[C_5H_7]^+$
55	52.0	$[C_4H_7]^+$
54	25.9	$[C_4H_6]^+$
42	27.4	$[C_2H_2O]^+$

Norcamphor-oximes [48]/[49]

Mass	Relative Abundance (%)	Ion
125	not observed	
124	not observed	
108	not observed	
95	8.1	$[C_7H_{11}]^+$
94	15.0	$[C_7H_{10}]^+$
82	30.7	$[C_6H_{10}]^+$
69	100.0	$[C_6H_9]^+$
68	27.3	$[C_5H_8]^+$
55	52.0	$[C_4H_7]^+$
54	25.9	$[C_4H_6]^+$
42	27.4	$[C_3H_6]^+$

Lactams **[50]/[51]**

Mass	Relative Abundance (%)	Ion
130	32.9	$[C_7H_{16}NO]^+$
129	5.9	$[C_7H_{15}NO]^+$
113	10.1	$[C_7H_{15}N]^+$
112	10.1	$[C_7H_{14}N]^+$
100	11.0	$[C_6H_{14}N]^+$
99	26.5	$[C_6H_{13}N]^+$
96	15.9	$[C_7H_{12}]^+$
95	8.1	$[C_7H_{11}]^+$
84	18.5	$[C_7H_{12}]^+$
83	40.7	$[C_6H_{11}]^+$
82	30.7	$[C_6H_{10}]^+$
72	3.3	$[C_4H_{10}N]^+$
70	17.8	$[C_6H_{10}]^+$
69	100.0	$[C_6H_9]^+$
68	27.3	$[C_5H_8]^+$
57	16.1	$[C_3H_7N]^+$
56	33.4	$[C_3H_6N]^+$
55	52.0	$[C_4H_7]^+$
45	24.7	$[C_2H_4O]^+$
44	15.2	$[C_2H_6N]^+$
43	96.1	$[C_2H_5N]^+$
42	27.4	$[C_3H_6]^+$

2'.2' Electron impact mass spectrum of the components of the brown viscous oil

2-Norbornanone [47]

Mass	Relative Abundance (%)	Ion
110	7.6	$[C_7H_{10}O]^+$
94	1.0	$[C_7H_{10}]^+$
82	4.6	$[C_6H_{10}]^+$
81	14.9	$[C_6H_9]^+$
69	5.5	$[C_5H_9]^+$
68	31.7	$[C_5H_8]^+$
67	100.0	$[C_5H_7]^+$
55	21.4	$[C_4H_7]^+$
54	18.9	$[C_4H_6]^+$
42	9.5	$[C_2H_2O]^+$
41	56.0	$[C_2HO]^+$
28	24.7	$[CO]^+$

Norcamphor-oximes [48]/[49]

Mass	Relative Abundance (%)	Ion
125	10.4	$[C_7H_{11}NO]^+$
124	0.8	$[C_7H_{10}NO]^+$
108	9.0	$[C_7H_{10}N]^+$
95	1.7	$[C_7H_{11}]^+$
94	1.0	$[C_7H_{10}]^+$
82	4.6	$[C_6H_{10}]^+$
69	5.5	$[C_5H_9]^+$
68	31.7	$[C_5H_8]^+$
55	21.4	$[C_4H_7]^+$
54	18.9	$[C_4H_6]^+$
42	9.5	$[C_3H_6]^+$
41	56.0	$[C_3H_5]^+$
17	5.8	$[OH]^+$

Lactams **[50]/[51]/[52]/53]**

Mass	Relative Abundance (%)	Ion
165	0.7	$[C_7H_{16}{}^{35}ClNO]^+$
163	1.7	$[C_7H_{14}{}^{35}ClNO]^+$
127	4.6	$[C_7H_{13}NO]^+$
126	2.4	$[C_7H_{12}NO]^+$
125	10.4	$[C_7H_{11}NO]^+$
110	7.6	$[C_7H_{12}N]^+$
96	15.9	$[C_7H_{12}]^+$
82	4.6	$[C_6H_{10}]^+$
69	5.5	$[C_6H_9]^+$
55	10.5	$[C_4H_7]^+$
45	24.7	$[C_2H_4O]^+$
41	56.0	$[C_3H_6]^+$
35	16.6	$[^{35}Cl]^+$
28	56.0	$[C_2H_4]^+$
27	38.0	$[C_2H_3]^+$

CHAPTER THREE

CONFIGURATIONS AT C-2 IN GEMINAL CHLORONITROSO DERIVATIVES OF BICYCLO-[2,2,1] HEPTANE

In Chapter 1, it was pointed out that it was not possible at the time to use early Cotton effect studies to assign the configurations at the chiral C-2 centre in the geminal chloronitroso derivatives of the bicyclo-[2,2,1]-heptanes. A combination of X-ray analysis and high resolution n.m.r. investigations on 10-bromo-2-chloro-2-nitrosocamphane **[32]**, and high resolution n.m.r. investigations on (-)-2-chloro-2-nitrosocamphane **[19]** and on racemic 2-chloro-2-nitrosonorbornane **[45]**, now enable the configurations at C-2 in the other chloronitroso derivatives to be unambiguously assigned. The results obtained for six of these compounds are shown in **Figure 3.1**. Davidson's suggestion[88] that when these substances are irradiated with visible light for a *short* time, the configuration at C-2 only inverts when the environment of the nitroso group is sterically congested seems to hold in compounds **[32],[19],[61]**, and **[29]** but not in the case of compound **[62]**. Why this substance does not appear to obey Davidson's reasoning is not yet understood.

	(+)-10-Bromo-2-chloro-2-nitroso camphane	(-) 2-Chloro-2-nitrosocamphane	2-Chloro-2-nitrosonorbornai	(+)-1-Carboxylic acid-2-chloro-2-nitrosoapocamphane	(+)-2-chloro-2-nitroso-10-sulfonic acid apocamphane, pyridine salt	(+)-2-Chloro-2-nitrosofenchane
References	(83), (88), (89)	(83), (86), (88)	(88)	(83)	(83)	(88)
Irradiated with	Red Visible Light	Red Visible Light	Red Visible Light	Red Visible Light	Red Visible Light	Red Visible Light
Cotton Effect (Unirradiated)	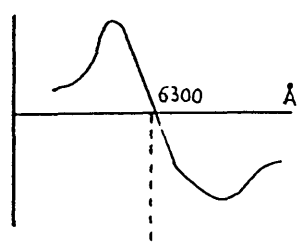	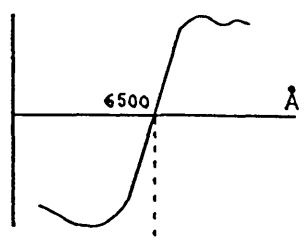	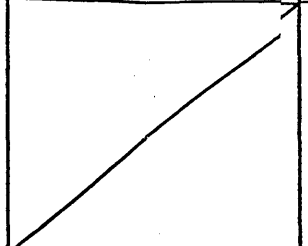	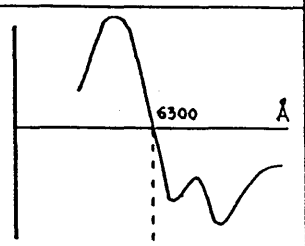	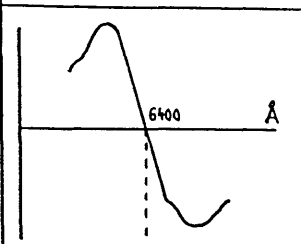	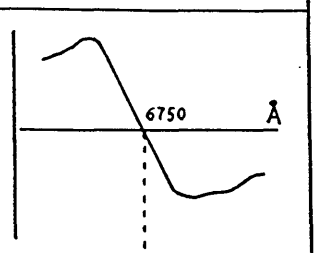
Cotton Effect (Irradiated)	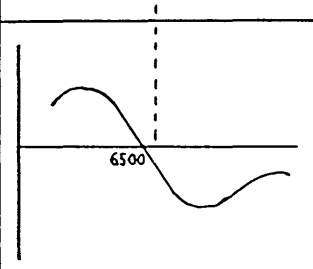	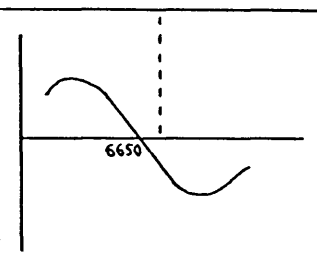	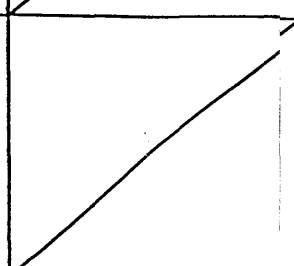	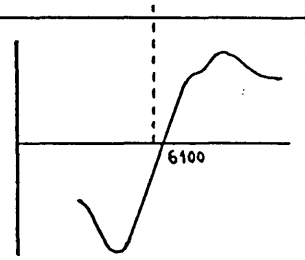	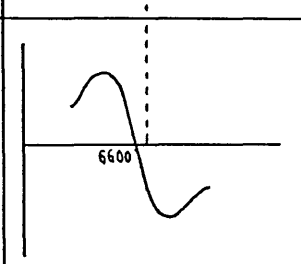	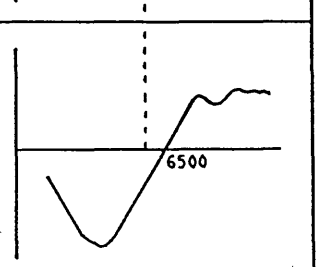
Spectrum Displacement	RED	RED	NONE	BLUE	RED	RED
Rotatory Dispersion Curve Displacement	RED	RED	NONE	BLUE	RED	RED
Suggested Structure (Before Irradiation)	[32] 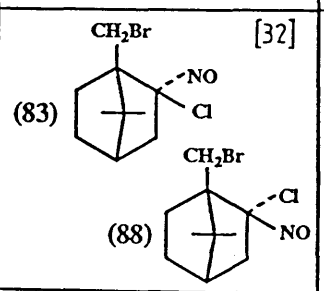	[19] 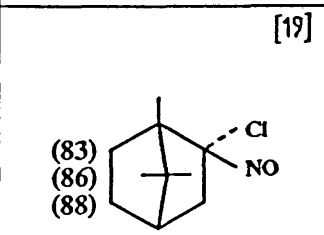	[45] 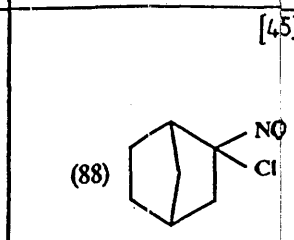	[61] 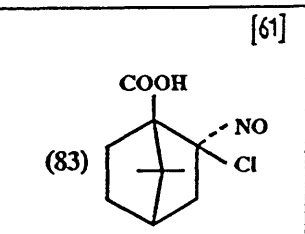	[62] 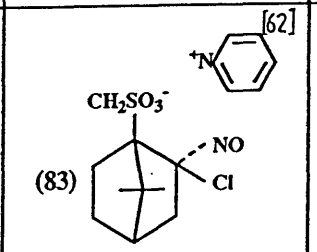	[29] 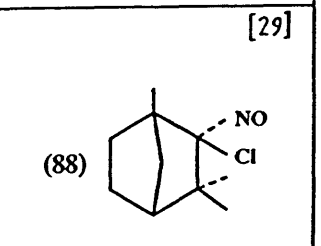
Actual Structure (Before Irradiation)	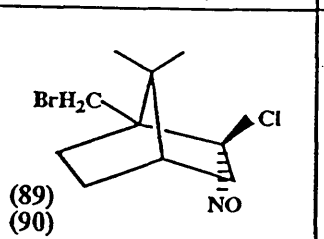	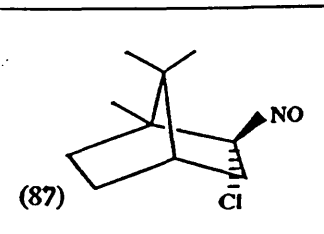	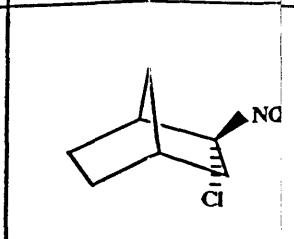	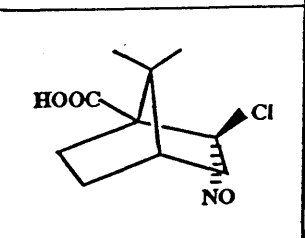	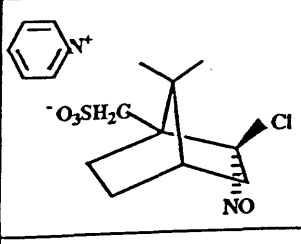	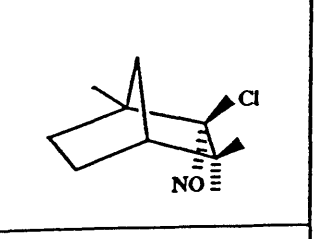
Actual Structure (After Irradiation for a very short time)	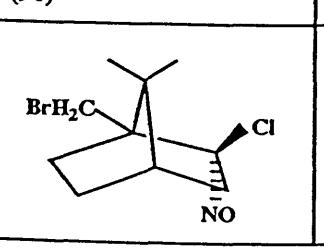	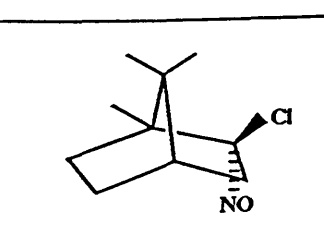		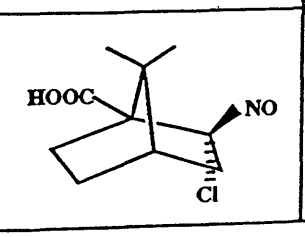	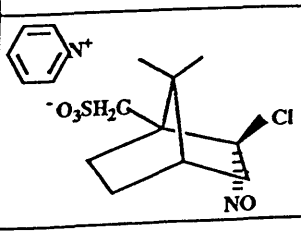	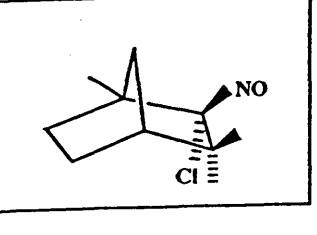

Figure 3.1

CHAPTER FOUR

THE ACTION OF NO AND NO_2 ON BIOLOGICALLY IMPORTANT SUBSTANCES

It has been known for quite a long time that several kinds of organic substances containing nitrogen are potent carcinogens. The poisoning of ruminants in Norway with nitrite-treated fish meal[100,101] was traced to N-nitrosodimethylamine, **[63]**. Fried cured bacon is known to contain small amounts of the carcinogen N-nitrosopyrrolidine, **[64]**, and bioassays of nitrosamines and nitrosamides, **[65]**, show that most of them are powerful carcinogens.[102]

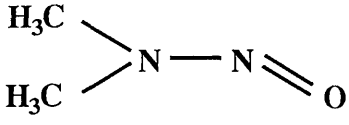

[63]

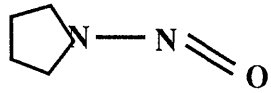

[64]

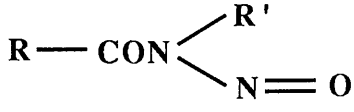

[65]

Amines such as 1,2-dimethylhydrazine, **[66]**, and azo derivatives like azoxymethane, **[67]**, are potent carcinogens that are used to induce tumours, in experimental animals.

[66]

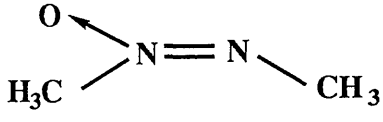

[67]

N,N-dimethylformamide, **[68]**, and 2-nitropropane, **[69]**, are known to cause severe adverse effects on the health of workers who use these compounds,[103] and nitric oxide seems to be implicated in the Endothelium Derived Relaxing Factor (E.D.R.F.) that plays a catastrophic role in toxic shock.[104]

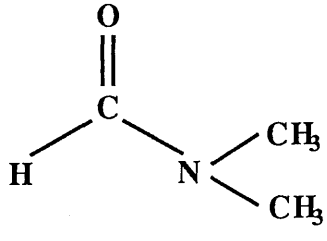

[68]

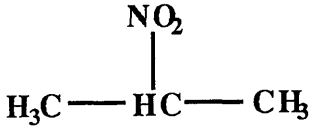

[69]

In Chapters 1 and 2, it was pointed out that similar N-nitrosamine derivatives, azoxy derivatives and derivatives of substituted amides are also encountered in the unstable intermediates that are produced in the red photolysis of aliphatic C-nitroso solids. Compounds **[63]-[69]** are all potent carcinogens but it is possible, as in the case of the red photolysis reactions described in the earlier parts of this thesis, that these substances in fact are precursors of the real carcinogens. The real carcinogens may, for example, be radicals similar to those described in Chapters 1 and 2.

The nitrosites of the terpenes are particularly easy to prepare: sodium nitrite and acetic acid are simply allowed to come into contact with the terpene at temperatures within the range 0^{o}-10^{o}C. Many kinds of biologically important substances contain olefinic residues and they can therefore be reasonably expected to undergo reactions of the kind mentioned in Chapters 1 and 2 when they are brought into contact with the oxides of nitrogen, either by direct contact with the gases, or by coming into contact with nitrite ion in the presence of an acid and air, for example with hydrochloric acid and air in the gut, or with weak organic acids encountered in decomposing meats or in agricultural environments.

Nitrates are used as fertilisers in agriculture and they are readily reduced to nitrites by several kinds of enzyme and bacteria that are present in soils and plants.[105] Nitrite can then enter the diet via drinking water, and levels of nitrates and nitrites in water supplies have recently attracted considerable political and media attention throughout the world.

Alkali nitrites are also present in smaller amounts in vegetables, particularly leaf and root crops, in cured meats and in other foodstuffs to which they are added to inhibit bacterial spoilage and food poisoning.

Nitrites inhibit the growth of the bacterium Clostridium Botulinum, whose toxins are highly poisonous: 1 mg of Botulinum toxin A can kill 30 million mice. Many meat products are therefore subjected to treatment with alkali nitrites, followed by some form of heat tratment during which the concentration of nitrite decreases.[106] Before the introduction of nitrites for this purpose, thousands of people used to be killed each year by botulin poisoning.

The work described in Chapters 1-3 may have significance for the botanical, agricultural and medical toxicology, including carcinogenisis, of compounds containing nitrogen, and it was therefore felt that at this point it would be worthwhile studying the reactions of these oxides of nitrogen with model examples of biologically important molecules. It was decided to examine reactions with unsaturated steroids, unsaturated fatty acids, pyrimidine and purine bases, and the results obtained from these studies are described in sub-chapters 4.1-4.4. The compounds chosen were cholesterol, cholesteryl-propionate, (-)-7-dehydrocholesterol, oleic acid, elaidic acid, linoleic acid, cytosine, thymine and adenine.

4.1 The action of NO and NO_2 on cholesterol and some of its derivatives

4.1.1 CHOLESTEROL

Cholesterol, cholest-5-ene-3-β-ol, $C_{27}H_{46}O$, **[70]**, obtained from Riedel-De Hahn Ag Seelze, was purified by recrystallisation, several times, from petroleum ether (40-60), and its purity was then checked by means of thin layer chromatography, using silica gel plates and hexane:ethylacetate (1:1) as eluent. Microanalytical data for the purified cholesterol are listed in **Table 4.1**.

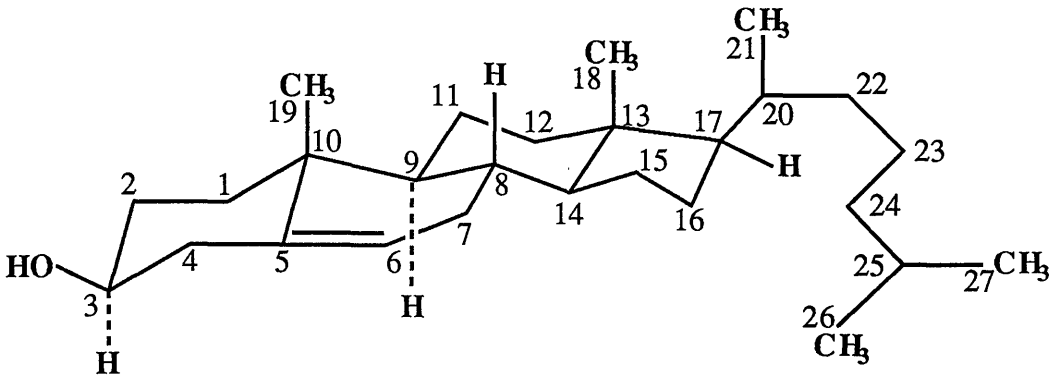

[70]

Table 4.1

Microanalyses data for cholesterol

Element	% Composition found	% Composition [expected for $C_{27}H_{46}O$]
C	83.72	83.94
H	12.19	11.92
O	4.09	4.14

Mass spectral data, together with infra red and ^1H n.m.r. data for the same sample are listed in **Tables 4.2, 4.3** and **4.4** respectively. Its infra red and ^1H n.m.r. spectra are shown in **Figures 4.1** and **4.2** respectively.

In cholesterol, the $-C(5)=C(6)<$ and $-C(3)$-OH residues might both react with the oxides of nitrogen to form the nitrosite[29]

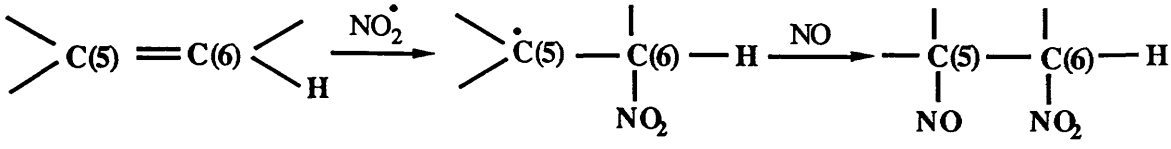

and the nitrite ester respectively.

The first of these reactions requires two equivalent of NO. The second requires one equivalent. The oxides of nitrogen are derived from the following sequence of reactions:

$$CH_3COOH + NaNO_2 \longrightarrow HNO_2 + CH_3COONa$$

$$3\,HNO_2 \longrightarrow HNO_3 + 2\,NO + H_2O$$

$$2\,NO + O_2 \longrightarrow 2\,NO_2$$

If the nitrite ester alone is formed, then one mole of cholesterol requires one formula weight of $NaNO_2$. However, if the nitrosite is also formed, then a further four formula weights of $NaNO_2$ are required per mole of cholesterol. Reactions involving relative ratios of cholesterol to sodium nitrite of **a)** 1:1, **b)** 1:3 and **c)** 1:8 were therefore investigated, with the following results.

Table 4.2
Electron impact mass spectrum of cholesterol [70]

Mass	Relative abundance (%)	Ion
386.1	68.74	$[C_{27}H_{46}O]^+$
371.1	21.55	$[C_{26}H_{43}O]^+$
368.1	33.01	$[C_{27}H_{44}]^+$
353.1	22.33	$[C_{26}H_{41}]^+$
301.1	33.20	$[C_{21}H_{33}O]^+$
275.1	33.40	$[C_{20}H_{35}]^+$
255.1	20.00	$[C_{19}H_{27}]^+$
231.0	17.67	$[C_{16}H_{23}O]^+$
213.1	27.96	$[C_{16}H_{21}]^+$
199.0	12.23	$[C_{15}H_{19}]^+$
178.0	12.43	$[C_{12}H_{32}O]^+$
173.1	14.95	$[C_{13}H_{17}]^+$
159.0	27.96	$[C_{12}H_{15}]^+$
145.0	40.00	$[C_{11}H_{13}]^+$
133.0	28.35	$[C_{10}H_{13}]^+$
119.0	31.84	$[C_9H_{11}]^+$
105.1	47.57	$[C_8H_9]^+$
95.1	48.74	$[C_7H_{11}]^+$
81.0	52.82	$[C_6H_9]^+$
69.0	38.06	$[C_5H_9]^+$
67.1	39.61	$[C_5H_7]^+$
57.1	52.62	$[C_4H_9]^+$
55.1	67.77	$[C_4H_7]^+$
43.1	100.00	$[C_3H_7]^+$
40.9	62.52	$[C_3H_5]^+$

Table 4.3

Infra red assignments of cholesterol

Band/cm^{-1}	Assignment
3430	Bonded OH
3040	CH stretching mode of >C=CH-
2960	Asymmetric stretching modes of CH_3 groups
2938	Asymmetric stretching modes of CH_2 groups
2900	CH group stretching vibration
2870	Symmetric stretching modes of CH_3 groups
2850	Symmetric stretching modes of CH_2 groups
1670-1620	>C=C< stretching vibrations
1468	Asymmetric deformation of CH_3 and CH_2 groups
1440	$>CH_2$ next to the double bond
1378/1368	symmetric deformations of CH_3 groups
1058	->C-O- stretching vibration

Table 4.4

^{1}H n.m.r. chemical shifts, δ_H, for cholesterol

δ_H(ppm)($CDCl_3$)

18-H	26/27-H	21-H
0.68	0.88	0.88
19-H	3-H	6-H
1.00	3.55	5.40

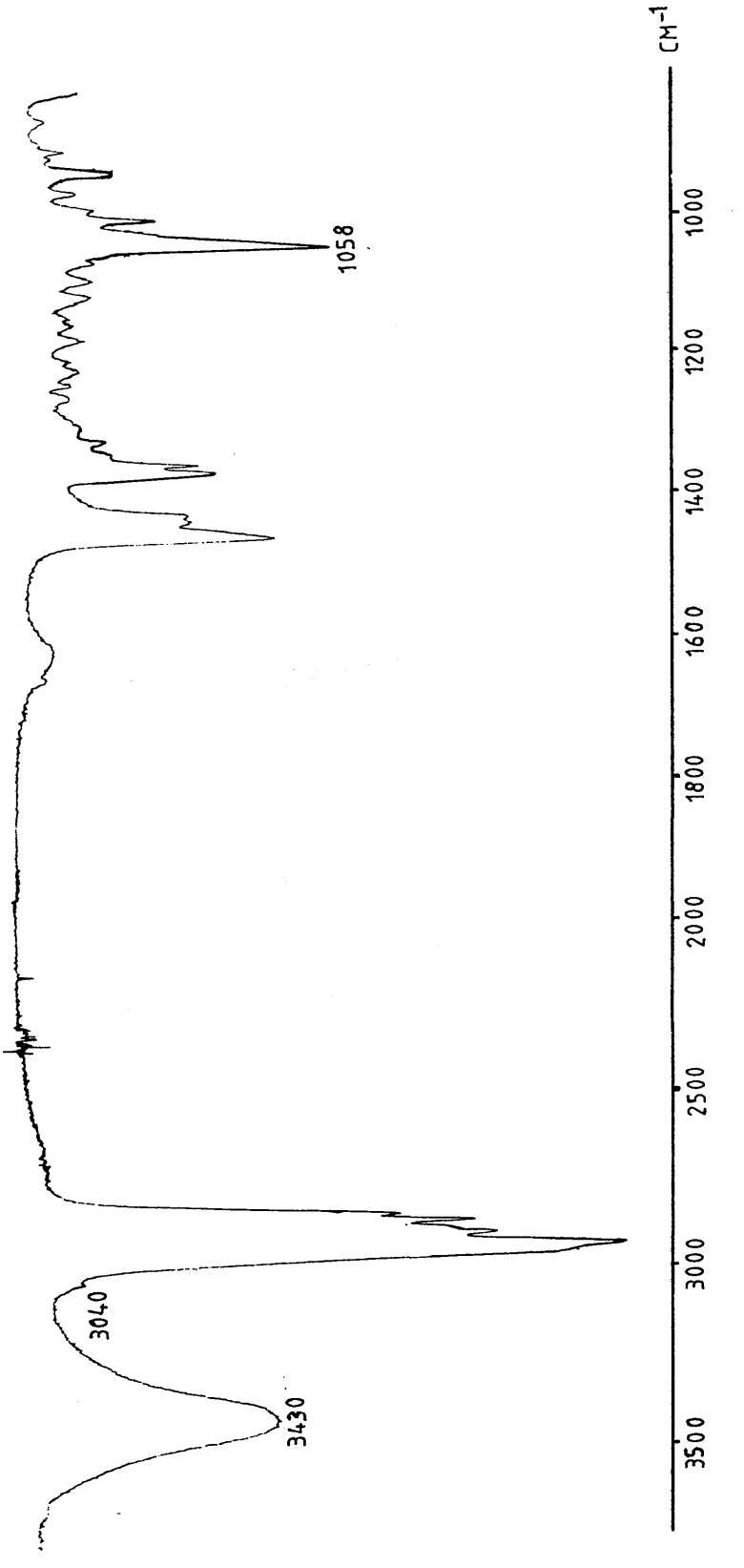

Figure 4.1 The infra red spectrum of cholesterol (KBr disc)

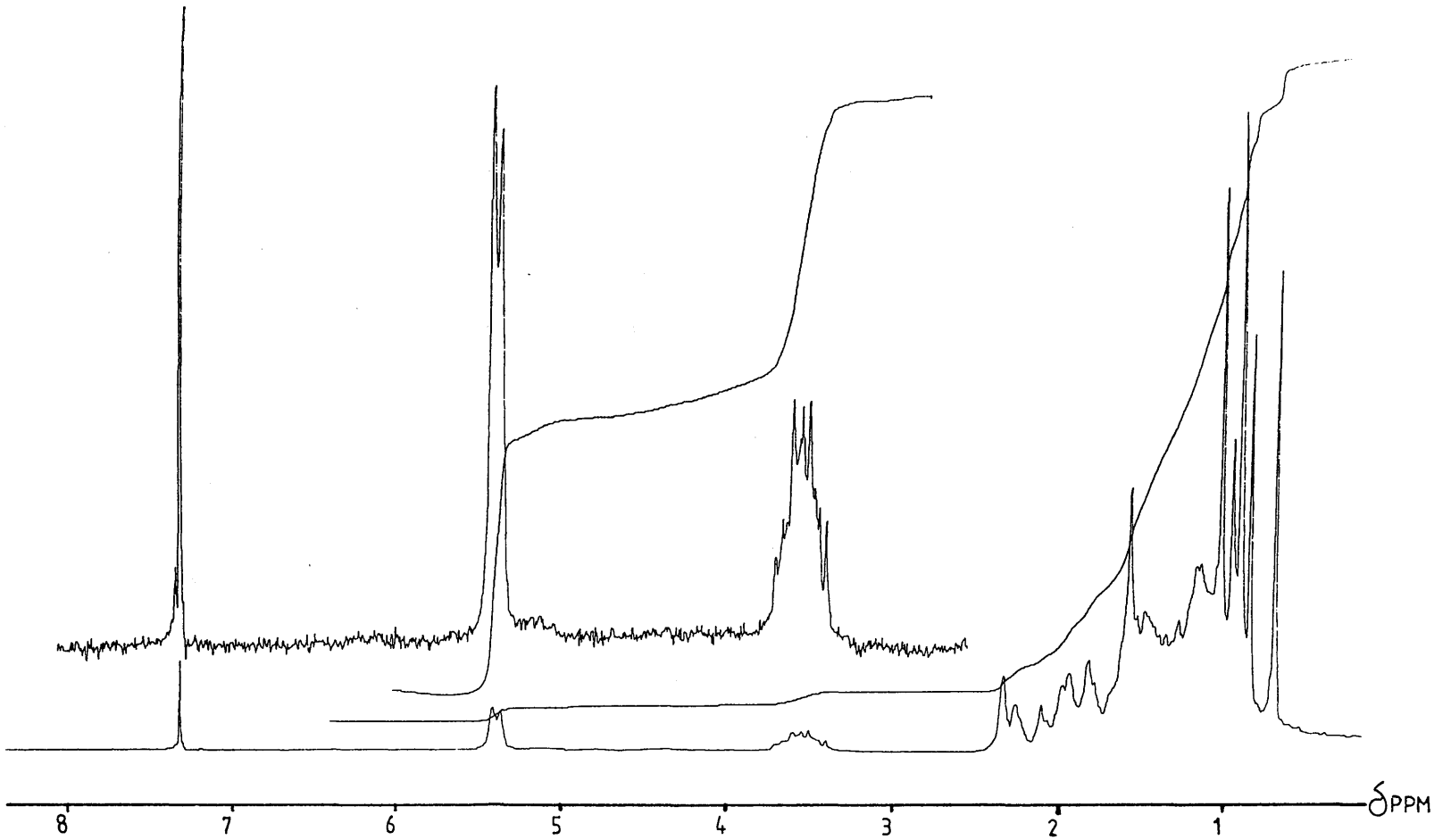

Figure 4.2 The 100.06 MHz ^{1}H n.m.r. spectrum of cholesterol in $CDCl_3$ solution, at ambient temperature

4.1.1.1 Cholesterol : $NaNO_2$ = 1:1

Figures 4.3 and **4.4** are infra red (KBr disc) and ^1H n.m.r. spectra, respectively, of the products that are obtained when 0.01M of solid cholesterol is treated, at ambient temperature, with 0.01M of $NaNO_2$ in the presence of acetic acid, using blue light and allowing a minimum amount of air into the reaction vessel.

The relative intensity of the bonded OH absorption, at 3430 cm^{-1}, in **Figure 4.3** has only 50% of its original intensity in pure cholesterol. The C–O stretching vibration intensity, at 1058 cm^{-1}, has also been slightly reduced in intensity. However, the >C=C< stretching vibrational frequency and its relative intensity are unaffected by these manipulations. The infra red spectrum, **Figure 4.3**, shows quite clearly that, under the conditions of the reaction, 50% of the cholesterol OH residue has reacted, and a nitrosite has not been formed. The following absorption peaks assigned to a nitrite residue are present in **Figure 4.3**.

1640 cm^{-1}: NO stretch 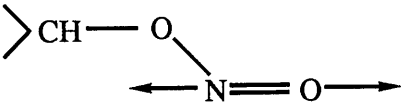 of the trans-isomer

1600 cm^{-1}: NO stretch 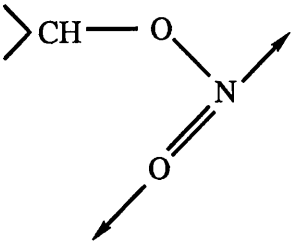 of the cis-isomer

821 cm^{-1}: =N-O stretch 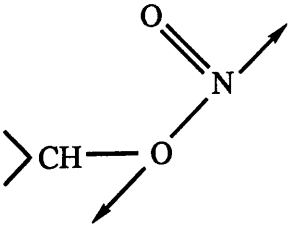 of the cis-isomer

787 cm^{-1}: =N-O stretch 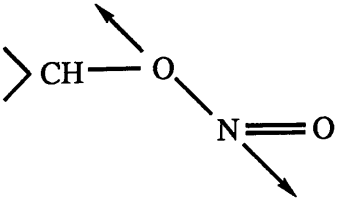 of the trans-isomer

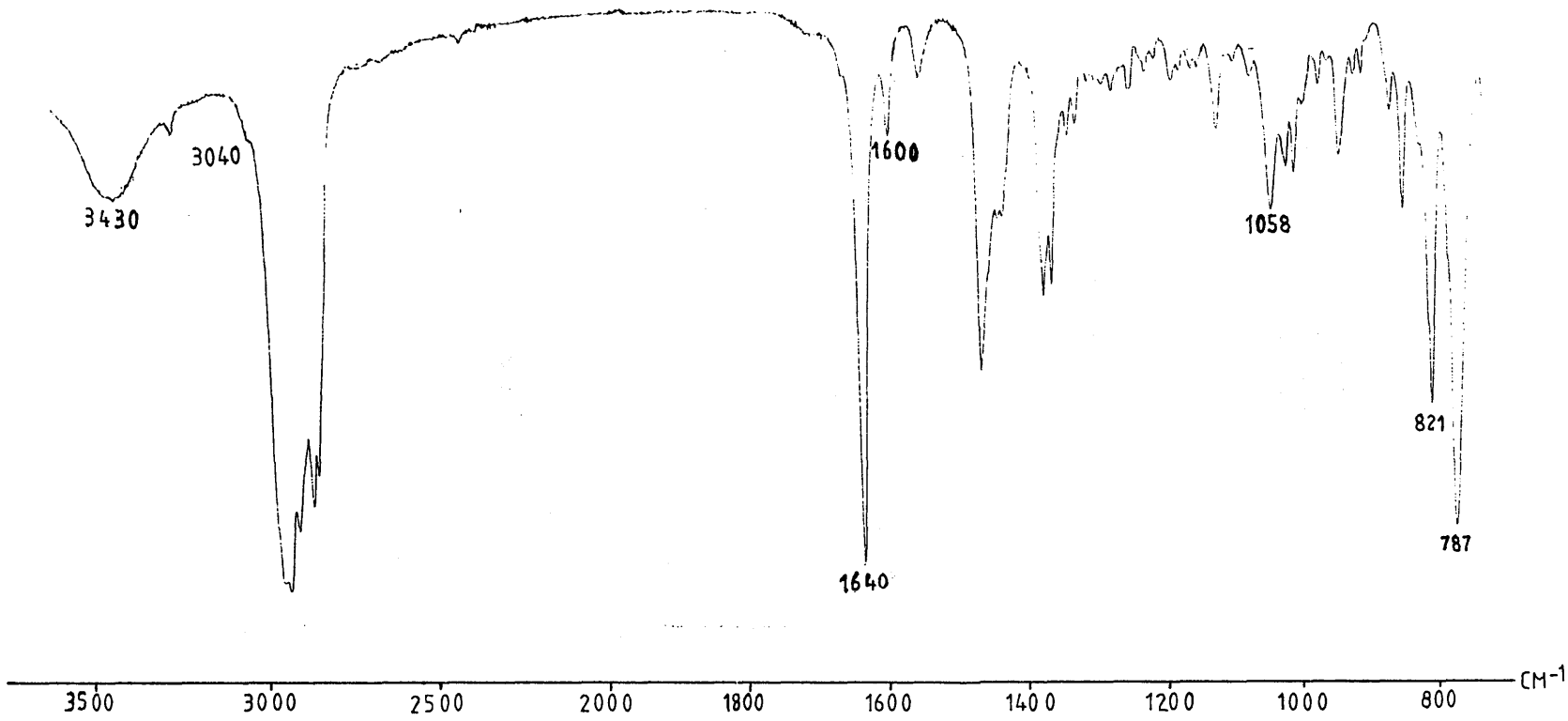

Figure 4.3 The infra red spectrum of the products obtained from the reaction of cholesterol : $NaNO_2$ = 1:1 (KBr disc)

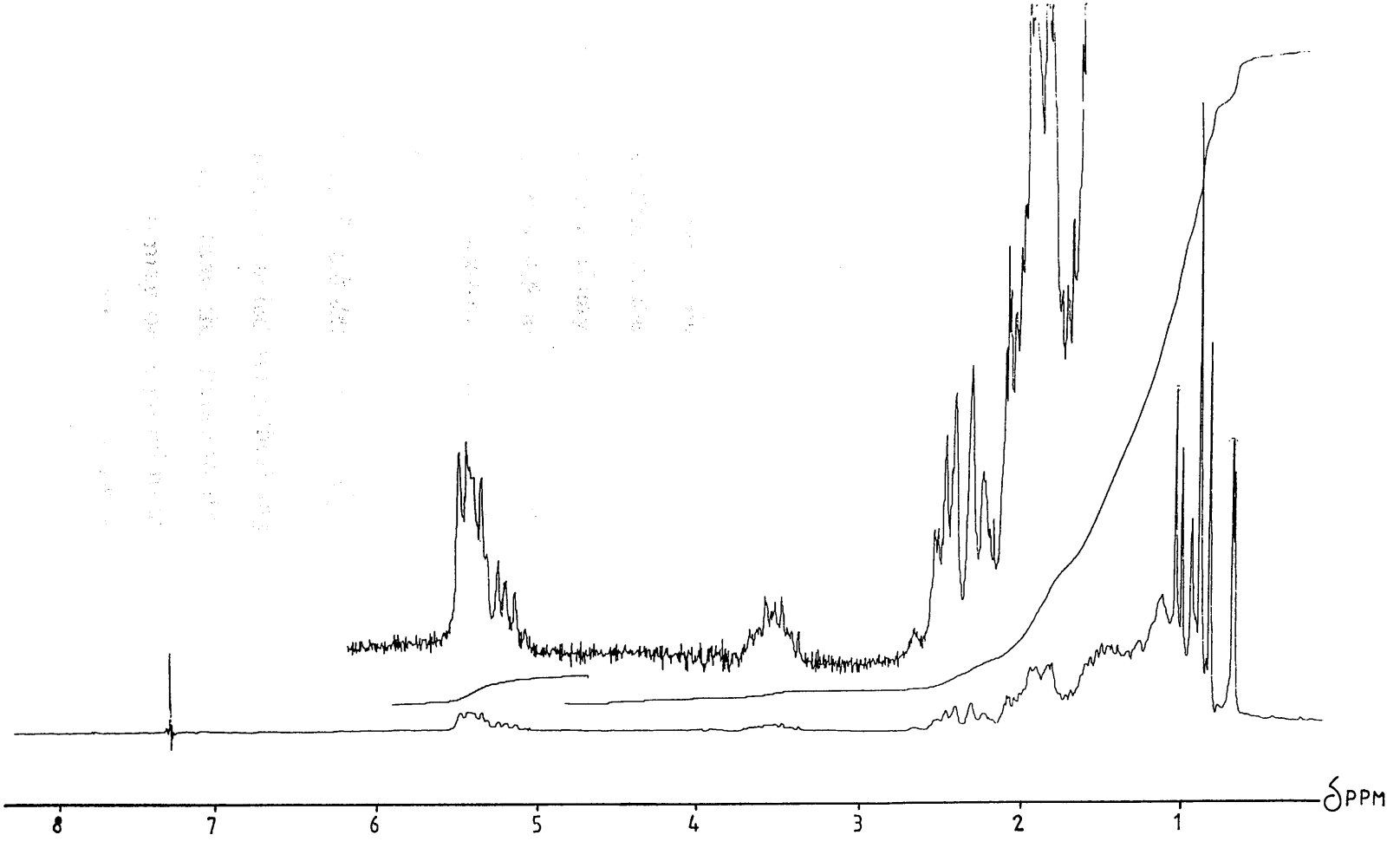

Figure 4.4 The 100.06 MHz ^{1}H n.m.r. spectrum of the products obtained from the reaction of cholesterol : $NaNO_2$ = 1:1 in $CDCl_3$ solution, at ambient temperature

The spectrum, in **Figure 4.3**, shows no evidence of infra red absorption of nitrate (1660-1625 cm^{-1} and 1285-1270 cm^{-1}),[107] nitro (1556-1545 cm^{-1} and 1390-1355 cm^{-1})[108] or nitroso monomer (1621-1539 cm^{-1}),[1] residues. It follows that under these conditions, cholesterol and acidified sodium nitrite react to form the ester cholesteryl nitrite *only*.

These conclusions are confirmed by the ^1H n.m.r. spectrum of the reaction products in $CDCl_3$, **Figure 4.4**. This also shows quite clearly that the >C(5)=C(6)< residue of cholesterol, at 5.40 ppm, is not affected.

4.1.1.2 Cholesterol : $NaNO_2$ = 1:3

Similar procedures carried out on a mixture of cholesterol : $NaNO_2$ in a ratio of 1:3, see **Figures 4.5** and **4.6** respectively, show that all of the $-$C(3)-OH residue of cholesterol has now been converted. **Figure 4.5** shows that all the cholesterol OH residue has disappeared and there is still no trace of any nitrate, nitro-alkyl or even nitroso-alkyl.

Figures 4.5 and **4.6** both show that *the olefinic residue of cholesterol, again, has not been affected by this reaction procedure.*

4.1.1.3 Cholesterol : $NaNO_2$ = 1:8

Yields obtained in synthesizing alkyl nitrosites are notoriously low, and so more than the theoretically minimum amount of cholesterol : $NaNO_2$ = 1:4 may be required to attack functional groups, in order to obtain a reasonable amount of nitrosite in the reaction products. However, if too large an excess amount of sodium nitrite is used in the reaction, then the excess NO and NO_2 that are generated can complicate

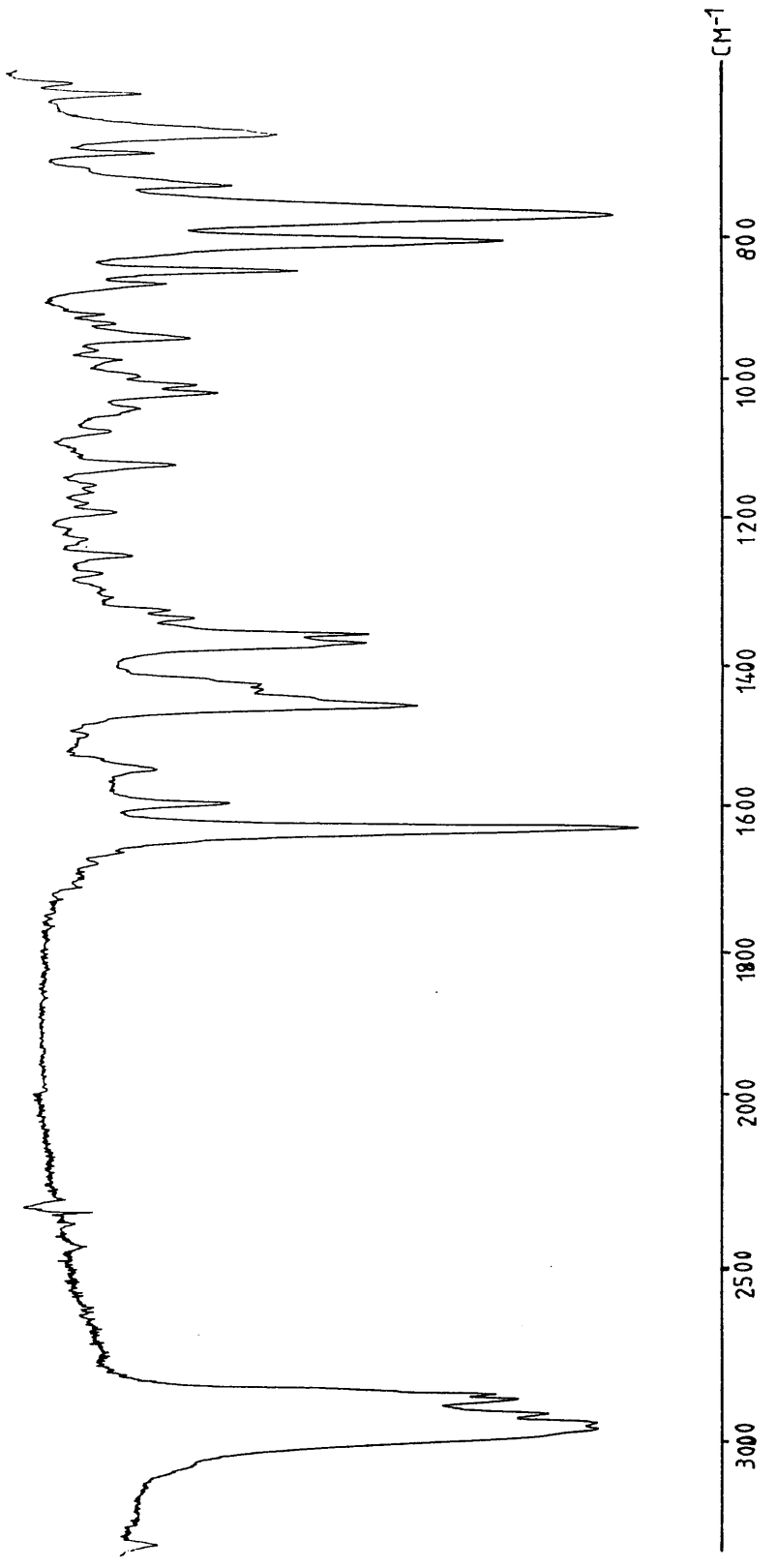

Figure 4.5 The infra red spectrum of the products obtained from the reaction of cholesterol : $NaNO_2$ = 1:3 (KBr disc)

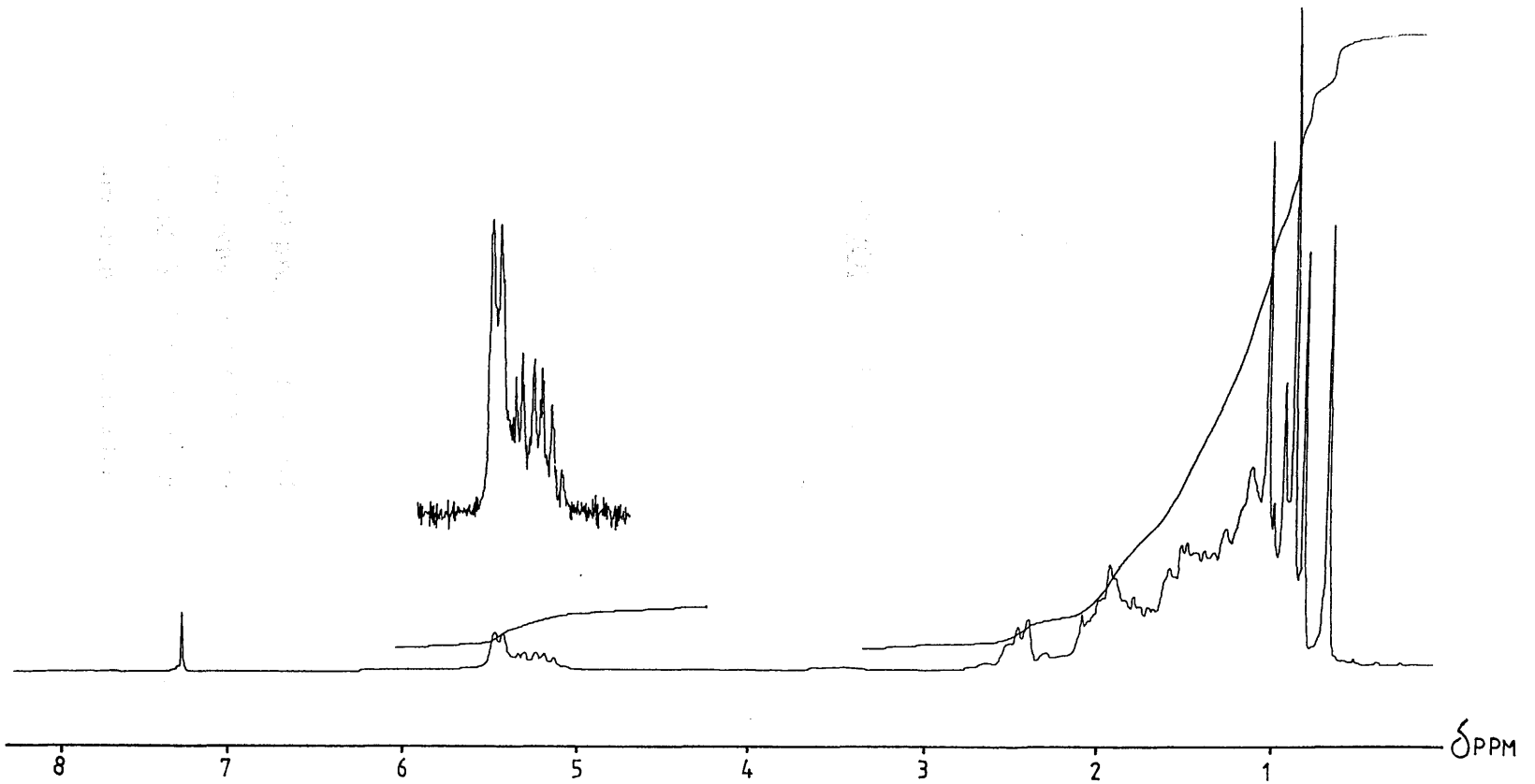

Figure 4.6 The 100.06 MHz ^{1}H n.m.r. spectrum of the products obtained from the reaction of cholesterol : $NaNO_2$ = 1:3 in $CDCl_3$ solution, at ambient temperature

matters as a result of their further secondary reactions with the nitrosites. Some compromise must therefore be made of the amount of $NaNO_2$ that is used. For these reasons, a third experiment was carried out in which the ratio of cholesterol : $NaNO_2$ is 1:8.

Infra red and ^1H n.m.r. spectra obtained from the products are shown in **Figures 4.7** and **4.8** respectively. They do not show any dramatic changes from the corresponding spectra of cholesterol : $NaNO_2$ = 1:3, **Figures 4.5** and **4.6**, and it therefore follows that no matter what amount of $NaNO_2$ is used under these conditions, only the nitrite ester of cholesterol is formed. The >C(5)=C(6)< olefinic residue does not react under these conditions.

4.1.2 CHOLESTERYL-PROPIONATE

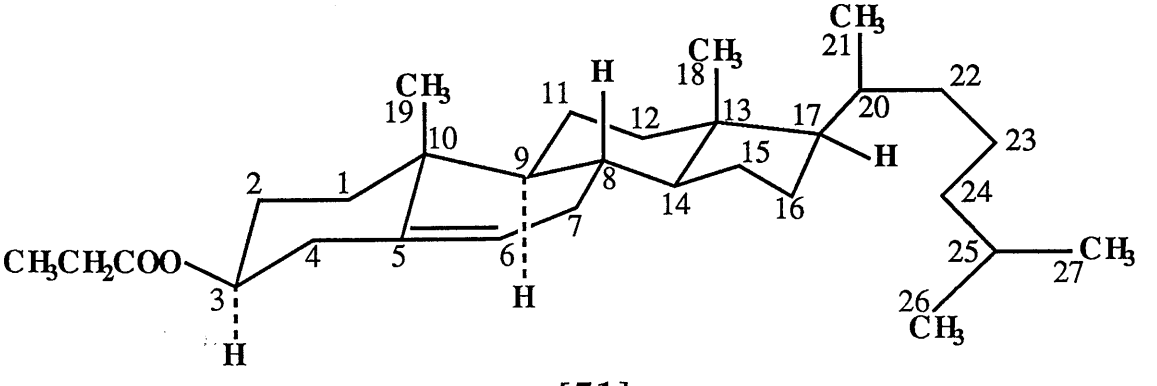

[71]

Cholesteryl-propionate, $C_{30}H_{50}O_2$, **[71]**, obtained from Professor C.J.W. Brooks, was purified by recrystallizing it once from petroleum ether (40-60) and finally checking its purity by means of thin layer chromatography, using silica gel and hexane-ethylacetate (1:1) as eluent. The microanalytical data for the purified sample of **[71]** are listed in **Table 4.5**.

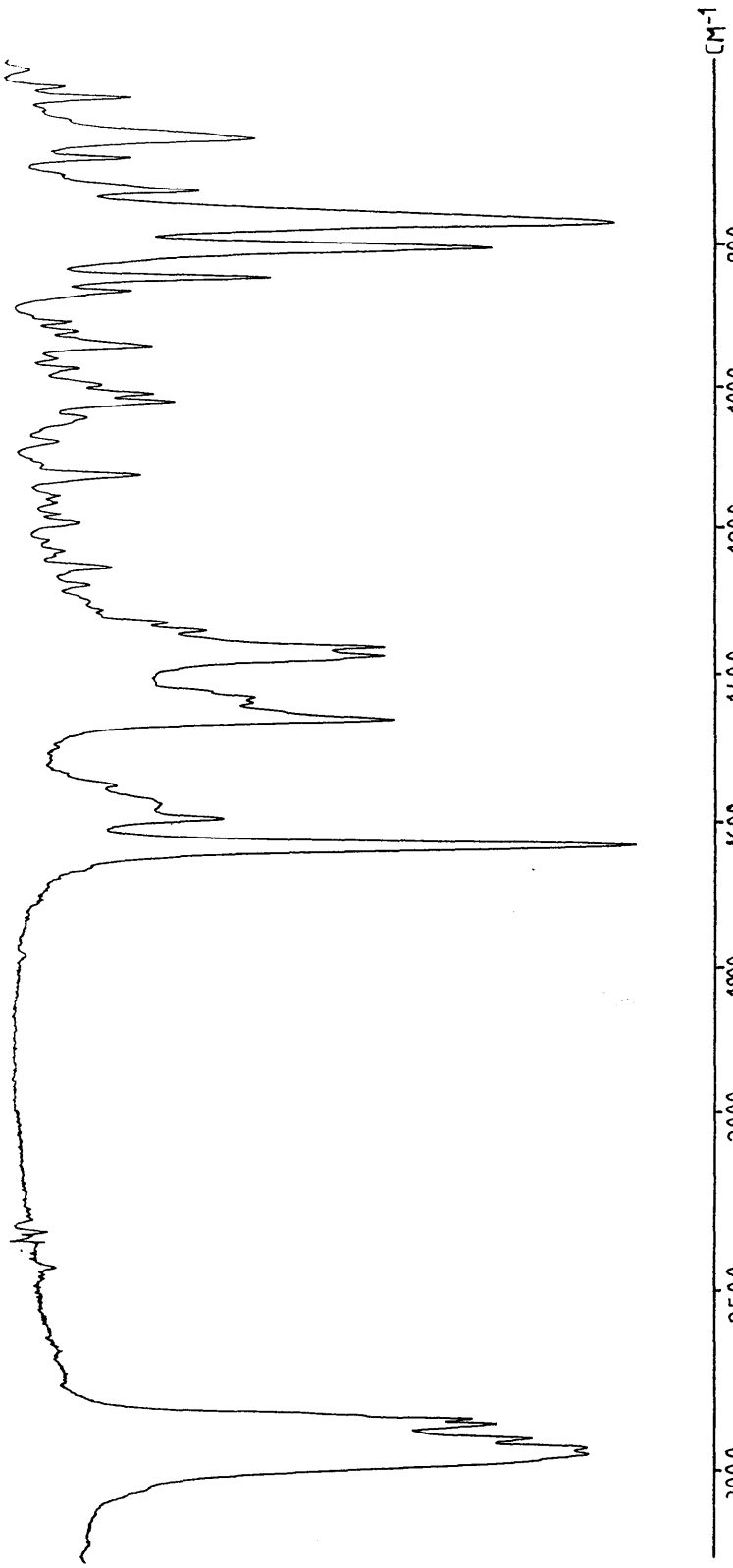

Figure 4.7 The infra red spectrum of the products obtained from the reaction of cholesterol : $NaNO_2$ = 1:8 (KBr disc)

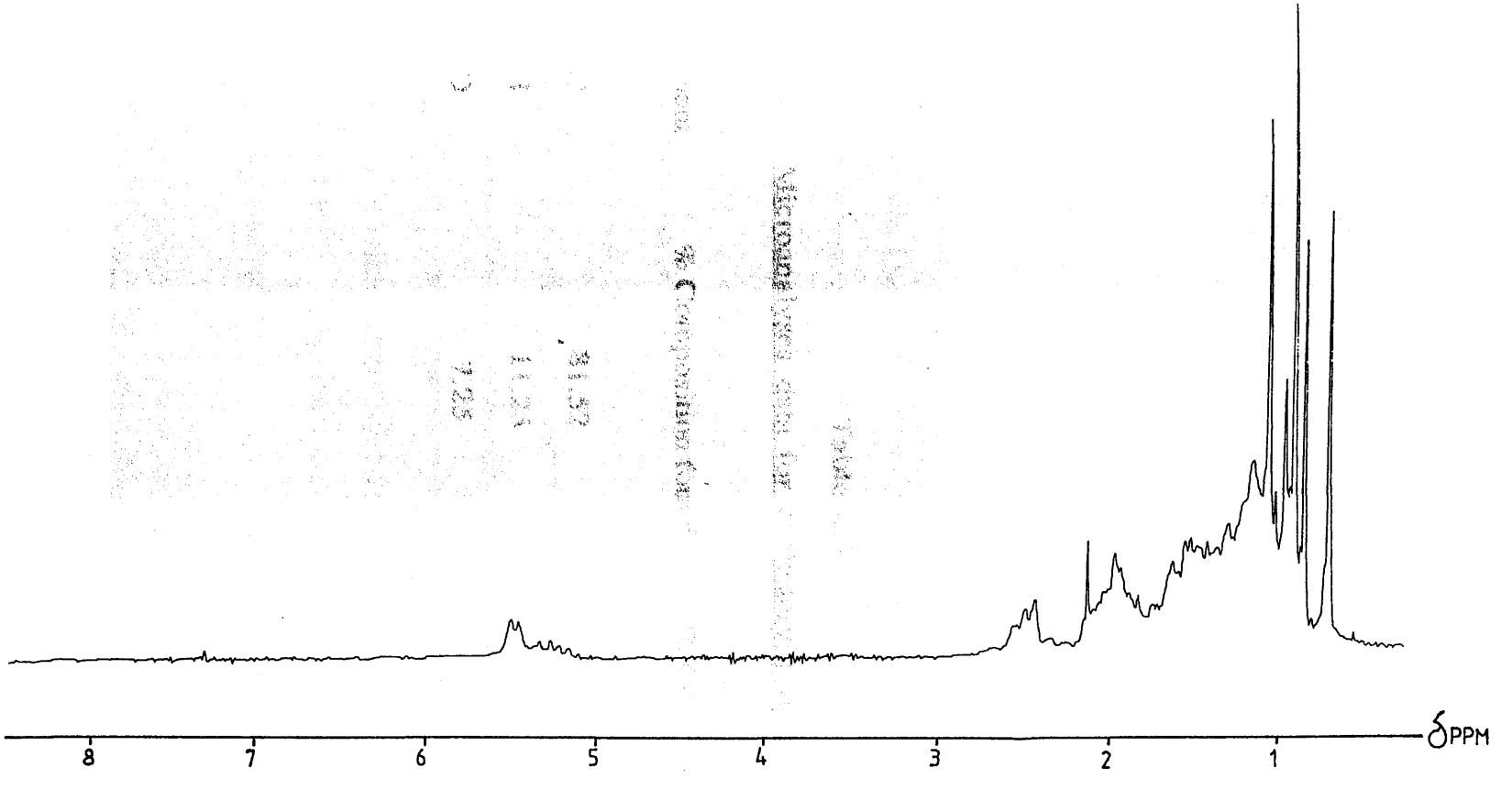

Figure 4.8 The 100.06 MHz ^{1}H n.m.r. spectrum of the products obtained from the reaction of cholesterol : $NaNO_2$ = 1:8 in $CDCl_3$ solution, at ambient temperature

Table 4.5

Microanalyses data for cholesteryl-propionate

Element	% Composition found	% Composition [expected for $C_{30}H_{50}O_2$]
C	81.52	81.45
H	11.23	11.31
O	7.25	7.24

Its infra red spectrum was then recorded, **Figure 4.9**. It shows particularly the characteristic peaks of an ester >C=O stretch frequency at 1732 cm^{-1}, $\geq$C-O- stretch frequency at 1200 cm^{-1} and a $\geq$C-O- bond stretching vibration of a secondary alcohol at 1082 cm^{-1}.

But, apart from these, almost all its other i.r. peaks are already present in the infra red spectrum of cholesterol, **Figure 4.1**.

4.1.2.1 Cholesteryl-Propionate : $NaNO_2$ = 1:1

Since cholesteryl-propionate contains only one double bond, and it can also be hydrolysed by the nitrous acid formed, it was decided to treat this substance with different amounts of $NaNO_2$ too.

The infra red spectrum of the products that are obtained when solid cholesteryl-propionate is treated with an equimolar amount of $NaNO_2$ and acetic acid was also recorded, **Figure 4.10**. It shows that in this reaction, very little seems to have happened, but two extra weak peaks appear in the infra red spectrum, at 1640 cm^{-1} and at 1560 cm^{-1}. This spectrum also shows quite clearly that neither a nitro- nor a nitrato- nor a nitroso- residue have been formed in this reaction. It also shows that the double bond is certainly not affected by the reaction procedures. The small additional peaks in the infra red spectrum reveal the presence of a small amount of cholesteryl nitrite (1640 cm^{-1}) and a small amount of an acid anion $RCOO^-$, indicating that a small amount of the cholesteryl-propionate has reacted.

$$C_{30}H_{50}O_2 + HNO_2 \xrightarrow[\text{sodium acetate buffer}]{} C_{27}H_{45}NO_2 + CH_3\text{-}CH_2\text{-}COOH$$

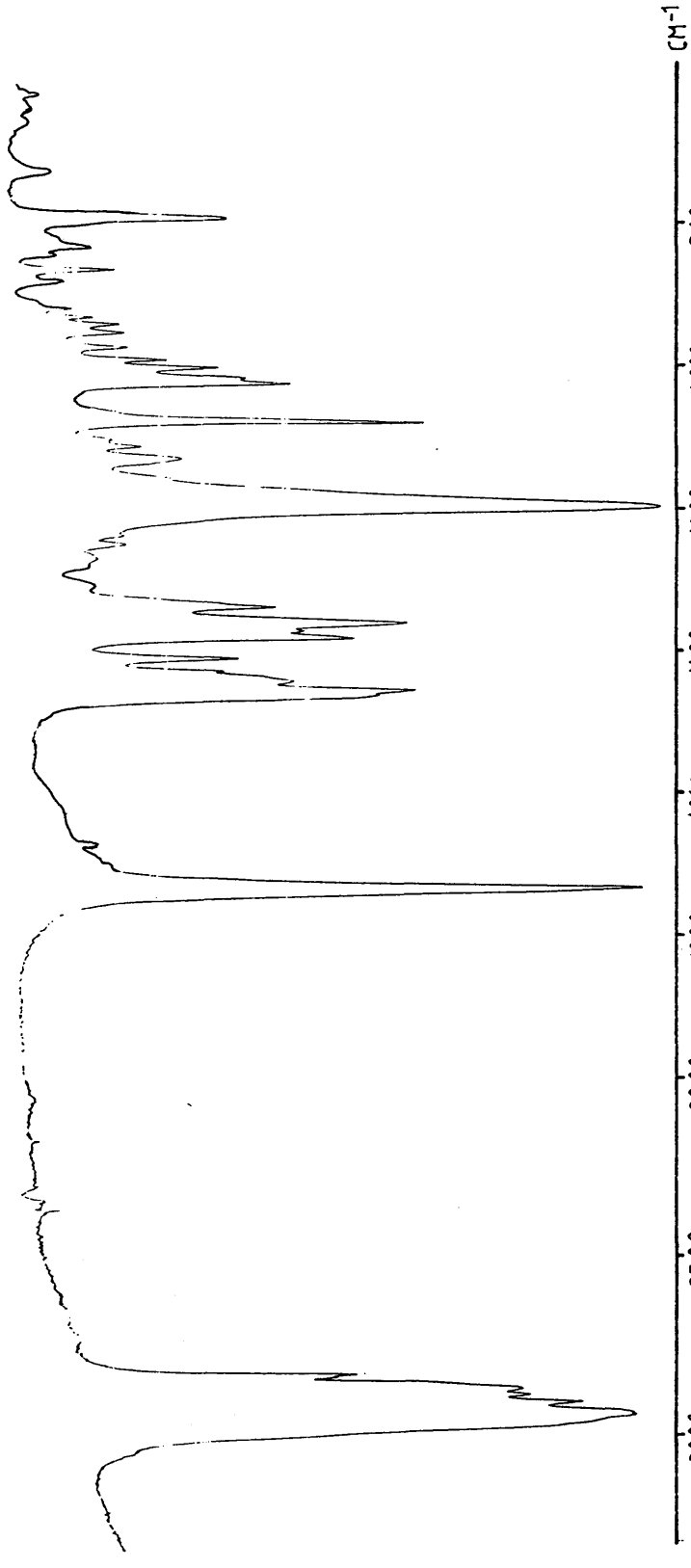

Figure 4.9 The infra red spectrum of cholesteryl-propionate (KBr disc)

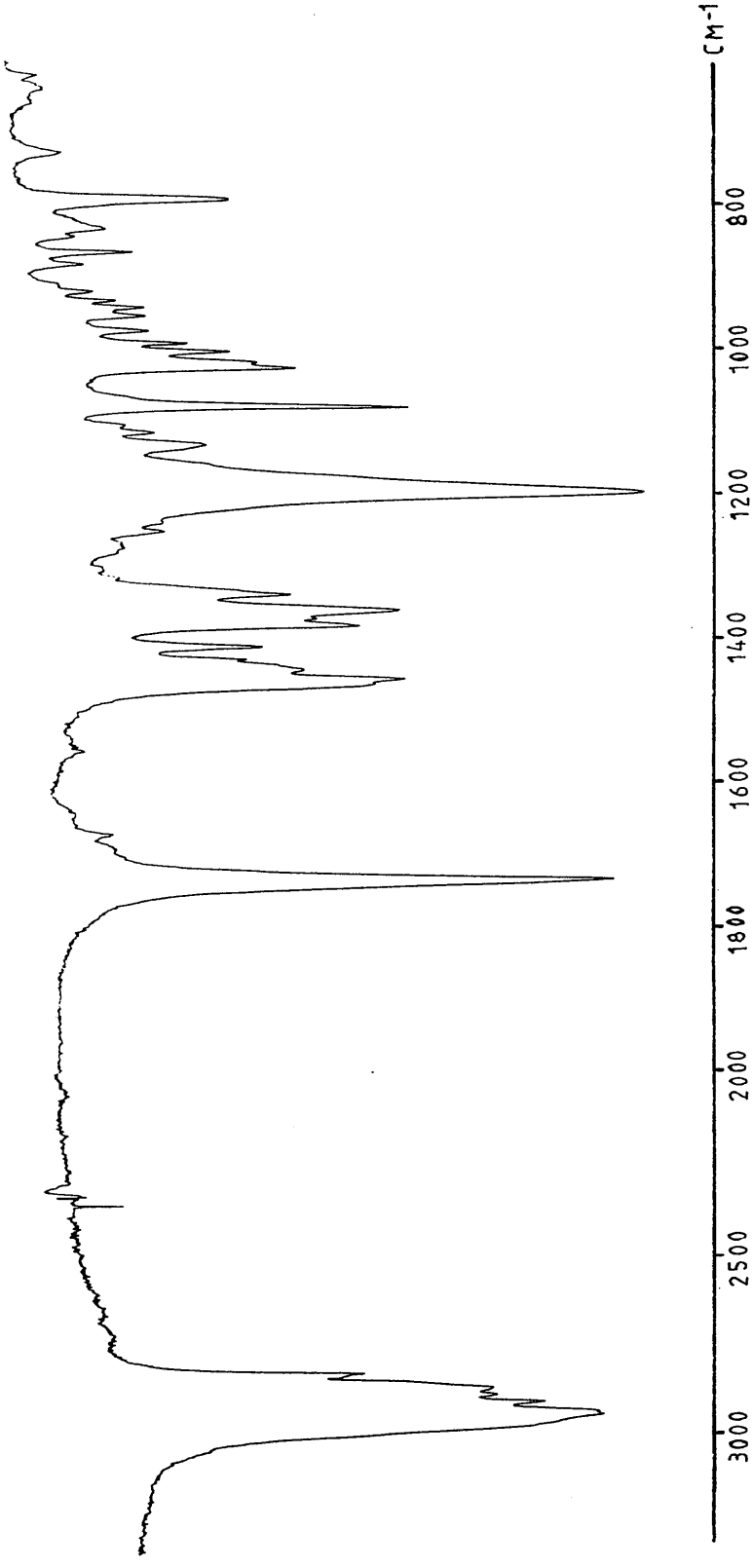

Figure 4.10 The infra red spectrum of the products obtained from the reaction of cholesteryl-propionate : $NaNO_2$ = 1:1 (KBr disc)

A thin layer chromatogram of the reaction products only reveals the presence of the original cholesteryl-propionate. This confirms that there has been very little effect on the original cholesteryl-propionate ester. The amounts of cholesteryl nitrite and sodium propionate formed are too small to be detected chromatographically.

4.1.2.2 Cholesteryl-Propionate : $NaNO_2$ = 1:3

On increasing the relative amounts of $NaNO_2$ and CH_3COOH by a factor of three and examining the reaction products by means of infra red spectroscopy, **Figure 4.11** was obtained. It quite clearly shows a markedly increased intensity of the weak peaks at 1640 cm^{-1} and 1560 cm^{-1}. Again, there is no evidence whatever of any reaction with the double bond. There is no evidence for the formation of a nitro-, or a nitrato- or even a nitroso- residue. As in the case of experiment *4.1.2.a*, the only thing that seems to have happened is that HNO_2 has caused a small amount of hydrolysis of the cholesteryl-propionate to take place, forming a small amount of cholesteryl nitrite and sodium propionate.

As in the case of cholesterol itself, the ester residue also appears to be protecting the cholesterol frame-work from attack by the oxides of nitrogen.

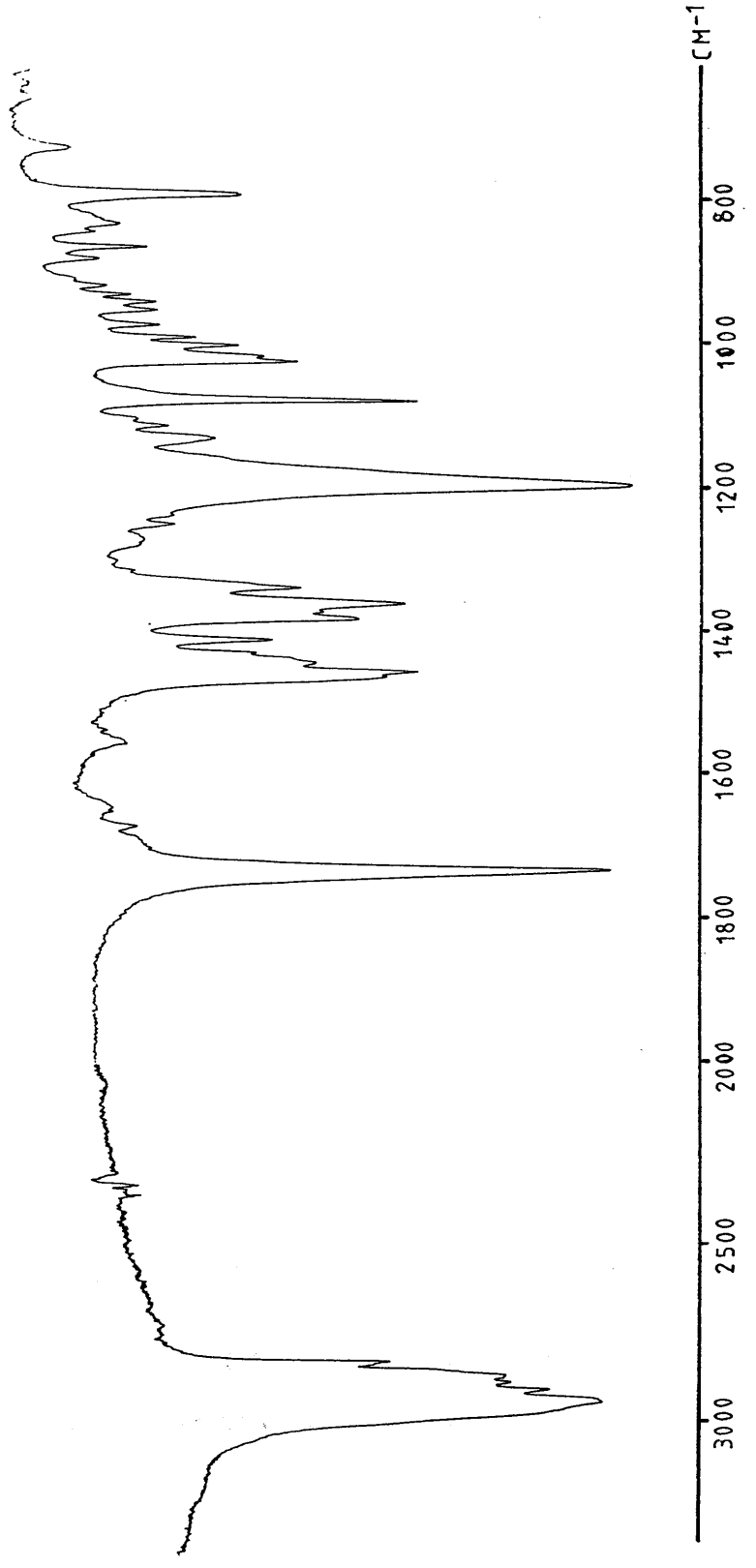

Figure 4.11 The infra red spectrum of the products obtained from the reaction of cholesteryl-propionate : $NaNO_2$ = 1:3 (KBr disc)

4.1.3 (-)-(7)-DEHYDROCHOLSTEROL:

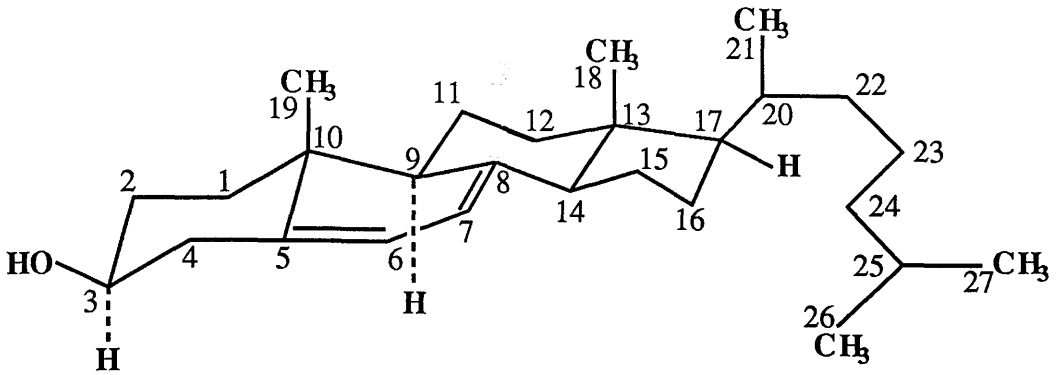

[72]

(-)-(7)-Dehydrocholesterol, (-)-cholesta-5,7-dien-3β-ol, $C_{27}H_{44}O$, **[72]**, obtained from Aldrich Chemical Company Inc., was used without further purification and was kept frozen. During all the experimental work, this compound was handled under nitrogen as it is air sensitive. Its C- and H- microanalytical and mass spectral data are listed in **Tables 4.6** and **4.7** respectively. Each peak in its infra red, ^{1}H n.m.r. and ^{13}C-$\{^{1}H\}$ n.m.r. spectra were then assigned. These spectra are shown in **Figures 4.12**, **4.13** and **4.14** respectively. Assignments obtained from the infra red, ^{1}H n.m.r.and ^{13}C n.m.r spectra are shown in **Tables 4.8**, **4.9** and **4.10** respectively.

4.1.3.1 The reaction of (-)-(7)-dehydrocholesterol with N_2O_3

A sample of (-)-(7)-dehydrocholesterol **[72]** was allowed to react with an equimolar amount of aqueous $NaNO_2$ and acetic acid under the same reaction conditions already outlined for cholesterol and cholesteryl-propionate. Analysis of the products by thin layer chromatography using

Table 4.6

Microanalyses data for (-)-(7)-dehydrocholesterol

Element	% Composition found	% Composition [expected for $C_{30}H_{50}O_2$]
C	84.50	84.38
H	11.44	11.46
O	4.06	4.16

Table 4.7
Electron impact mass spectrum of (-)-(7)-dehydrocholesterol [72]

Mass	Relative abundance (%)	Ion
384.1	61.95	$[C_{27}H_{44}O]^+$
366.1	11.22	$[C_{27}H_{42}]^+$
351.1	71.57	$[C_{26}H_{39}]^+$
325.1	40.09	$[C_{23}H_{33}O]^+$
271.1	10.79	$[C_{19}H_{27}O]^+$
253.1	15.60	$[C_{19}H_{25}]^+$
211.1	22.59	$[C_{16}H_{19}]^+$
199.0	12.23	$[C_{15}H_{19}]^+$
197.1	19.53	$[C_{15}H_{17}]^+$
185.1	12.23	$[C_{14}H_{17}]^+$
183.1	19.53	$[C_{14}H_{15}]^+$
178.0	12.43	$[C_{11}H_{30}O]^+$
171.0	24.78	$[C_{13}H_{15}]^+$
169.0	18.08	$[C_{13}H_{13}]$
157.1	33.01	$[C_{12}H_{13}]^+$
155.1	17.49	$[C_{12}H_{11}]^+$
143.1	50.87	$[C_{11}H_{11}]^+$
119.0	28.43	$[C_9H_{11}]^+$
105.1	26.09	$[C_8H_9]^+$
95.1	24.20	$[C_7H_{11}]^+$
81.0	32.07	$[C_6H_9]^+$
69.0	29.01	$[C_5H_9]^+$
55.2	52.04	$[C_4H_7]^+$
43.2	100.00	$[C_3H_7]^+$
41.0	62.39	$[C_3H_5]^+$

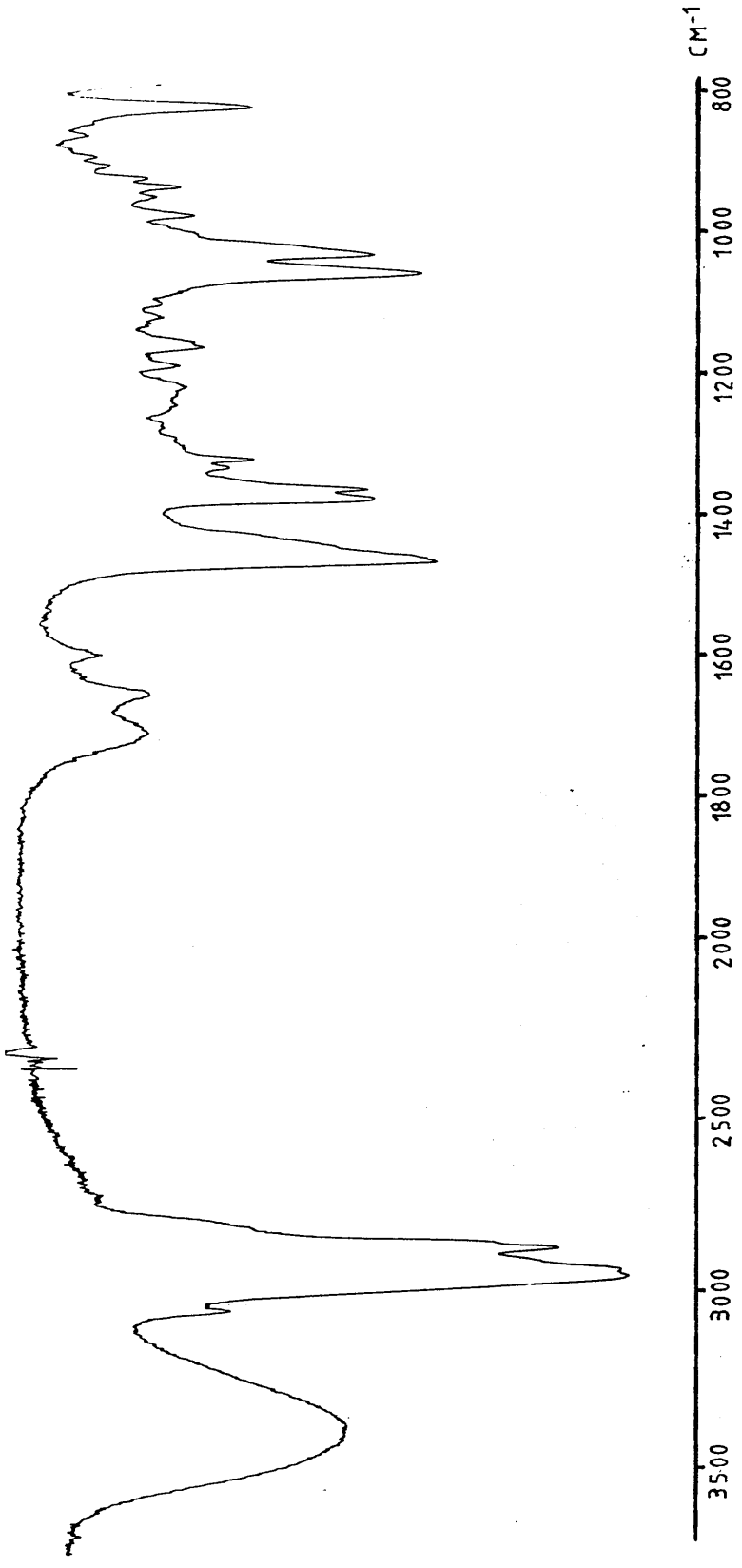

Figure 4.12 The infra red spectrum of (-)-(7)-dehydrocholesterol (KBr disc)

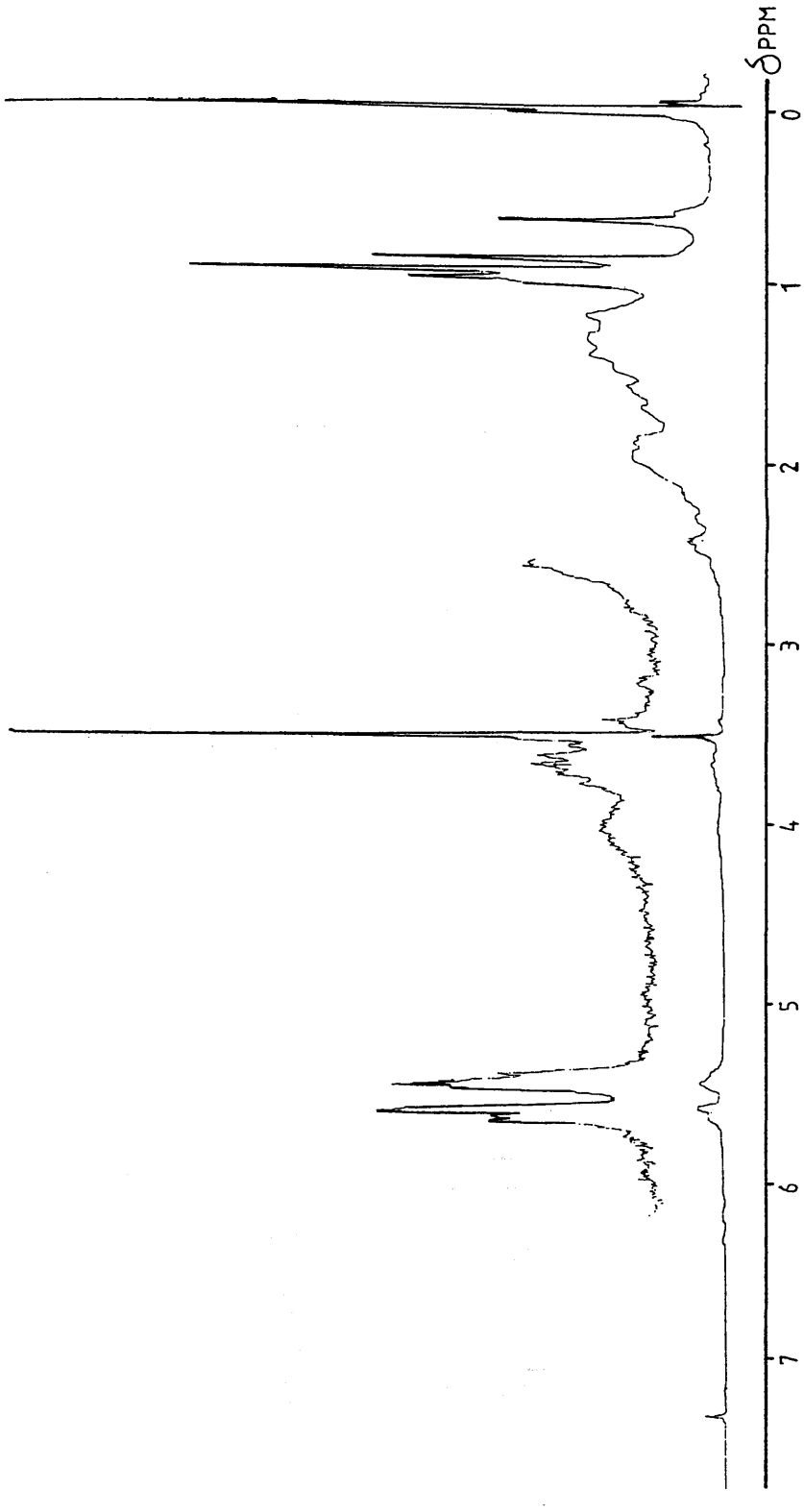

Figure 4.13 The 100.06 MHz ^{1}H n.m.r. spectrum of (-)-(7)-dehydrocholesterol in $CDCl_3$ solution, at ambient temperature

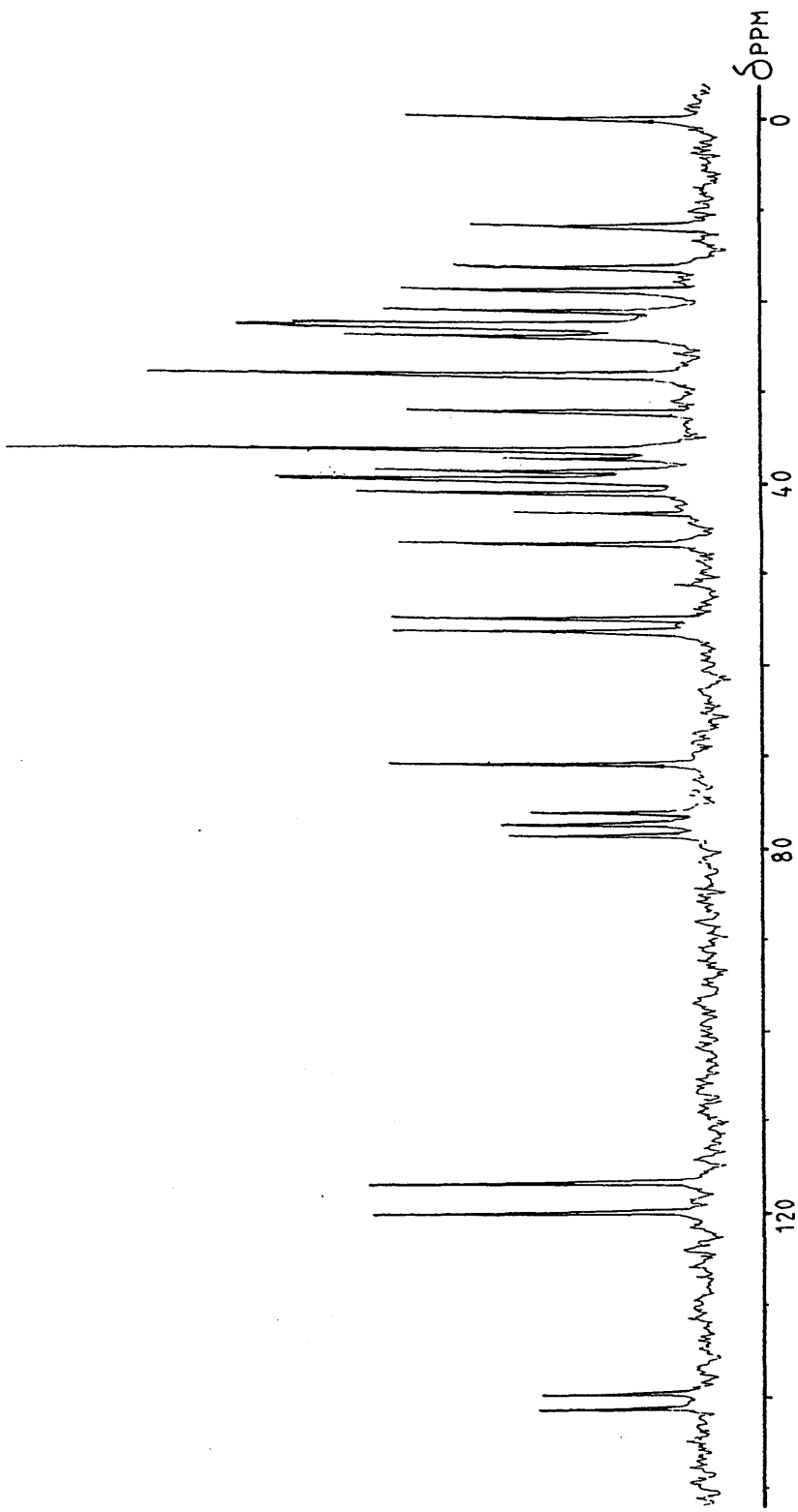

Figure 4.14 (A) The 25.160 MHz ^{13}C-{^{1}H} n.m.r. spectrum of (-)-(7)-dehydrocholesterol in $CDCl_3$ solution, at ambient temperature

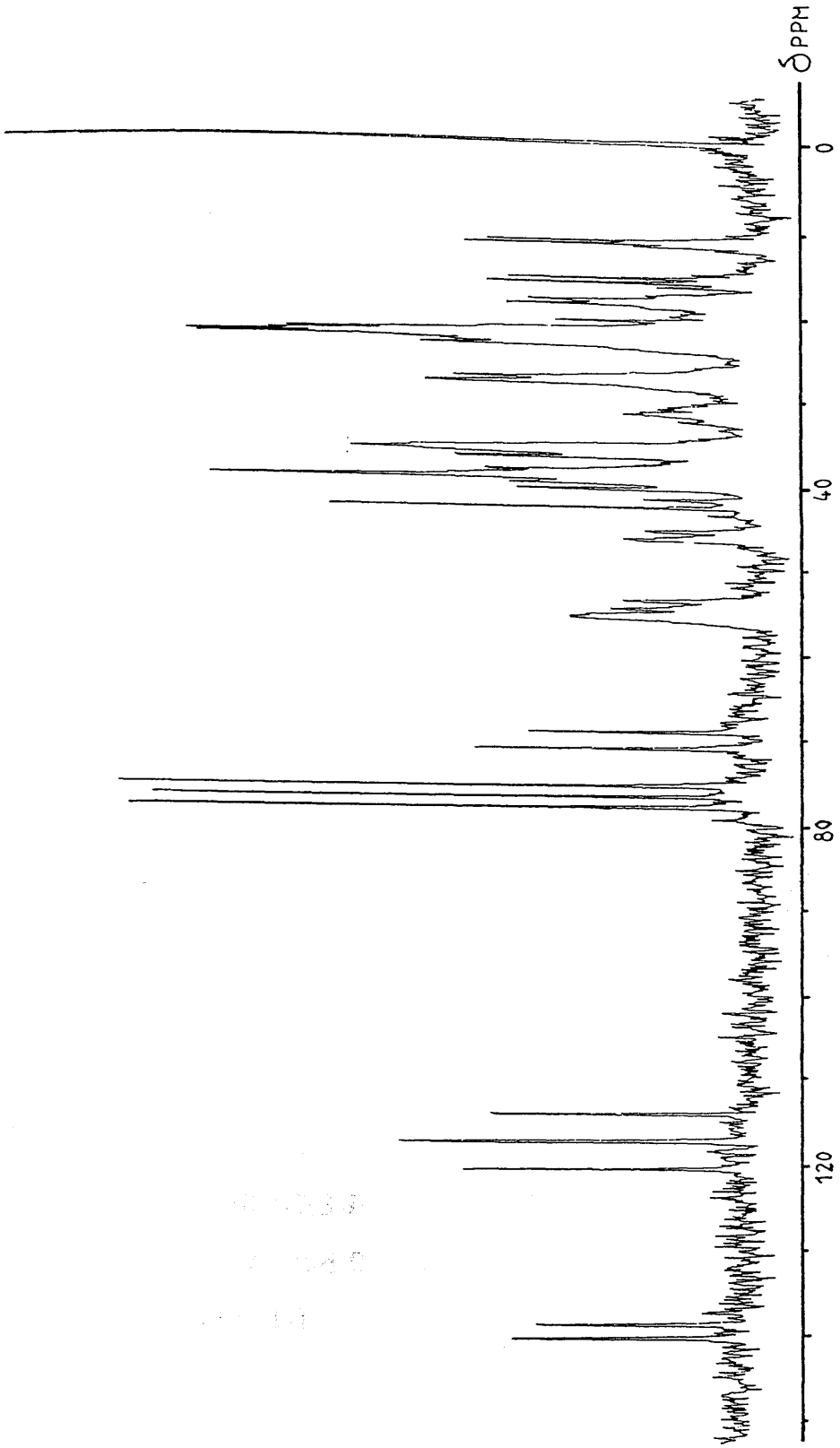

Figure 4.14 (B) The 25.160 MHz ^{13}C n.m.r. spectrum of (-)-(7)-dehydrocholesterol in $CDCl_3$ solution, at ambient temperature

Table 4.8

Infra red assignments of (-)-7-dehydrocholesterol

ν_{max} (cm^{-1})/(KBr disc)

3380 [bonded OH]; 3040 [=C(6)-H and =C(7)-H]; 2950, 2930, 2870, 2855, and 1468 [CH_3 and CH]; 1710 [>C=O, considered as an impurity]; 1655, 1600, 832, and 800 [2xC=C]; 1378, and 1368 [$>C(CH_3)_2$]; 1062, and 1039 [C-O].

Table 4.9

^{1}H n.m.r. chemical shifts, δ_H, for (-)-7-dehydrocholesterol

δ_H (ppm)/($CDCl_3$)

5.62 and 5.44 [2H, AB specrum, J_{AB}=6Hz, =C(6)H-C(7)H=], 3.68 [C(3)-H], 3.58 [C(3)H-OH], 2.42 [C(4)-He], 2.15 [C(4)-Ha], 0.99 [$C(19)H_3$], 0.99 and 0.94 [C(20)H-$C(21)H_3$], 0.94 and 0.88 [C(25)H] and 0.66 [$C(18)H_3$].

Table 4.10

^{13}C n.m.r. chemical shifts, δ_C, for (-)-7-dehydrocholesterol

CARBON NUMBER	CHEMICAL SHIFT	MULTIPLICITY
1	39.262	t
2	32.016	t
3	70.483	d
4	36.159	t
5	141.445	s
6	119.659	d
7	116.324	d
8	139.801	s
9	55.963	d
10	38.423	s
11	21.161	t
12	23.915	t
13	42.963	s
14	54.543	d
15	23.023	t
16	39.517	t
17	46.302	d
18	22.832	q
19	22.594	q
20	37.054	d
21	18.865	q
22	36.159	t
23	40.814	t
24	32.016	t
25	28.061	d
26/27	11.846/16.310	q/q

hexane:ethylacetate = 1:1 as eluent showed that two other species are present in the products, in addition to the unsaturated (-)-(7)-dehydrocholesterol. The unreacted (-)-(7)-dehydrocholesterol was then removed from the reaction products by extracting it with petroleum ether (40-60).

The electron impact mass spectrum, infra red spectrum, ^{1}H n.m.r. and ^{13}C n.m.r. spectra of the residual products are shown in **Table 4.11** and in **Figures 4.15**, **4.16**, and **4.17** respectively.

The infra red spectrum, in **Figure 4.15**, clearly shows that the OH absorption at 3380 cm^{-1} in **[72]** has not been affected at all by this reaction, contrary to the OH residue of cholesterol. However, the (-)-(7)-dehydrocholesterol olefinic >C= and -CH= stretches are no longer present in these residues, and hence addition across the olefinic system of **[72]** has taken place. Furthermore, these reaction products exhibit the following peaks in the infra red spectrum[90]

υmax (KBr)	1630, 1275, 838 and 732 ($R\text{-}ONO_2$)
	1540, 1340 and 860 ($R\text{-}NO_2$)

Reaction of (-)-(7)-dehydrocholesterol therefore produces a mixture of compounds containing alkyl nitrate, $R\text{-}ONO_2$, and nitro-alkane, $R\text{-}NO_2$, residues. Furthermore, in these reaction products, the $R\text{-}ONO_2$ absorption at 1630 cm^{-1} has almost the same intensity as the absorption at 1540 cm^{-1}, i.e. the reaction products contain essentially equal amounts of $R\text{-}ONO_2$ and $R\text{-}NO_2$ residues: this point follws immediately when the relative intensities of these reaction products are compared with the corresponding region of the infra red spectrum of nitronitrato-humulene, where the ratio of ONO_2:NO_2 residues is also 1:1.

Inspection of the ^{1}H n.m.r. spectrum of the reaction products, **Figure 4.16**, confirms the deductions made from the infra red spectrum.

Table 4.11
Electron impact mass spectrum of the reaction products of (-)-(7)-dehydrocholesterol : $NaNO_2$ = 1:1

Mass	Relative abundance (%)	Ion
384.1	6.23	$[C_{27}H_{44}O]^+$
351.1	7.37	$[C_{26}H_{39}]^+$
279.0	3.12	$[C_{19}H_{35}O]^+$
267.1	2.27	$[C_{18}H_{35}O]^+$
253.1	4.82	$[C_{19}H_{25}]^+$
250.0	1.42	$[C_{18}H_{34}]^+$
211.1	4.53	$[C_{16}H_{19}]^+$
209.0	6.23	$[C_{15}H_{29}]^+$
197.1	6.23	$[C_{15}H_{17}]^+$
195.1	6.23	$[C_{14}H_{27}]^+$
183.1	5.38	$[C_{14}H_{15}]^+$
181.0	5.38	$[C_{13}H_{25}]^+$
179.0	5.10	$[C_{13}H_{23}]^+$
171.0	5.95	$[C_{13}H_{15}]^+$
166.0	16.15	$[C_{12}H_{22}]^+$
165.0	15.01	$[C_{12}H_{21}]^+$
143.1	9.92	$[C_{11}H_{11}]^+$
105.1	12.18	$[C_8H_9]^+$
81.0	13.60	$[C_6H_9]^+$
76.0	8.50	$[N_2O_3]^+$
55.2	39.66	$[C_4H_7]^+$
46.1	3.40	$[NO_2]^+$
43.2	100.00	$[C_3H_7]^+$
41.0	69.97	$[C_3H_5]^+$

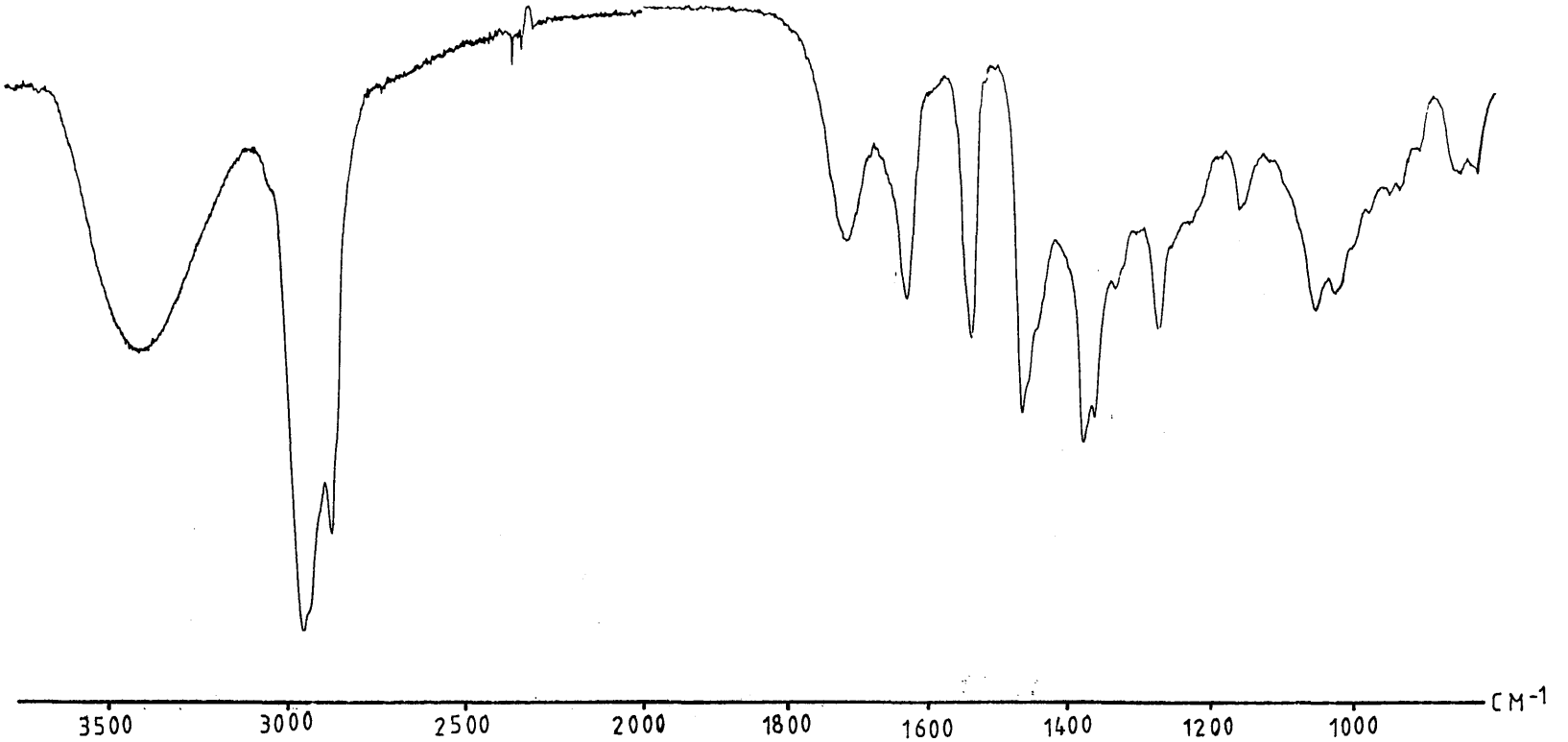

Figure 4.15 The infra red spectrum of the products obtained from the reaction of (-)-(7)-dehydrocholesterol : $NaNO_2$ = 1:1 (KBr disc)

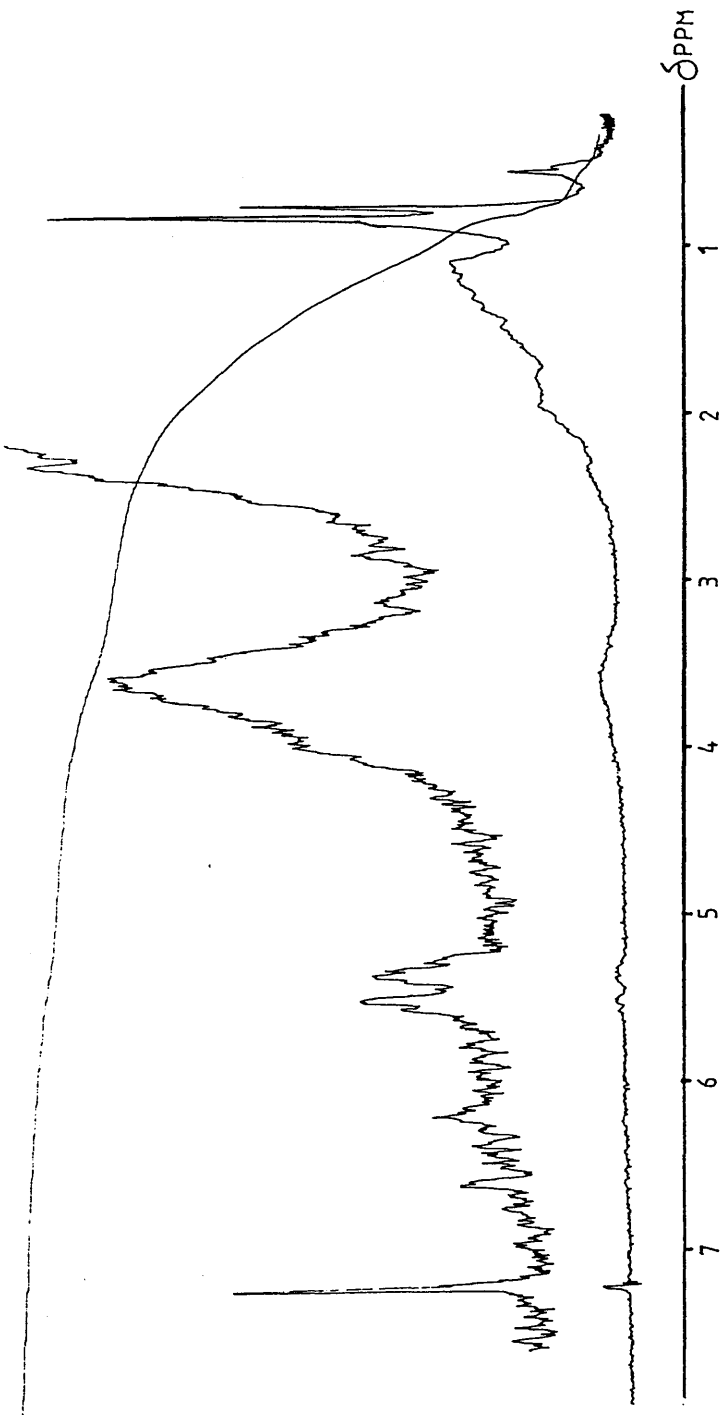

Figure 4.16 The 60 MHz ^1H n.m.r. spectrum of the products obtained from the reaction of (-)-(7)-dehydrocholesterol : $NaNO_2$ = 1:1 in $CDCl_3$ solution, at ambient temperature

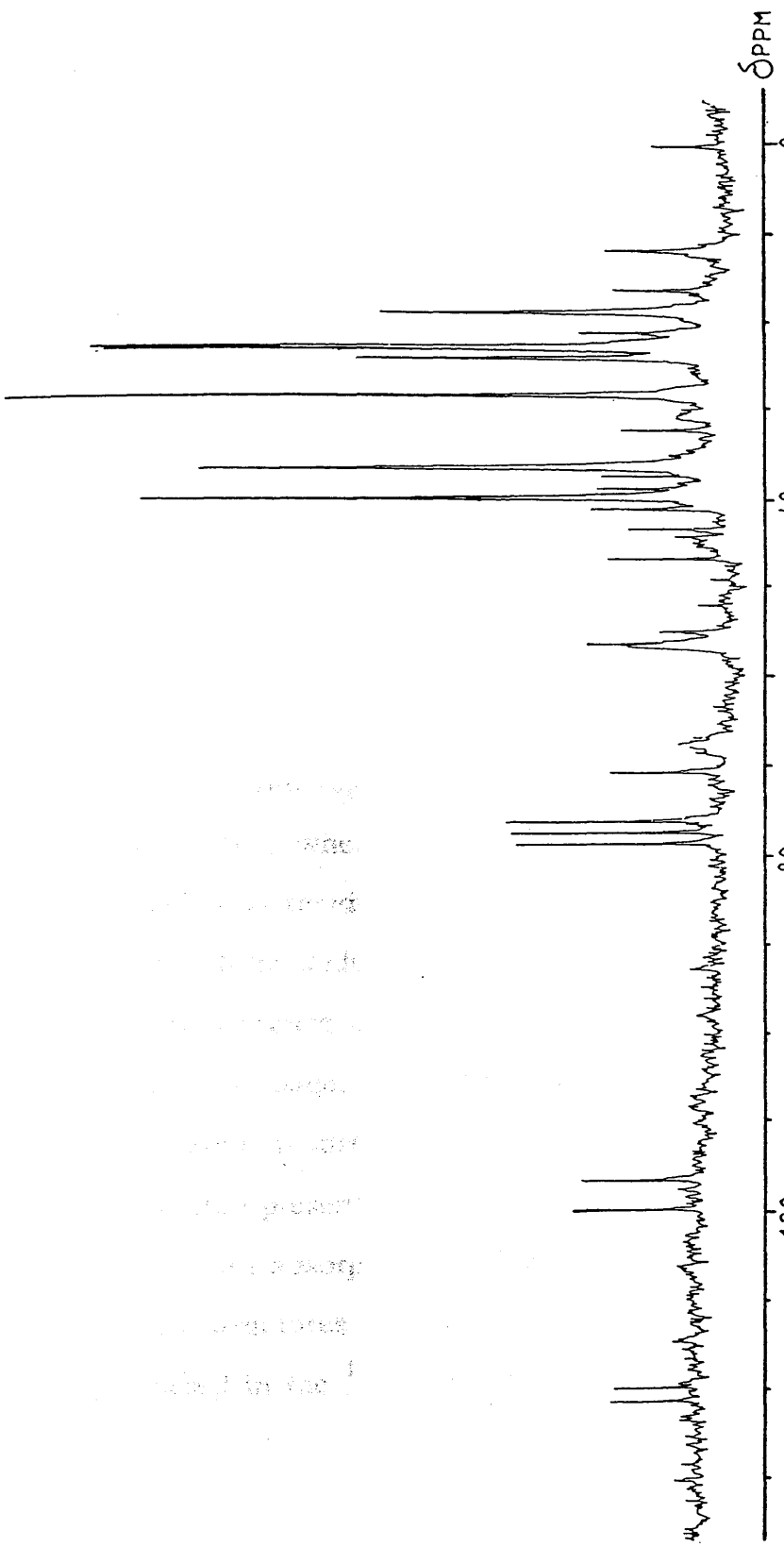

Figure 4.17 The 25.160 MHz ^{13}C-{^{1}H} n.m.r. spectrum of the products obtained from the reaction of (-)-(7)-dehydrocholesterol : $NaNO_2$ = 1:1 in $CDCl_3$ solution, at ambient temperature

Figure 4.16 contains only weak absorption peaks in the olefinic region, and these are assigned to a small amount of the parent (-)-(7)-dehydrocholesterol that still remains in the residue. The peaks in **Figure 4.16** in the region δ=3.60 ppm, overlapping with signals arising from the hydroxyl proton of the >C(3)H-OH residue, shows that addition across the olefinic residues forms >CH-ONO_2 groups and not >CH-NO_2 groups.

The electron impact mass spectrum, **Table 4.11**, shows extra peaks at m/z=46, 76, 149, 165, 166, 167, 178, 179, 181, 195, 209, 250, 267 and 279. m/z=46 corresponds to $[NO_2]^+$ and m/z=76 corresponds to $[N_2O_3]^+$. The others are assigned as shown in **Table 4.11**. It should be noticed that the O-NO_2 groups are cleaved in the mass spectrometer.

The ^{13}C n.m.r. spectrum, **Figure 4.17**, shows extra broad absorptions in the regions $68.60 \geq \delta \geq 67.80$ and $56.25 \geq \delta \geq 55.66$ ppm. These show that when (-)-(7)-dehydrocholesterol reacts with N_2O_3, several >CH-O- residues are produced. These observations, when combined with the deductions made from the ^1H n.m.r spectrum, seem to indicate the presence of at least the two isomers **[73]** and **[74]**, shown in the following page, formed by addition across the butadiene residue. Other isomers may also be produced, but further work would be needed to confirm their presence.

^{13}C n.m.r absorptions arising from the -C(5)-NO_2 and -C(8)-NO_2 residues in structures **[73]** and **[74]** in the reaction products have not been detected in the ^{13}C n.m.r. spectrum, shown in **Figure 4.17**. At present, it is not clear why these should be missing. Possibly nuclear Overhauser effects may be responsible.

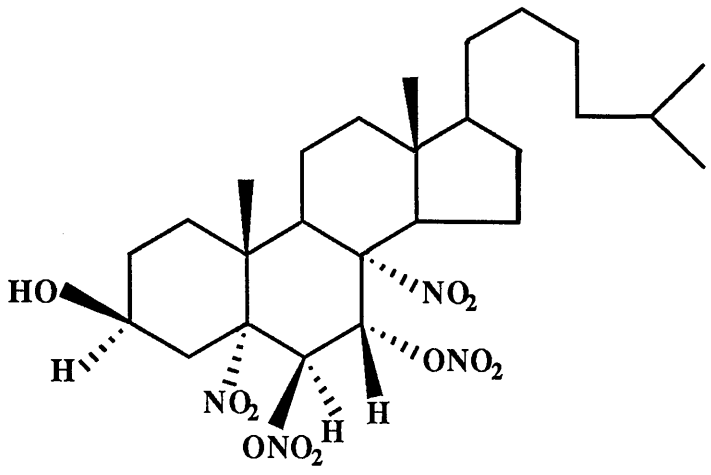

[73]

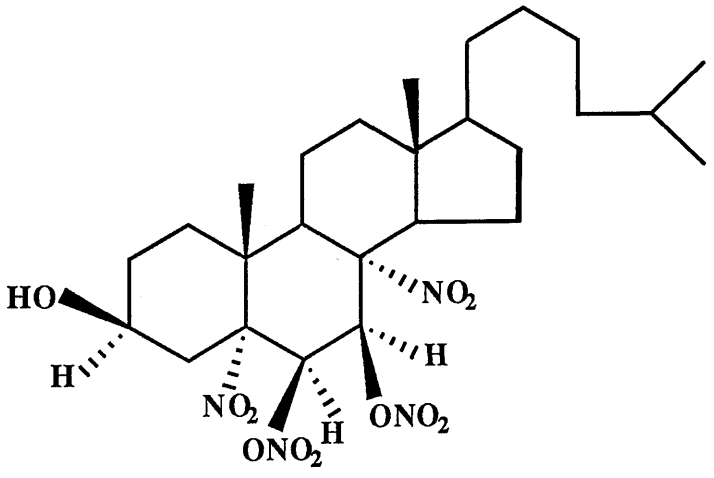

[74]

4.1.4 CONCLUSIONS

Treatment of either cholesterol, or cholesteryl esters, with sodium nitrite and acetic acid produces cholesteryl nitrite. Large yields of cholesteryl nitrite can be obtained from cholesterol, sodium nitrite and acetic acid, but the yield of cholesteryl nitrite obtained under similar conditions, from esters of cholesterol, sodium nitrite and acetic acid, is very much smaller.

It was noticed that when colourless solid cholesteryl nitrite is allowed to stand in contact with the atmosphere, it develops a steadily deepening yellow colour. The reaction responsible for producing this colour is not yet understood.

The >C(5)=C(6)< olefinic residues of cholesterol and cholesteryl-propionate do not react with N_2O_3 under the reaction conditions described in this work. However, (-)-(7)-dehydrocholesterol behaves quite differently. Its butadiene residue, in the second ring, readily reacts with N_2O_3 to give mixtures of nitronitrato derivatives and prior formation of these products appear to protect the >C(3)H-OH residue from reaction with at least, limited amounts of the oxides of nitrogen. Additional amounts of N_2O_3 probably convert the >C(3)H-OH residue to the corresponding nitrite ester, but further work is needed to check this point.

Cholesterol, and possibly other naturally occuring alcohols including sugars, may be able to store NO and NO_2 in this way, and thereby transport these gases to sites remote from the point of entry into plants and animals.

4.2 The action of NO and NO_2 on unsaturated fatty acids

4.2.1 OLEIC ACID

Oleic acid, cis-octadec-9-enoic acid, $C_{18}H_{34}O_2$, **[75]**, obtained from the departmental stores, was subjected to elemental analyses, without any further purification. Its electron impact mass spectrum, its infra red, its ^1H n.m.r., its ^{13}C-{^1H}, and its ^{13}C-{^1H} 90° and 135° D.E.P.T. spectra were all recorded and fully analyzed.

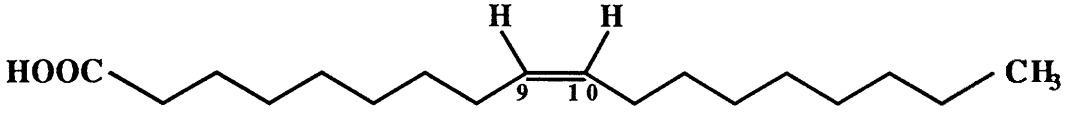

[75]

4.2.1.1 Elemental analyses of oleic acid

Elemental analyses of a liquid sample of oleic acid gave the percentage abundances for carbon and hydrogen listed in **Table 4.12.** Oxygen was calculated by difference. The results indicate that the sample is mainly oleic acid.

Table 4.12

Microanalyses data for oleic acid

Element	% Composition [found]	% Composition [expected for $C_{18}H_{34}O_2$]
C	76.52	76.60
H	12.22	12.06
O	11.26	11.34

4.2.1.2 ^{13}C and ^{1}H nuclear magnetic resonance studies of $CDCl_3$ solutions of oleic acid

4.2.1.2.1 The 50.323 MHz ^{13}C-nuclear magnetic resonance spectra

The ^{13}C-{^{1}H}, and the ^{13}C-{^{1}H} 90° and 135° D.E.P.T. spectra of the sample of oleic acid in $CDCl_3$ solution, at 298 K, are shown in **Figures 4.18A**, **4.18B** and **4.18C** respectively. These spectra show clearly that the solution in fact, contains two species, which turn out to be oleic acid, 90%, **[75]**, and linoleic acid, 10%, **[76]**. Particular attention was paid to the olefinic region, $130.5 \geq \delta \geq 127.5$ ppm, which shows two intense peaks arising from the olefinic carbons of oleic acid, and unexpectedly, in addition, four weak peaks that correspond to the olefinic carbons of linoleic acid. **Figures 4.18A** and **4.18C** also show some extra peaks that arise from methylene $>CH_2$ residues of linoleic acid. Detailed assignments of the n.m.r. data are shown in **Tables 4.13 and 4.14.**[109]

4.2.1.2.2 The 200.132 MHz ^{1}H-nuclear magnetic resonance spectrum

The proton magnetic resonance spectrum of the same solution of oleic acid is shown in **Figure 4.19**. It also confirms that the solution contains two components, oleic acid, 90%, and a small amount of linoleic acid, 10%. This latter is easily identified by the presence in the ^{1}H n.m.r. spectrum of a multiplet at around δ=2.78 ppm which is also present in the ^{1}H n.m.r. spectrum of pure linoleic acid, shown in **Figure 4.20**. The ratio of oleic acid:linoleic acid, roughly about 9:1, as shown in **Table 4.15**, hardly affects the interpretation of the microanalyses results already mentioned in **Table 4.12**

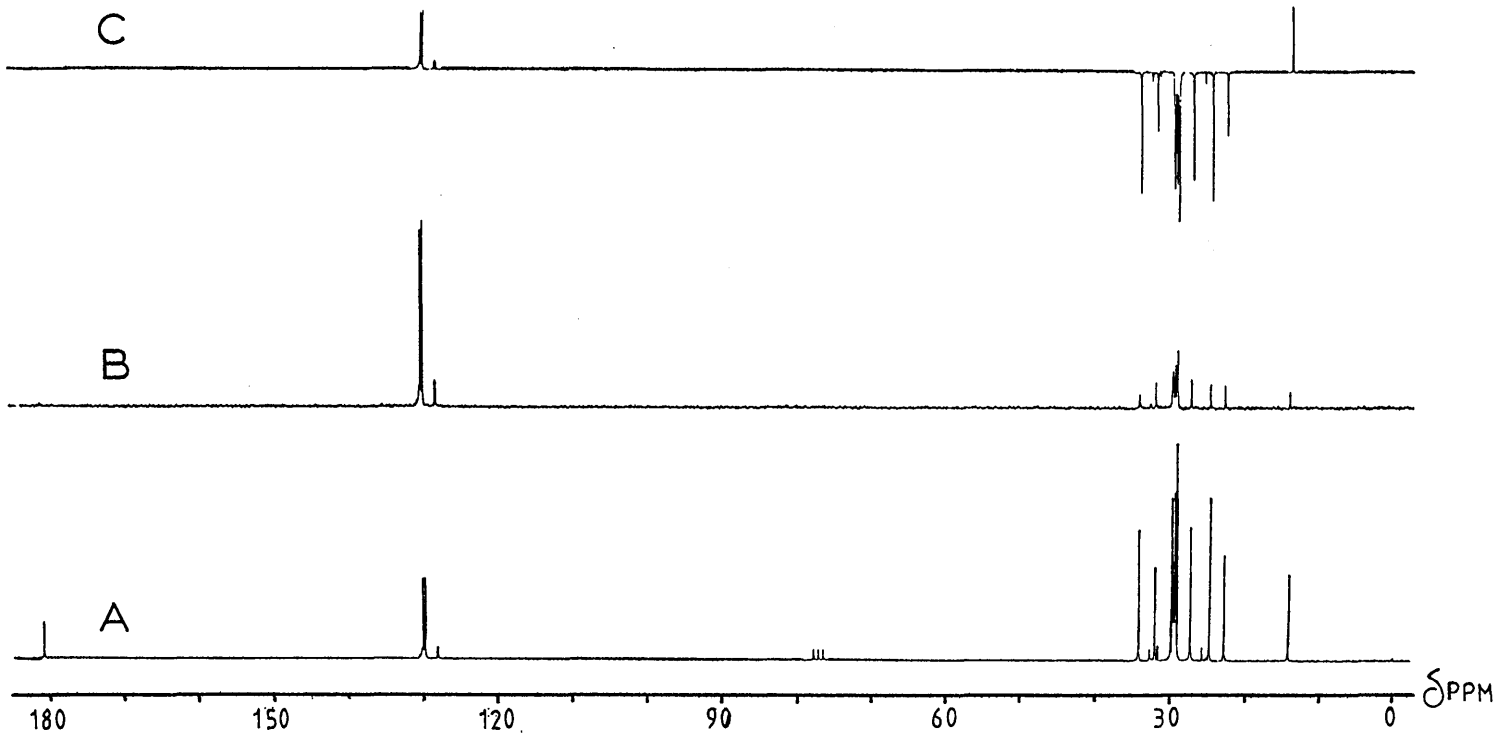

Figure 4.18 The 25.160 MHz ^{13}C-{^{1}H} n.m.r. spectrum, {A}, and the corresponding $\Theta = 90^{o}$, {B}, and $\Theta = 135^{o}${C}, D.E.P.T. spectra of oleic acid (90%) + linoleic acid (10%) in $CDCl_3$ solution, at ambient temperature

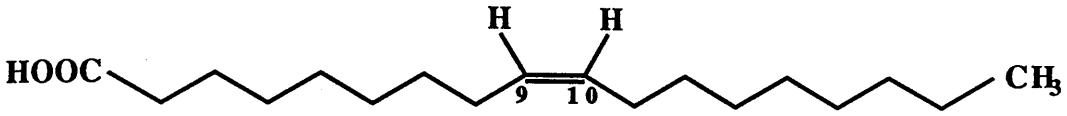

[75]

Table 4.13

^{13}C n.m.r. chemical shifts of oleic acid

δ_c(ppm)($CDCl_3$)

C-1	C-2	C-3	C-4	C-5	C-6	C-7	C-8
180.58	34.06	24.59	←———	29.72-29.02	———	→	27.15

C-9	C-10	C-11	C-12	C-13	C-14	C-15
129.58	129.87	27.09	←———	29.72-29.02	———	→

C-16	C-17	C-18
31.89	22.65	14.02

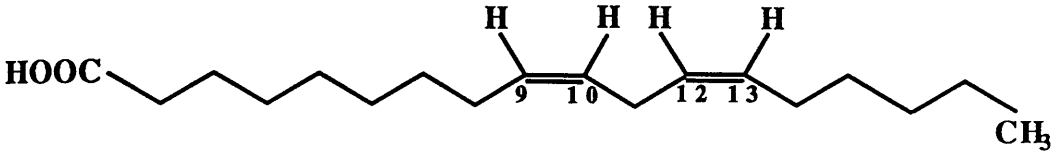

[76]

Table 4.14

^{13}C n.m.r. chemical shifts of linoleic acid present with oleic acid

δ_c(ppm)($CDCl_3$)

C-1	C-2	C-3	C-4	C-5	C-6	C-7	C-8
/	32.57	25.55	/	/	/	/	/

C-9	C-10	C-11	C-12	C-13
130.01/129.69	127.98/127.81	/	127.81/127.98	129.69/130.01

C-14	C-15	C-16	C-17	C-18
/	/	31.49	22.54	/

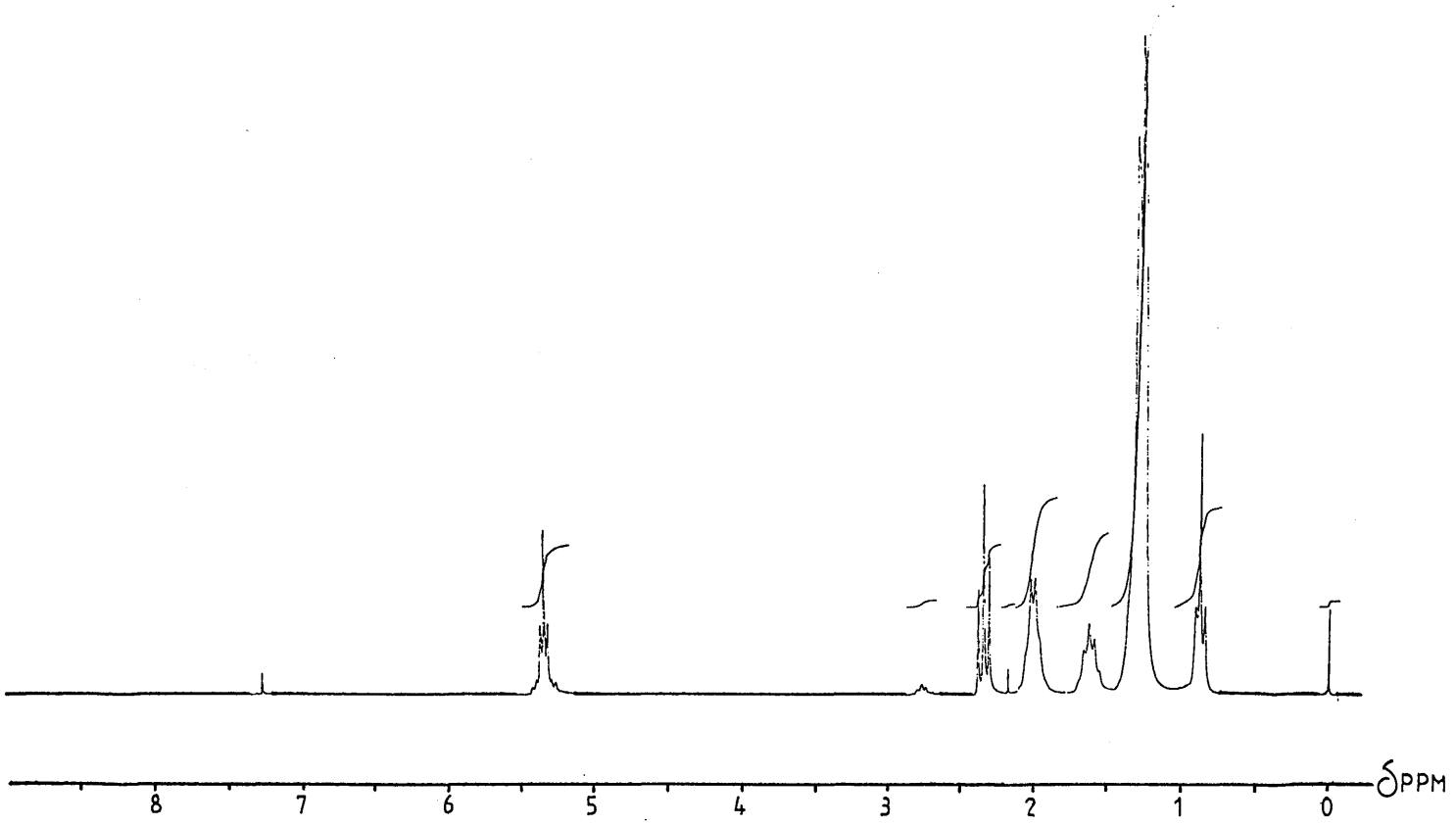

Figure 4.19 The 200.132 MHz ^{1}H n.m.r. spectrum of oleic acid (90%) + linoleic acid (10%) in $CDCl_3$ solution, at ambient temperature

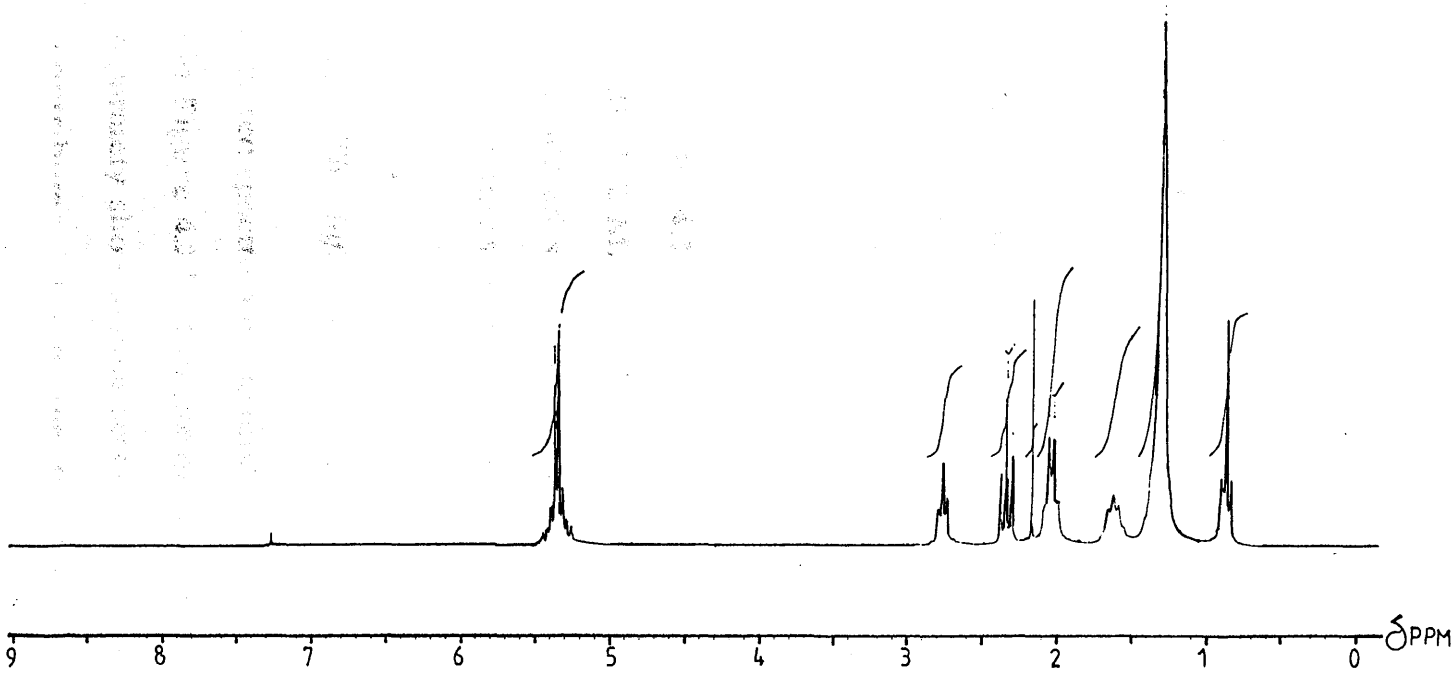

Figure 4.20 The 200.132 MHz ^{1}H n.m.r. spectrum of linoleic acid in $CDCl_3$ solution, at ambient temperature

Table 4.15

Microanalyses data for oleic acid : linoleic acid = 9 : 1

Element	% Composition found	% Composition 100% oleic acid	% Composition 90% oleic acid 10% linoleic acid
C	76.52	76.60	76.65
H	12.22	12.06	12.00
O	11.26	11.34	11.35

The ^{1}H n.m.r. chemical shifts and the ^{1}H-^{1}H coupling constants are listed in **Table 4.16.**

The olefinic region, $5.50 \geq \delta \geq 5.00$ ppm, of the 200.132 MHz ^{1}H n.m.r. spectrum has been subjected to a detailed analysis, and spin-Hamiltonian parameters for all proton interactions that influence this region of the oleic acid spectrum have been identified. The parameters are listed in **Table 4.17** and a spectrum, for a proton resonance frequency of 200.132 MHz, calculated from them is shown in **Figure 4.21.** This calculated spectrum is compared with the corresponding experimental ^{1}H n.m.r. spectrum, in **Figure 4.22.**

4.2.1.3 The infra red spectrum of oleic acid

The infra red spectrum of the mixture of oleic acid : linoleic acid = 9:1, shown in **Figure 4.23,** does not distinguish between the two acids since they separately show similar sets of absorptions, and the linoleic acid only contributes 10% to the observed spectrum. Detailed assignments of the vibrational frequencies are given in **Table 4.18.**

Table 4.16

^{1}H n.m.r. chemical shifts, δ_H, and ^{1}H-^{1}H coupling constants ($J_{H,H}$) for oleic acid

Chemical Shift	Hydrogen Number	$J_{H,H}$
0.867	18	7.5
1.260	1/4-7/12-17	/
1.620	3	7.5
1.998	8/11	5.0
2.334	2	7.5
5.331	9/10	/

Table 4.17

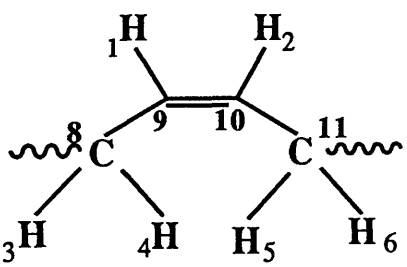

$J_{H,H}$/Hz

J_{12}= 11.15	J_{13}= 4.95	J_{14}= 9.20	J_{15}= -1.95	J_{16}= -1.95
J_{23}= -1.95	J_{24}= -1.95	J_{25}= 9.20	J_{26}= 4.95	
J_{34}= 14.00	J_{35}= 0.00	J_{36}= 0.00		
J_{45}= 0.00	J_{56}= 0.00			
J_{56}= 14.00				

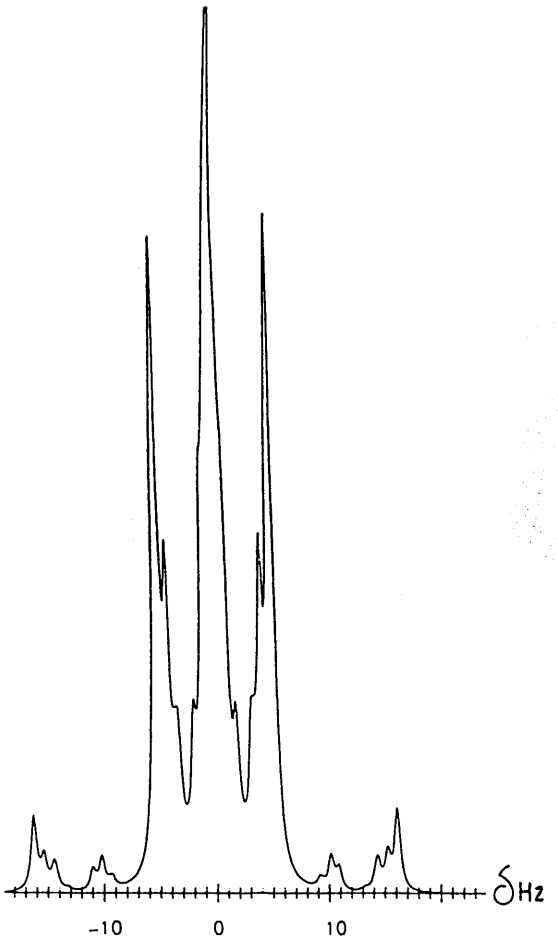

Figure 4.21 The calculated ^{1}H n.m.r. spectrum of the olefinic region of oleic acid

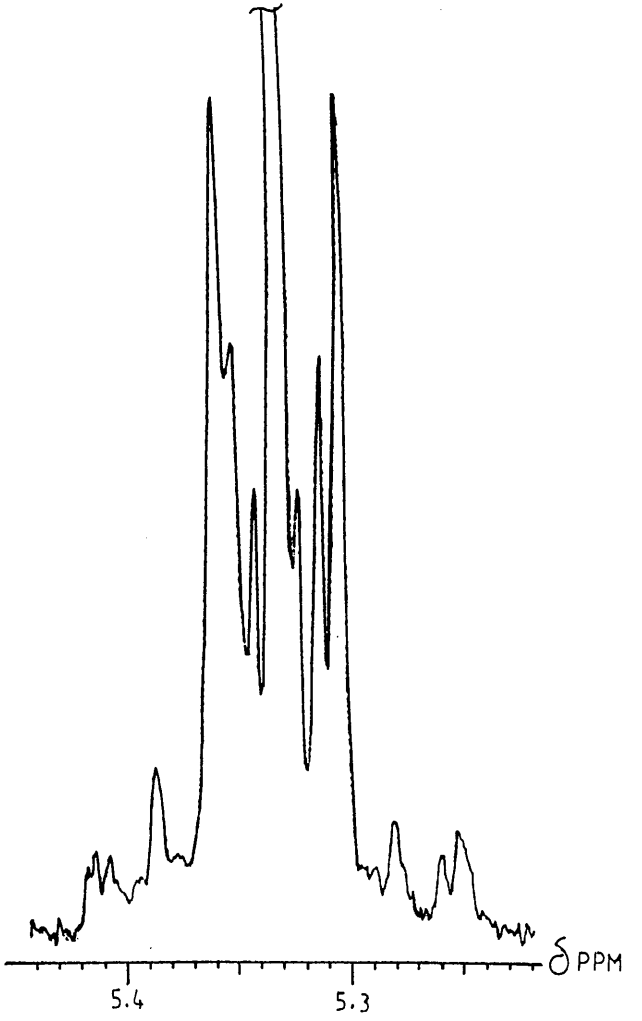

Figure 4.22 The experimental 200.132 MHz ^{1}H n.m.r. spectrum of the olefinic region of oleic acid (90%) + linoleic acid (10%) in $CDCl_3$ solution, at ambient temperature

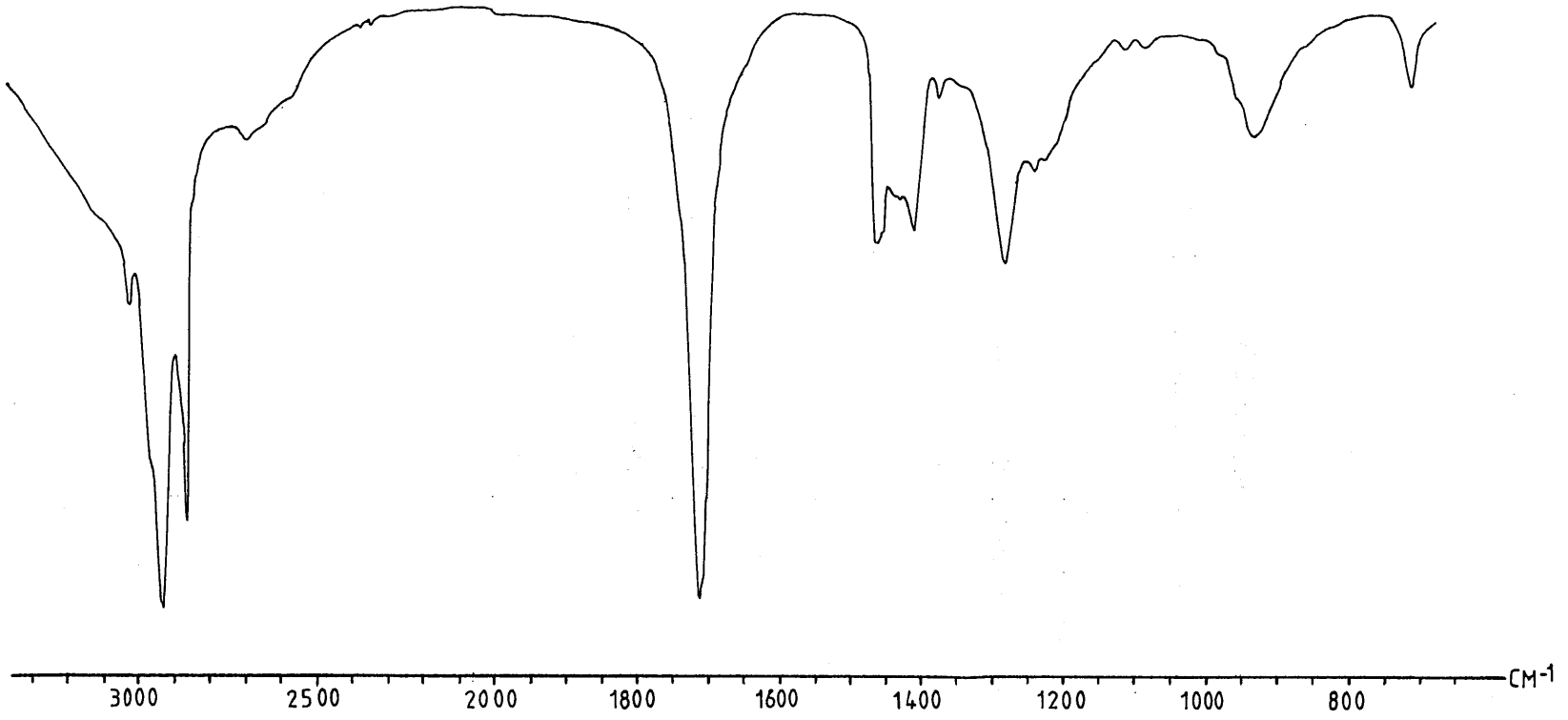

Figure 4.23 The infra red spectrum of oleic acid (90%) + linoleic acid (10%) (KBr disc)

Table 4.18

Infra red assignments of oleic acid

Band/cm^{-1}	Assignment
3004	>CH-, stretching mode of-CH=CH-
2950	$-CH_3$, asymmetric stretching mode
2930/2922	$>CH_2$, asymmetric stretching modes
2855	$-CH_3$, asymmetric stretching mode
2858	$>CH_2$, symmetric stretching mode
1711	>C=O, stretching mode
1465/1412	$>CH_2$, deformation modes and $-CH_3$, asymmetric deformation modes
1378	$-CH_3$, symmetric deformation mode
1285	$>CH_2$, wags
940	unassigned
722	>CH-, wag of cis olefinic

4.2.1.4 The electron impact mass spectrum of oleic acid

The electron impact mass spectrum also establishes that the major component in the investigated fatty acid sample, is oleic acid, and it too confirms the presence of a small amount of linoleic acid. A fragment observed at m/z=66 is characteristic of the -CH=CH-CH_2-CH=CH- fragment of linoleic acid, which is not present in oleic acid. A more complete description of the mass spectrum cracking pattern and the cracking pattern mechanisms are given in detail, in **Table 4.19.**

4.2.1.5 The action of NO and NO_2 on oleic acid

4.2.1.5.1 Oleic acid : $NaNO_2$ = 1:1

Oleic acid was vigorously shaken at room temperature, in a stoppered flask, with an aqueous solution containing an equimolar amount of sodium nitrite and acetic acid. Small amounts of air were periodically allowed into the reaction flask, which was then immediately re-stoppered. The infra red spectrum of the reaction products, obtained by this treatment, is as shown in **Figure 4.24.** The spectrum shows that only 50% of the oleic acid -CH=CH- residue has reacted and in addition to the absorption spectrum of the starting oleic acid sample, weak extra peaks, marked * in the figure, appear in the region $1650 \geq \upsilon \geq 1500$ cm^{-1} and $1000 \geq \upsilon \geq 850$ cm^{-1}. These reveal the formation of small amounts of >CH-NO_2 and >C=N-OH residues.

4.2.1.5.2 Oleic acid : $NaNO_2$ = 1:2

It was then decided to increase the amount of $NaNO_2$ by a factor of two, in order to force the double bond to react totally. The infra red spectrum, shown in **Figure 4.25,** indicates that there is further reaction

Table 4.19
Electron impact mass spectrum of oleic acid [75]

Mass	Relative Abundance (%)	Ion
282	2.8	$[C_{18}H_{34}O_2]^+$
265	2.3	$[C_{18}H_{33}O]^+$
264	9.9	$[C_{18}H_{32}O]^+$
222	2.8	$[C_{16}H_{30}]^+$
209	1.5	$[C_{15}H_{29}]^+$
194	3.3	$[C_{14}H_{26}]^+$
181	4.1	$[C_{13}H_{25}]^+$
167	4.8	$[C_{12}H_{23}]^+$
153	4.5	$[C_{11}H_{21}]^+$
139	6.3	$[C_{10}H_{19}]^+$
125	9.5	$[C_9H_{17}]^+$
124	7.9	$[C_9H_{16}]^+$
111	18.3	$[C_8H_{15}]^+$
110	13.5	$[C_8H_{14}]^+$
109	13.9	$[C_8H_{13}]^+$
98	18.6	$[C_7H_{14}]^+$
97	34.9	$[C_7H_{13}]^+$
96	22.1	$[C_7H_{12}]^+$
95	25.7	$[C_7H_{11}]^+$
85	10.3	$[C_6H_{13}]^+$
84	20.2	$[C_6H_{12}]^+$
83	45.5	$[C_6H_{11}]^+$
69	56.7	$[C_5H_9]^+$
55	100.0	$[C_4H_7]^+$
41	96.7	$[C_3H_5]^+$
27	23.9	$[C_2H_3]^+$

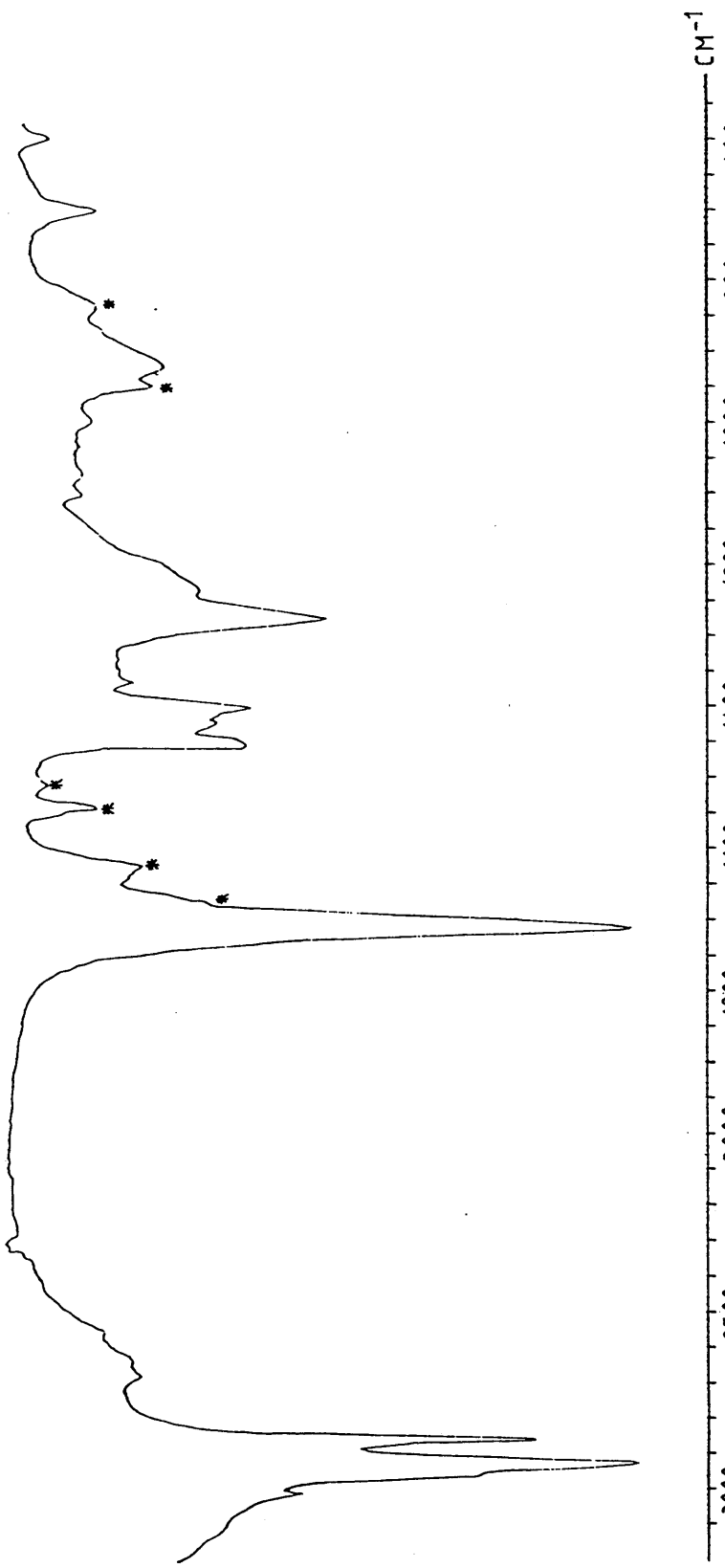

Figure 4.24 The infra red spectrum of the products obtained from the reaction of oleic acid : $NaNO_2$ = 1:1 (KBr disc)

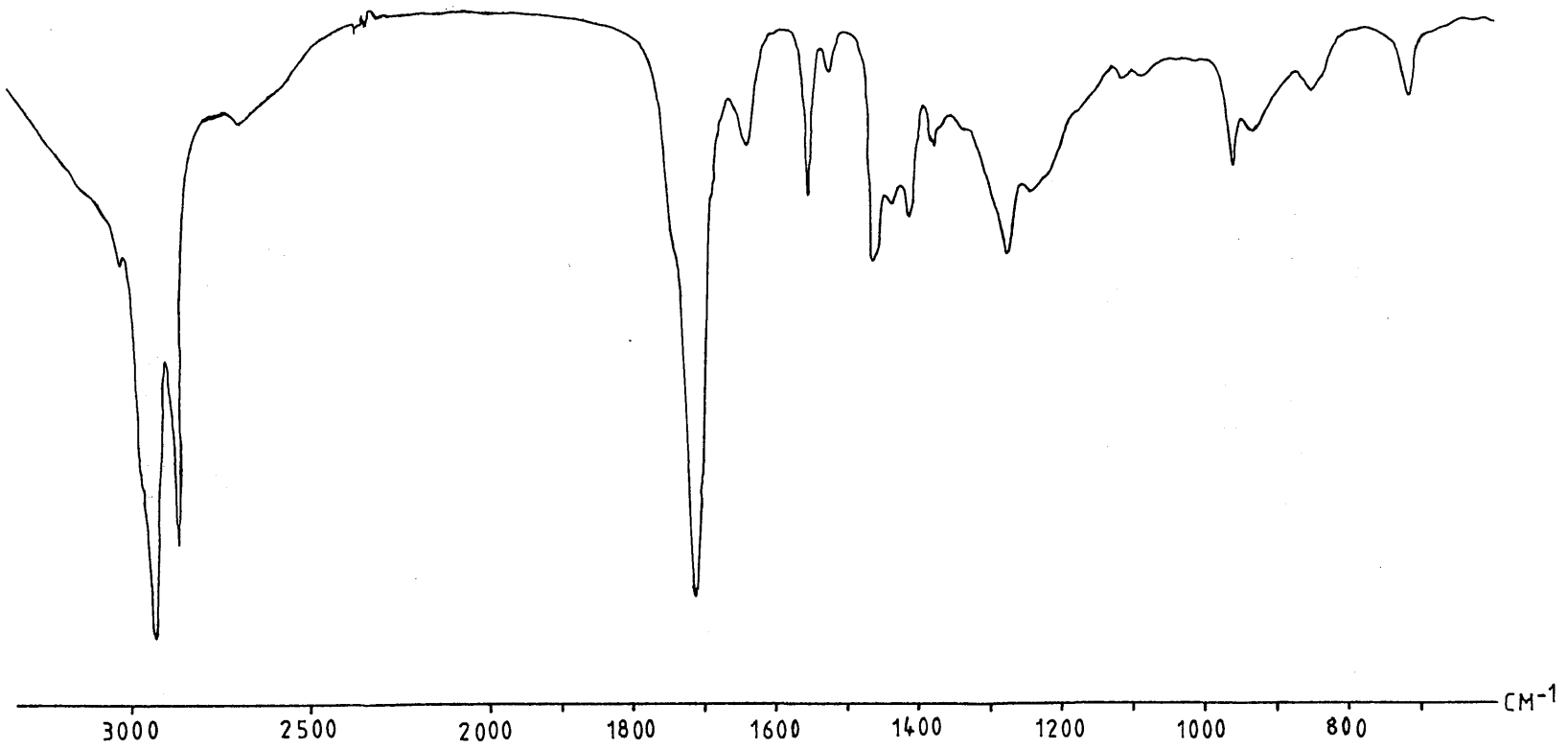

Figure 4.25 The infra red spectrum of the products obtained from the reaction of oleic acid : $NaNO_2$ = 1:2 (KBr disc)

of the -CH=CH- residue, but still not all the oleic acid has reacted. However, the extra peaks are now much more obvious.

4.2.1.5.3 Oleic acid : $NaNO_2$ = 1:3

Further increasing the amount of $NaNO_2$ this time trebles the number of double bond residues that react with the oxides of nitrogen produced by the action of acid and air on the sodium nitrite.

The ^{13}C-{^{1}H}, and its ^{13}C-{^{1}H} 90° and 135° D.E.P.T., the ^{1}H n.m.r. and the infra red spectra of the reaction products were all recorded and fully analyzed.

4.2.1.5.3.a The 50.323 MHz ^{13}C n.m.r spectra of $CDCl_3$ solutions of the products obtained when oleic acid reacts with sodium nitrite solution

The ^{13}C-{^{1}H}, and the ^{13}C-{^{1}H} 90° and 135° D.E.P.T.spectra of the reaction products in $CDCl_3$ solution are shown in **Figures 4.26A**, **4.26B** and **4.26C** respectively. Comparing these spectra with those of the starting material, shown in **Figures 4.18A**, **4.18B** and **4.18C**, shows that the original oleic acid is still present, but the linoleic acid seems to have totally disappeared. Furthermore, two extra peaks appear in the olefinic region of **Figure 4.26A**. These arise from the trans-isomer of oleic acid, elaidic acid, **[77]**, whose ^{13}C-{^{1}H}, ^{13}C-{^{1}H} 90° and 135° D.E.P.T. spectra are shown in **Figures 4.27A**, **4.27B** and **4.27C**. The ^{13}C n.m.r. chemical shifts, shown in these figures and the expanded region $34.5 \geq \delta \geq 14.0$, **Figure 4.28**, have been unambiguously assigned to either oleic acid or elaidic acid : the assignments for elaidic acid are shown in detail, in **Table 4.20**.[109] The relative intensities of the olefinic peaks show that after reaction, the

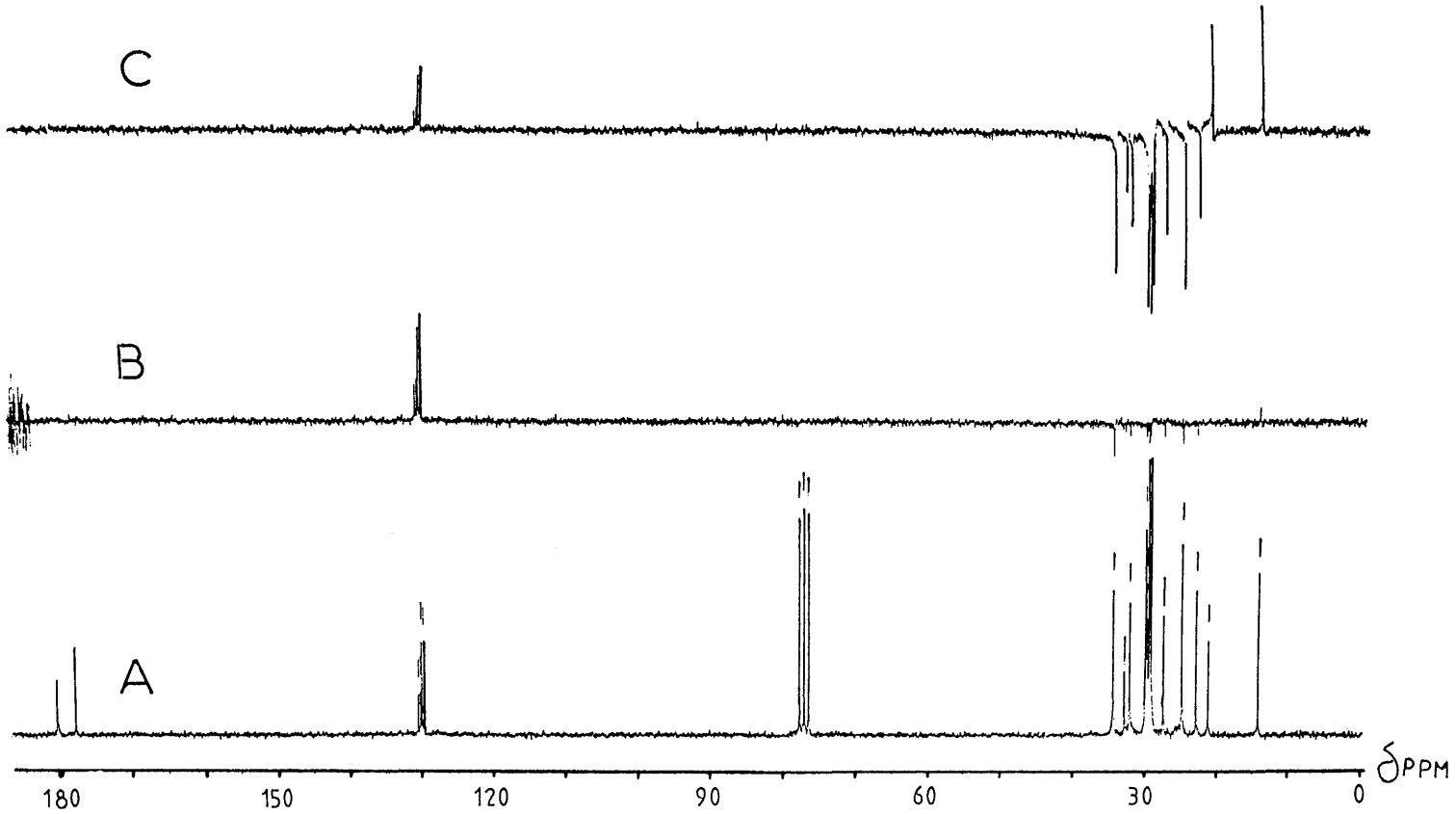

Figure 4.26 The 50.323 MHz ^{13}C-{^{1}H} n.m.r. spectrum, {A}, and the corresponding $\Theta = 90^{o}$, {B}, and $\Theta = 135^{o}${C}, D.E.P.T. spectra of the products obtained from the reaction of oleic acid : $NaNO_2$ = 1:3 in $CDCl_3$ solution, at ambient temperature

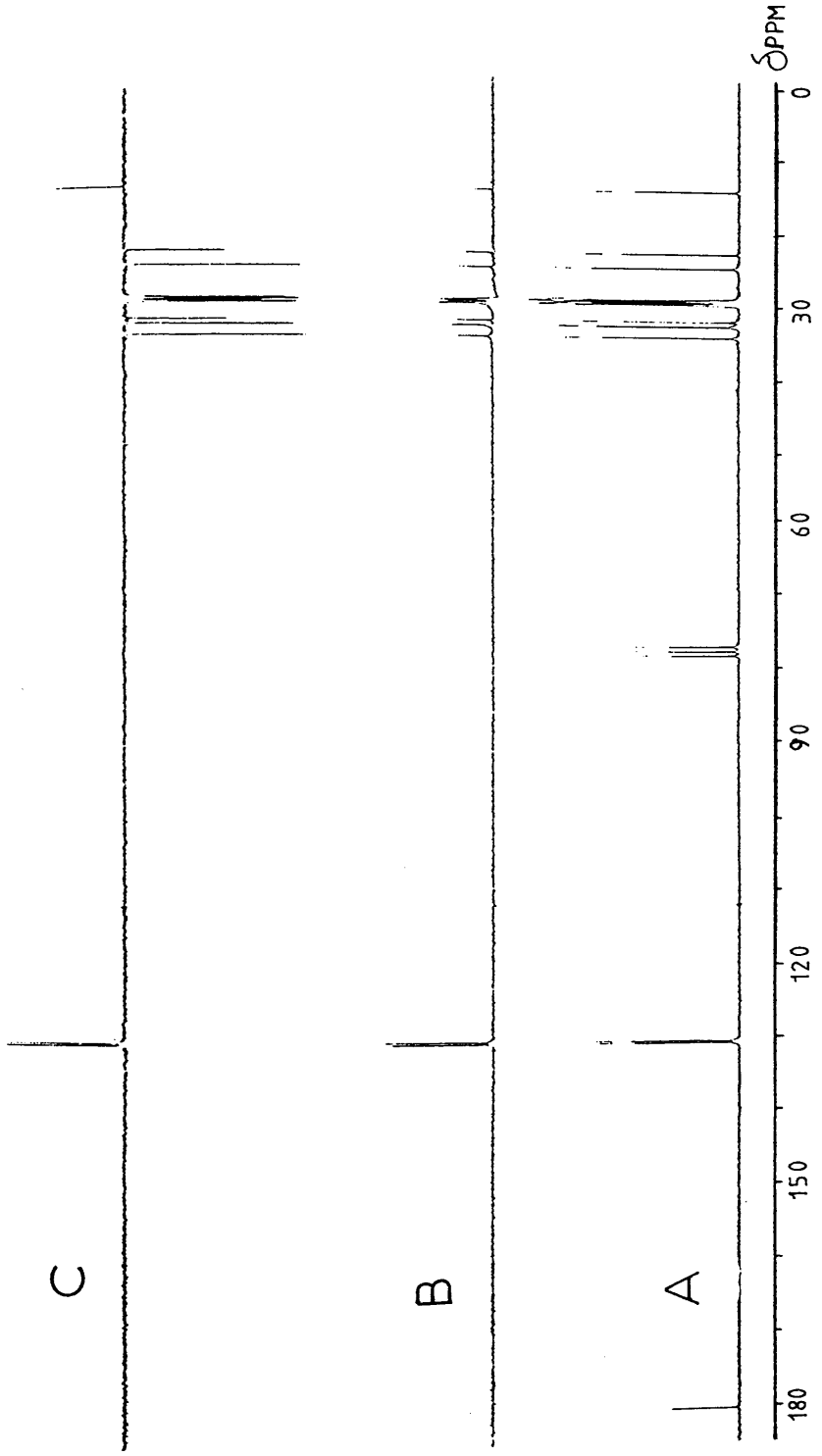

Figure 4.27 The 50.323 MHz ^{13}C-{^{1}H} n.m.r. spectrum, {A}, and the corresponding $\Theta = 90^{o}$, {B}, and $\Theta = 135^{o}${C}, D.E.P.T. spectra of elaidic acid in $CDCl_3$ solution, at ambient temperature

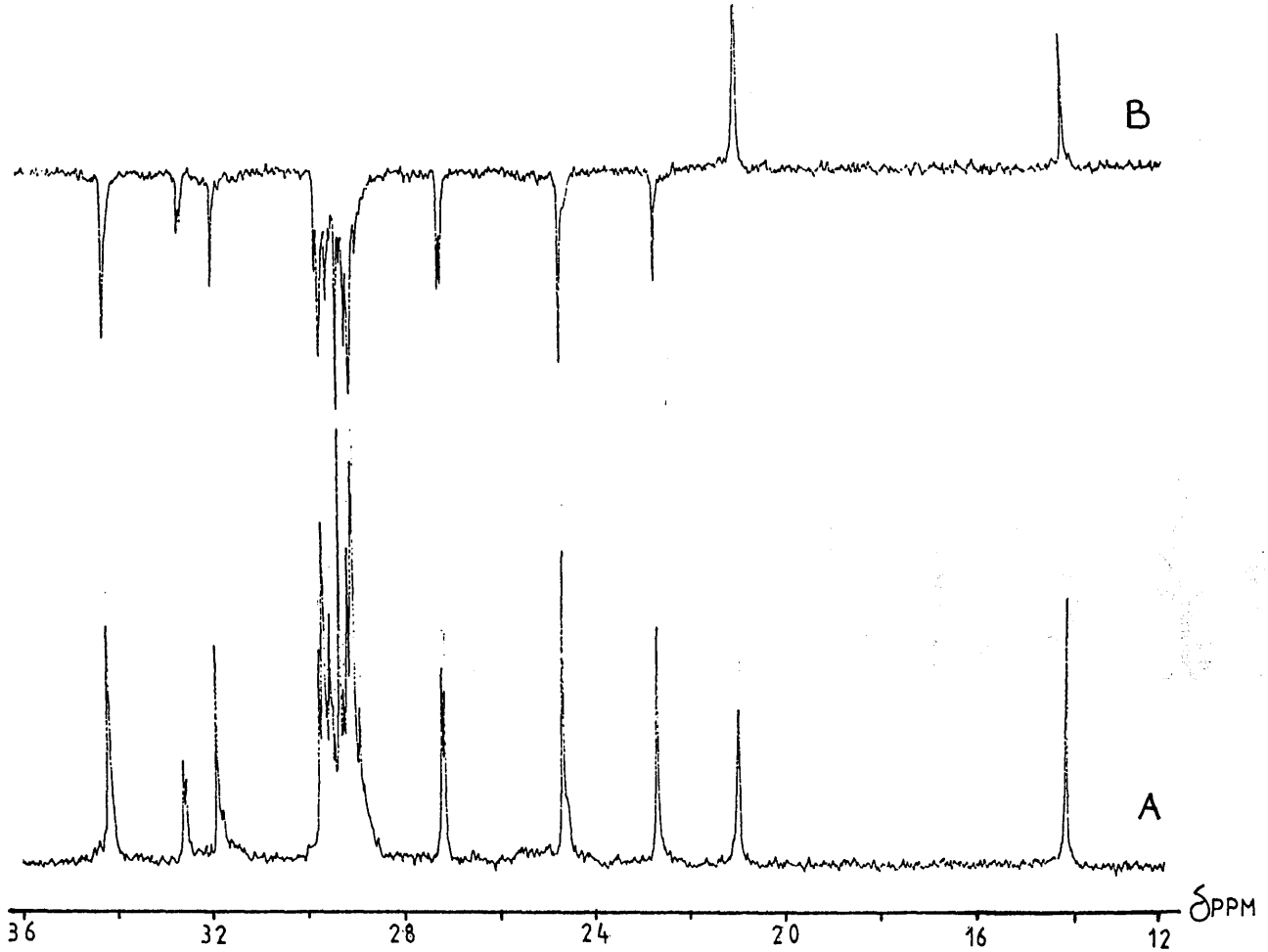

Figure 4.28 The expanded 50.323 MHz ^{13}C-{^{1}H} n.m.r. spectrum, {A}, and the corresponding $\Theta = 135^{o}$, {B}, D.E.P.T. spectrum of the mixture of oleic acid and elaidic acid in $CDCl_3$ solution, at ambient. temperature

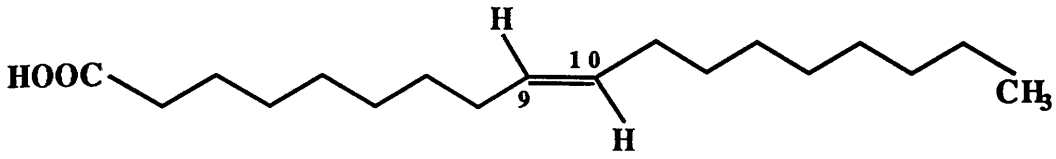

[77]

Table 4.20

^{13}C n.m.r. chemical shifts of elaidic acid present in the mixture

δ_c(ppm)($CDCl_3$)

C-1	C-2	C-3	C-4	C-5	C-6	C-7	C-8
180.45	34.14	24.65	/	29.6 - 28.9		/	32.52

C-9	C-10	C-11	C-12	C-13	C-14	C-15
130.15	130.45	32.58	/	29.6 - 28.9		/

C-16	C-17	C-18
31.87	22.66	14.09

ratio of oleic acid:elaidic acid = 3:1. Finally, in the spectrum in **Figure 4.26A**, two extra weak peaks were noticed at δ=177.87 ppm and δ=20.96 ppm. They arise from the acetic acid which was present in excess, in the reaction mixture.

4.2.1.5.3.b *The 200.132 MHz ^1H n.m.r. spectrum of $CDCl_3$ solutions of the products obtained when oleic acid reacts with sodium nitrite solution*

This spectrum is shown in **Figure 4.29**. Its expanded version, **Figure 4.30**, shows very dramatic changes, particularly in the olefinic region, $5.40 \geq \delta \geq 5.30$ ppm, and also in the line shape of the neighbouring methylene $>CH_2$ region, $2.05 \geq \delta \geq 1.90$ ppm, when compared with the corresponding regions of the spectrum of the original, unreacted acid. By judiciously combining the ^1H n.m.r. spectra of the -CH=CH- residues of the oleic acid (90%) + linoleic acid (10%), and the ^1H n.m.r. spectrum of the -CH=CH- residue of elaidic acid, **[77]**, as shown in **Figures 4.31A** and **Figure 4.31B** respectively, the ^1H n.m.r. spectrum of the reaction products was reconstructed, as shown in **Figure 4.32** and is compared to the ^1H n.m.r. spectrum, shown in **Figure 4.30**. **Figures 4.29-4.32** confirm the earlier conclusions that the reaction mixture contains oleic acid and its trans isomer elaidic acid, in the ratio oleic acid:elaidic acid = 3:1.

4.2.1.5.3.c *The infra red analyses of the products obtained when oleic acid reacts with sodium nitrite solution*

The infra red spectrum of the reaction products, shown in **Figure 4.33**, shows a total absence of i.r. absorption at 962 cm^{-1}, characteristic of the trans =CH- wag ~~in elaidic acid~~, as shown in **Figure 4.34**. Furthermore, additional characteristic i.r. absorptions of a $\geq C\text{-}NO_2$ residue appear at 1552, 1360 and 890 cm^{-1}, as well as of a >C=N-OH residue at 1650 and 968 cm^{-1}.

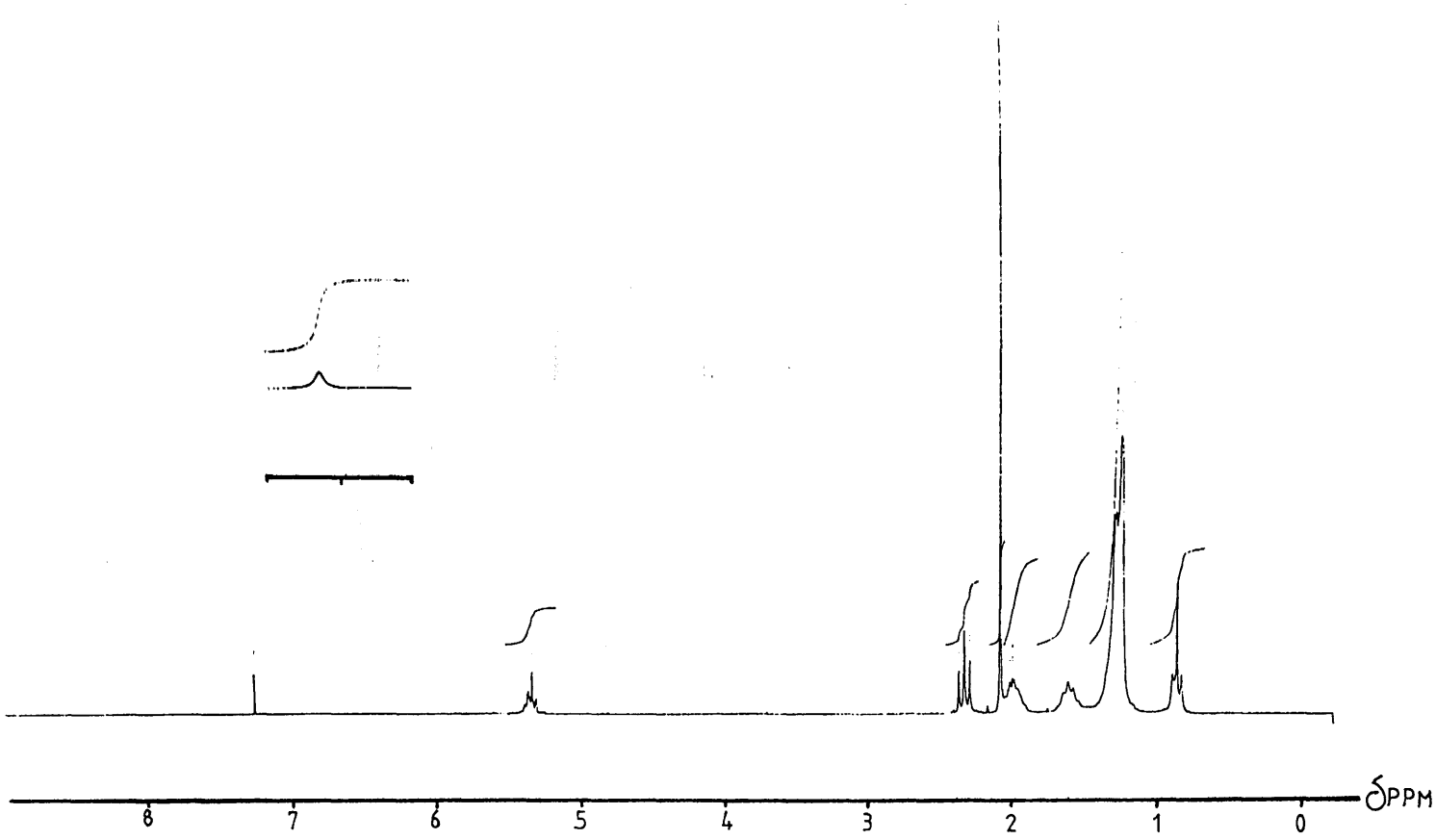

Figure 4.29 The 200.132 MHz ^{1}H n.m.r. spectrum of the products obtained from the reaction of oleic acid : $NaNO_2$ = 1:3 in $CDCl_3$ solution, at ambient temperature

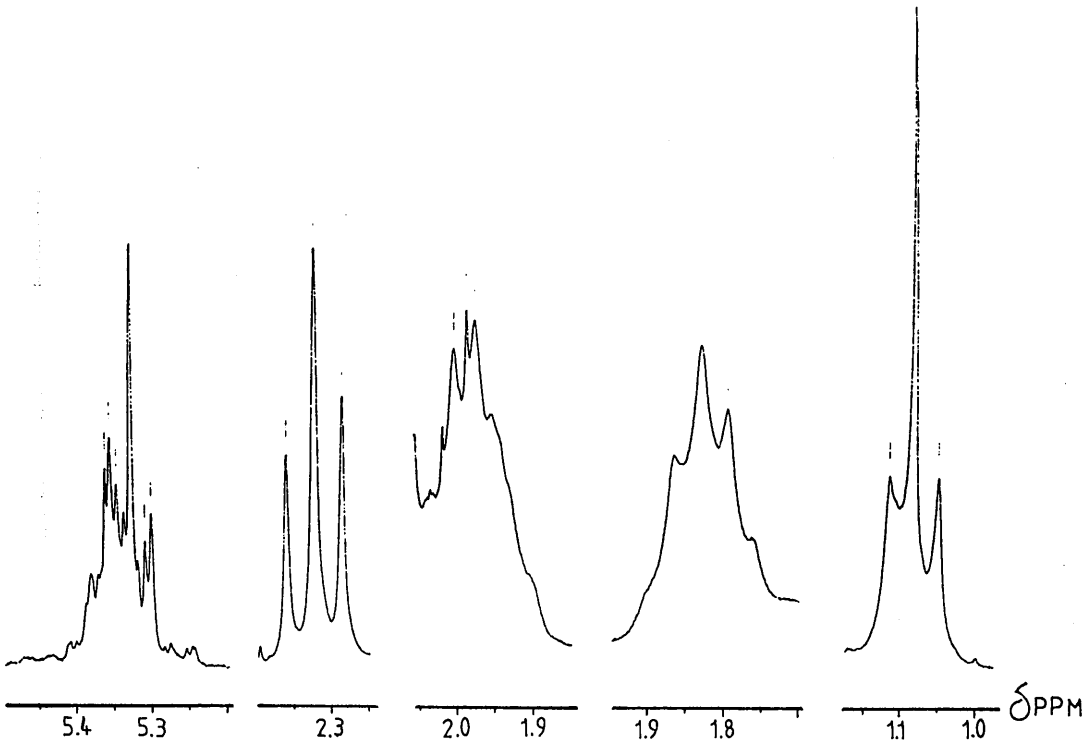

Figure 4.30 The expanded 200.132 MHz ^{1}H n.m.r. spectrum of the products obtained from the reaction of oleic acid : $NaNO_2$ = 1:3 in $CDCl_3$ solution, at ambient temperature

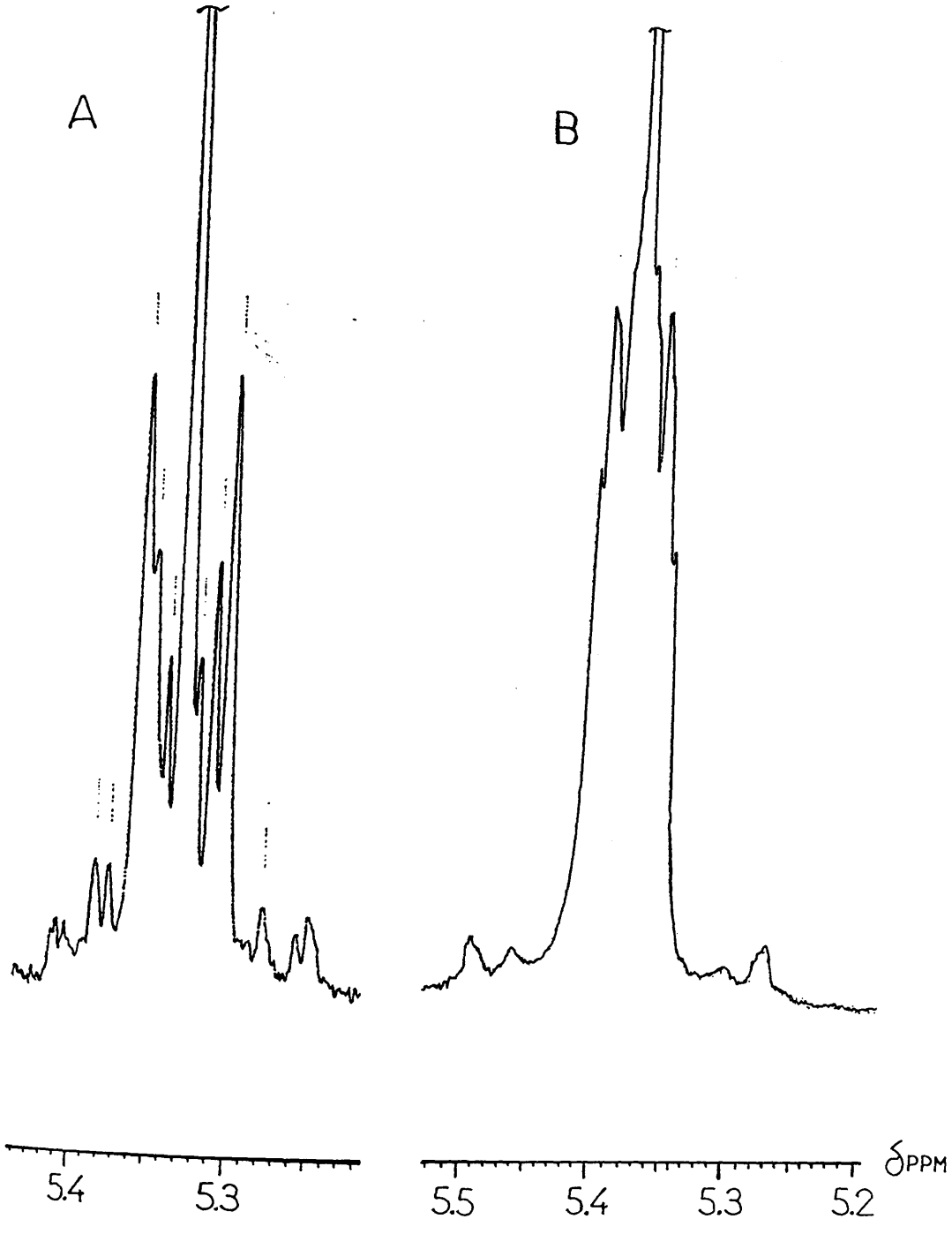

Figure 4.31 The 200.132 MHz ^{1}H n.m.r. spectra of the olefinic region of oleic acid (90%) + linoleic acid (10%), {**A**}, and of the olefinic region of elaidic acid, {**B**}, in $CDCl_3$ solution, at ambient temperature

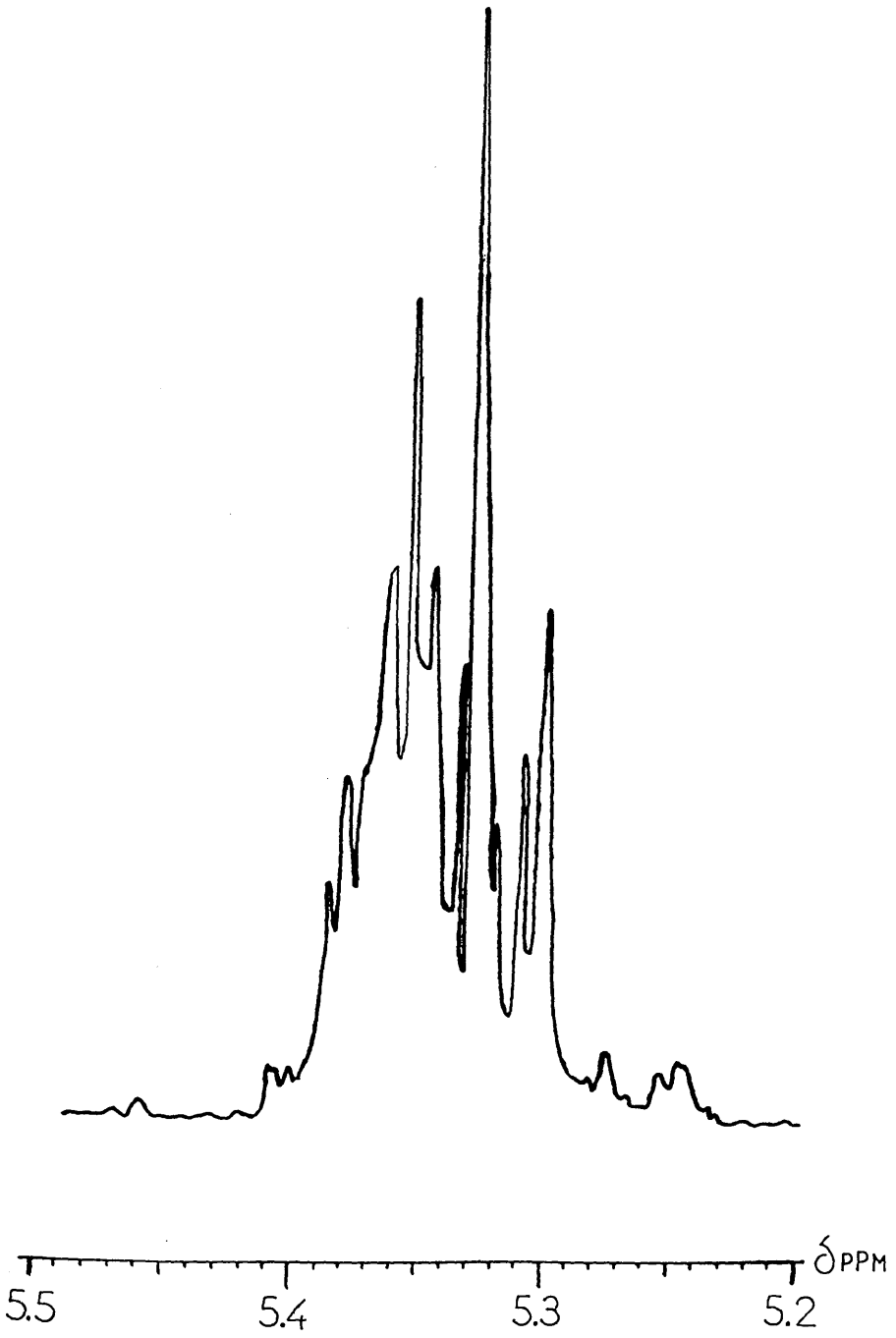

Figure 4.32 The calculated ^{1}H n.m.r. spectrum of the olefinic region of the products obtained from the reaction of oleic acid : $NaNO_2$ = 1:3

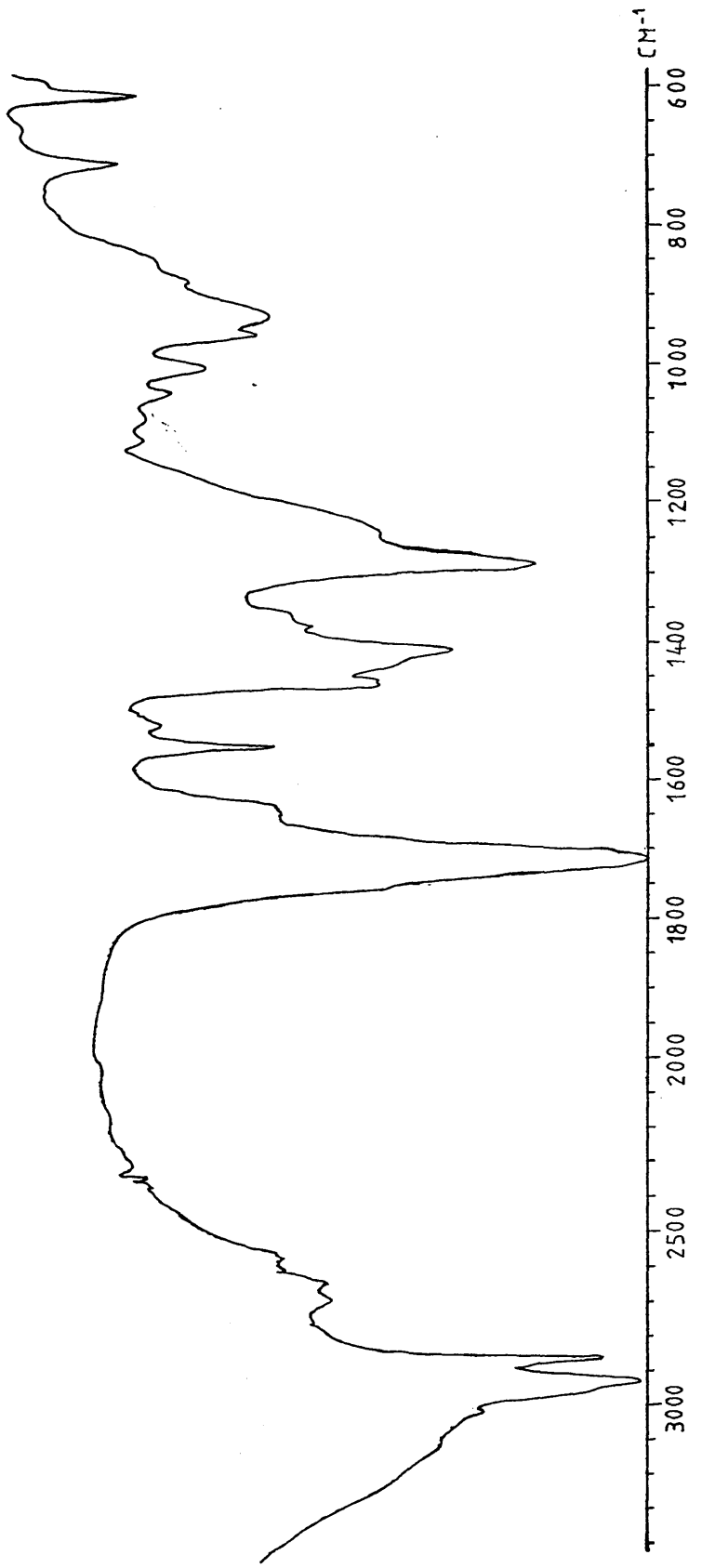

Figure 4.33 The infra red spectrum of the products obtained from the reaction of oleic acid : $NaNO_2$ = 1:3 (KBr disc)

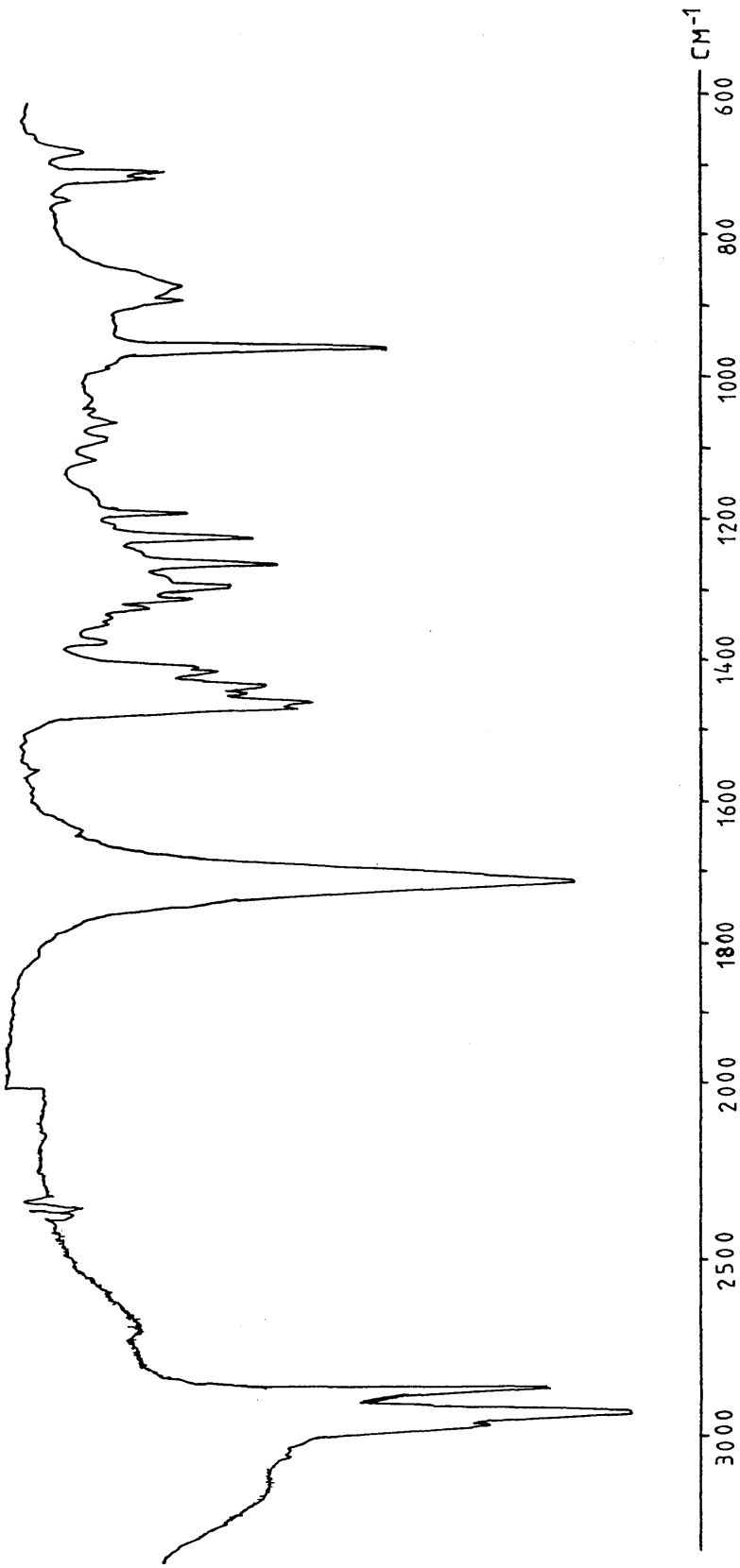

Figure 4.34 The infra red spectrum of elaidic acid (KBr disc)

4.2.1.6 *Conclusions:* The chemically significant points in this work are as follows.

The sample of oleic acid examined, in fact, contained 10% of linoleic acid

The conformation in the neighbourhood of the olefinic residue of oleic acid has been deduced from the detailed ^{1}H n.m.r. data, listed in **Table 4.17**, by applying the relationship $^{3}J_{H,H} = 10\cos^{2}\vartheta - \cos\vartheta + 2$.[110] The deduced angles with the preferred conformation are as shown in the diagram below.

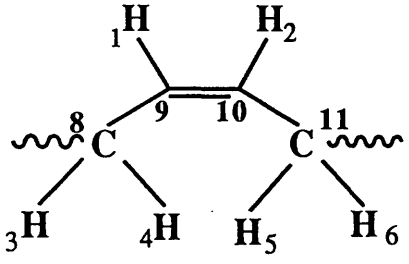

$$\vartheta_{13} = \vartheta_{26} = 53^{\circ}$$

$$\vartheta_{14} = \vartheta_{25} = 143^{\circ}$$

When oleic acid is brought into contact with acidified sodium nitrite, some of it is converted into its trans isomer, elaidic acid. Detailed analyses of the alkenic region of the ^{1}H n.m.r. spectrum of elaidic acid, shows that the important dihedral angles in its preferred conformation are

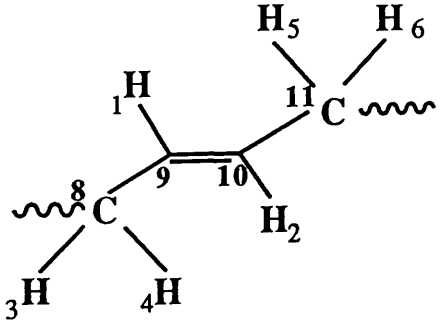

$$\vartheta_{13} = \vartheta_{26} = 40^{\circ}$$

$$\vartheta_{14} = \vartheta_{25} = 131^{\circ}$$

These angles were deduced from the following $^{3}J_{H-H}$ values obtained from a complete analysis of the 200.132 MHz ^{1}H n.m.r. spectrum of this compound

$J_{12} = 15.0,\ J_{13} = 7.0,\ J_{14} = 7.0,\ J_{15} = -1.9,\ J_{16} = -1.9$
$J_{23} = -1.9,\ J_{24} = -1.9,\ J_{25} = 7.0,\ J_{26} = 7.0$
$J_{34} = 14.0,\ J_{35} = 0.0,\ J_{36} = 0.0$
$J_{45} = 0.0,\ J_{46} = 0.0$
$J_{56} = 14.0$

$\geqslant C\text{-}NO_2$ and >C=N-OH residues have not been detected in the n.m.r. spectra of oleic acid after being brought into contact with acidified sodium nitrite. However, these residues are detected in the appropriate i.r. spectrum. It is therefore believed that the mechanisms involved in the cis-trans isomerisation are as outlined in **Scheme 4.1**. In this, $\cdot NO_2$ first attacks the double bond in oleic acid, thereby forming the unstable radical intermediate **[78]**.

Route 1 is eliminated on the basis of the ^{13}C n.m.r. spectrum of the products: a ^{13}C signal from the $>\underline{C}H\text{-}(NO_2)$ residue would appear at about 85-90 ppm[111] and it is not observed in **Figure 4.26**. Furthermore, the olefinic residues in **[79]** are not observed in the corresponding ^{1}H n.m.r. spectrum, **Figure 4.28**.

Route 3 is of minor importance since its products are not observed in the n.m.r. spectra but only, as weak absorptions, in the infra red spectrum of the products.

Route 2 is obviously the main one whereby the oxides of nitrogen convert oleic acid into its geometrical isomer elaidic acid. The life time of the the intermediate radical **[78]** must be too short to allow the reaction in route 3 to become important. This life time and the time required for the rotation of the radical **[78]** about >C(9)-C(10)< bond must be of the same order of magnitude.

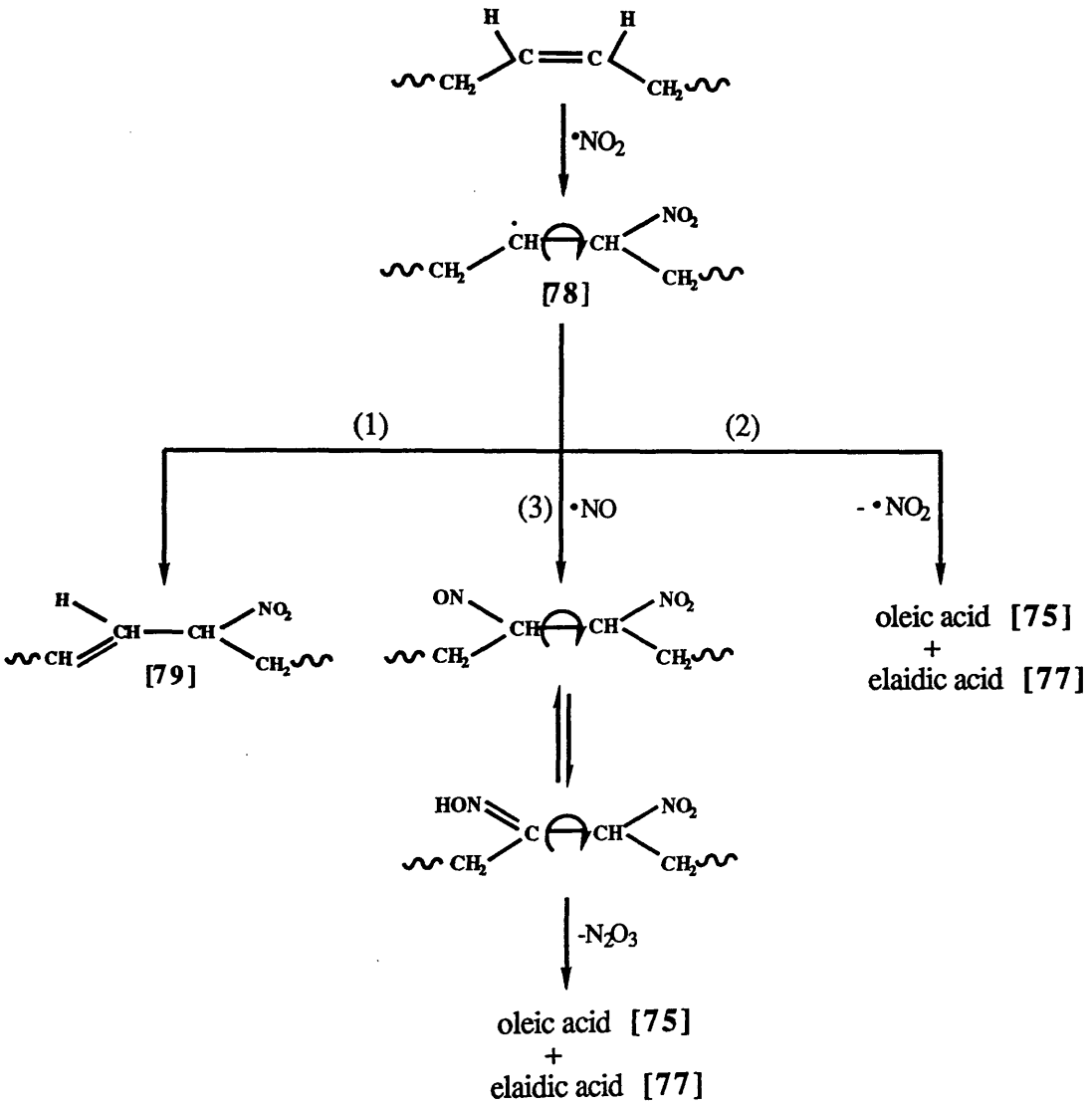
H
H
C
C
CH2
CH2
•NO2
NO2
CH
CH
CH2
CH2
[78]
(1)
(2)
(3) •NO
- •NO2
H
CH
CH
NO2
CH
CH2
[79]
ON
CH
CH
NO2
CH2
oleic acid [75]
+
elaidic acid [77]
HON
C
CH
NO2
CH2
CH2
-N2O3
oleic acid [75]
+
elaidic acid [77]

Scheme 4.1

4.2.2. ELAIDIC ACID

Elaidic acid, trans-octadec-9-enoic acid, $C_{18}H_{34}O_2$, [77], was obtained from the departmental stores.

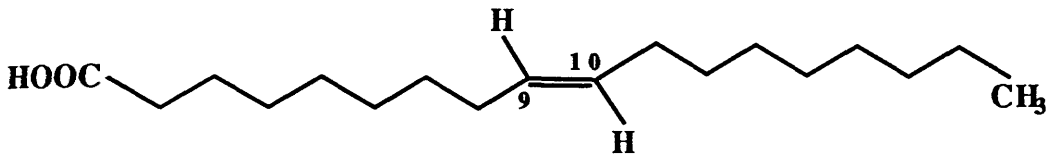

[77]

A sample of elaidic acid, has already been investigated by means of infra red and nuclear magnetic resonance spectroscopy, see Section 4.2.1 of this thesis.

Its elemental analyses, electron impact mass spectrum, and *its* reaction with acidified sodium nitrite are now considered in greater detail.

4.2.2.1 Elemental analyses of elaidic acid

A solid sample of elaidic acid was subjected to standard elemental analyses, yielding the results shown in **Table 4.21**. Oxygen content was estimated by difference.

Table 4.21

Microanalyses data for elaidic acid

Element	% Composition [found]	% Composition [expected for $C_{18}H_{34}O_2$]
C	75.75	76.60
H	13.47	12.06
O	10.78	11.34

4.2.2.2 *Electron impact mass spectrum of elaidic acid*

The electron impact mass spectum establishes that the sample analysed is mainly elaidic ecid. A more complete description of the mass spectrum cracking pattern is given below, in Table 4.22.

Table 4.22

Electron impact mass spectrum of elaidic acid [77]

Mass	Relative Abundance (%)	Ion
282	3.6	$[C_{18}H_{34}O_2]^+$
264	11.4	$[C_{18}H_{32}O]^+$
222	3.3	$[C_{16}H_{30}]^+$
194	1.8	$[C_{14}H_{26}]^+$
193	2.0	$[C_{14}H_{25}]^+$
180	2.8	$[C_{13}H_{24}]^+$
167	2.1	$[C_{12}H_{23}]^+$
153	3.2	$[C_{11}H_{21}]^+$
139	5.0	$[C_{10}H_{19}]^+$
125	9.7	$[C_9H_{17}]^+$
124	8.4	$[C_9H_{16}]^+$
111	16.5	$[C_8H_{15}]^+$
110	14.5	$[C_8H_{14}]^+$
109	10.0	$[C_8H_{13}]^+$
98	19.8	$[C_7H_{14}]^+$
97	34.8	$[C_7H_{13}]^+$
96	19.6	$[C_7H_{12}]^+$
95	14.3	$[C_7H_{11}]^+$
85	10.0	$[C_6H_{13}]^+$

Mass	Relative Abundance (%)	Ion
84	25.3	$[C_6H_{12}]^+$
83	45.9	$[C_6H_{11}]^+$
69	62.5	$[C_5H_9]^+$
55	100.0	$[C_4H_7]^+$
43	62.1	$[C_3H_7]^+$
42	14.3	$[C_3H_6]^+$
41	89.5	$[C_3H_5]^+$
29	34.1	$[C_2H_5]^+$
28	22.1	$[C_2H_4]^+$
27	17.9	$[C_2H_3]^+$

4.2.2.3 The action NO and NO_2 on elaidic acid

By analogy with the reaction carried out on oleic acid, elaidic acid was allowed to react with an acidified solution of sodium nitrite, (elaidic acid:$NaNO_2$ = 1:3). The ^{13}C-{^{1}H} n.m.r. spectrum of the products, at 50.323 MHz, was then recorded and fully analyzed. This spectrum is shown in **Figure 4.35**. By compairing it with that obtained from the starting material, as well as those obtained from oleic acid before and after reaction, it turns out that the reaction mixture consists mainly of elaidic and oleic acids in a ratio of 6:1. The ^{13}C n.m.r. chemical shifts assignments are shown in detail, in **Table 4.23**.[109] The two peaks that arise at δ=177.85 ppm and δ=21.22 ppm are due to the acetic acid present in excess in the reaction mixture. This shows quite dramatically that part of the original elaidic acid was isomerized to oleic acid, in a similar way, as was found for oleic acid itself.

Table 4.23

^{13}C n.m.r. chemical shifts, δ_C, of the olefinic residue of elaidic acid present in the reaction mixture

C-9	C-10
130.15	130.44

^{13}C n.m.r. chemical shifts, δ_C, of the olefinic residue of oleic acid present in the reaction mixture

C-9	C-10
129.68	129.97

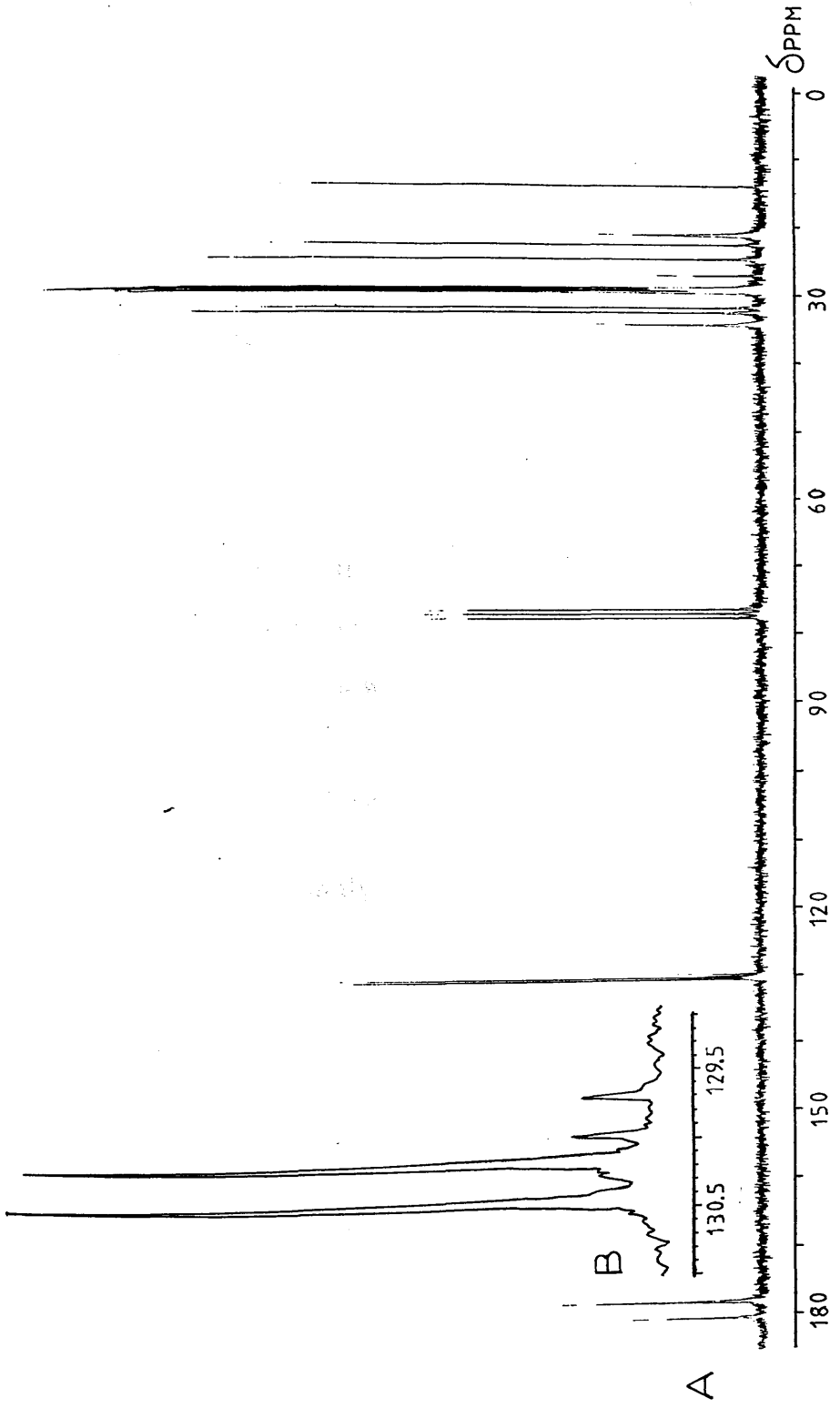

Figure 4.35 The 50.325 MHz ^{13}C-{^{1}H} n.m.r. spectrum, {A}, and the corresponding extended spectrum of the olefinic region, {B},of the products obtained from the reaction of elaidic acid : $NaNO_2$ = 1:3 in $CDCl_3$ solution, at ambient temperature

4.2.3. LINOLEIC ACID

Linoleic acid, cis, cis-octadeca-9, 12-dienoic acid, $C_{18}H_{32}O_2$, **[76]**, was obtained from the departmental stores, and was used without further purification.

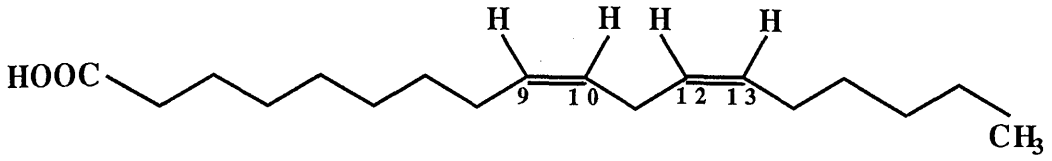

[76]

A sample of linoleic acid was then subjected to elemental analyses. Its electron impact mass spectrum, its infra red spectrum, its ^{1}H n.m.r., its ^{13}C-{^{1}H} n.m.r., its ^{13}C-{^{1}H} 90° and 135° D.E.P.T. spectra, as well as its two dimensional HETCOR ^{13}C-^{1}H direct correlation and long-range correlation spectra were all recorded and fully analyzed.

4.2.3.1 Elemental analyses of linoleic acid

Elemental analyses of a solid sample of linoleic acid gave the percentage abundances for carbon and hydrogen that are listed in **Table 4.24**. Oxygen content was estimated by difference.

Table 4.24

Microanalyses data for linoleic acid

Element	% Composition [found]	% Composition [expected for $C_{18}H_{32}O_2$]
C	76.99	77.14
H	11.30	11.43
O	11.71	11.43

4.2.3.2 ^{13}C and ^{1}H nuclear magnetic resonance studies of $CDCl_3$ solutions of linoleic acid

The ^{13}C-{^{1}H}, and the ^{13}C-{^{1}H} 90° and 135° D.E.P.T. spectra of the sample of linoleic acid in $CDCl_3$ solution, at 298 K, are shown in **Figures 4.36A, 4.36B and 4.36C** respectively. The spectra show clearly that the solute contains only linoleic acid. Resonances from C(1), C(17) and (18) were unambiguously assigned in these figures, but signals from the individual alkenic carbons and from the individual aliphatic residues could not be assigned from these same figures, themselves. The ^{13}C-^{1}H direct correlation and the ^{13}C-^{1}H long-range correlation, two dimensional HETCOR spectra were therefore recorded and are shown in **Figures 4.37** and **4.38** respectively. By combining information from all these spectra with the information obtained from the 200.132 MHz ^{1}H n.m.r. spectrum, shown in **Figure 4.39**, all the remaining carbon resonances were then unambiguously assigned. ^{13}C n.m.r. chemical shifts of all the carbon nuclei in linoleic acid,[109] as well as the ^{1}H n.m.r. chemical shifts, obtained by using these procedures are listed in **Table 4.25**. A close look at the ^{1}H n.m.r. spectrum of linoleic acid, **Figure 4.39**, indicates that four equivalent hydrogens give rise to the 1:3:3:1 quartet at δ_H = 2.035 ppm. These hydrogens can only be attached to C(8) and C(14). From this conclusion, it was then easy to determine the exact ^{13}C n.m.r. chemical shifts, as well as the ^{1}H n.m.r. chemical shifts, by combining all the spectra shown in **Figures 4.36-4.39.**

For example, since δ_H = 2.035 ppm corresponds to the hydrogens attached to C(8) and C(14), the ^{13}C n.m.r. chemical shifts corresponding to these two carbons are $\delta_{C(8)} = \delta_{C(14)}$ = 27.14 ppm; deduced from **Figure 4.37**. The ^{13}C-^{1}H long-range HETCOR spectra in

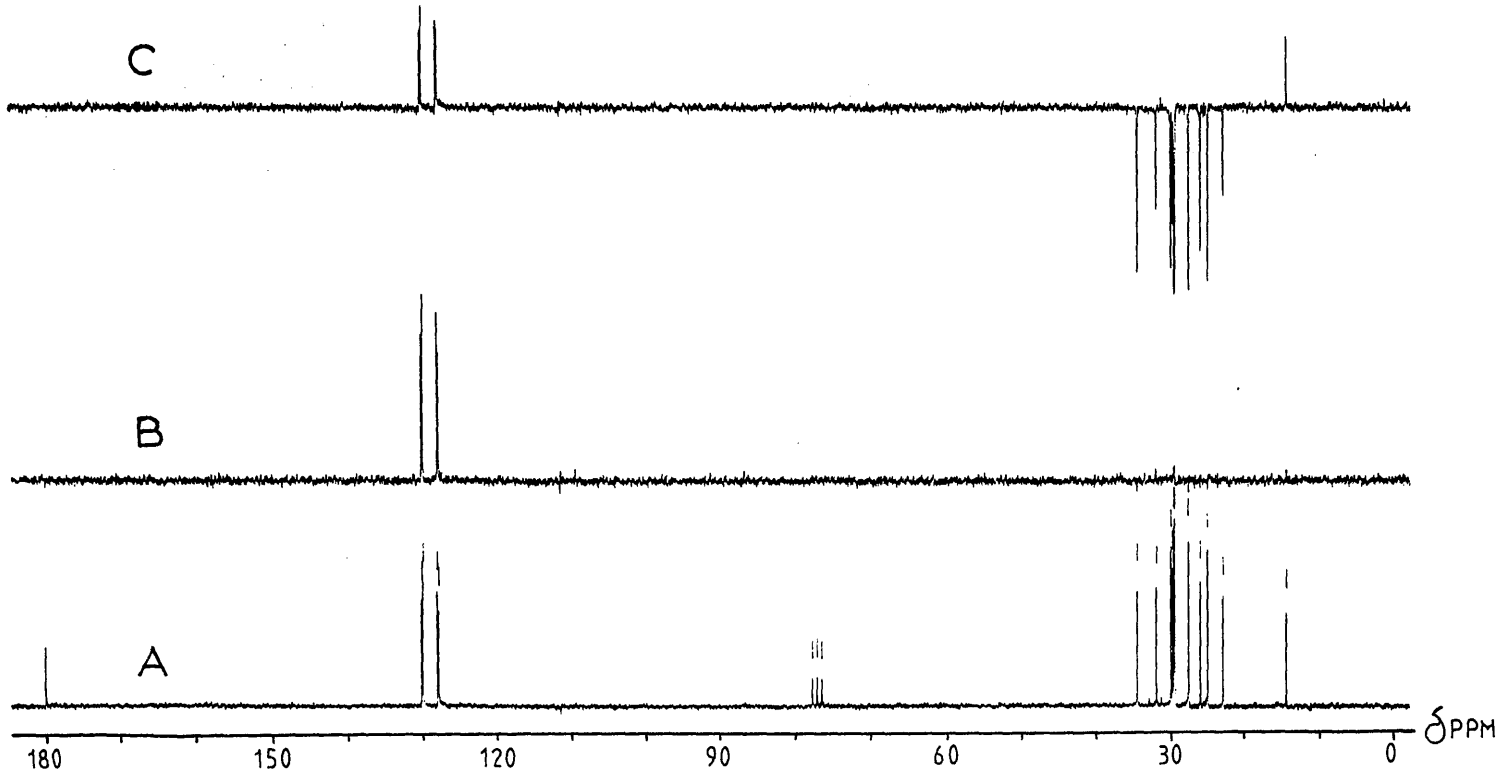

Figure 4.36 The 50.325 MHz ^{13}C-{^{1}H} n.m.r. spectrum, {A}, and the corresponding $\Theta = 90^{o}$, {B}, and $\Theta = 135^{o}${C}, D.E.P.T. spectra of linoleic acid in $CDCl_3$ solution, at ambient temperature

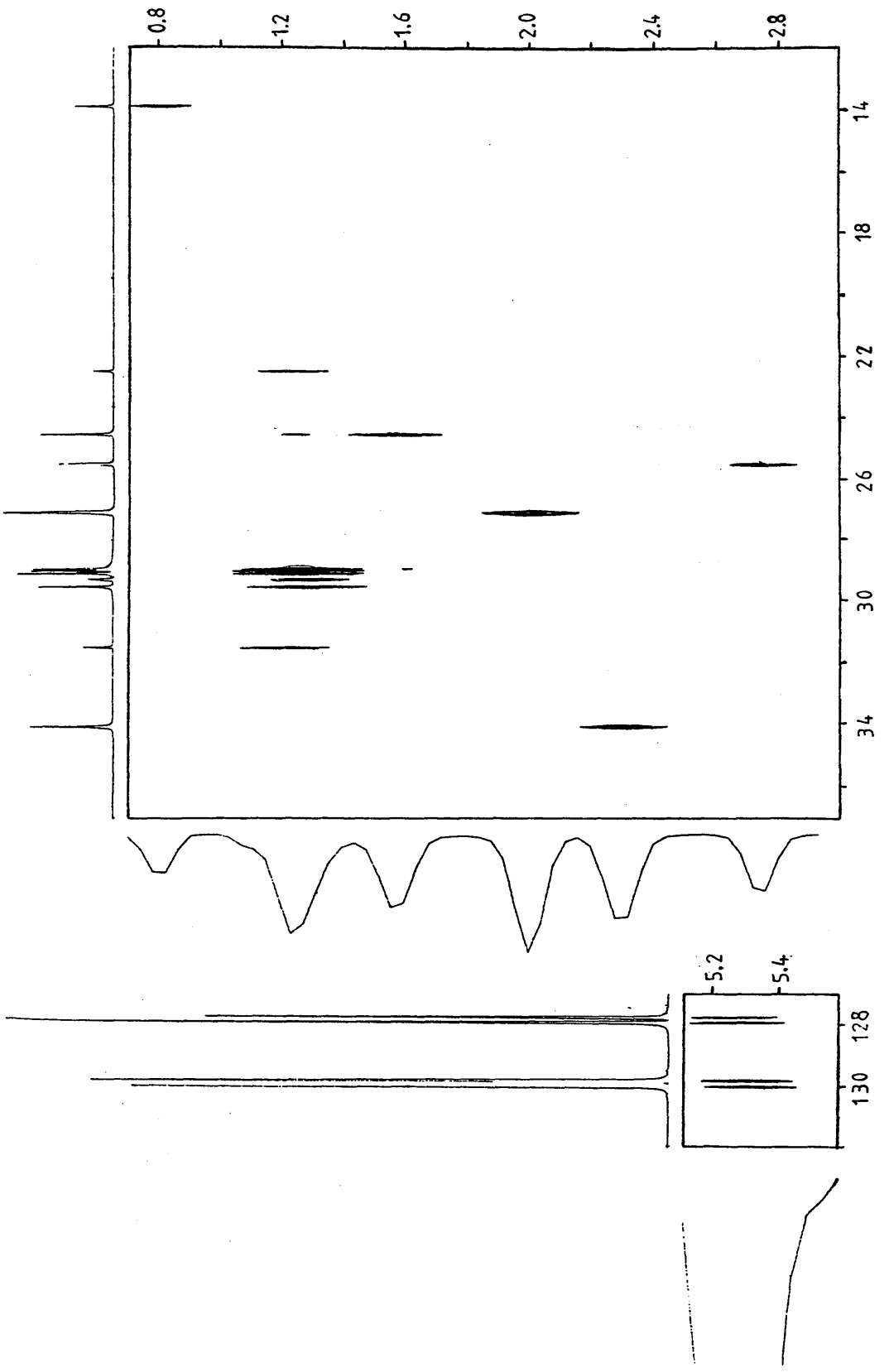

Figure 4.37 The ^{13}C-^{1}H direct correlation, two dimensional HETCOR spectrum of linoleic acid

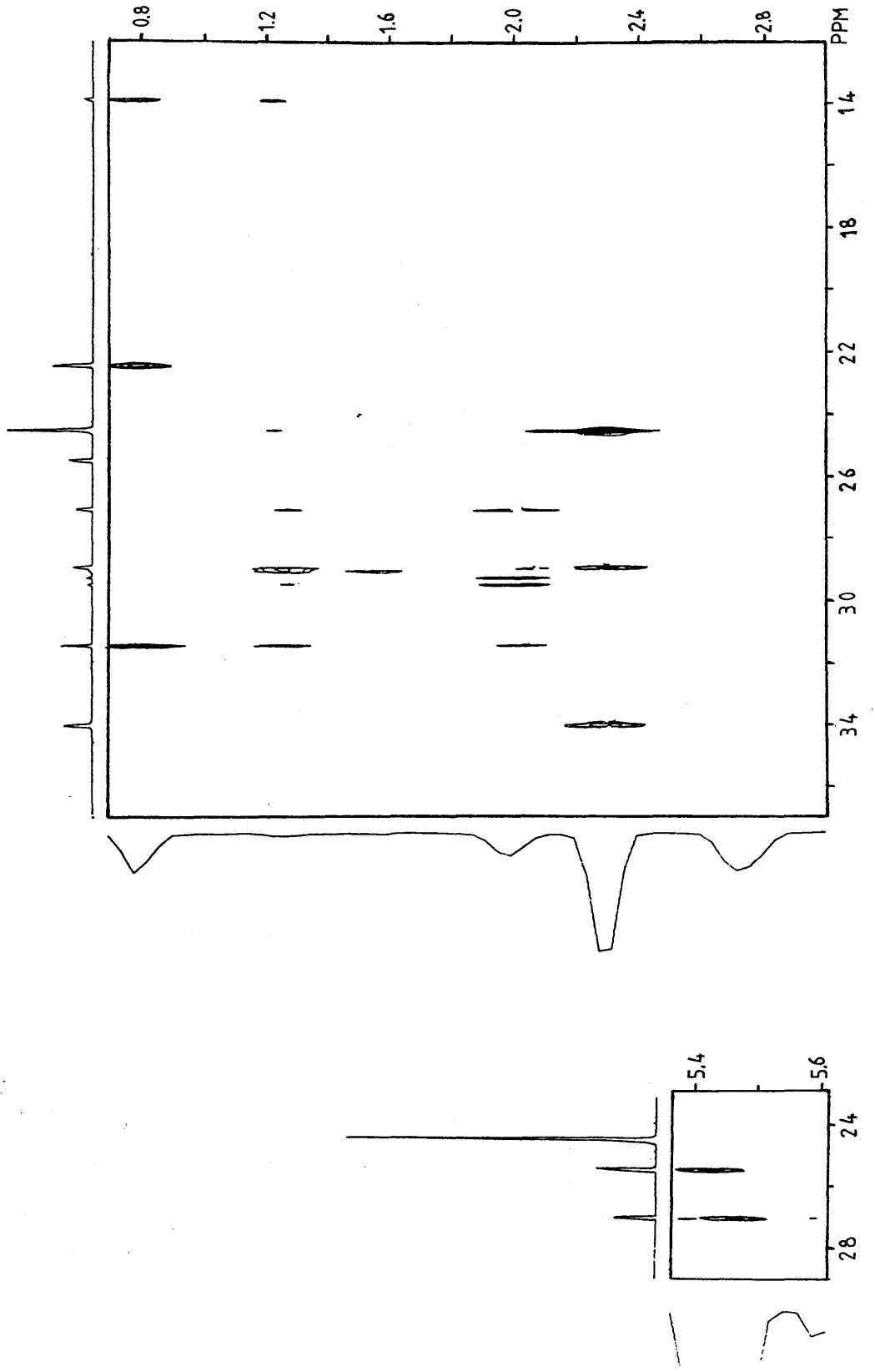

Figure 4.38 The ^{13}C-^{1}H long-range correlation, two dimensional HETCOR spectrum of linoleic acid

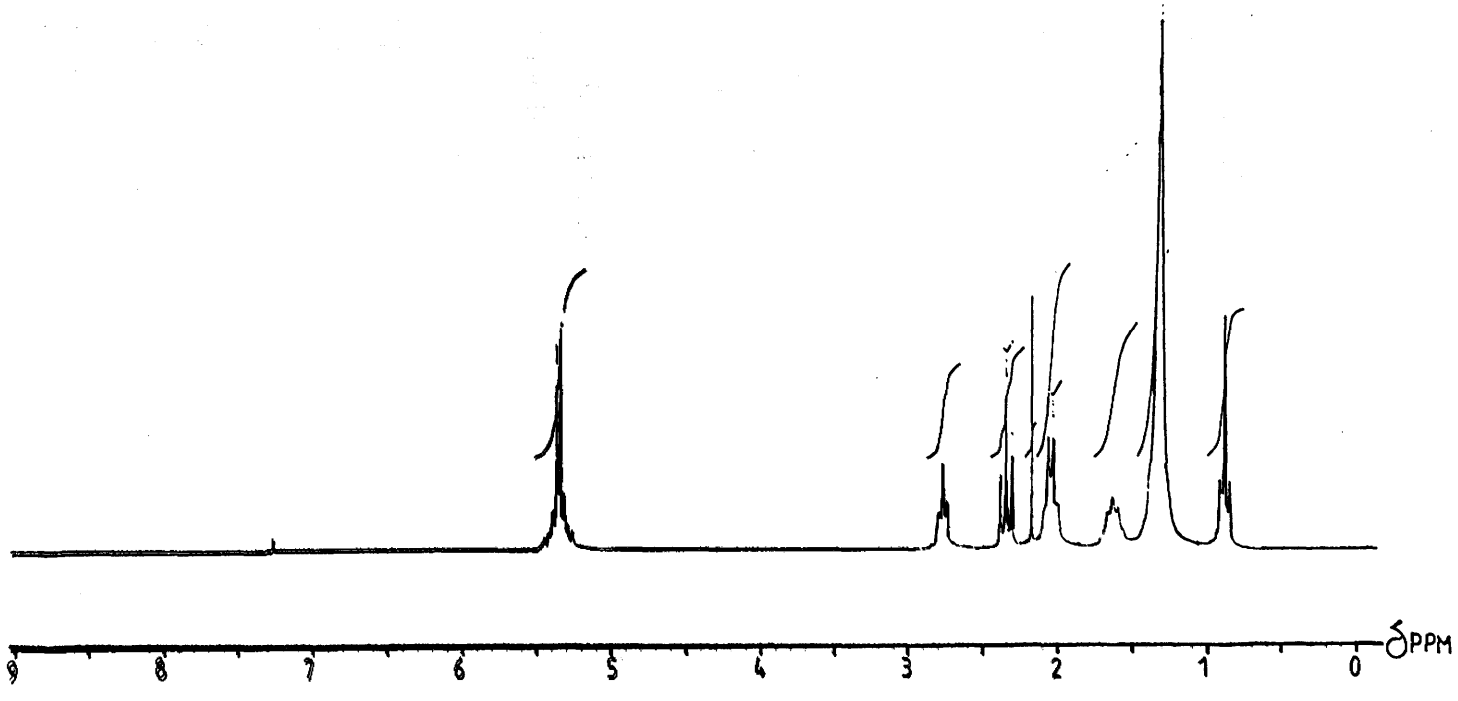

Figure 4.39 The 200.132 MHz ^{1}H n.m.r. spectrum of linoleic acid in $CDCl_3$ solution, at ambient temperature

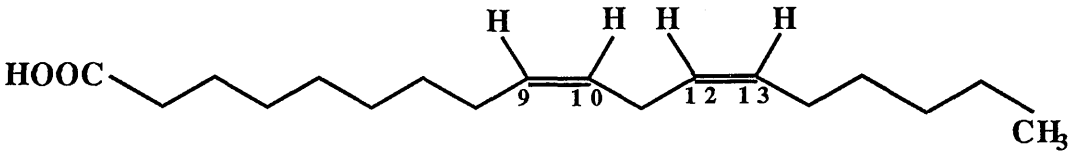

Table 4.25

^{13}C n.m.r. chemical shifts, δ_C, for linoleic acid

δ_C(ppm)($CDCl_3$)

C-1	C-2	C-3	C-4	C-5	C-6
180.48	34.07	24.60	28.99	29.11	29.03
	C-7	C-8	C-9		
	29.31/29.54	27.15	130.14/129.95		
	C-10	C-11	C-12		
	128.01/127.85	25.58	127.85/128.01		
C-13	C-14	C-15	C-16	C-17	C-18
129.95/130.14	27.15	29.54/29.31	31.46	22.54	14.02

^{1}H n.m.r. chemical shifts, δ_H, for linoleic acid

δ_H(ppm)($CDCl_3$)

Chemical Shift	Hydrogens
5.320	/-C<u>H</u>=CH-CH_2-CH=C<u>H</u>-/
5.230	/-CH=C<u>H</u>-CH_2-C<u>H</u>=CH-/
2.775	/-CH=CH-C<u>H_2</u>-CH=CH-/
2.332	HOOC-C<u>H_2</u>-CH_2-/
2.035	/-C<u>H_2</u>-CH=CH-CH_2-CH=CH-C<u>H_2</u>-/
1.620	HOOC-CH_2-C<u>H_2</u>-/
1.212	HOOC-CH_2-CH_2-(C<u>H_2</u>)$_4$-//-(C<u>H_2</u>)$_3$-CH_3
0.874	/-CH_2-C<u>H_3</u>

Figure 4.38 then enable the signals centred at δ_H = 5.320 ppm to be assigned to the olefinic protons C(9)-H and C(13)-H, so that the remaining olefinic proton signals centred at δ_H = 5.230 ppm can now be assigned to C(10)-H and C(12)-H. The ^{13}C-^{1}H direct HETCOR spectra on **Figure 4.37** then enable the ^{13}C resonances from C(9) and C(13) to be discriminated from corresponding resonances from C(10) and C(12).

Similar, cyclic, reasoning was then applied to the spectra in **Figures 4.37-4.39** until the assignments become self-consistent, and eventually chemical shifts were thus assigned to all the ^{13}C and ^{1}H nuclei in linoleic acid. These assignments are as already given in **Table 4.25**.

A summary of the procedures used to assign the ^{13}C and ^{1}H n.m.r. signals is given in the following page.

The ^{13}C n.m.r. assignments are almost identical to the corresponding assignments made by J.G. Batchelor *et al.*,[109] with a small chemical shift difference of about ± 0.30 ppm. In addition, the chemical shifts of C(4)-C(7) are now distinguishable because the spectra were recorded on a 50.323 MHz computer-controlled Fourier transform system, instead of a 22.6 MHz used earlier.

SUMMARY OF THE PROCEDURES USED

1/ $\delta(H_2)_8 = \delta(H_2)_{14}$ = 2.035 ppm (4H, quartert)/{**Figure 4.39**}

2/ $\delta(C)_8 = \delta(C)_{14}$ = 27.15 ppm/{**Figure 4.37**}

3/ $\delta(H)_9 = \delta(H)_{13}$ = 5.320 ppm/{**Figure 4.38**}

4/ $\delta(H)_{10} = \delta(H)_{12}$ = 5.230 ppm/{**Figure 4.38**}

5/ $\delta(C)_{11}$ = 25.58 ppm/{**Figure 4.38**}

6/ $\delta(H_2)_{11}$ = 2.775 ppm/{**Figure 4.37**}

7/ $\delta(C)_{9/13}$ = 130.14/129.04 ppm/{**Figure 4.37**}

8/ $\delta(C)_{10/12}$ = 128.01/127.85 ppm/{**Figure 4.37**}

9/ $\delta(C)_1$ = 180.48 ppm/{**Figure 4.36**}

10/ $\delta(H_2)_2$ = 2.332 ppm (2H, triplet)/{**Figure 4.39**}

11/ $\delta(C)_2$ = 34.07 ppm/{**Figure 4.37**}

12/ $\delta(H_2)_3$ = 1.620 ppm (2H, quintet)/{**Figure 4.39**}

13/ $\delta(C)_3$ = 24.60 ppm/{**Figure 4.37**}

14/ $\delta(C)_{18}$ = 14.02 ppm/{**Figure 4.36**}

15/ $\delta(H_3)_{18}$ = 0.874 ppm (3H, triplet)/{**Figure 4.37**}

16/ $\delta(C)_{17}$ = 22.54 ppm/{**Figure 4.38**}

17/ $\delta(H_2)_{17}$ = 1.212 ppm (3H, triplet)/{**Figure 4.37**}

18/ $\delta(C)_4$ = 28.99 ppm/{**Figure 4.38**}

19/ $\delta(H_2)_4$ = 1.212 ppm (3H, triplet)/{**Figure 4.37**}

20/ $\delta(C)_{16}$= 31.49 ppm/{**Figure 4.38**}

21/ $\delta(H_2)_{16}$ = 1.212 ppm (3H, triplet)/{**Figure 4.37**}

22/ $\delta(C)_4$ = 29.544/29.31 ppm/{**Figure 4.38**}

23/ $\delta(C)_6$= 29.03 ppm/{**Figure 4.38**}

24/ $\delta(C)_5$= 29.11 ppm/{**Figure 4.38**}

4.2.3.3 The olefinic region of the ^1H n.m.r. spectrum of linoleic acid

The olefinic region of the ^1H n.m.r. spectrum of linoleic acid was subjected to an especially detailed analysis, and all its relevant spin-Hamiltonian parameters were evaluated. These are given in **Table 4.26.** A spectrum, for a proton resonance frequency of 200.132 MHz, calculated using these parameters is shown in **Figure 4.40.** The corresponding experimental spectrum is shown in **Figure 4.41.**

Table 4.26

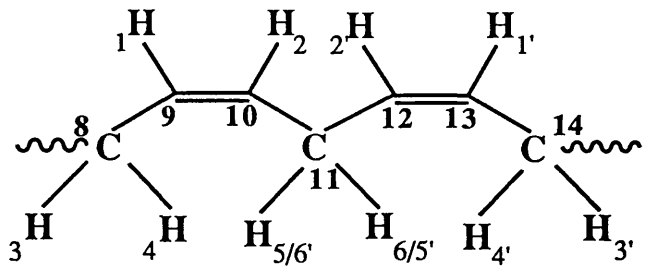

Relative Chemical Shifts/Hz

$\delta_1 = 0.00,\ \delta_2 = 9.80,\ \delta_3 = 509.34,\ \delta_4 = 509.34,\ \delta_5 = 657.43,$

$\delta_6 = 657.43,\ \delta_{1'} = 1.20,\ \delta_{2'} = 11.00,\ \delta_{3'} = 509.34,$

$\delta_{4'} = 509.34,\ \delta_{5'} = 657.43,\ \delta_{6'} = 657.43$

$J_{H,H}$/Hz

$J_{12}=J_{1'2'}=10.75,\ J_{13}=J_{1'3'}=-1.80,\ J_{14}=J_{1'4'}=-1.80,\ J_{15}=J_{1'5'}=2.85,$

$J_{16}=J_{1'6'}=2.85,\ J_{23}=J_{2'3'}=11.00,\ J_{24}=J_{2'4'}=11.00,\ J_{25}=J_{2'5'}=-1.80,$

$J_{26}=J_{2'6'}=-1.80,\ J_{34}=J_{3'4'}=14.00,\ J_{35}=J_{3'5'}=0.00,\ J_{36}=J_{3'6'}=0.00,$

$J_{45}=J_{4'5'}=0.00,\ J_{46}=J_{4'6'}=0.00,\ J_{56}=J_{5'6'}=14.00,$

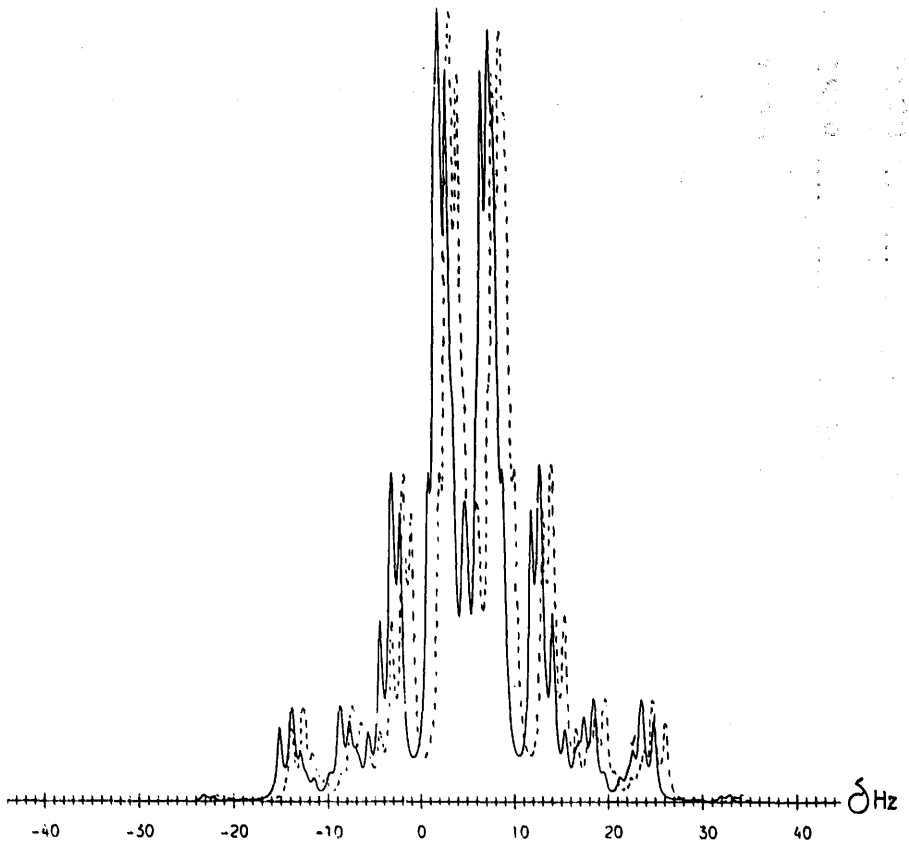

Figure 4.40 The calculated ^{1}H n.m.r. spectrum of the olefinic region of linoleic acid

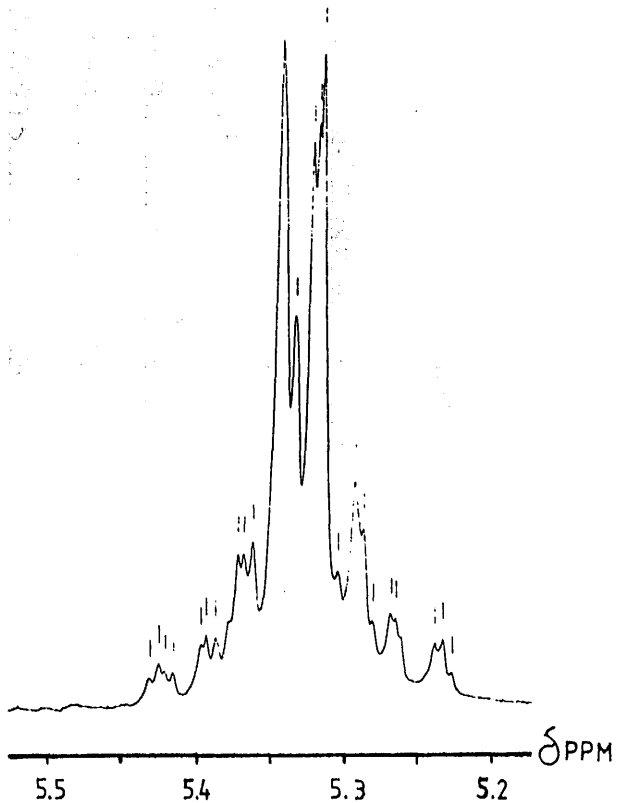

Figure 4.41 The experimental 200.132 MHz ^{1}H n.m.r. spectrum of the olefinic region of linoleic acid

4.2.3.4 Infra red analyses of linoleic acid

The infra red spectum of linoleic acid is shown in **Figure 4.42**, and detailed assignments of the vibrational frequencies are listed in **Table 4.27**.

Table 4.27

Infra red assignments of linoleic acid

Band/cm^{-1}	Assignment
3010	-CH=, stretching mode of -CH=CH-
2960	$-CH_3$, asymmetric stretching mode
2930/2915	$>CH_2$, asymmetric stretching modes
2870	$-CH_3$, asymmetric stretching mode
2859	$>CH_2$, symmetric stretching mode
1720	>C=O, stretching mode
1460/1412	$>CH_2$, deformation modes and $-CH_3$, asymmetric deformation modes
1380	$-CH_3$, symmetric deformation mode
1285/1250/1220	$>CH_2$, wags
940	unassigned
722	-CH=, wag of cis olefinic

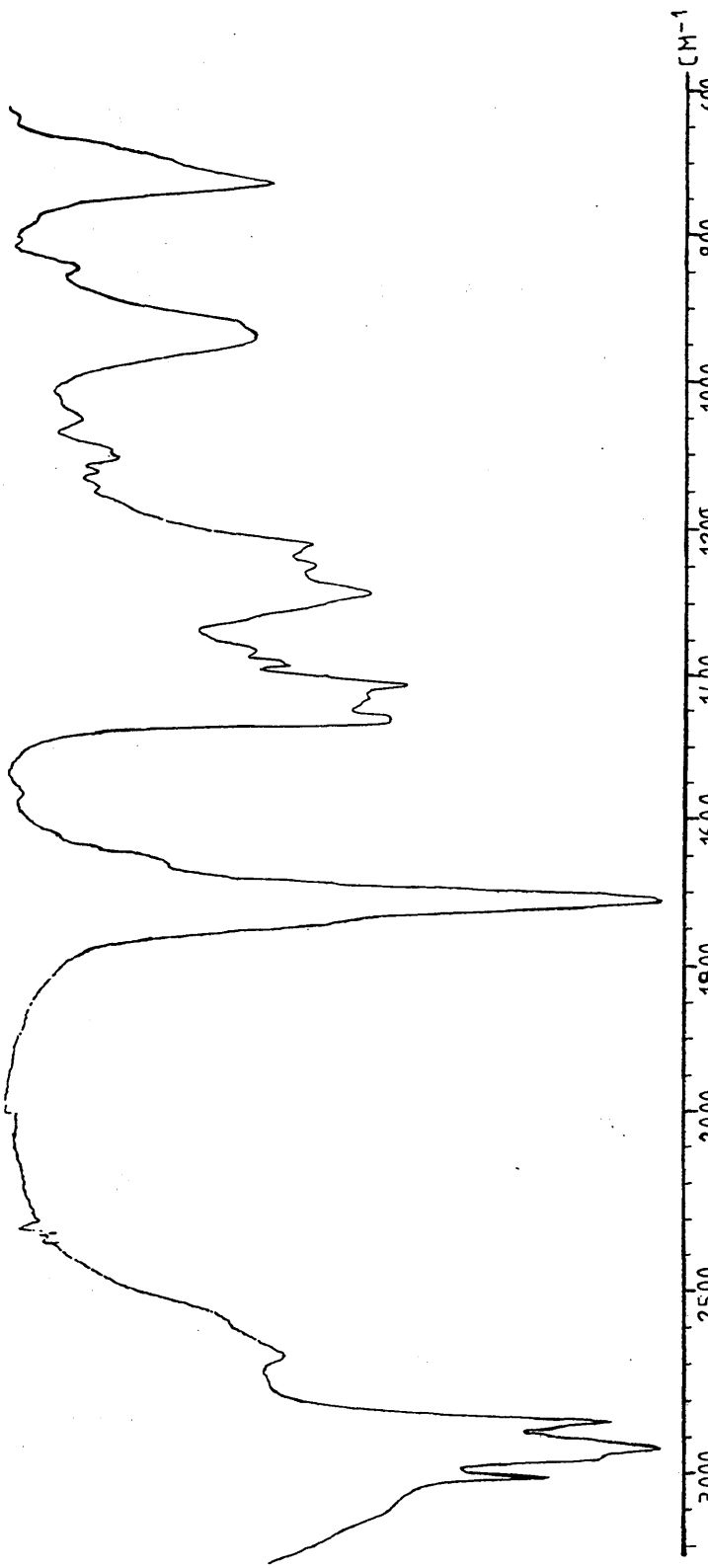

Figure 4.42 The infra red spectrum of linoleic acid (Thin Film)

4.2.3.5 Electron impact mass spectrum of linoleic acid

The electron impact mass spectum shows clearly that the investigated fatty acid sample is of linoleic acid. A detailed more complete description of the mass spectrum cracking pattern is given in **Table 4.28.**

Table 4.28
Electron impact mass spectrum of linoleic acid [76]

Mass	Relative Abundance (%)	Ion
281	2.1	$[^{13}C^{12}C_{17}H_{32}O_2]^+$
280	10.6	$[C_{18}H_{32}O_2]^+$
262	0.7	$[C_{17}H_{32}O]^+$
223	0.8	$[C_{14}H_{23}O_2]^+$
210	1.2	$[C_{13}H_{22}O_2]^+$
196	1.5	$[C_{12}H_{20}O_2]^+$
182	2.0	$[C_{11}H_{18}O_2]^+$
168	1.7	$[C_{10}H_{16}O_2]^+$
164	2.2	$[C_{12}H_{20}]^+$
163	1.9	$[C_{12}H_{19}]^+$
150	4.2	$[C_{11}H_{18}]^+$
149	3.3	$[C_{11}H_{17}]^+$
136	4.5	$[C_{10}H_{16}]^+$
135	4.0	$[C_{10}H_{15}]^+$
123	7.4	$[C_9H_{15}]^+$
122	4.7	$[C_9H_{14}]^+$
121	4.8	$[C_9H_{13}]^+$
109	16.6	$[C_8H_{13}]^+$

Mass	Relative Abundance (%)	Ion
108	5.1	$[C_8H_{12}]^+$
107	5.7	$[C_8H_{11}]^+$
96	26.5	$[C_7H_{12}]^+$
95	41.8	$[C_7H_{11}]^+$
82	36.5	$[C_6H_{10}]^+$
81	68.2	$[C_6H_9]^+$
80	18.2	$[C_6H_8]^+$
79	41.2	$[C_6H_7]^+$
70	32.5	$[C_5H_{10}]^+$
69	36.8	$[C_5H_9]^+$
68	95.5	$[C_5H_8]^+$
55	76.9	$[C_4H_7]^+$
54	39.1	$[C_4H_6]^+$
53	16.5	$[C_3H_5]^+$
45	13.3	$[CHO_2]^+$
43	33.5	$[C_4H_7]^+$
42	13.6	$[C_4H_6]^+$
41	100.0	$[C_4H_5]^+$
39	23.7	$[C_3H_3]^+$
29	45.0	$[C_2H_5]^+$
28	13.2	$[C_2H_4]^+$
27	25.3	$[C_2H_3]^+$

4.2.3.6 The action of NO and NO_2 on linoleic acid

4.2.3.6.1 Linoleic acid:$NaNO_2$ = 1:1

Linoleic acid was allowed to react with an aqueous solution containing an equimolar amount of sodium nitrite in a stoppered flask, at room temperature. The mixture was vigorously shaken, and small amounts of air were periodically allowed into the the reaction flask. The infra red spectrum of the reaction products, obtained by this procedure, was recorded and is shown in **Figure 4.43**. It shows that about 55-60% of the linoleic acid -CH=CH- residues have reacted and weak extra absorptions, now appear in the regions 1755 cm^{-1}, 1555 cm^{-1}, 1360 cm^{-1} and 890 cm^{-1}. These characterise the formation of >C=N-OH and >CH-NO_2 residues and other groups to be characterized later in this thesis.

4.2.3.6.2 Linoleic acid:$NaNO_2$ = 1:2

Since not all the linoleic acid has reacted with the gases generated from an equimolar amount of $NaNO_2$, it was decided to double this amount. The infra red spectrum, shown in **Figure 4.44**, indicates that there is still some unreacted linoleic acid, though there is further reaction of the -CH=CH- residues.

4.2.3.6.3 Linoleic acid:$NaNO_2$ = 1:4

The amount of sodium nitrite was further increased by a factor of four, so that all the linoleic acid could eventually react. The infra red spectrum of the resultant products, **Figure 4.45**, shows that most of the original fatty acid has now reacted and that only about 10% is left unreacted in this case. ^{13}C-{^{1}H}, ^{13}C-{^{1}H} 90° and 135° D.E.P.T. and ^{1}H n.m.r. spectra of these products were also examined.

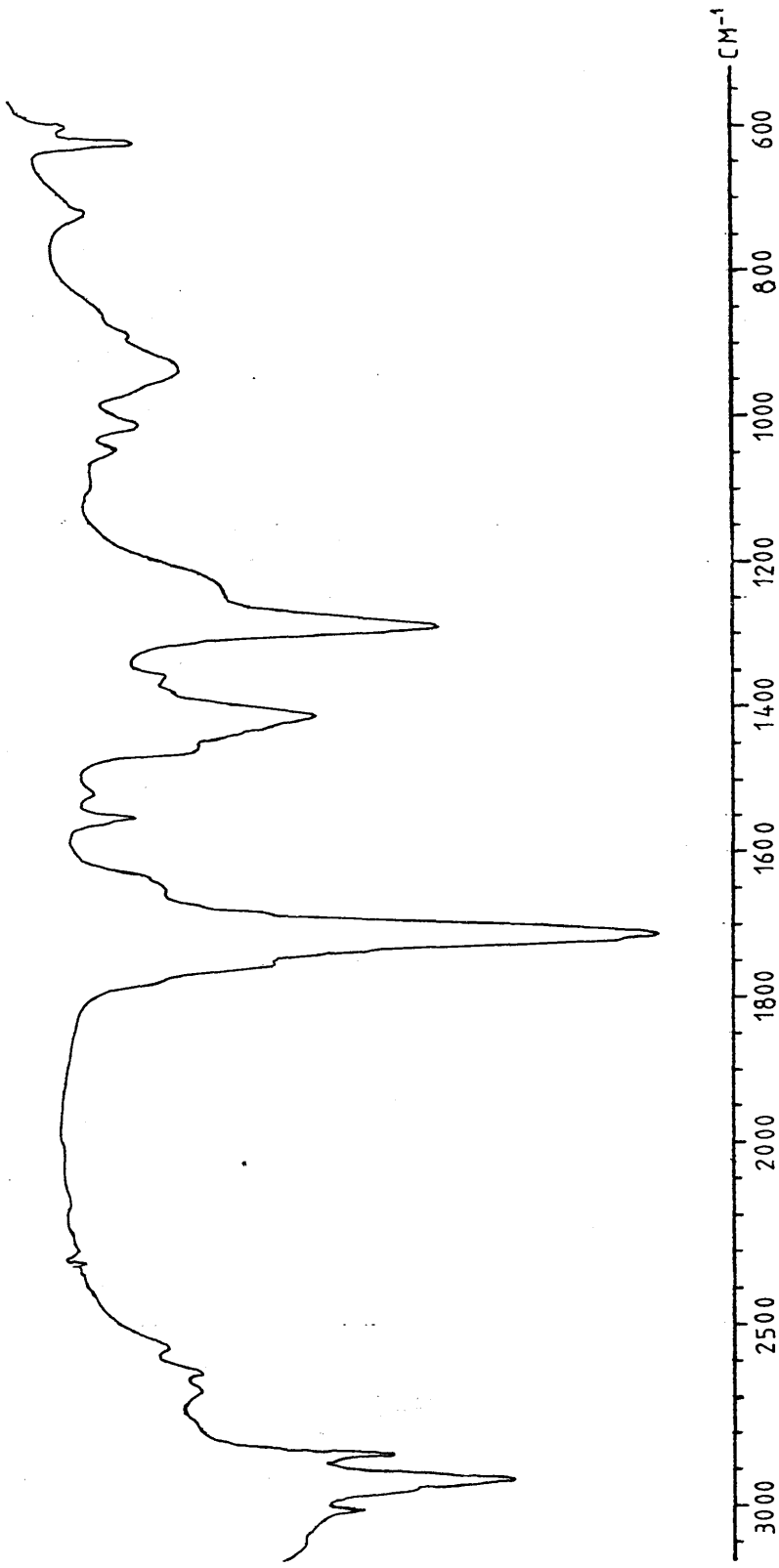

Figure 4.43 The infra red spectrum of the products obtained from the reaction of linoleic acid : $NaNO_2$ = 1:1 (Thin Film)

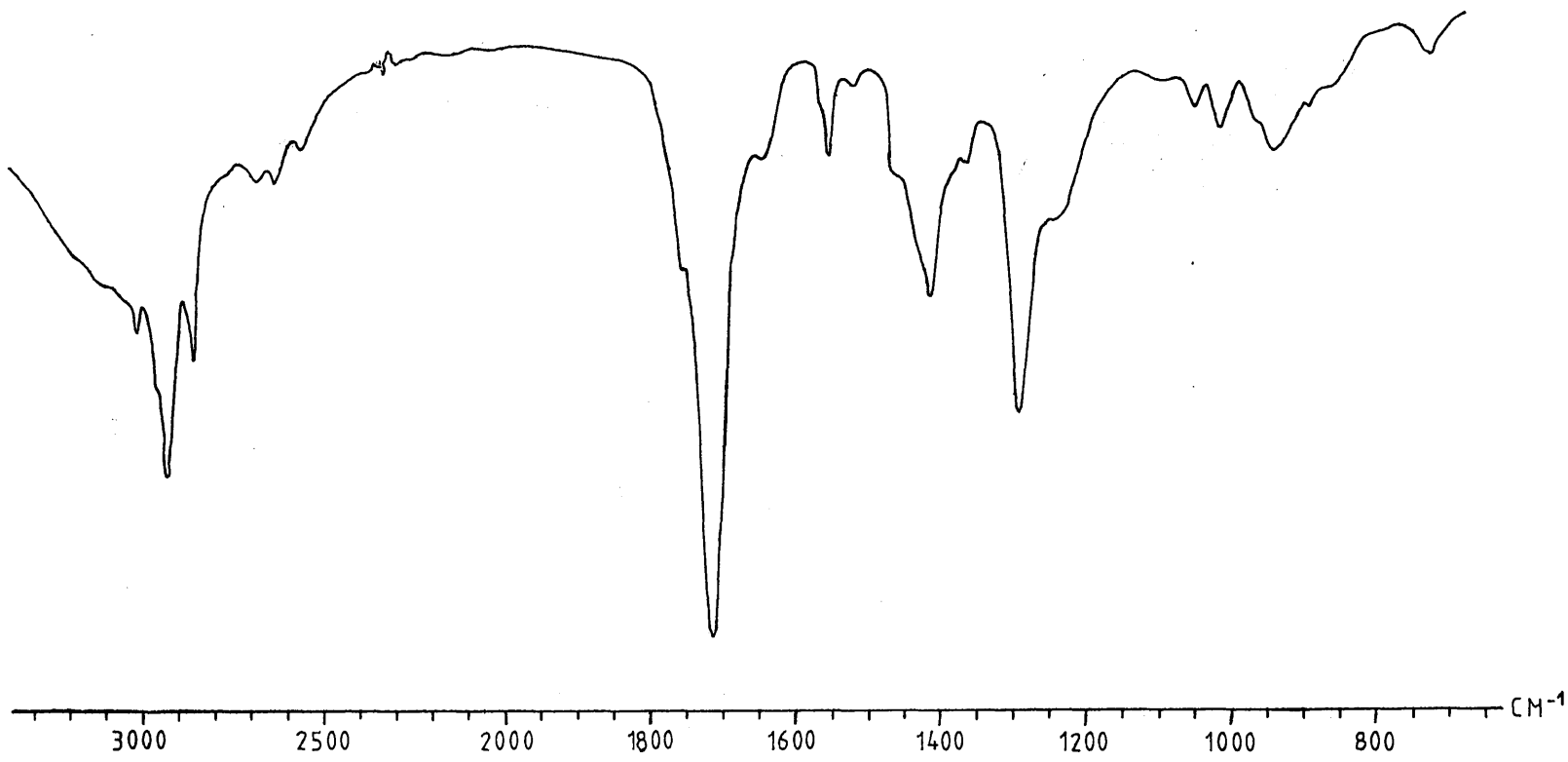

Figure 4.44 The infra red spectrum of the products obtained from the reaction of linoleic acid : $NaNO_2$ = 1:2 (Thin Film)

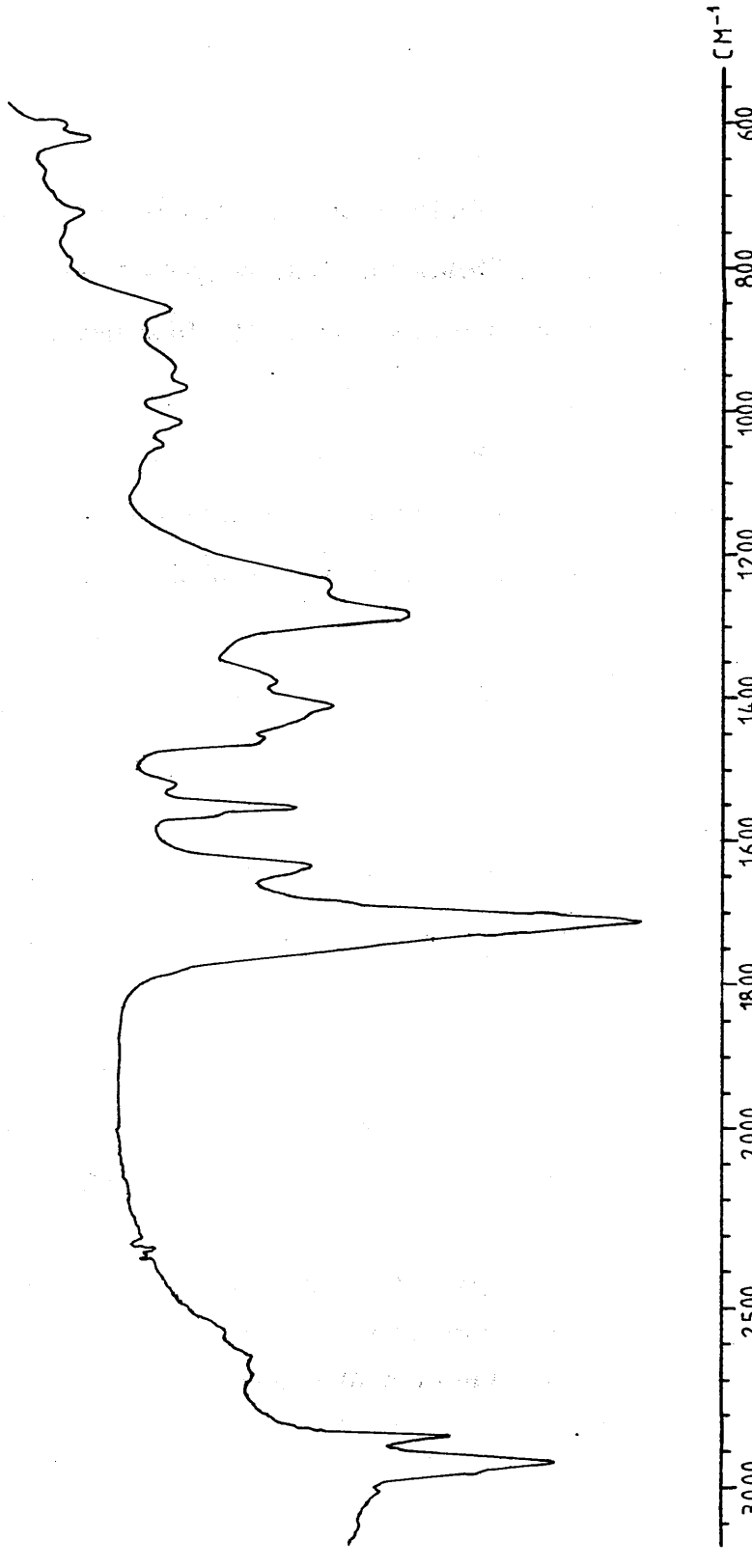

Figure 4.45 The infra red spectrum of the products obtained from the reaction of linoleic acid : $NaNO_2$ = 1:4 (Thin Film)

4.2.3.6.3.a The 50.323 MHz ^{13}C n.m.r. spectra of $CDCl_3$ solutions of the products obtained when linoleic acid reacts with sodium nitrite solution

The ^{13}C-{^{1}H}, and the ^{13}C-{^{1}H} 90° and 135° D.E.P.T.spectra of the reaction products in $CDCl_3$ solution were all recorded and are shown in **Figures 4.46A**, **4.46B** and **4.46C** respectively, and they should be compared with the corresponding spectra of the starting material shown in **Figures 4.36A-4.36C**. The expanded spectrum, **Figure 4.47**, shows that the reaction products contain more than the four olefinic =CH- residues, of linoleic acid. In addition to the original linoleic acid olefinic ^{13}C residues, signals from the other three geometrical isomers, the (Z,E), the (E,Z) and the (E,E) forms of this fatty acid are also present in **Figure 4.47**: there are sixteen olefinic =CH- peaks in all. The ^{13}C assignments in **Figure 4.47**, are shown in detail, in **Table 4.29**. The relative intensities of the olefinic peaks show that the approximate ratio of the fatty acids present in the mixture is: (Z,Z) : (Z,E) : (E,Z) : (E,E) = 3:2:2:1 respectively. Two extra weak peaks can also be observed in **Figure 4.46A**, at δ=177.53 ppm and δ=20.87 ppm: they arise from the acetic acid which was present in excess, in the reaction mixture and is carried through in the procedure used to isolate the reaction products.

4.2.1.5.3.b The 200.132 MHz ^{1}H n.m.r. spectrum of $CDCl_3$ solutions of the products obtained when linoleic acid reacts with sodium nitrite solution

The ^{1}H n.m.r. spectrum is shown in **Figure 4.48**. The expanded version of the olefinic region $5.50 \geq \delta \geq 5.20$ ppm, **Figure 4.49**, shows an interesting and dramatic change in the line shape in the region

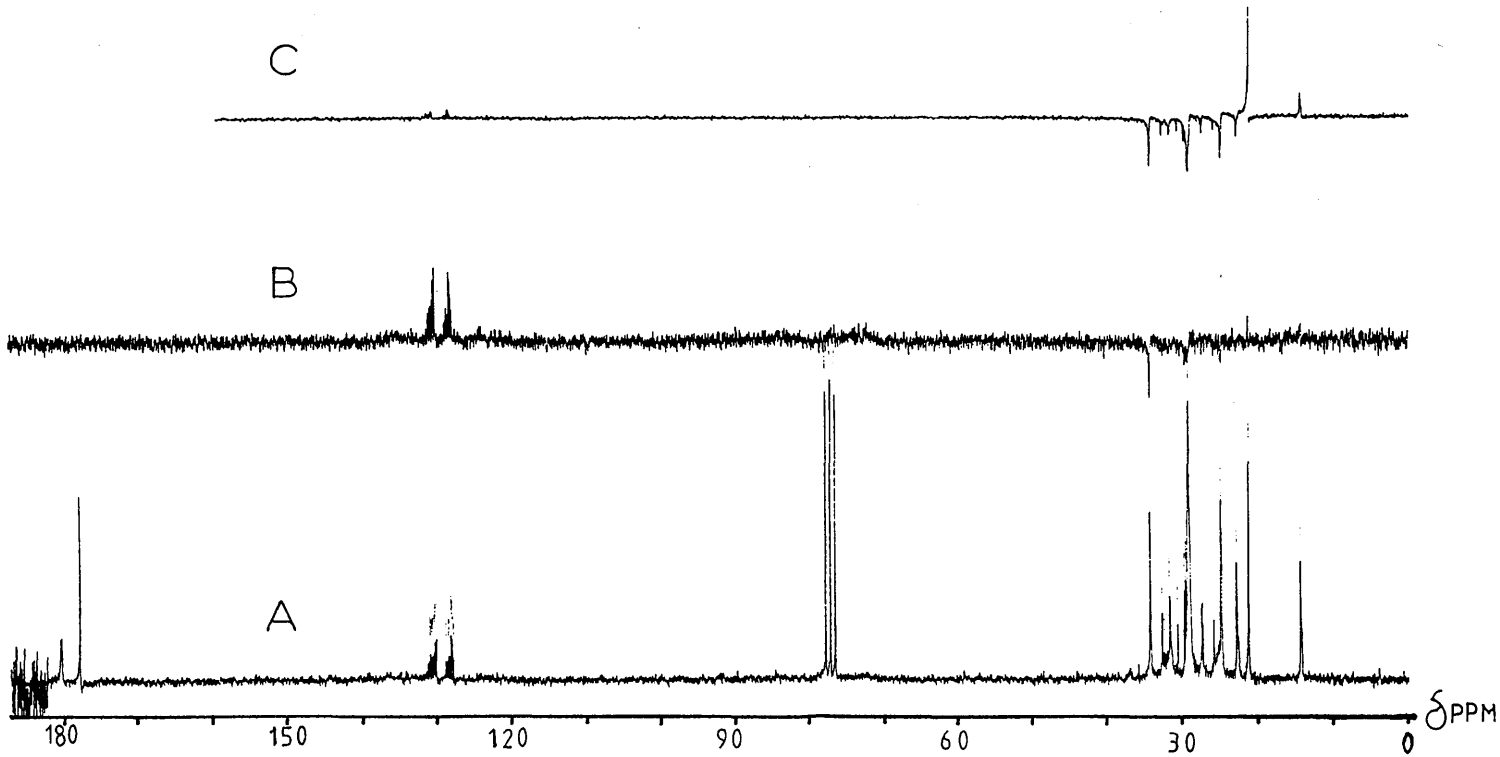

Figure 4.46 The 50.323 MHz ^{13}C-{^{1}H} n.m.r. spectrum, {A}, and the corresponding $\Theta=90^{o}$, {B}, and $\Theta=135^{o}$, {C}, D.E.P.T. spectra of the products obtained from the reaction of linoleic acid : $NaNO_2$ = 1:4 in $CDCl_3$ solution, at ambient temperature

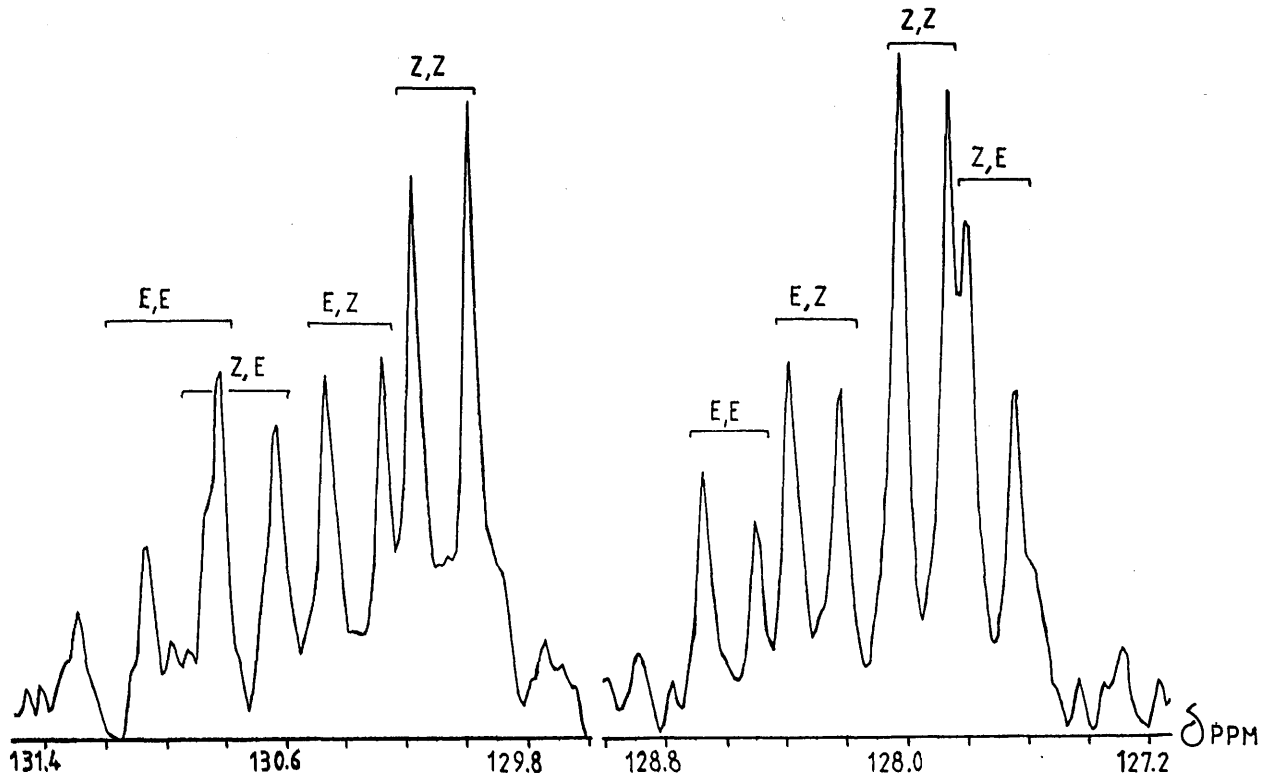

Figure 4.47 The expanded ^{13}C-{^{1}H} n.m.r. spectrum of the olefinic region of the products obtained from the reaction of linoleic acid : $NaNO_2$ = 1:4 in $CDCl_3$ solution, at ambient temperature

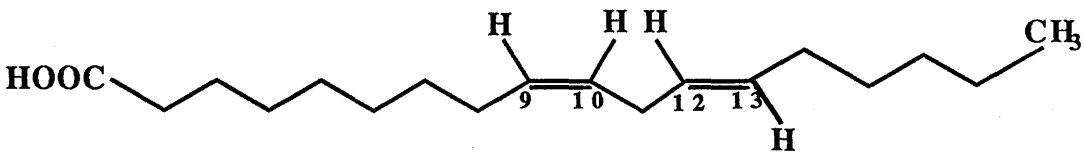

[80]

The (Z,E) isomer of linoleic acid

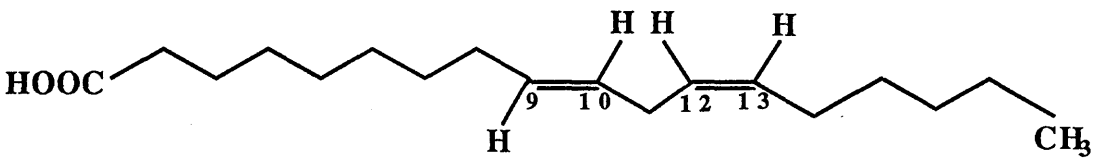

[81]

The (E,Z) isomer of linoleic acid

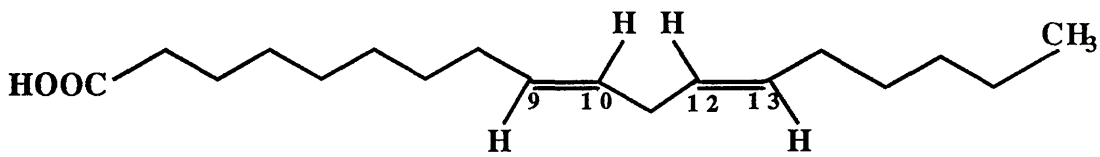

[82]

The (E,E) isomer of linoleic acid: linelaidic acid

Table 4.29 {A}

^{13}C n.m.r. chemical shifts, δ_C, for the (Z,E) isomer of linoleic acid **[80]**

δ_C(ppm)($CDCl_3$)

C-1	C-2	C-3	C-4	C-5	C-6
180.32	34.07	24.59	28.94	29.14	29.00
	C-7	C-8		C-9	
	29.35/29.49	27.10		130.48	
	C-10	C-11		C-12	
	127.77	25.54		127.64	
C-13	C-14	C-15	C-16	C-17	C-18
130.27	26.98	29.26	30.04	22.22	13.94

^{13}C n.m.r. chemical shifts, δ_C, for the (E,Z) isomer of linoleic acid **[81]**

δ_C(ppm)($CDCl_3$)

C-1	C-2	C-3	C-4	C-5	C-6
180.19	32.44	24.52	28.85	29.14	29.00
	C-7	C-8		C-9	
	29.35/29.49	26.98		130.63	
	C-10	C-11		C-12	
	128.38	25.54		128.22	
C-13	C-14	C-15	C-16	C-17	C-18
130.84	27.10	29.26	31.43	22.48	13.99

Table 4.29 {B}

^{13}C n.m.r. chemical shifts, δ_C, for the (E,E) isomer of linoleic acid: linelaidic acid [82]

δ_C(ppm)($CDCl_3$)

C-1	C-2	C-3	C-4	C-5	C-6
180.19	32.44	24.52	28.85	29.14	29.00
	C-7	C-8		C-9	
	29.35/29.49	26.98		131.28	
	C-10	C-11		C-12	
	131.67	25.54		128.50	
C-13	C-14	C-15	C-16	C-17	C-18
131.06	26.98	29.26	30.35	22.22	13.94

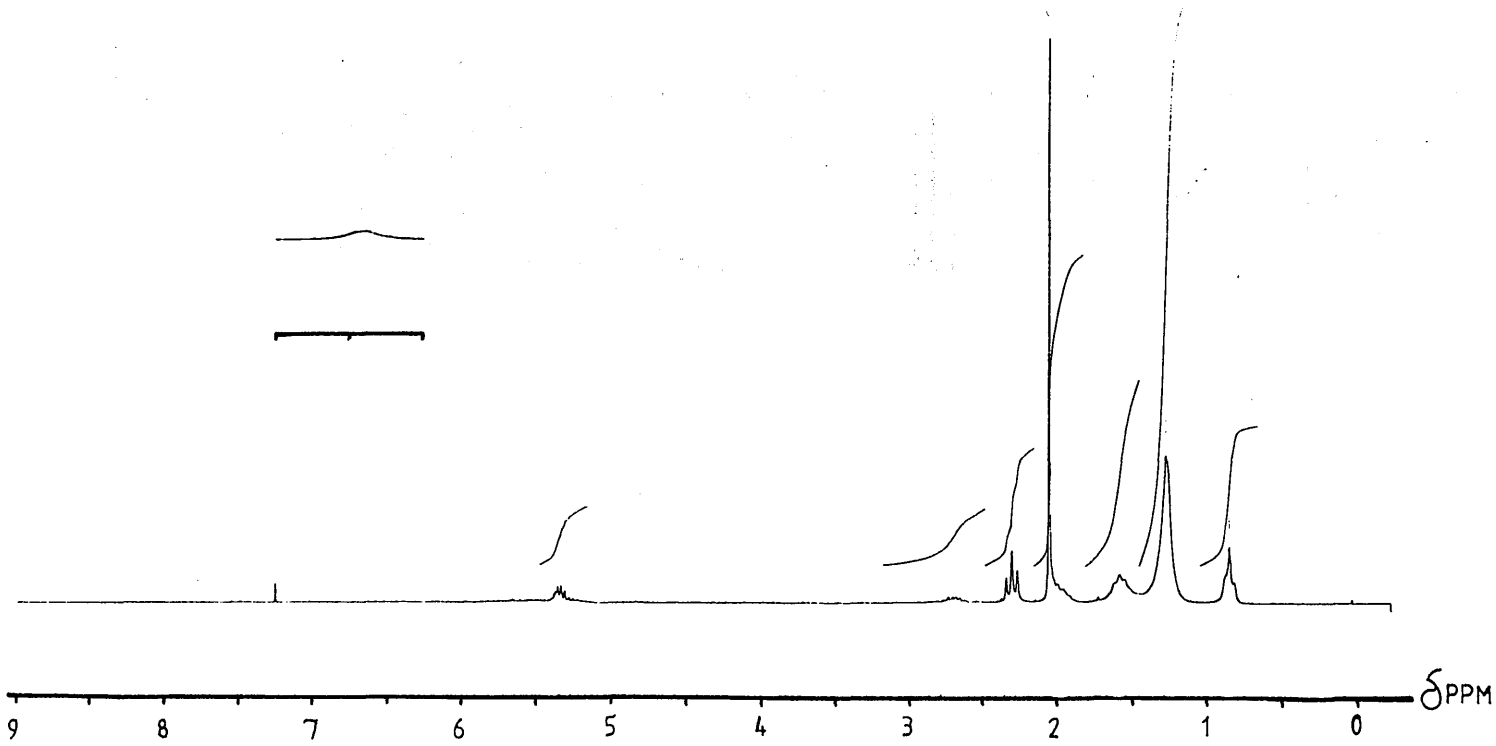

Figure 4.48 The 200.132 MHz ^{1}H n.m.r. spectrum of the products obtained from the reaction of linoleic acid : $NaNO_2$= 1:4 in $CDCl_3$ solution, at ambient temperature

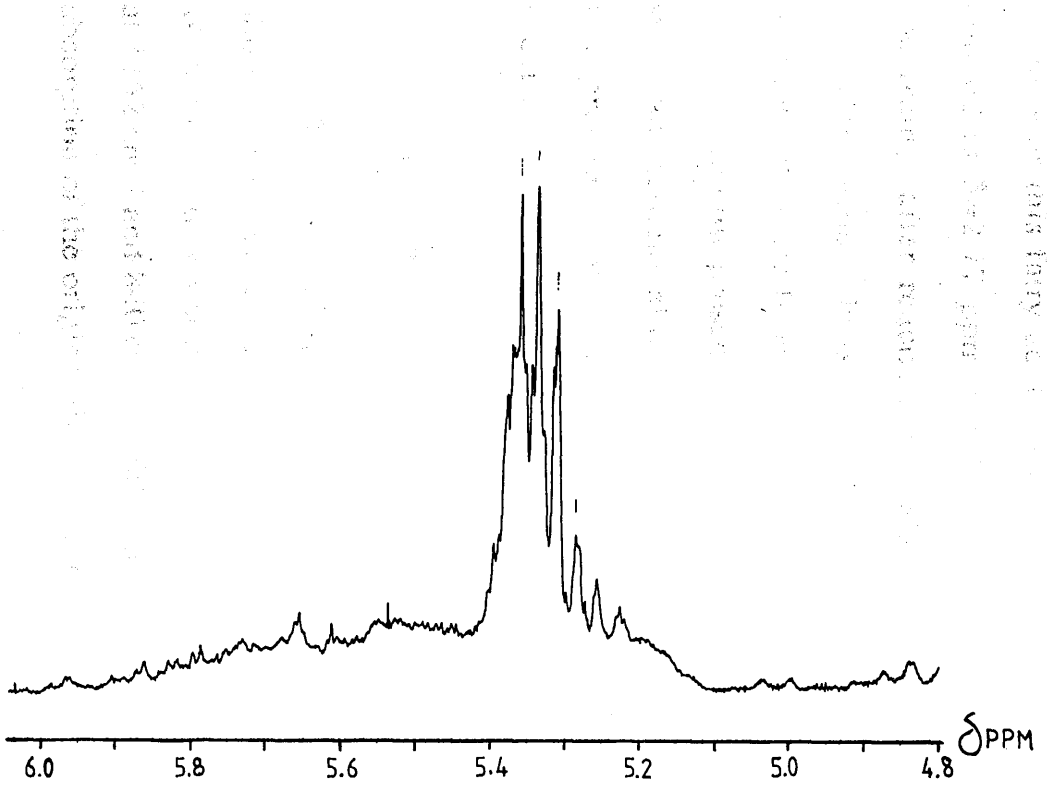

Figure 4.49 The expanded ^{1}H n.m.r. spectrum of the olefinic region of the products obtained from the reaction of linoleic acid : $NaNO_2$ = 1:4 in $CDCl_3$ solution, at ambient temperature

$5.50 \geq \delta \geq 5.33$ ppm, whereas virtually no change seems to be observed in the region $5.33 \geq \delta \geq 5.20$ ppm, when the linoleic acid reacts with the oxides of nitrogen. The ^{1}H n.m.r. spectrum confirms that there is effectively still some unreacted linoleic acid and that the three geometrical isomers of this fatty acid are formed. Other dramatic changes are also noticed at $\delta=2.77$ ppm and $\delta=2.03$ ppm of the original linoleic acid spectrum, after reaction has taken place. These correspond to the methylene groups in α-positions to the olefinic =CH- residues. After reaction, they are broad, as would be expected since all the geometrical isomers are now present in the reaction mixture. The other regions of the spectrum remain almost unchanged. These results also confirm the interpretations made earlier of the linoleic acid ^{13}C and ^{1}H n.m.r. spectra.

4.2.3.7 Infra red analyses of the reaction products

The infra red spectrum of the reaction products, **Figure 4.45**, shows characteristic infra red. absorptions of a >C=N-OH residue at 1635 cm^{-1} and 968 cm^{-1}, as well as absorptions due to $>CH-NO_2$ residue at 1552 cm^{-1} and 840 cm^{-1}, with the 1360 cm^{-1} absorption masked by the absorption of the original linoleic acid.

4.2.3.8 *Conclusions:* The chemically significant points that emerge from this work are as follows.

^{13}C and ^{1}H n.m.r. signals of linoleic acid have been assigned. Changes that take place in the molecular structure of the acid can now be readily monitored by means of magnetic resonance spectroscopy.

The conformations in the neighbourhood of the olefinic residues in linoleic acid are deduced from the spin-Hamiltonian parameters obtained by analyzing the ^{1}H n.m.r. spectrum, **Table 4.26.** The conformations follow from the relationship $^{3}J_{H,H} = 10\cos^{2}\vartheta - \cos\vartheta + 2$,[110] that connects $^{3}J_{H,H}$ with the dihedral angle ϑ between the H-C-C and C-C-H planes in the molecular fragment H-C-C-H.

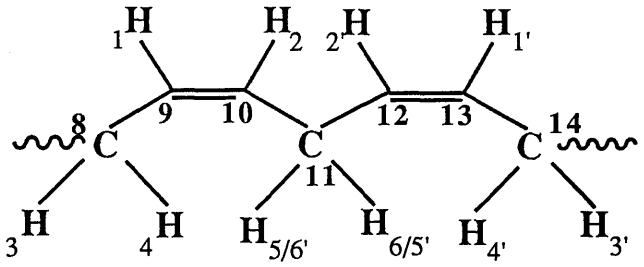

In this case, it was asumed that the dihedral angle for the fragment H(1)-C-C-H(3) equals the dihedral angle for the fragment H(2)-C-C-H(5) which equals also the dihedral angle for the fragments H(1')-C-C-H(3') and H(2')-C-C-H(5') and that the dihedral angle for the fragment H(1)-C-C-H(4) equals the dihedral angle for the fragment H(2)-C-C-H(6) which in its turn equals the dihedral angle for the fragments H(1')-C-C-H(4') and H(2')-C-C-H(6'). It was also assumed that the olefinic residues are almost staggered with respect to the carbon spine in the molecule.

Application of the relationship mentioned above then leads to the following dihedral angles:

$\vartheta_{H(1)\text{-}C\text{-}C\text{-}H(3)} = \vartheta_{H(2)\text{-}C\text{-}C\text{-}H(5)} = \vartheta_{H(1')\text{-}C\text{-}C\text{-}H(3')} = \vartheta_{H(2')\text{-}C\text{-}C\text{-}H(5')} = 154^{o}$

$\vartheta_{H(1)\text{-}C\text{-}C\text{-}H(4)} = \vartheta_{H(2)\text{-}C\text{-}C\text{-}H(6)} = \vartheta_{H(1')\text{-}C\text{-}C\text{-}H(4')} = \vartheta_{H(2')\text{-}C\text{-}C\text{-}H(6')} = 69^{o}$

As was found for oleic acid, linoleic acid is also converted into a mixture of its geometric isomers when it is brought into contact with an aqueous solution of $NaNO_2$ acidified with acetic acid. The ^{13}C n.m.r. spectrum shows that relative amounts of these isomers are: linoleic acid (Z,Z) : (Z,E) : (E,Z) : (E,E) = 3 : 2 : 2 : 1. Other fatty acids isomeric with linoleic acid were not detected during this work, i.e. no evidence has been found in this work that allylic shifts within the $-H_2C(8)$-C(9)H=C(10)H-C(11)H_2-C(12)H=C(13)H-C(14)H_2- residue take place when linoleic acid is brought into contact with the oxides of nitrogen, at least under the conditions used in this work.

We speculate at this point that all unsaturated aliphatic fatty acids undergo partial geometric isomerisation when brought into contact with the oxides of nitrogen.

Nitro-oximes could not be isolated in this work but monitoring the infra red spectrum of linoleic acid when it reacts with acidified aqueous solutions of $NaNO_2$ reveals minute amounts of an oxime >C=N-OH and an aliphatic >CH-NO_2 residue. It is therefore believed that the mechanism of isomerisation of linoleic acid is similar to that involved in the isomerisation of oleic acid, as shown in **Scheme 4.2.**

For reasons similar to those outlined for oleic acid, **page 154**, route 1 can be ruled out, route 3 is of minor importance, and route 2 appears to be the major path whereby linoleic acid is converted into its geometric isomers.

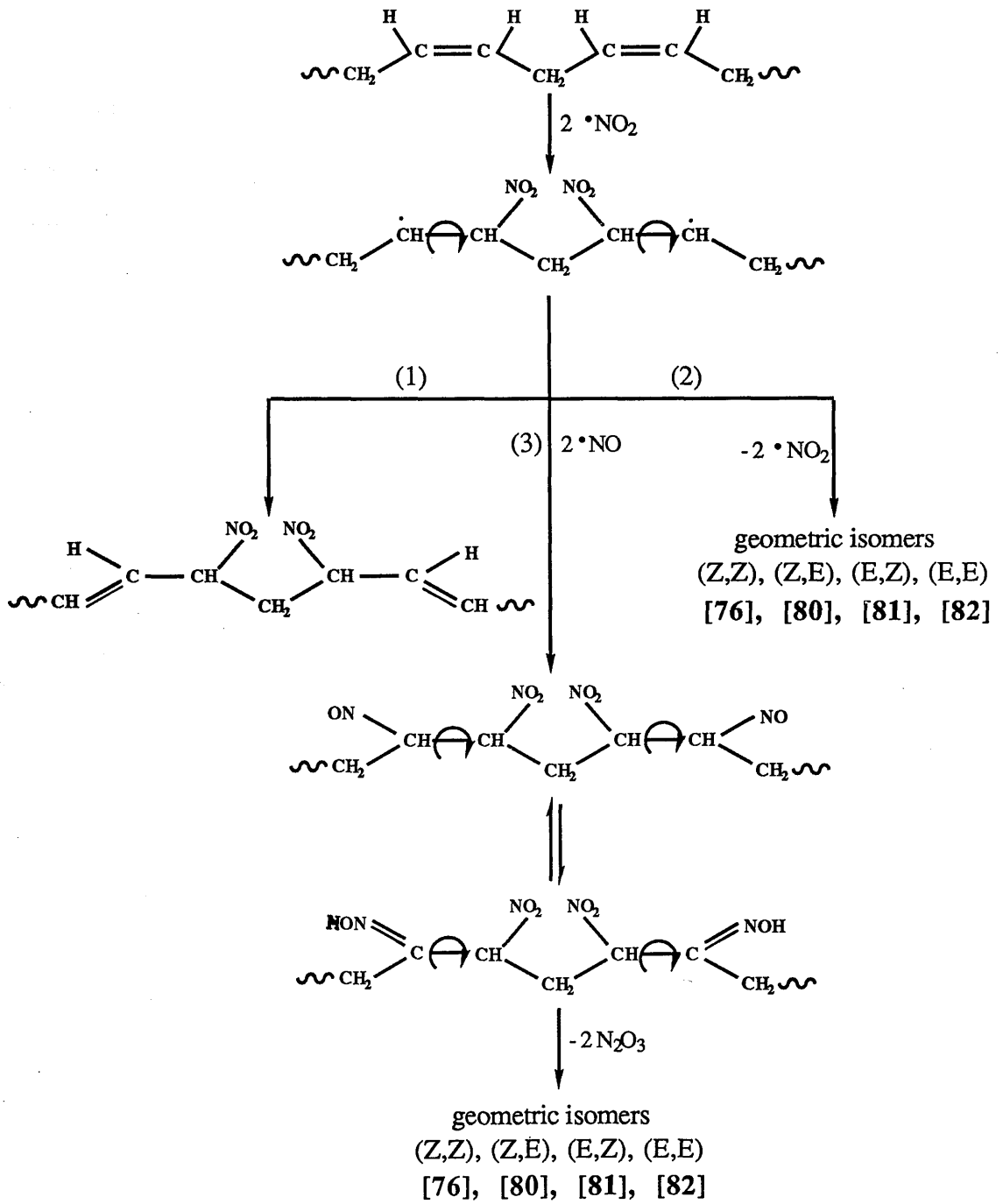
2 •NO2
(1)
(2)
(3) 2 •NO
-2 •NO2
geometric isomers
(Z,Z), (Z,E), (E,Z), (E,E)
[76], [80], [81], [82]
-2 N2O3
geometric isomers
(Z,Z), (Z,E), (E,Z), (E,E)
[76], [80], [81], [82]

Scheme 4.2

It would be very interesting to obtain the spin-Hamiltonian parameters, and thence information about the configuration in the olefinic regions, of the geometric isomers of linoleic acid. The overlapping of the olefinic regions of the ^{1}H n.m.r. spectra of the mixture made it impossible to obtain these parameters. However, the isomers of linoleic acid can be obtained from natural sources and it might be worthwhile examining their ^{13}C and ^{1}H n.m.r. spectra.

It should be possible to use n.m.r. spectra to deduce conformations in these geometric isomers and it would then be an easy matter to predict some of the consequences of exposing the membrane of a biological cell to the oxides of nitrogen. It follows from this work that a mixture of NO_2 and NO must affect the geometry of a lipid double layer in the membrane of any animal or plant cell and thence the permeability of the membrane and the sequencing of metabolic reactions that take place within the cell. The effects of these oxides of nitrogen on the permeabilities of the cell membrane become obvious when space filling models of the isomeric acids are examined, as in **Figures 4.50-4.55.**

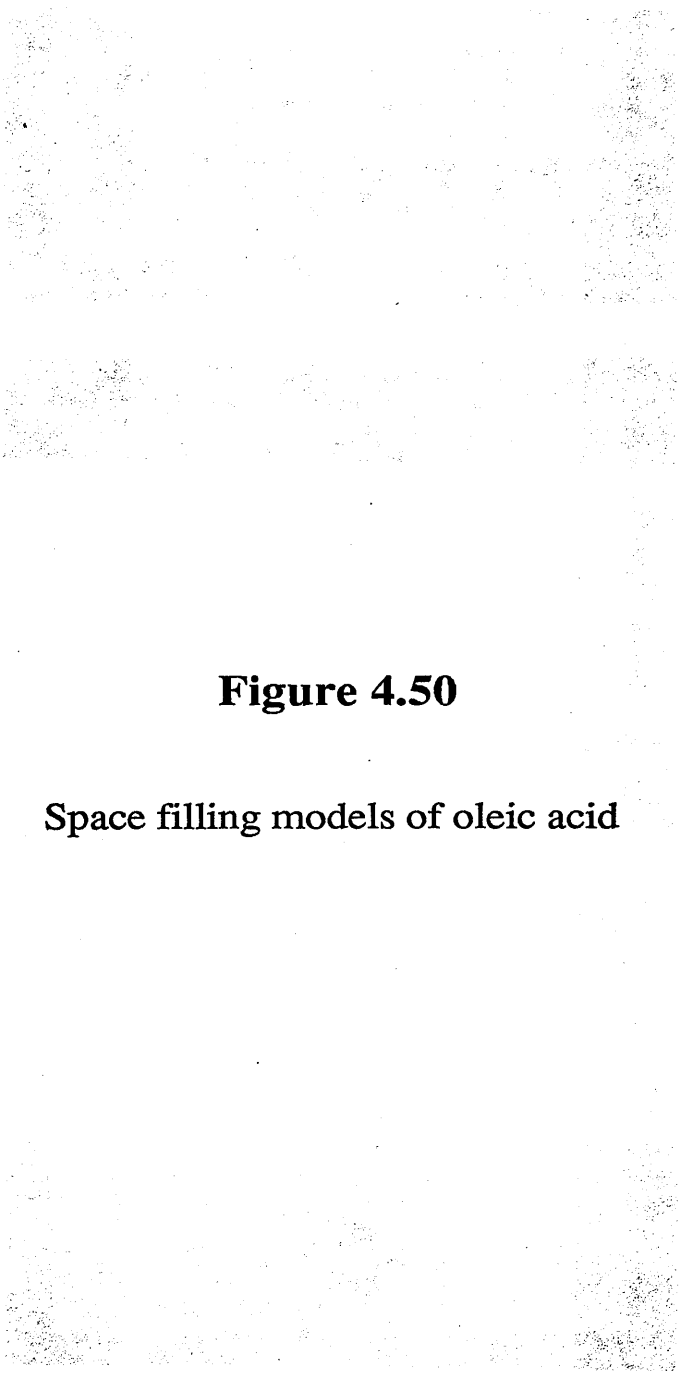

Figure 4.50

Space filling models of oleic acid

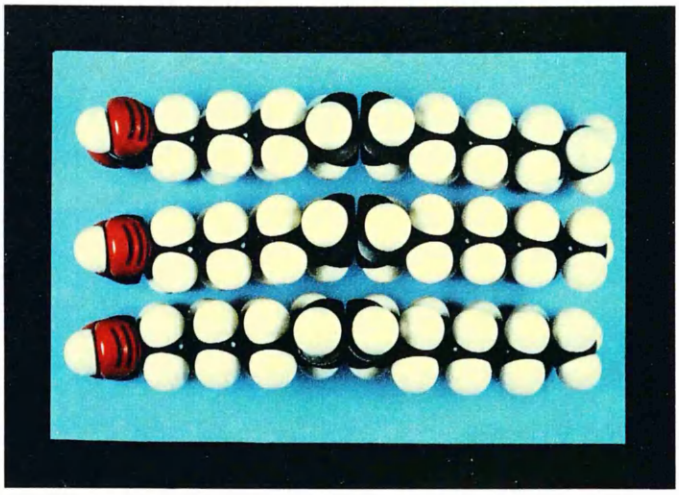

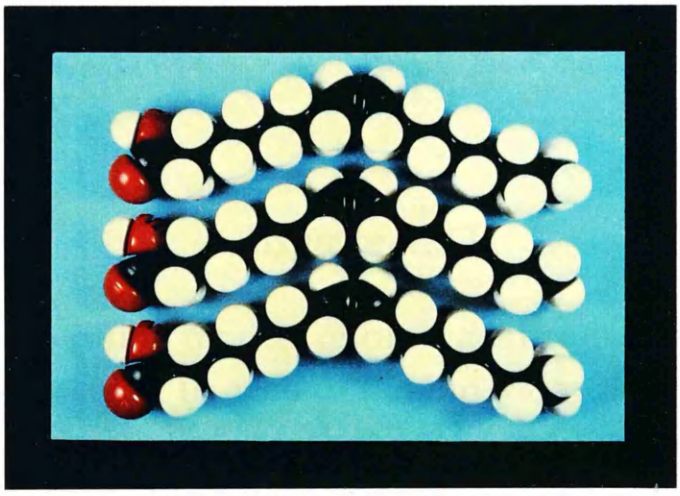

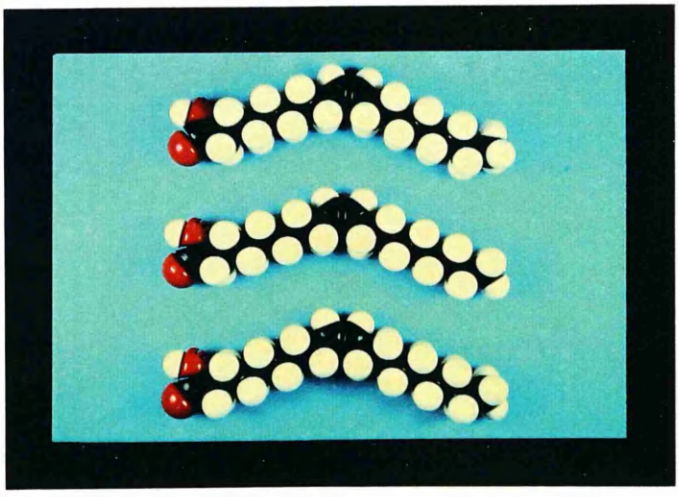

Figure 4.51

Space filling models of oleic acid containing elaidic acid. In each of the three figures, the outer molecules are oleic acid, and the inner molecule is elaidic acid

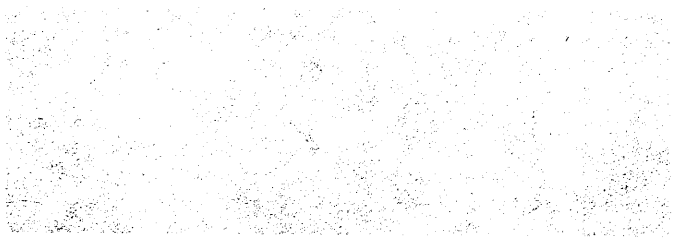

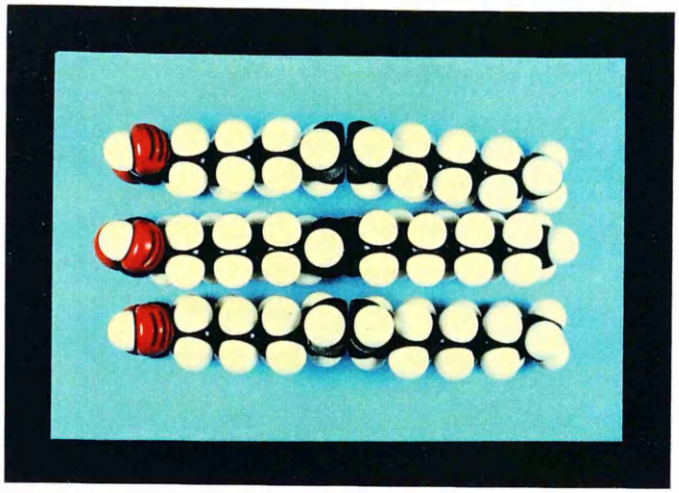

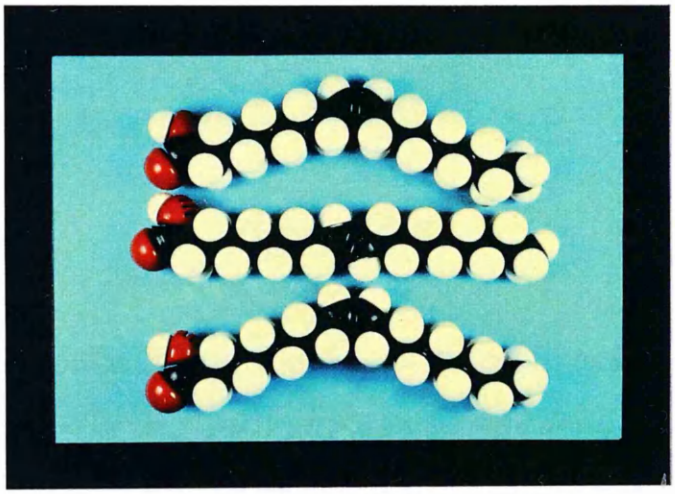

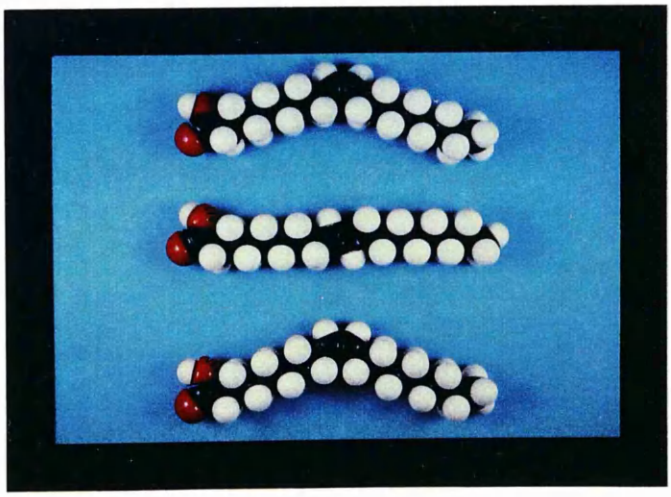

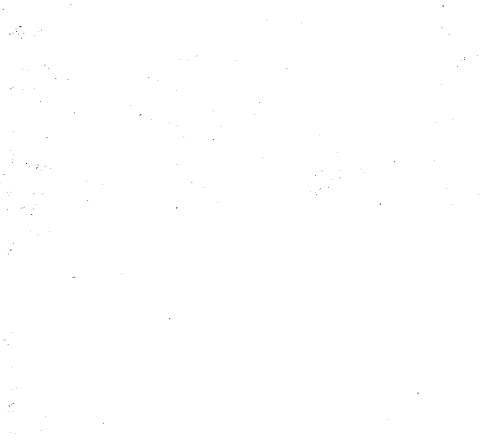

Figure 4.52

Space filling models of linoleic acid

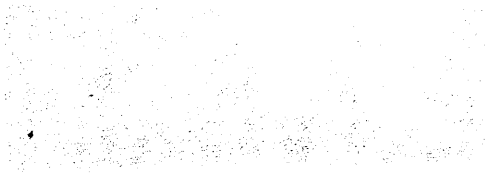

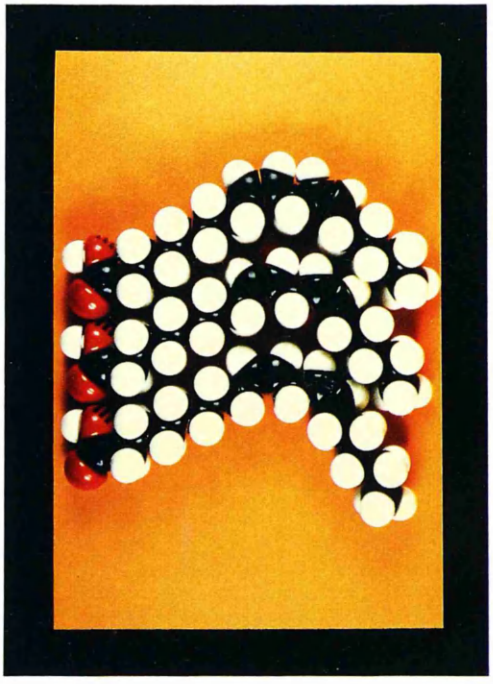

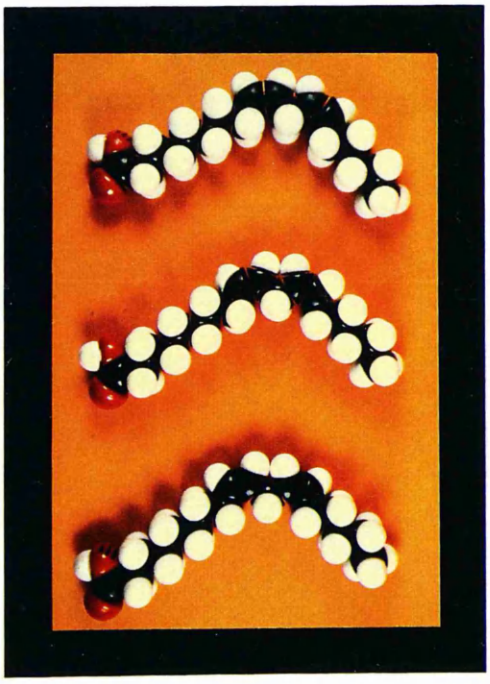

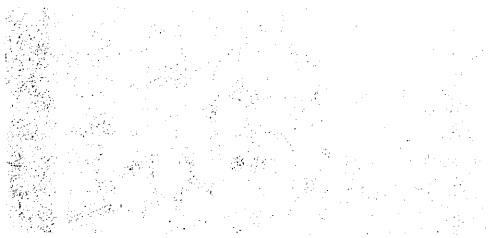

Figure 4.53

Space filling models of linoleic acid containing its (Z,E) isomer. In each of the three figures, the outer molecules are linoleic acid, and the inner molecule is its (Z,E) isomer

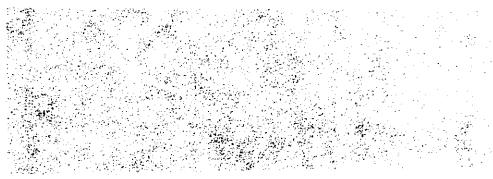

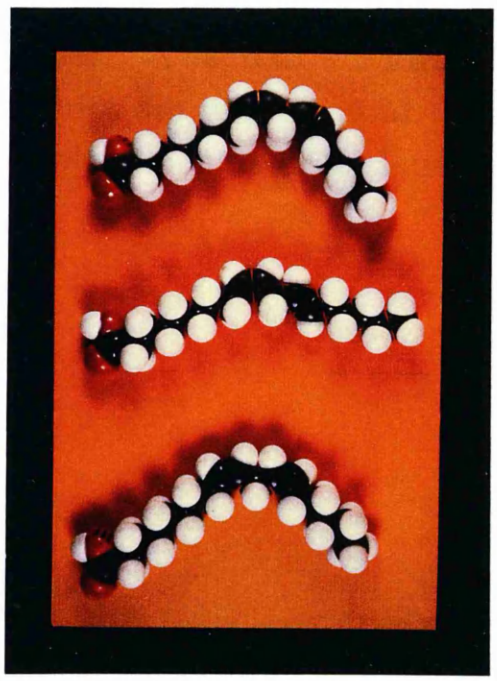

Figure 4.54

Space filling models of linoleic acid containing its (E,Z) isomer. In each of the three figures, the outer molecules are linoleic acid, and the inner molecule is its (E,Z) isomer

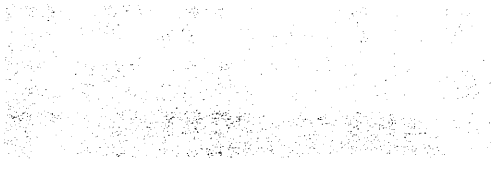

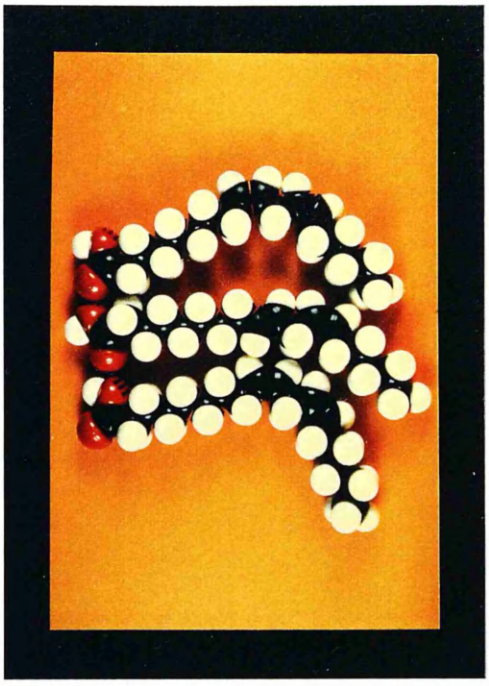

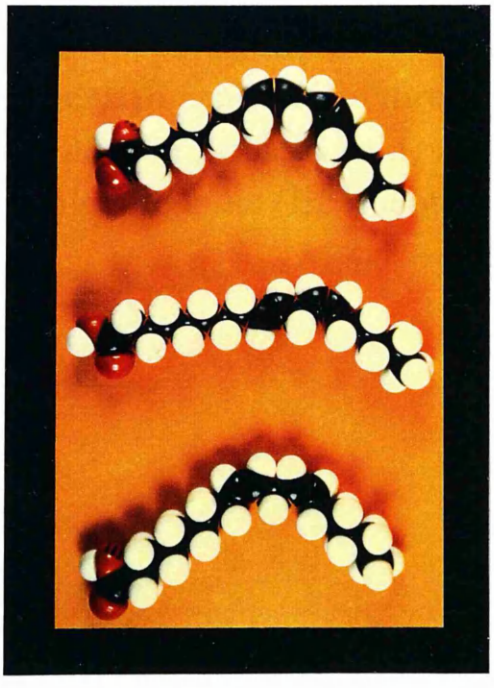

Figure 4.55

Space filling models of linoleic acid containing its (E,E) isomer. In each of the three figures, the outer molecules are linoleic acid, and the inner molecule is its (E,E) isomer

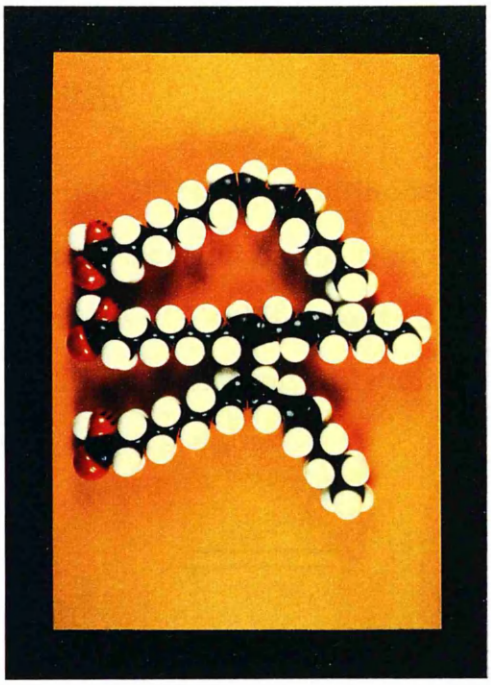

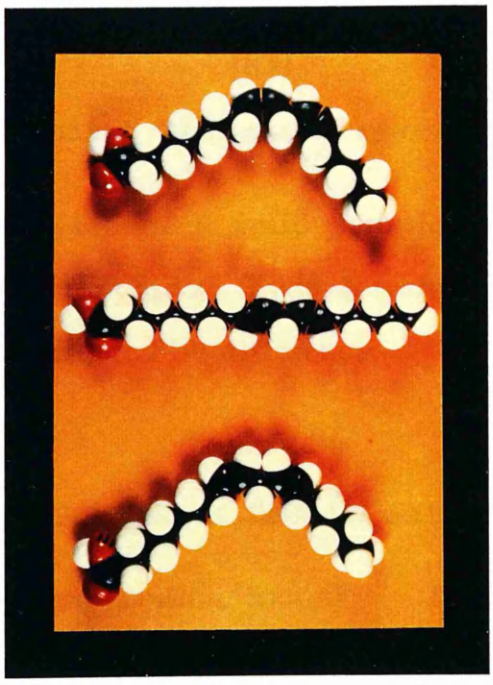

4.3 The action of NO and NO_2 on pyrimidine and purine bases

4.3.1 CYTOSINE

Cytosine, 4-amino-2(1H)-pyrimidinone, $C_4H_5N_3O$, **[83]**, was subjected to elemental analyses and its electron impact mass spectrum, its infra red, its ^1H n.m.r., its ^{13}C-{^1H}, and its ^{13}C-{^1H} 90° and 135° D.E.P.T. spectra were all recorded and fully analyzed.

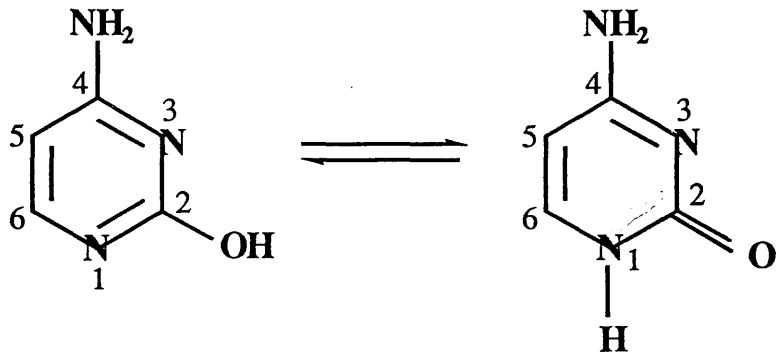

OH-form **NH-form**

[83]

4.3.1.1 Elemental analyses of cytosine

Elemental analyses of a solid sample of cytosine gave the percentage abundances for carbon, hydrogen and nitrogen listed in **Table 4.30**. Oxygen was calculated by difference.

Table 4.30

Microanalyses data for cytosine

Element	% Composition [found]	% Composition [expected for $C_4H_5N_3O$]
C	43.51	43.32
H	4.50	4.50
N	37.71	37.84
O	14.28	14.34

4.3.1.2 The electron impact mass spectrum, the infra red spectrum, and the 200.132 MHz ^{1}H and 50.324 MHz ^{13}C n.m.r. spectra of cytosine

These spectra all establish the 100% purity of the cytosine that was examined. The mass spectrum cracking pattern details are listed in **Table 4.31.** The infra red spectrum is shown in **Figure 4.56,** and detailed assignments of the vibrational frequencies are listed in **Table 4.32.**[112] The ^{1}H n.m.r. spectrum in dimethylsulphoxide solution is shown in **Figure 4.57** and ^{1}H chemical shifts[113] and $J_{(^{1}H,^{1}H)}$ values are listed in **Table 4.33.** ^{13}C-{^{1}H}, and ^{13}C-{^{1}H} 90° and 135° D.E.P.T. spectra are shown in **Figures 4.58A, 4.58B** and **4.58C** respectively. ^{13}C chemical shifts are listed in **Table 4.34.**[113]

Table 4.31

Mass Spectrum Cracking Pattern of Cytosine

Measured Mass (m/z)	% Intensity	Fragment
111	100.0	$[C_4H_5N_3O]^+$
83	23.1	$[C_3H_3N_2O]^+/[C_3H_5N_3]^+$
69	38.9	$[C_3H_3NO]^+/[C_3H_5N_2]^+$
68	26.4	$[C_3H_2NO]^+/[C_3H_4N_2]^+$
67	28.1	$[C_3HNO]^+/[C_3H_3N_2]^+$
43	14.1	$[CHNO]^+$
42	27.6	$[CNO]^+$
41	42.0	$[C_2H_3N]^+$
40	29.9	$[C_2H_2N]^+$
28	36.1	$[CO]^+$

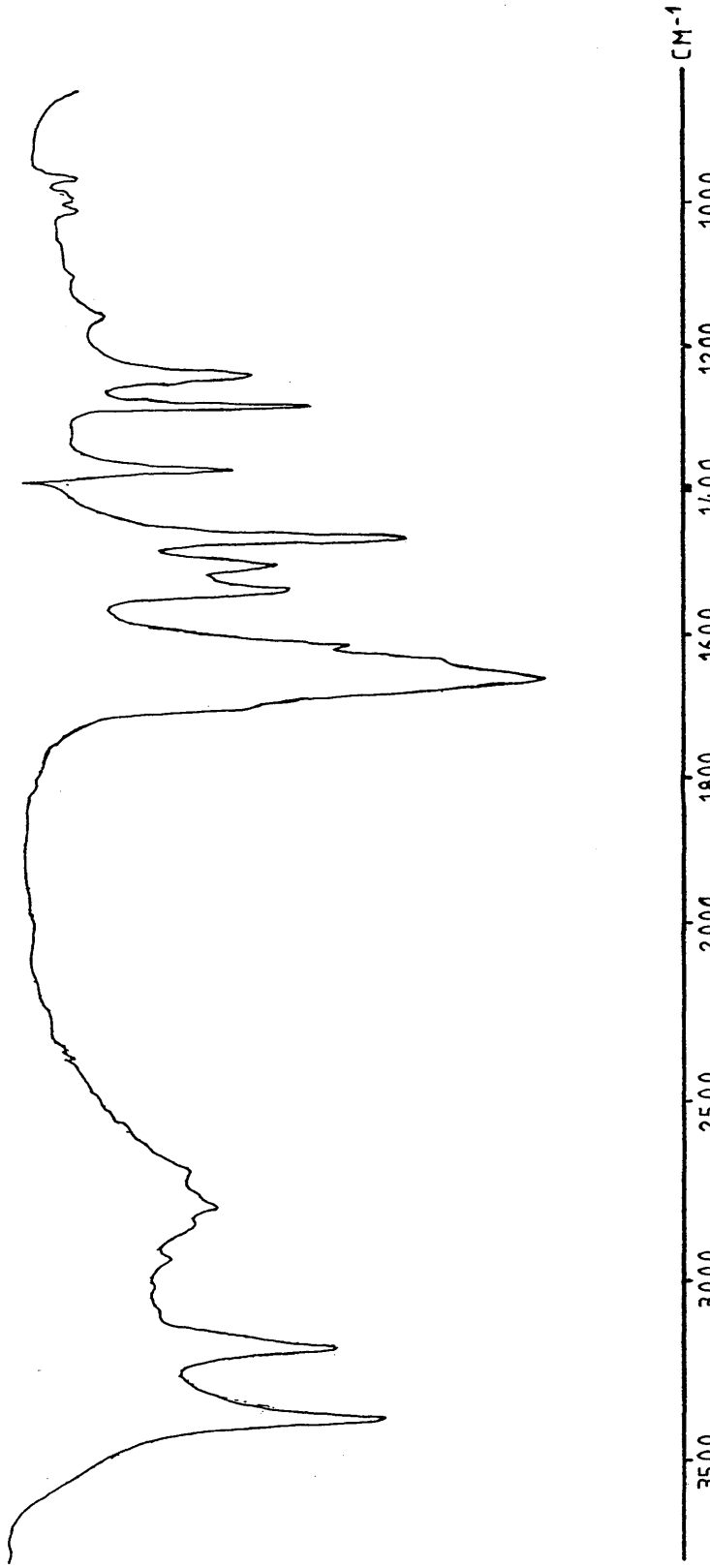

Figure 4.56 The infra red spectrum of cytosine (KBr disc)

Table 4.32

Infra red assignments, KBr disc, in cytosine

Band/cm^{-1}	Assignment
3380	$-NH_2$, asymmetric stretching mode
3180	$-NH_2$, symmetric stretching mode
1660	>C=O, stretching mode
1638	>C=C<, stretching vibration
1615	$-NH_2$, deformation mode
1585	ring stretching modes
1500	
1465	
1370	
1280	$=C-NH_2$, outside the ring
1240	C-N, in the ring
800	=CH-, wag of >C=C<

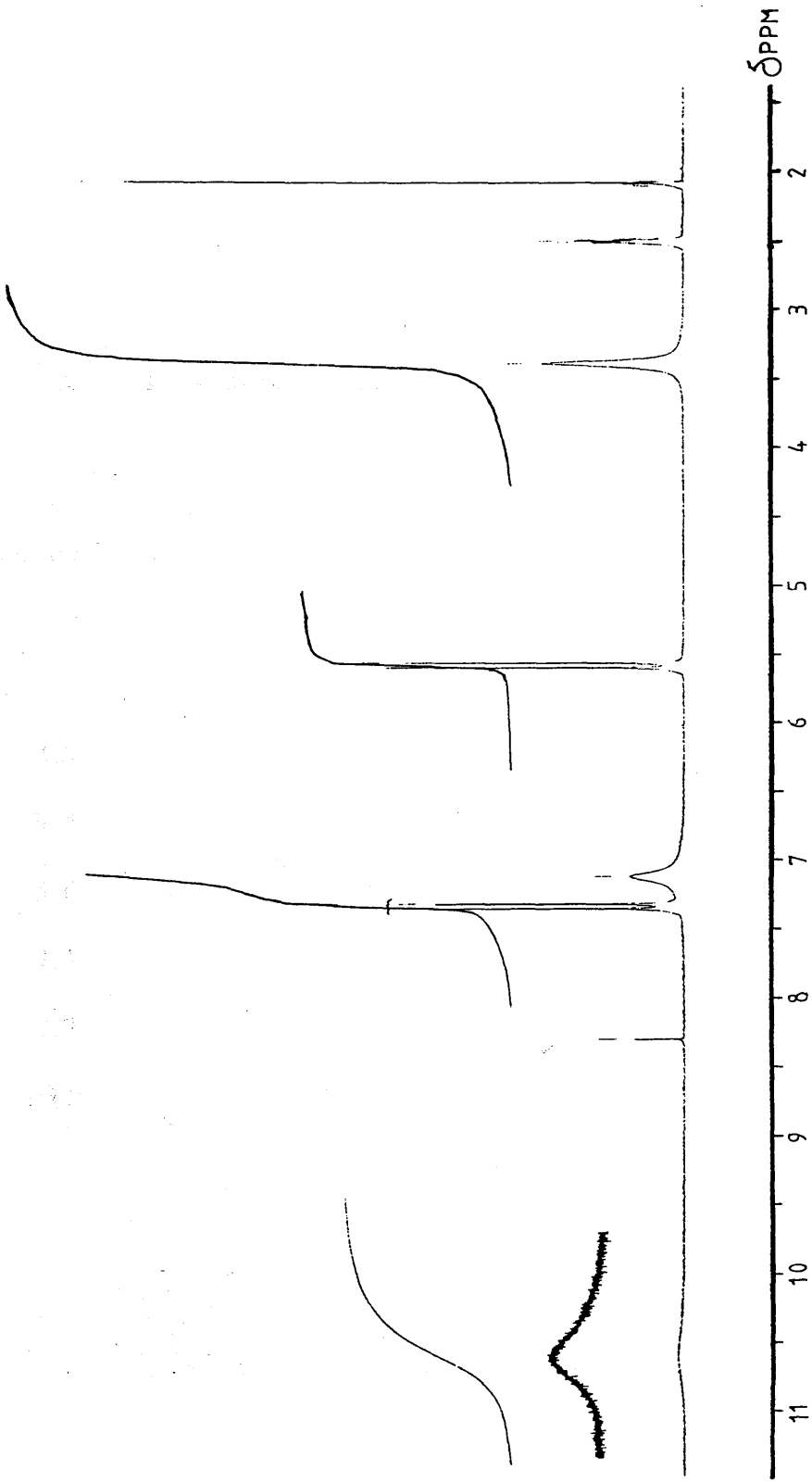

Figure 4.57 The 200.132 MHz ^{1}H n.m.r. spectrum of cytosine in dimethylsulphoxide

Table 4.33

^{1}H n.m.r. chemical shifts, δ_H, and ^{1}H-^{1}H coupling constants ($J_{H,H}$) of cytosine

Chemical Shift	Hydrogen Number	$J_{H,H}$	Multiplicity
2.0			
		dimethylsulphoxide	
2.5			
3.4		Impurity in the solvent	
5.6	C(5)-H	7	doublet
7.1	C(4)-NH_2	/	broad
7.3	C(6)-H	7	doublet
10.5	C(6)-NH-C(2)	/	broad

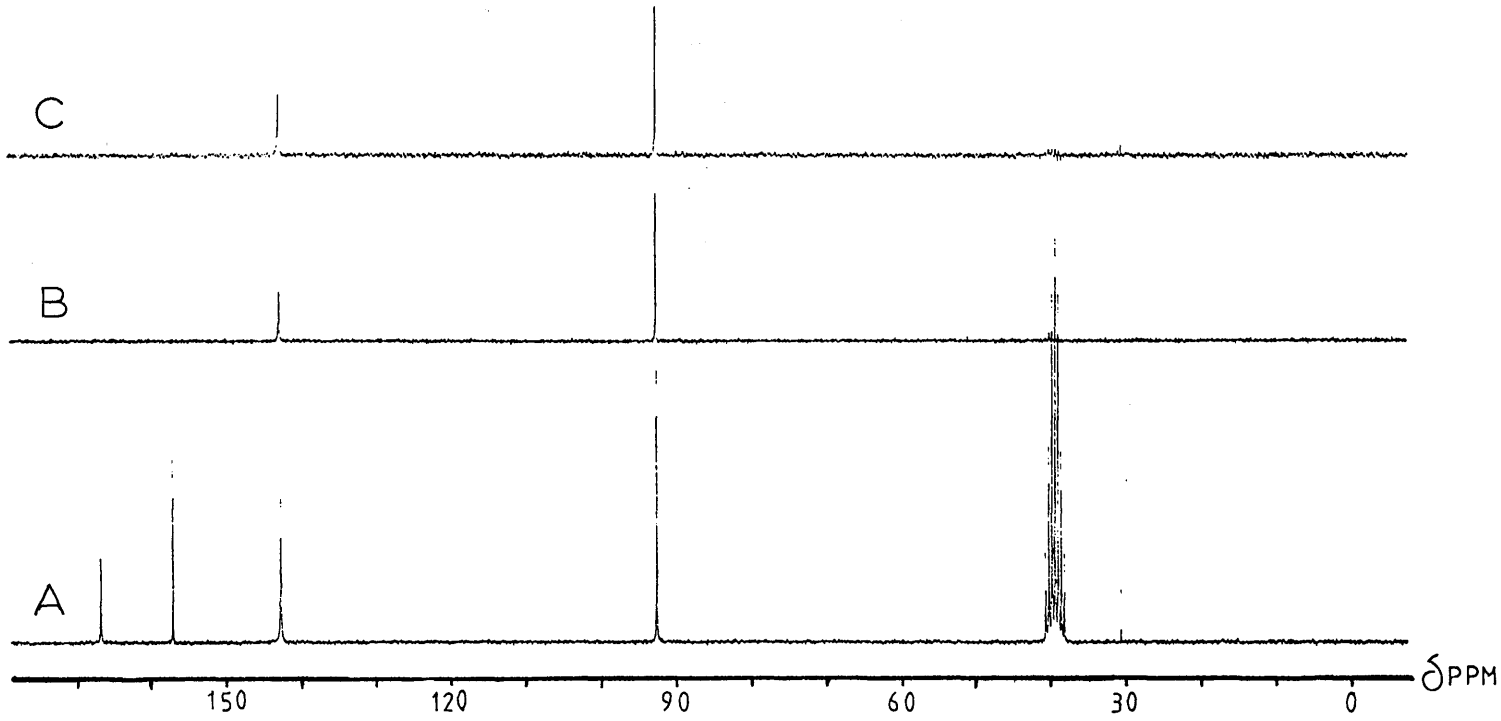

Figure 4.58 The 50.324 MHz ^{13}C-{^{1}H} n.m.r. spectrum, {A}, and the corresponding $\Theta = 90^{o}$, {B}, and $\Theta = 135^{o}$, {C}, of cytosine in dimethylsulphoxide

Table 4.34

^{13}C n.m.r. chemical shifts, δ_C, of cytosine

δ_C (ppm)(DMSO at 39.5 ppm)

C-2	C-4	C-5	C-6
166.78	157.09	92.86	142.75

4.3.1.3 The action of NO and NO_2 on cytosine

A solution of cytosine, in dimethylsulphoxide, was allowed to react with an equimolar saturated aqueous solution of soduim nitrite and acetic acid, as described earlier in this thesis. On adding the acetic acid, some brownish fumes were formed, but these disappeared as soon as the solution is mixed thoroughly. However, the solution was slightly coloured at this point: it turned yellow/brown. The precipitate was then analyzed by means of infra red and electron mass spectroscopy.

The infra red spectrum of the reaction products is shown in **Figure 4.59** and when this is compared with the infra red spectrum of the pure cytosine **[83]**, shown in **Figure 4.56**, it follows that the cytosine has dramatically changed when treated with the oxides of nitrogen. Comparaison of **Figure 4.59** with the the infra red spectrum of uracil **[84]**, **Figure 4.60**, and also the corresponding mass spectra, **Tables 4.31** and **4.35**, shows that this reaction converts cytosine into uracil.[114]

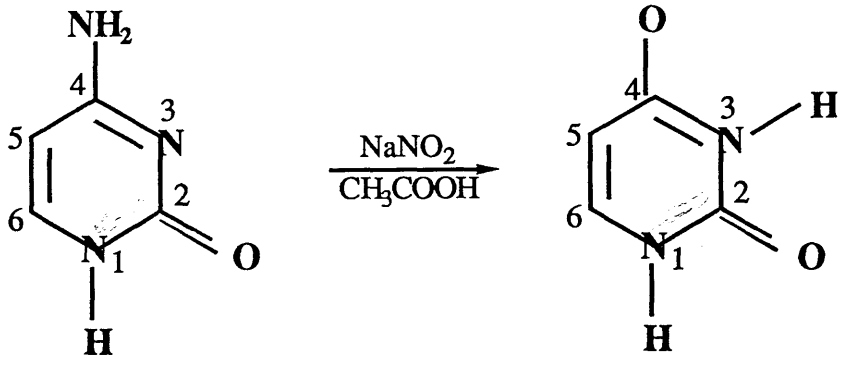

[83] **[84]**

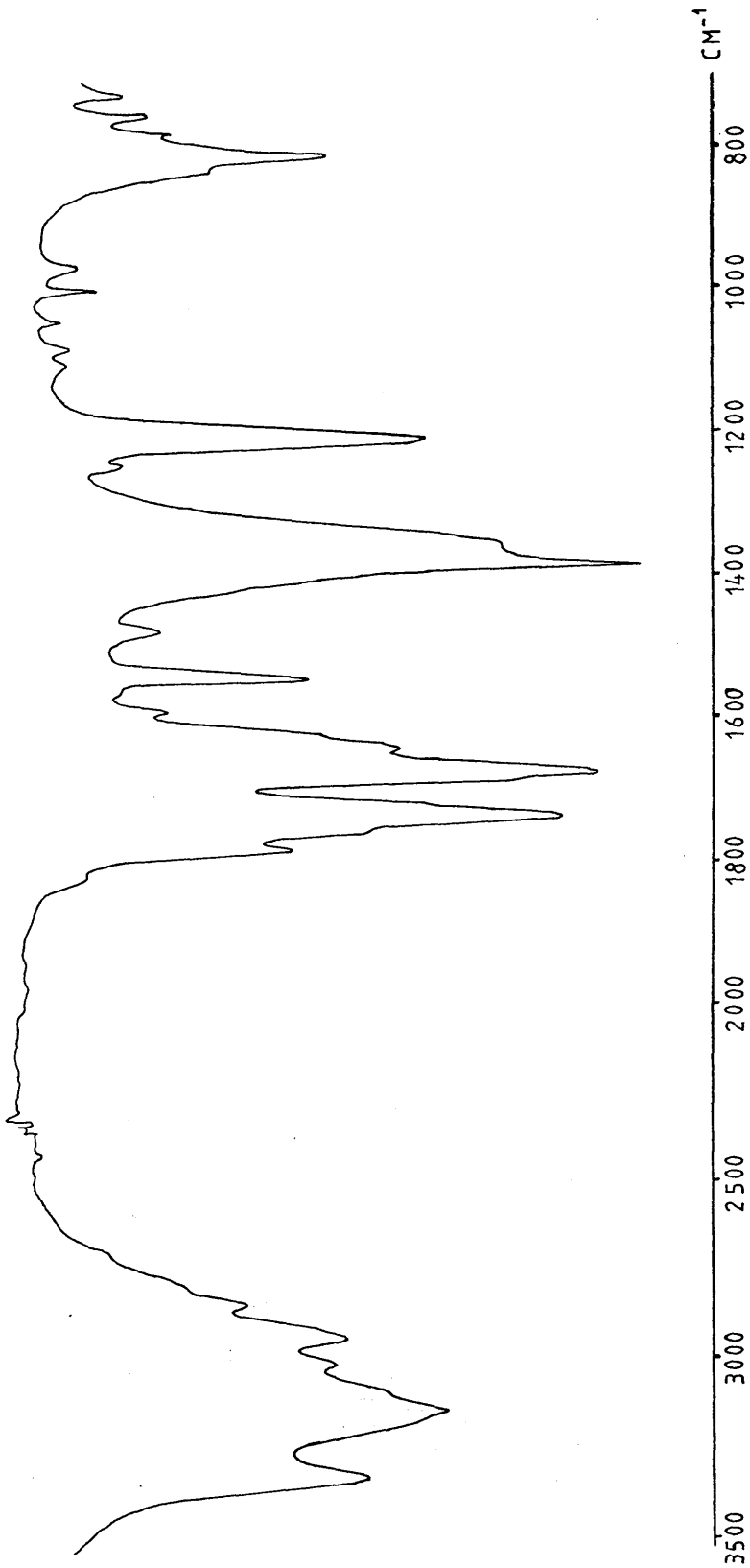

Figure 4.59 The infra red spectrum of the products obtained from the reaction of cytosine : $NaNO_2$ = 1:1(KBr disc)

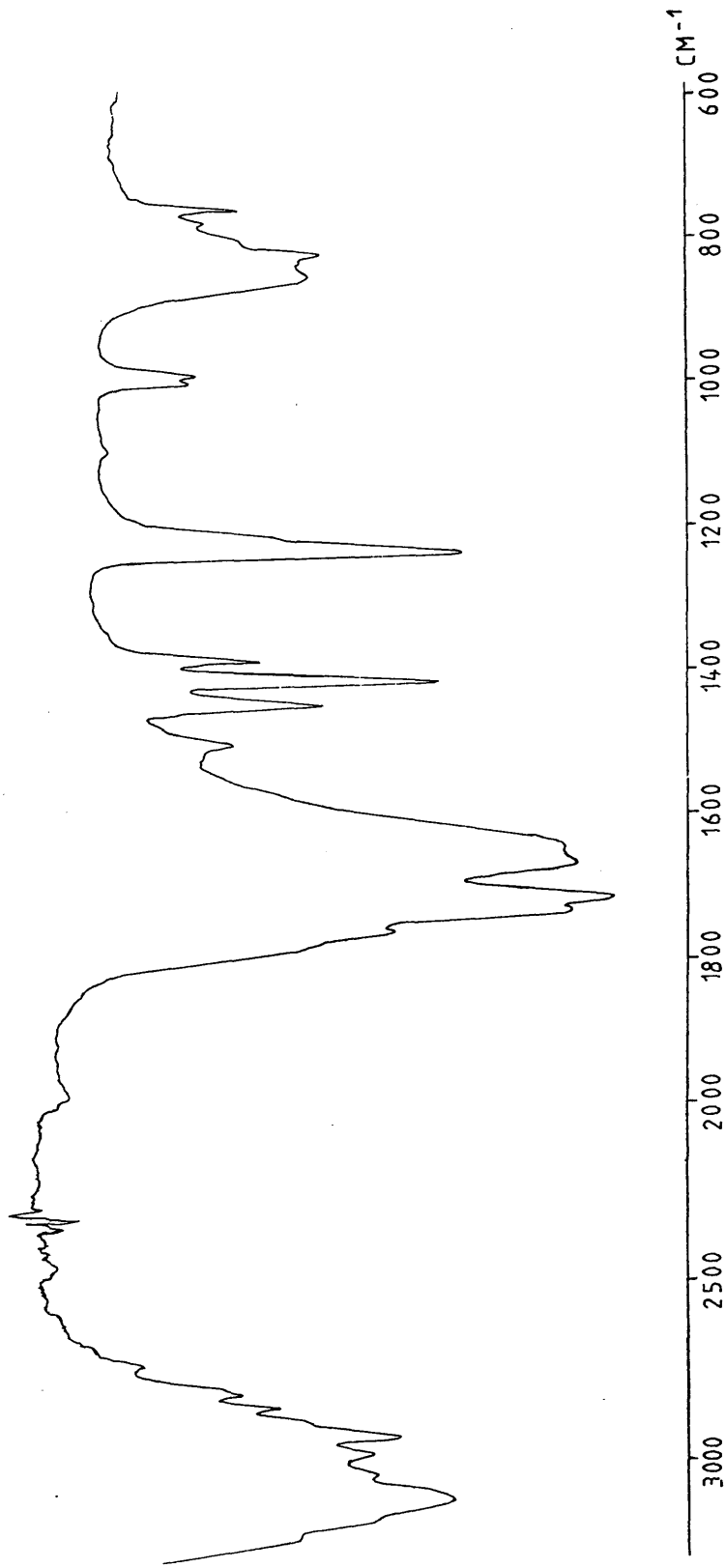

Figure 4.60 The infra red spectrum of uracil (KBr disc)

Table 4.35

Mass spectrum cracking pattern of the parent uracil, {A}, and of uracil present in the reaction mixture, {B}

Measured Mass (m/z)	% Intensity {A}	% Intensity {B}	Fragment
112	100.0	8.6	$[C_4H_4N_2O_2]^+$
70	9.4	2.7	$[C_3H_4NO]^+$
69	70.2	53.4	$[C_3H_3NO]^+$
68	23.6	30.7	$[C_3H_2NO]^+$
43	12.9	23.7	$[CHNO]^+$
42	72.5	44.9	$[CNO]^+$
41	43.9	64.1	$[C_2H_3N]^+$
40	40.5	53.1	$[C_2H_2N]^+$
39	10.7	19.0	$[C_2HN]^+$
28	74.6	81.9	$[CO]^+$

4.3.2 THYMINE

Thymine, 5-methyl-2,4(1H,3H)-pyrimidinedione, $C_5H_6N_2O_2$, **[85]**, was also included at this stage of the project. Microanalytical data and electron impact mass spectrum data for the sample that was used are listed in **Tables 4.36** and **4.37** respectively.

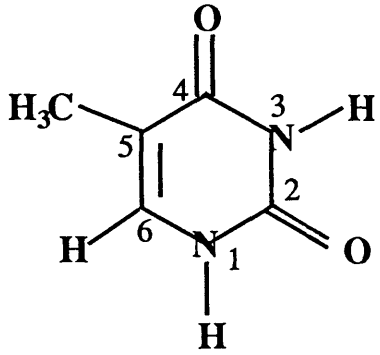

[85]

Table 4.36

Microanalyses data for thymine

Element	% Composition [found]	% Composition [expected for $C_5H_6N_2O_2$]
C	47.53	47.62
H	4.70	4.76
N	22.26	22.22
O	25.51	25.40

Table 4.37

Mass Spectrum Cracking Pattern of Thymine

Measured Mass (m/z)	% Intensity	Fragment
126	67.7	$[C_5H_6N_2O_2]^+$
83	13.4	$[C_4H_5NO]^+$
55	100.0	$[C_3H_5N]^+$
54	51.2	$[C_3H_4N]^+$
52	14.8	$[C_3H_2N]^+$
39	11.0	$[C_3H_3]^+$
28	62.8	$[CO]^+$
27	23.8	$[C_2H_3]^+$
26	29.9	$[C_2H_2]^+$

The infra red spectrum, and the 200.132 MHz ^{1}H and the 50.324 MHz ^{13}C-{^{1}H} n.m.r. spectra of this same sample are shown in **Figures 4.61, 4.62 4.63** respectively. Assignments of the main regions of the infra red spectrum are listed in **Table 4.38**,[112] and ^{1}H and ^{13}C chemical shifts are listed in **Tables 4.39**[115] and **4.40**[116] respectively

4.3.2.1 The action of NO and NO_2 on thymine

As in the case of cytosine, thymine in dimethylsulphoxide solution was then brought into contact with a saturated solution of sodium nitrite in the presence of acetic acid. Ratios of thymine : $NaNO_2$ of 1:1 and 1:2 were employed and the precipitates obtained from the reaction mixture were then examined by infra red and mass spectroscopy. The infra red spectra of the products are shown in **Figures 4.64** and **4.65**, and the main peaks of the mass spectra are listed in **Tables 4.41** and **4.42.**

The results of this work show quite clearly that the thymine has not reacted under the conditions that were used. No evidence was obtained that indicated either that the >C(5)=C(6)< residue or

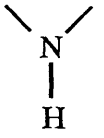

residues of the thymine molecule react with the oxides of nitrogen under the conditions used.

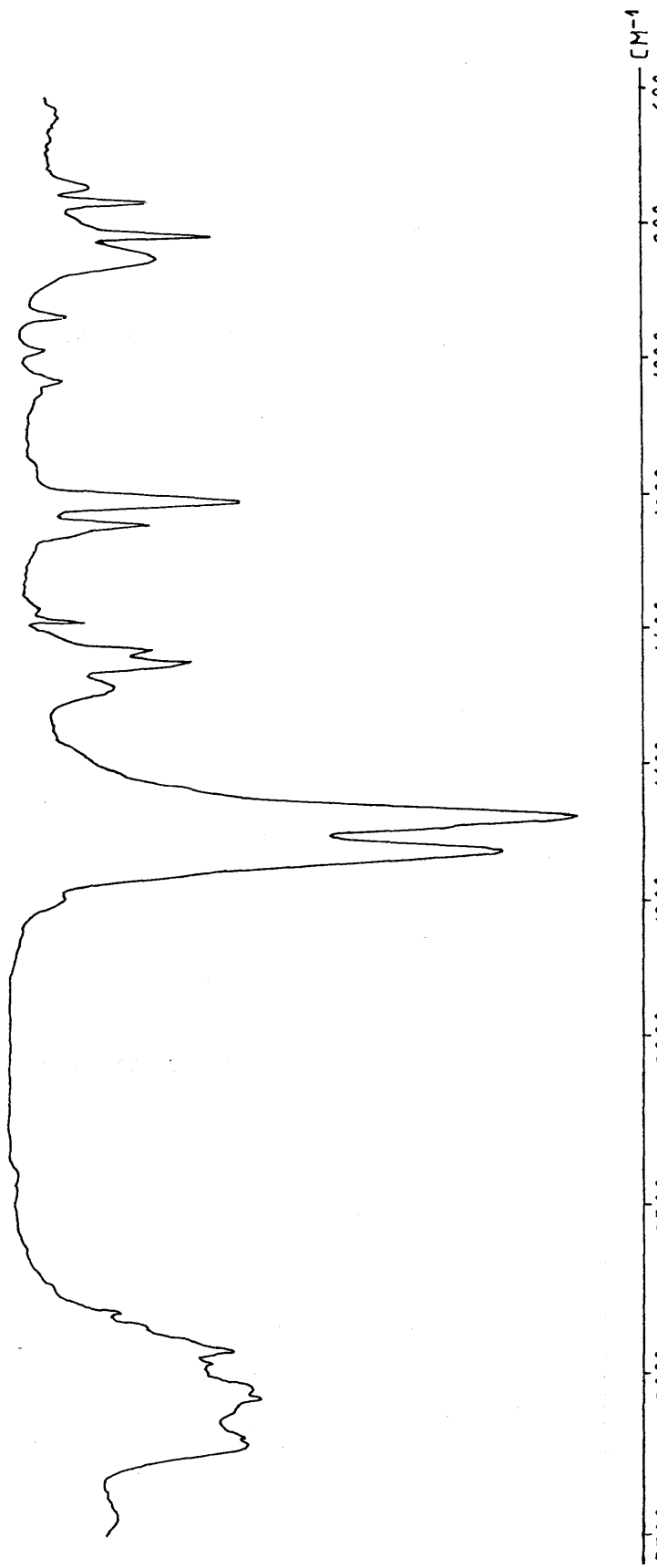

Figure 4.61 The infra red spectrum of thymine (KBr disc)

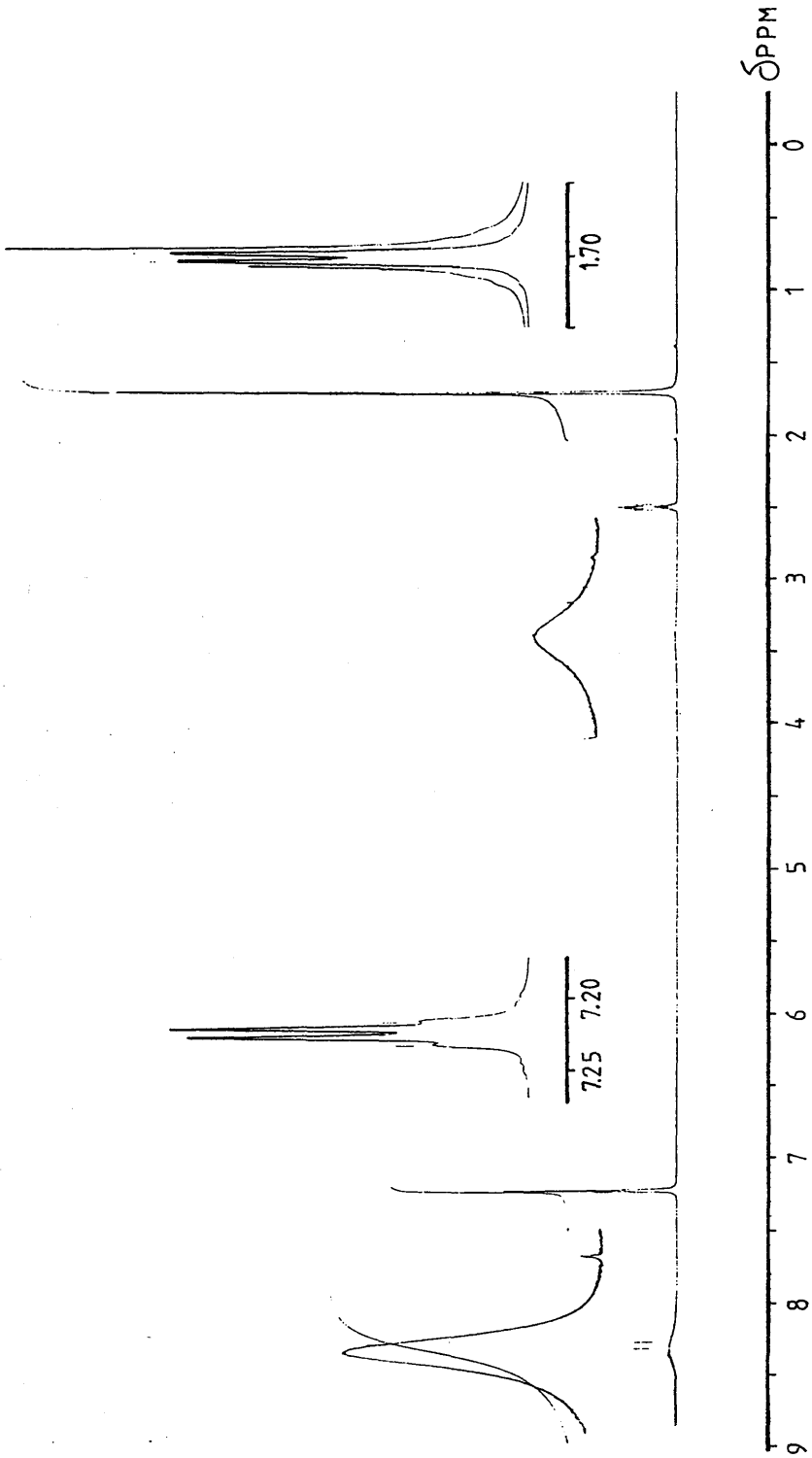

Figure 4.62 The 200.132 MHz ^{1}H n.m.r. spectrum of thymine in dimethylsulphoxide

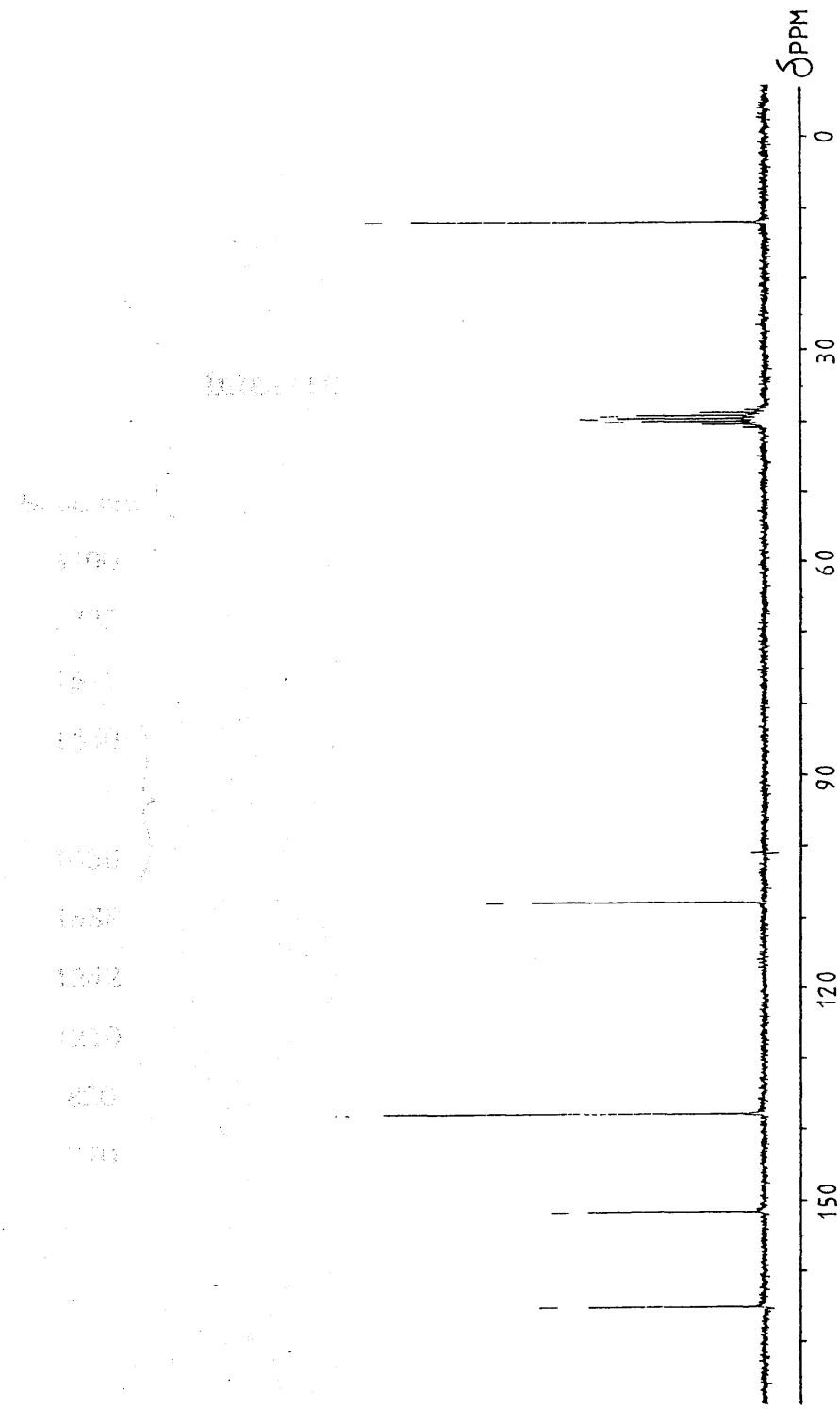

Figure 4.63 The 50.324 MHz ^{13}C-{^{1}H} n.m.r. spectrum, of thymine in dimethylsulphoxide

Table 4.38

Infra red assignments, KBr disc, in thymine

Band/cm^{-1}	Assignment
3400	-NH, stretching mode
1725	>C=O, stretching mode
1675	>C=C<, stretching vibration
1450 – 1430	CNH, bending modes
1388	CH_3, deformation
1242	=C-NH, outside the ring
1210	C-N, in the ring
820	=CH-, wag of >C=C<
770	>NH, wagging

Table 4.39

^{1}H n.m.r. chemical shifts, δ_H, of thymine

Chemical Shift	Hydrogen Number	Multiplicity
1.7	C(5) -C<u>H</u>$_3$	doublet
2.5	dimethylsulphoxide	
7.2	C(6)-<u>H</u>	quartet
8.3	C(6)-N<u>H</u>-C(2)/C(4)-N<u>H</u>-C(2)	broad

Table 4.40

^{13}C n.m.r. chemical shifts, δ_C, of thymine

δ_C (ppm)(DMSO at 39.5 ppm)

C-2	C-4	C-5	C-6
151.60	165.02	107.82	137.82

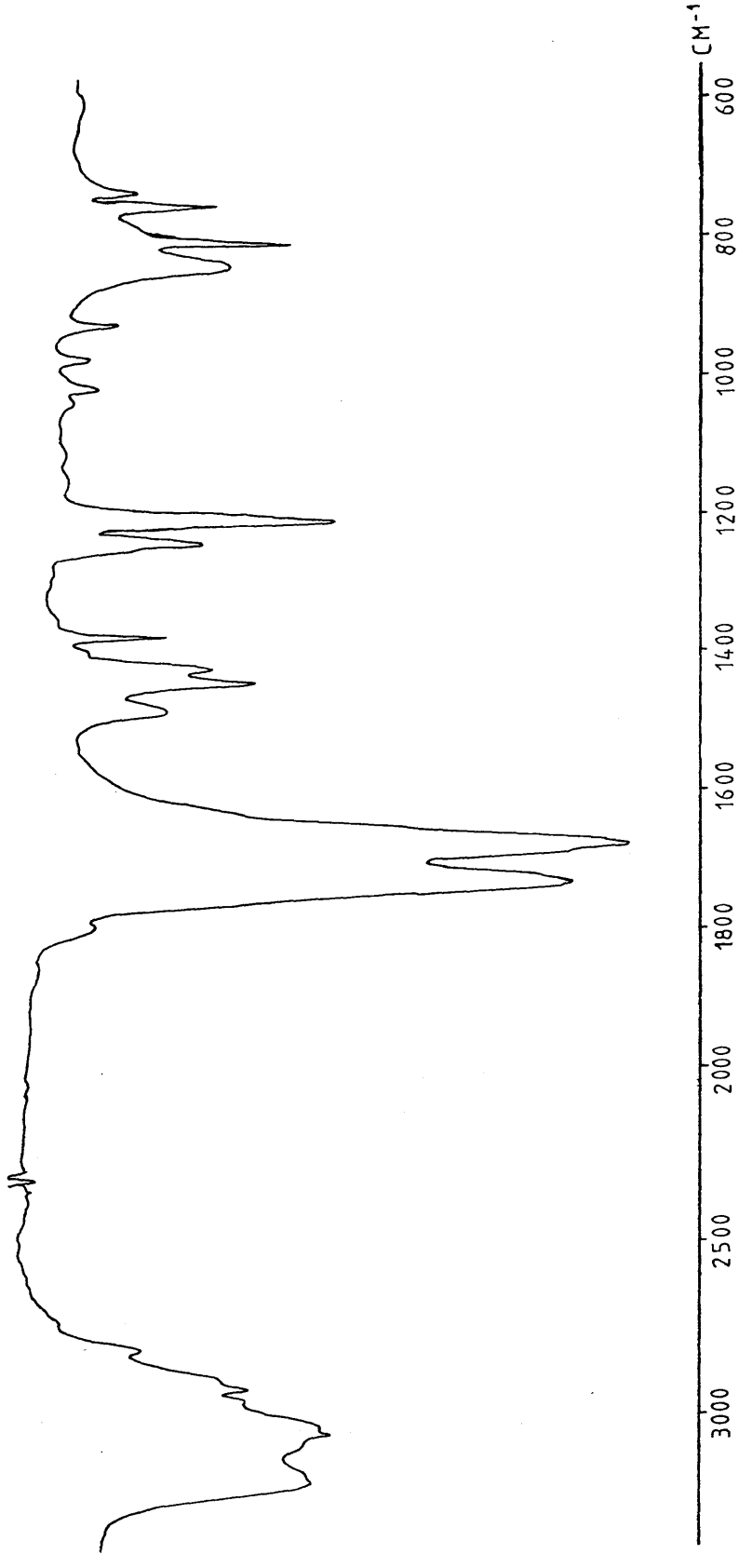

Figure 4.64 The infra red spectrum of the products obtained from the reaction of thymine : $NaNO_2$ = 1:1(KBr disc)

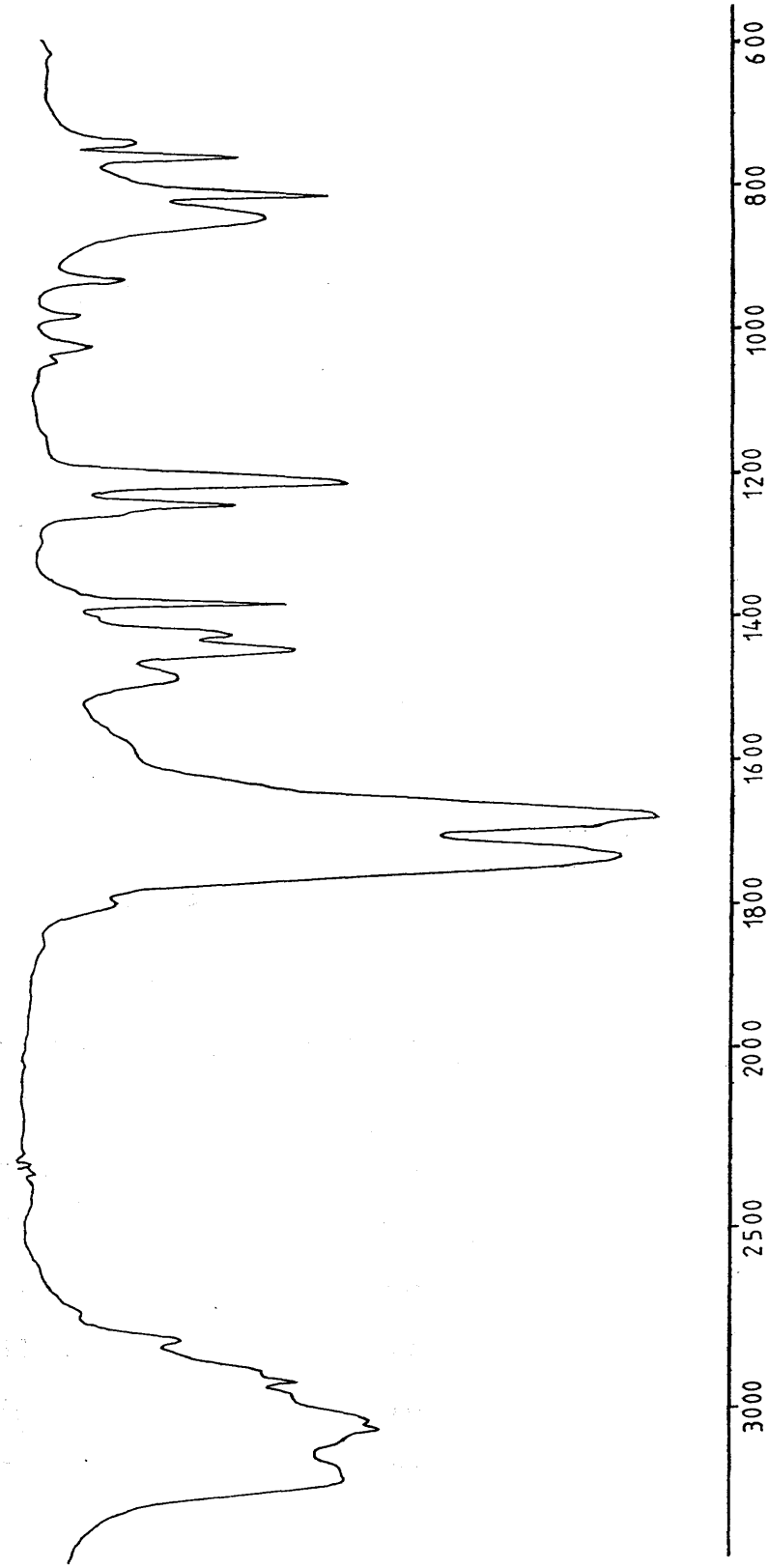

Figure 4.65 The infra red spectrum of the products obtained from the reaction of thymine : $NaNO_2$ = 1:2(KBr disc)

Table 4.41

Mass Spectrum Cracking Pattern of the Reaction Products of Thymine : $NaNO_2$=1:1

Measured Mass (m/z)	% Intensity	Fragment
126	98.2	$[C_5H_6N_2O_2]^+$
83	16.2	$[C_4H_5NO]^+$
55	100.0	$[C_3H_5N]^+$
54	46.0	$[C_3H_4N]^+$
52	12.8	$[C_3H_2N]^+$
39	11.0	$[C_3H_3]^+$
28	73.3	$[CO]^+$
27	24.3	$[C_2H_3]^+$
26	12.4	$[C_2H_2]^+$

Table 4.42

Mass Spectrum Cracking Pattern of the Reaction Products of Thymine : $NaNO_2$=1:2

Measured Mass (m/z)	% Intensity	Fragment
126	61.3	$[C_5H_6N_2O_2]^+$
83	11.0	$[C_4H_5NO]^+$
55	100.0	$[C_3H_5N]^+$
54	48.8	$[C_3H_4N]^+$
52	13.6	$[C_3H_2N]^+$
39	10.5	$[C_3H_3]^+$
28	61.4	$[CO]^+$
27	22.9	$[C_2H_3]^+$
26	11.6	$[C_2H_2]^+$

4.3.1 ADENINE

Adenine, 6-aminopurine, $C_5H_5N_5$, **[86]**, exists in two tautomeric forms, the 9H-form and the 7H-form. The 7H-form is known to be favoured in the free base.[117]

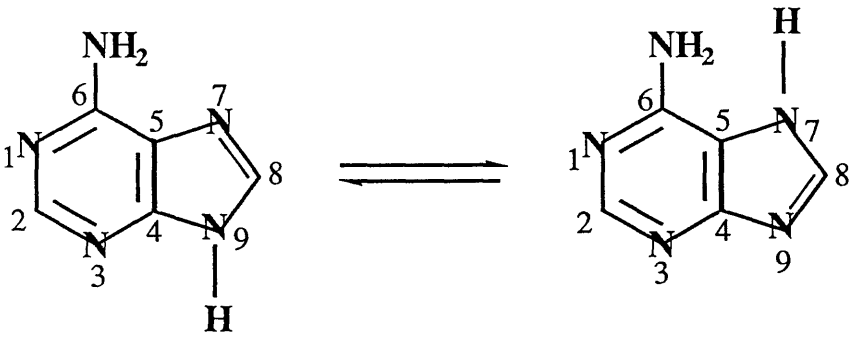

[86]

9H-Form 7H-Form

Microanalytical data for the adenine sample used in this work is given in **Table 4.43.**

Table 4.43

Microanalyses data for adenine

Element	% Composition [found]	% Composition [expected for $C_5H_5N_5$]
C	44.56	44.44
H	3.75	3.71
N	51.69	51.85

The infra red spectrum and the electron impact mass spectrum data are shown in **Figure 4.66** and **Table 4.44** respectively. Assignments of the vibrational frequencies are listed in **Table 4.45.**

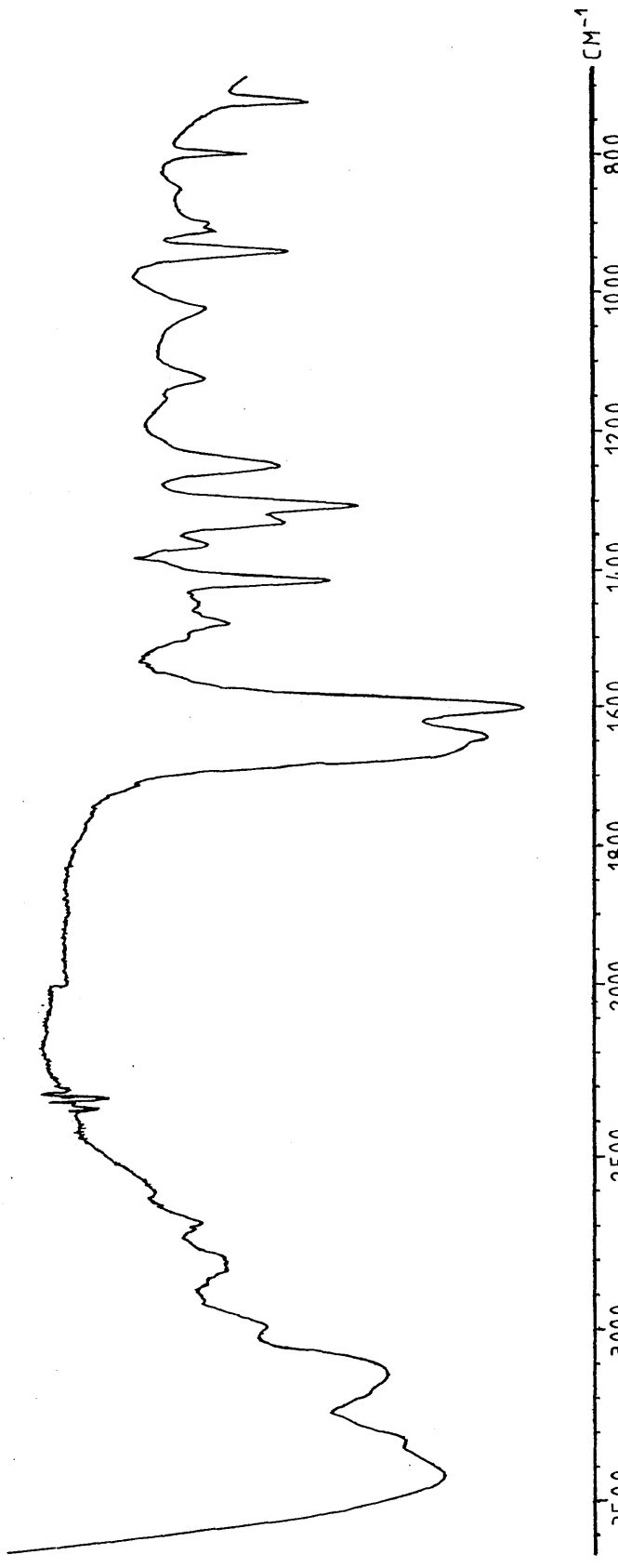

Figure 4.66 The infra red spectrum of adenine (KBr disc)

Table 4.44

Mass Spectrum Cracking Pattern of Adenine

Measured Mass (m/z)	% Intensity	Fragment
135	100.0	$[C_5H_5N_5]^+$
110	37.6	$[C_4H_4N_4]^+$
81	16.6	$[C_3H_3N_3]^+$
66	12.2	$[C_3HN_2]^+$
54	23.1	$[C_2H_2N_2]^+$
53	26.7	$[C_2HN_2]^+$
43	10.1	$[CH_3N_2]^+$
28	67.8	$[CH_2N]^+$

Table 4.45

Infra red assignments, KBr disc, in adenine

Band/cm^{-1}	Assignment
3320	$-NH_2$, asymmetric stretching mode
3130	$-NH_2$, symmetric stretching mode
1645	>C=, stretching vibration
1600	$-NH_2$, deformation
1415	CNH, bending modes
1310	$=C-NH_2$, bending modes
1250	=C-NH, outside the ring
1130	unassigned
1020	$-NH_2$, rocking
940	=CH-, rocking
800	=CH-, wagging
722	>NH, wagging

4.3.3.1 The action of NO and NO_2 on adenine

Adenine in dimethylsulphoxide solution was brought into contact with a saturated solution of sodium nitrite in the presence of acetic acid (adenine : $NaNO_2$ = 1:1), and as in the case of thymine, the precipitate obtained from the reaction products was subjected to electron impact mass spectral and infra red analyses. The mass spectral data are listed in **Table 4.46** and the infra red spectrum is shown in **Figure 4.67**. The adenine **[86]** has obviously reacted with the oxides of nitrogen under these conditions to form hypoxanthine **[87]**. Details from the mass spectral cracking pattern and the infra red spectrum of a pure sample of hypoxanthine **[87]** can be obtained from **Table 4.47** and from **Figure 4.68** respectively.

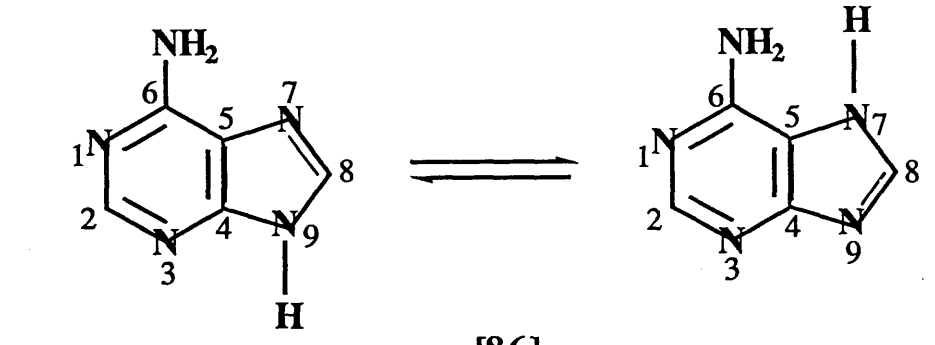

[86]

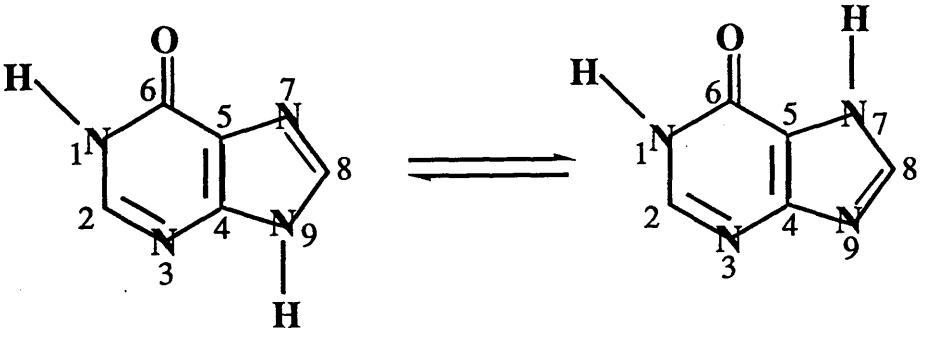

[87]

1,9-Dihydro-form 1,7-Dihydro-form

Table 4.46

Mass Spectrum Cracking Pattern of the Products of the Reaction of Adenine : $NaNO_2$=1:1

Measured Mass (m/z)	% Intensity	Fragment
136	9.1	$[C_5H_6N_5]^+$
81	17.6	$[C_3H_3N_3]^+$
54	24.0	$[C_2H_2N_2]^+$
53	24.1	$[C_2HN_2]^+$
39	5.4	$[C_2HN]^+$
38	7.8	$[C_2N]^+$
29	9.7	$[CH_3N]^+$
28	68.4	$[CH_2N]^+$
27	9.9	$[CHN]^+$

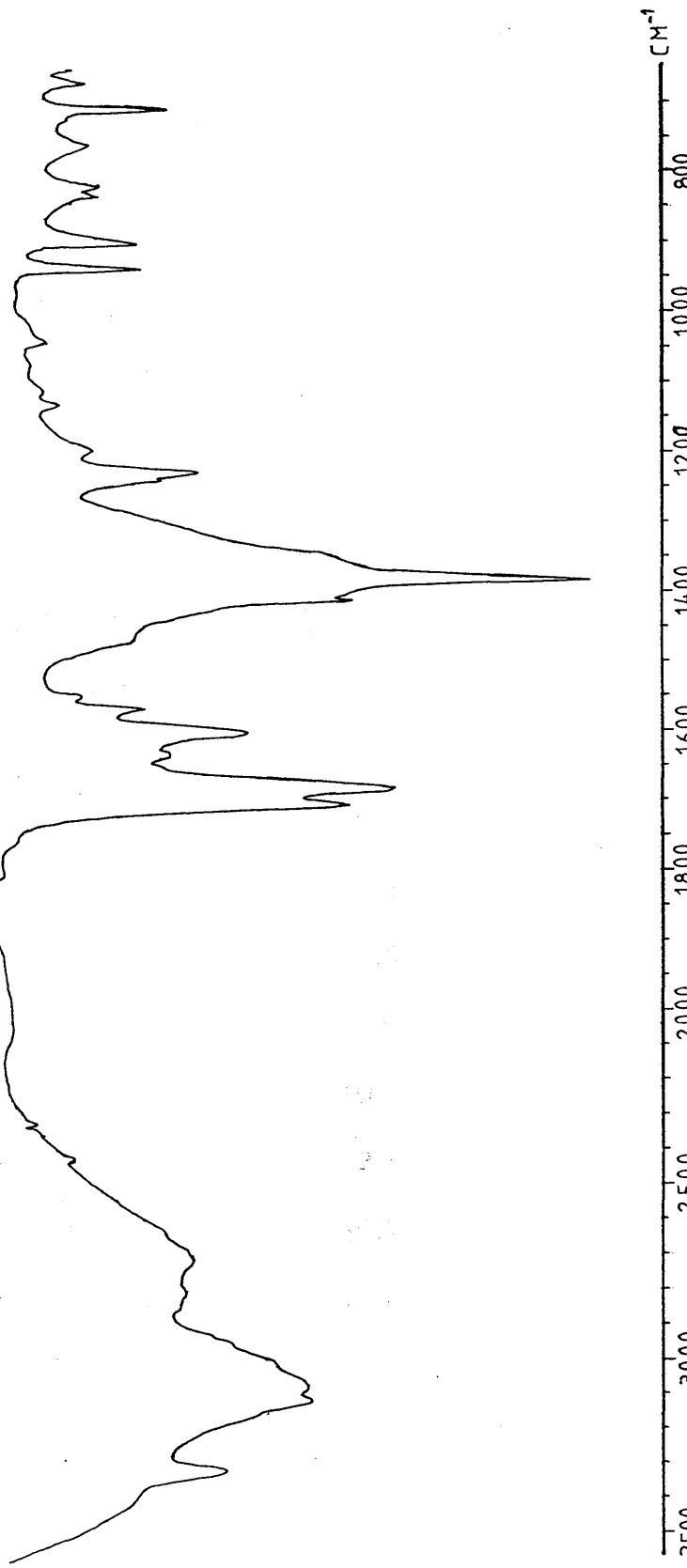

Figure 4.67 The infra red spectrum of the products obtained from the reaction of adenine : $NaNO_2$ = 1:1(KBr disc)

Table 4.47

Mass Spectrum Cracking Pattern of Hypoxanthine

Measured Mass (m/z)	% Intensity	Fragment
136	100.0	$[C_5H_6N_5]^+$
81	14.9	$[C_3H_3N_3]^+$
54	49.2	$[C_2H_2N_2]^+$
53	26.5	$[C_2HN_2]^+$
39	10.0	$[C_2HN]^+$
38	10.3	$[C_2N]^+$
29	12.3	$[CH_3N]^+$
28	80.2	$[CH_2N]^+$
27	14.0	$[CHN]^+$

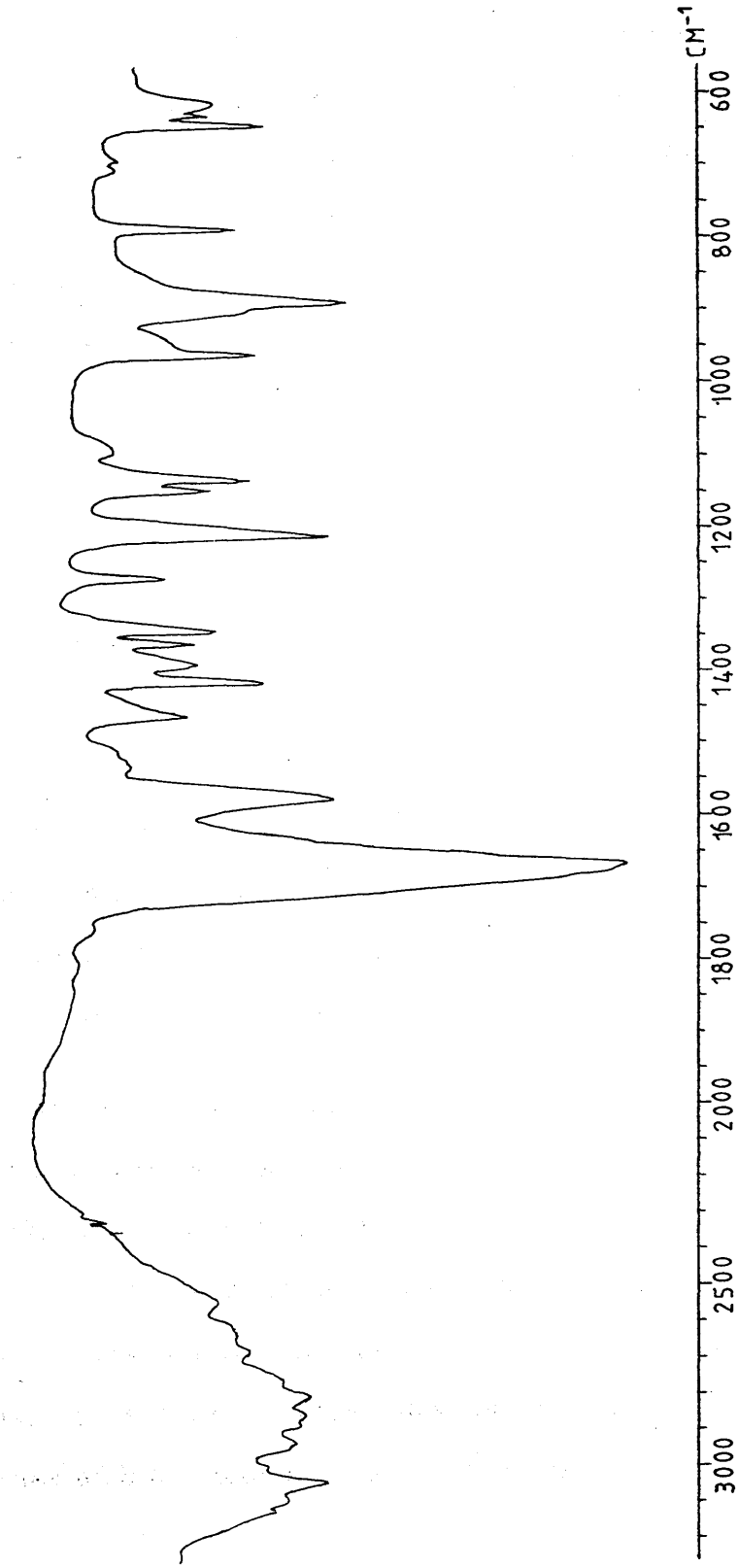

Figure 4.68 The infra red spectrum of hypoxanthine (KBr disc)

4.3.4 CONCLUSIONS

In the time availible for this work, it was not possible to study the effects of the oxides of nitrogen on other pyrimidine or purine bases, or on nucleic acids which include these bases, but from the pilot studies that have been described in this thesis, it seems that under very mild conditions, amino- pyrimidines and amino-purines react to give the corresponding hydroxy compounds. This reaction may well be responsible for the damage inflicted by nitrous acid or by the oxides of nitrogen, and therefore by nitrites on DNA and RNA, thereby giving rise to mutations in plants and animals. In the nucleic acids that are involved in transmission of genetic information, thymine is paired with adenine through specific hydrogen bonds, and cytosine is similarly paired with guanine. The conversion of cytosine to uracil and guanine to hypoxanthine, when these substances react with acidified sodium nitrite, must change the way the bases are paired, and therefore must change the genetic code. Guanine almost certainly reacts with acidified sodium nitrite in a similar manner, as also must naturally occurring amino acid residues, or any molecular fragment that contains an $-NH_2$ residue.

Acidified sodium nitrite affects steroids, and almost certainly carbohydrates. It affects unsaturated fatty acids, and therefore almost certainly permeability through cell membranes. It affects pyrimidines and purine bases, and almost certainly nucleosides, nucleotides and amino acids. It also affects amino acids and proteins. Acidified sodium nitrite has a devastating effect on the molecules encountered in living systems, and it interferes with the genetic code. NO and NO_2 must be implicated in some areas of carcinogenesis. They may well be implicated also in bacterial toxic shock.

REFERENCES

1 B. G. Gowenlock and W. Lüttke, *Quart. Rev.*, 1958, **12**, 321.

2 H. Mausser and H. H. Heitzer, *Z. Naturforsch*, 1965, **20B**, 200.

3 A. Mackor, Th. A. J. W. Wajer, and Th. J. de Boer, *Tetrahedron Lett.*, 1966, **19**, 2115.

4 A. Mackor, Th. A. J. W. Wajer, and Th. J. de Boer, *Tetrahedron Lett.*, 1967, **29**, 2757.

5 R. Hoffmann, R. Gleiter, and F. B. Mallory, *J. Amer. Chem. Soc.*, 1970, **92**, 1460.

6 B. G. Gowenlock and J. Trotman, *J. Chem. Soc.*, 1956, 1670.

7 V. Keussler and W. Lüttke, *Z. Electrochem.*, 1959, **63**, 614.

8 R. R. Holmes, *J. Org. Chem.*, 1964, **29**, 3076.

9 W. Höbold, U. Prietz, and W. Pritzkow, *J. Prakt. Chem.*, 1969, **311**, 260.

10 Y. L. Chow, "The Chemistry of Amino, Nitroso and Nitro Compounds and their Derivatives", Ed. S. Patai, Interscience, New York, 1982, vol.1, p.181.

11 E. T. Storm and A. L. Bluhm, *Chem. Comm.*, 1966, 115.

12 Th. A. J. W. Wajer, A. Mackor, and Th. J. de Boer, *Tetrahedron*, 1967, **23**, 4021.

13 Th. J. de Boer, *Can. J. Chem.*, 1982, **60**, 1602.

14 B. G. Gowenlock, G. Kresze, and J. Pfab, *Tetrahedron Lett.*, 1972, **1**, 593.

15 C. Chatgilialoglu and K. U. Ingold, *J. Amer. Chem. Soc.*, 1981, **103**, 4833.

16 D. K. MacAlpine, A. L. Porte, and G. A. Sim, *J. Chem. Soc., Perkin Trans. 1*, 1981, 2533.

17 A. A. Freer, D. K. MacAlpine, J. Peacock, and A. L. Porte, *J. Chem. Soc., Perkin Trans. 2*, 1985, 971.

18 B. G. Gowenlock, G. Kresze, and J. Pfab, *Tetrahedron*, 1973, **29**, 3587.

19 B. G. Gowenlock, G. Kresze, and J. Pfab, *J. Chem. Soc., Perkin Trans. 2*, 1974, 511.

20 B. G. Gowenlock, G. Kresze, and J. Pfab, *Justus Liebigs Ann. Chem.*, 1975, **16**, 1903.

21 D. Forrest, B. G. Gowenlock, and J. Pfab, *J. Chem. Soc., Perkin Trans. 2*, 1978, 242.

22 D. Forrest, B. G. Gowenlock, and J. Pfab, *J. Chem. Soc., Perkin Trans. 2*, 1979, 576.

23 T. A. B. M. Bolsman and Th. J. de Boer, *Tetrahedron*, 1973, **29**, 3579.

24 A. H. M. Kayen and Th. J. de Boer, *Rec. Trav. Chim.*, 1977, **96**, 237.

25 D. H. Hammick and M. W. Lister, *J. Chem. Soc.*, 1937, 489.

26 S. T. R. S. Mitchell and J. Cameron, *J. Chem. Soc.*, 1938, 1964.

27 L. Creagh and I. Trachtenberg, *J. Org. Chem.*, 1969, **34**, 1307.

28 E. F. J. Duyntsee and M. E. A. H. Mevis, *Rec. Trav. Chim.*, 1971, **90**, 932.

29 D. K. MacAlpine, A.L. Porte, and G. A. Sim, *J. Chem. Soc., Perkin Trans. 1*, 1981, 999.

30 S. F. Nelson, "Free Radicals", Ed. J. K. Kochi, Interscience, New York, 1973, vol.2, p.545.

31 H. G. Aurich and W. Weiss, "Topics in Current Chemistry", Ed. F. Boschke, Springer-Verlag, Berlin, 1975, vol.59, p.65.

32 A. Mackor, Th. A. J. W. Wajer, and Th. J. de Boer, *Tetrahedron*, 1968, **24**, 1623.

33 S. Forshult, C. Lagercrantz, and K. Torssell, *Acta Chem. Scand.*, 1969, **23**, 522.

34 C. Lagercrantz, *J. Phys., Chem.*, 1971, **75**, 3406.

35 E. G. Janzen, *Accounts of Chem. Res.*, 1971, **4**, 31.

36 J. A. Mansen, H. Hittenhausen, and Th. A. J. W. de Boer, *Tetrahedron Letters*, 1971, 3213.

37 A. A. McConnell, S. T. R. S. Mitchell, A. L. Porte, J. S. Roberts, and C. Thomson, *J. Chem. Soc. (B)*, 1970, 833.

38 A. Mackor, Th. A. J. W. Wajor, Th. J de Boer, and J.D.W. van Voorst, *Tetrahedron Letters*, 1966, 2115.

39 M. Gomberg, *J. Amer. Chem. Soc.*, 1900, **22**, 757.

40 O. Piloty and B. G. Schwerin, *Ber.*, 1901, **34**, 1870.

41 A. Briere, H. Lemaire, and A. Rassat, *Bull. Soc. Chim. Franç.*, 1965, 3273.

42 E. G. Rozantsev, "Free Nitroxyl Radicals", Plenum Press, New York, 1970, 125.

43 O. Kikuchi, *Bull. Soc. Chim. Jap.*, 1969, **42**, 47.

44 H. G. Aurich, K. Hahn, K. Stork, and W. Weiss, *Tetrahedron*, 1977, **33**, 969.

45 A. Calder and A. R. Forrester, *J. Chem. Soc. (C)*, 1969, 1459.

46 R. W. Kreilick, "Advances in Magnetic Resonance", Ed. J. S. Waugh, Academic Press, 1973, vol.6, p.41.

47 Y. Notake, M. Okazaki, and K. Kawata, *J. Amer. Chem. Soc.*, 1977, **99**, 5198.

48 A. Aebi, D. H. R. Barton, and A. S. Lindsey, *J. Chem. Soc.*, 1953, 3124.

49 F. Šorm, V. Jarolim, M. Streibl, L. Dolejš, *Chem. Ind. (London)*, 1956, 154.

50 J. M. Robertson, "International Review of Science, Serie 2, Physical Chemistry, Chemical Crystallography", Butterworths, London, 1975, vol.11, p.57.

51 D. M. Hawley, J. S. Roberts, G. Ferguson, and A. L. Porte, *Chem. Comm.*, 1967, 942.

52 D. M. Hawley, G. Ferguson, and J. M. Robertson, *J. Chem. Soc. (B)*, 1968, **11**, 1255.

53 O. Schreiner and C. F. James, Pharm. Arch., 1898, **1**, 213.

54 S. T. R. S. Mitchell, *J. Chem. Soc.*, 1928, 3258.

55 S. T. R. S. Mitchell, *J. Chem. Soc. (A)*, 1930, **34**, 3258.

56 R. M. Hoffman, *J. Amer. Chem. Soc.*, 1934, **56**, 1894.

57 A. A. McConnell, *Ph.D. Thesis*, University of Glasgow, 1970.

58 A. A. McConnell, S. T. R. S. Mitchell, A. L. Porte, J. S. Roberts, and C. Thomson, *J. Chem. Soc. (B)*, 1970, 833.

59 F. Šorm, J. Mleziva, A. Arnold, and J. Pliva, *Collect. Czech. Chem. Comm.*, 1949, **14**, 699.

60 V. Herout, M. Streibl, J. Mleziva, and F. Šorm, *Collect. Czech. Chem. Comm.*, 1949, **14**, 716.

61 F. Šorm, M. Streibl, J. Pliva, and V. Herout, *Collect. Czech. Chem. Comm.*, 1952, **16**, 639.

62 F. Šorm, M. Streibl, V. Jarolim, L. Novotny, L. Dolejš, and V. Herout, *Collect. Czech. Chem. Comm.*, 1954, **19**, 570.

63 G. R. Clemo and J. O. Harris, *J. Chem. Soc.*, 1951, 22.

64 G. R. Clemo and J. O. Harris, *J. Chem. Soc.*, 1952, 665.

65 J. O. Harris, *J. Chem. Soc.*, 1953, 184.

66 W. R. Fawcett and J. O. Harris, *J. Chem. Soc.*, 1954, 2673.

67 P. Clarke and G. R. Ramage, *J. Chem. Soc.*, 1954, 4345.

68 R. P. Hildebrand, M. D. Sutherland, and O. J. Waters, *Chem. Ind. (London)*, 1959, 489.

69 S. Dev, *Tetrahedron*, 1960, **9**, 1.

70 J. B. Hendrickson, *Tetrahedron*, 1959, **7**, 82.

71 M. D. Sutherland and O. J. Waters, *Aust. J. Chem.*, 1961, **14**, 596.

72 A. T. McPhail, R. I. Reed, and G. A. Sim, *Chem. Ind. (London)*, 1964, 976.

73 J. A. Hartsuck and I. C. Paul, *Chem. Ind. (London)*, 1964, 977.

74 A. T. McPhail and G. A. Sim, *J. Chem. Soc. (B)*, 1966, 112.

75 A. C. Chapman, *J. Chem. Soc.*, 1895, **67**, 54.

76 A. C. Chapman, *J. Chem. Soc.*, 1895, **67**, 780.

77 Z. F. Khan and A. L. Porte, *J. Chem. Soc., Perkin Trans. 2*, 1989, 1599.

78 Z. F. Khan, A. L. Porte, and J. E. Schubert, *J. Chem. Soc., Perkin Trans. 2*, 1989, 1605.

79 A. H. M. Kayen, L. R. Subramanian, and Th. J. de Boer, *Recl. Trav.Chim. Pays-Bas*, 1971, **90**, 866.

80 G. Kresze, B. Ascherl, H. Braun, and H. Felder, *Org. Prep. Proc. Int.*, 1987, **19**, 329.

81 S. T. R. S. Mitchell and S. C. Carson, *J. Chem. Soc.*, 1936, 1005.

82 S. T. R. S. Mitchell and J. Cameron, *J. Chem. Soc.*, 1938, 1964.

83 J. Veitch, *Ph.D. Thesis*, University of Glasgow, 1953.

84 A. J. N. Hope and S. T. R. S. Mitchell, *J. Chem. Soc.*, 1954, 4215.

85 S. T. R. S. Mitchell, J. S. Watson, and W. Dunlop, *J. Chem. Soc.*, 1950, 3440.

86 A. J. N. Hope and S. T. R. S. Mitchell, *J. Chem. Soc.*, 1953, 3483.

87 N. N. Majeed, G. S. MacDougall, A. L. Porte, and I. H. Sadler, *J. Chem. Soc., Perkin Trans. 2*, 1988, 1027.

88 J. S. Davidson, *Ph.D. Thesis*, University of Glasgow, 1958.

89 G. Ferguson, G. J. Fritchie, J. M. Robertson, and G. A. Sim, *J. Chem. Soc.*, 1961, 1976.

90 N. N. Majeed and A. L. Porte, *J. Chem. Soc., Perkin Trans. 2*, 1987, 1139.

91 J. Lub and Th. J. de Boer, *Recl. Trav. Chim. Pays-Bas,* 1984, **103**, 328.

92 J. Lub, M. L. Beekes, and Th. J. de Boer, *Recl. Trav. Chim. Pays-Bas,* 1986, **105**, 22.

93 P. Tarte, *Bull. Soc. Chim. Belge,*1954, **63**, 525.

94 C. J. Groombridge, R. K. Harris, K. J. Packer, B. J. Say, and S. F. Tanner, *J. Chem. Soc., Chem. Comm.*, 1980, 174.

95 N. Zumbulyadis, P. M. Henrichs, and R. H. Young, *J. Chem. Phys.*, 1981, **75**, 1603.

96 W. Lüttke, *Angew. Chem.*, 1956, **68**, 417.

97 W. Lüttke, *Angew. Chem.*, 1957, **69**, 99.

98 W. Lüttke, *Z. Elektrochem.*, 1957, **61**, 302.

99 G. E. Hawkes, K. Herwig, and J. D. Roberts, *J. Org. Chem.*, 1974, **39**, 1022.

100 G. Ender, G. Harre, A. Helgebostad, N. Koppang, R. Madsen, and L. Ceh, *Naturwissenschaften*, 1964, **51**, 637.

101 J. Sakshang, E. Sognen, M. A. Hansen, and N. Koppang, *Nature (London)*, 1965, **206**, 1261.

102 R. C. Shank and P. N. Magee, "Mycotoxins and N-Nitrosocompounds: Environmental Risks", Ed. R. C. Shank, C. R. C. Press Inc., Boca Raton, Florida, U. S. A., 1981, **1**, 185, and references therein.

103 A. Gescher, *Chemistry in Britain,* 1990, **26**, 435.

104 A. Butler, *Chemistry in Britain,* 1990, **26**, 419.

105 C. Glidewell, *Chemistry in Britain,* 1990, **26**, 137.

106 J. A. Perigo, E. Whiting, and T. E. Bashford, *J. Food Technol.*, 1967, **2**, 377.

107 R. A. G. Carrington, *Spectrochim. Acta,* 1960, **16**, 1279.

108 W. H. Lunn, *Spectrochim. Acta,* 1960, **16**, 1279.

109 J. G. Batchelor, R. J. Cushley, and J. G. Prestegard, *J. Org. Chem.*, 1974, **39**, 1698.

110 M. Karplus, *J. Amer. Chem. Soc.,* 1963, **85**, 2870.

111 A. Ejchardt, *Org. Magn. Res.,* 1977, **10**, 263.

112 E. R. Blout and M. Fields, *J. Amer. Chem. Soc.,* 1950, **72**, 479.

113 F. Coletta, R. Ettore, and A. Gambaro, *J. Magn. Res.,* 1976, **22**, 453.

114 T. Lindhal and B. Nyberg, *Biochemistry,* 1974, **13**, 3405.

115 J. L. Wong and D. S. Fuchs, *J. Org. Chem.,* 1970, **11**, 3786.

116 P. D. Ellis, R. B. Dunlap, A. L. Pollard, K. Seidman, and A. D. Cardin, *J. Amer. Chem. Soc.,* 1973, **95**, 4398.

117 P. Karran and T. Lindhal, *Biochemistry,* 1980, **19**, 6005.